THE UNIVERSITY
of EDINBURGH

Characterising the roles of the members of the nuclear-encoded Rubisco small subunit family in *Arabidopsis thaliana*

Panupon Khumsupan

Doctor of Philosophy

Institute of Molecular Plant Sciences

The University of Edinburgh

2019

Supervisor:

Dr Alistair J. McCormick

Declaration

I hereby declare that this thesis is an original piece of work that embodies the results of my own research. All work presented in here has not been submitted for any other degree or professional qualification. I acknowledge the nature and extend of work carried out in collaboration with others below:

Chapter 4 – The gRNAs that target homologous regions in the 1B-3B locus was designed by Billy Aldridge, Oleg Raitskin and Nicola Patron, Earlham Institute. The Rubisco content assay was performed by Douglas Orr and Elizabete Carmo-Silva, Lancaster University.

Panupon Khumsupan

Acknowledgements

I would like to take this opportunity to thank everyone who has supported me through my PhD career. First of all, I would like to thank Alistair for taking a risk on and offering me the PhD position. Your guidance has fostered many of my skills and was absolutely vital to my scientific and personal growth. I will continue to model after you. I would like to thank Andrew for chatting with me about my work despite the busy schedule. I would also like to also thank Naomi; without you I would have been lost in my first two years.

This PhD would have been nearly impossible if I had not met Sophie. A PhD is a unique and challenging experience but I am glad that I had someone who was going through the exact same thing and could understand and sympathise the ups and downs. I will remember our Friday night movies, Bene's fish and chips and many random deep conversations. We made the right decision moving in together, and I have made another sister.

I am grateful for the members of the McCormick lab. Thank you Nicky and Livia for taking a role of (fun) mothers when mine own is far and be the voice of reason. I wish there were more people like you. Thank you Grant, Ale, Alex, Anton and Liat for being the coolest office neighbours. You guys have made us the best lab in IMPS!

During my time in Edinburgh, I have also made friends outside of the lab. I would like to thank my friend Bartosz for always inviting me for the 50% off dinner and cinema combo, and JR for many gym sessions and countless things we do together. You both have qualities that I admire and aspire to develop as I grow.

I would like to extend my gratitude to members of IMPS and their contribution to my research as well as free cake and alcohol. I would like to give a special thanks to Muriel. In a sorrow time, we found great friendship. Thank you for all the traveling memories and pictures that you took for me.

This PhD would not have been possible without the funding from the Darwin Trust of Edinburgh and the University of Edinburgh Innovation Initiative Grant who have funded my research and my stay in the UK.

Lastly, I would like to pay the deepest gratitude to my parents and sister. I could not have asked for a better family. Thank you for the support, patience, dedication, acceptance and, most importantly, love. This thesis is for you - ด้วยรักและเคารพ

Love is love

ความรักคือความรัก

List of abbreviations

Rubisco	Ribulose-1,5-bisphosphate carboxylase/oxygenase
RuBP	Ribulose-1,5-bisphosphate
CO_2	Carbon dioxide
O_2	Oxygen
3PGA	3-phosphoglycerate
2PGA	2-phosphoglycolate
CCM	Carbon concentrating mechanism
LSU	Large subunits
RbcL	Rubisco large subunit gene
RbcS	Rubisco small subunit gene
SSU	Small subunits
NT	N-terminus
CT	C-terminus
PDB	Protein Data Bank
$S_{c/o}$	CO_2/O_2 specificity
$V_{c,max}$	Maximum rate of Rubisco carboxylation
$k_{\mathrm{cat,c}}$	Turnover rate of carbon

CRISPR	Clustered regularly interspaced short palindromic repeats
Cas9	CRISPR associated protein
gRNA	guide RNA
PAM	Protospacer adjacent motif
DSB	Double strand break
NHEJ	Non-homologous end joining
HDR	Homology-directed repair
ZFN	Zinc finger nucleases
TALEN	TAL effector nuclease
CaMV35S	Cauliflower mosaic virus
T-DNA	Transfer-DNA
UTR	Untranslated region
PCR	Polymerase chain reaction
RT-qPCR	Reverse transcription-quantitative PCR
LB	Left border
DAG	Days after germination
FW	Fresh weight
DW	Dry weight

SLA	Specific leaf area
PSII	Photosystem II
F_v/F_m	Maximum quantum efficiency of PSII
SEM	Standard error of mean
KO	Knock-out
WT	Wild-type
PM	Point mutation
BB	BigBoi, *rbcs1a2b3b* KO mutant based on the *rbcs1a2b* T-DNA line
BG	BigGurl, *rbcs1a2b3b* KO mutant based on the *rbcs1a3b* T-DNA line
CC	CRISPR/Cas9 KO mutant
PAR	Photosynthetically active radiation
A	CO_2 Assimilation
C_i	Sub-stomatal CO_2 concentrations
J_{max}	Maximum photosynthetic electron transport rate
R_d	Mitochondrial respiration in the light
g_s	Stomatal conductance
ZT	Zeitgeber time
DC	Dark control

BL	Blue light
RL	Red light
FRL	Far-red light
HL	High light (white light at 1000 µmol photon m^{-2} s^{-1})
ML	Medium light (white light at 200 µmol photon m^{-2} s^{-1})
LL	Low light (white light at 50 µmol photon m^{-2} s^{-1})
HT	High temperature (30^{o}C)
LT	Low temperature (10^{o}C)

Lay summary

Photosynthesis is a process where plants use carbon dioxide (CO_2), water and light to produce food (in a form of sugars) for themselves. The enzyme that is responsible for fixing CO_2 during photosynthesis is called Rubisco. Most plants produce an abundance of Rubisco, as much as 40% of total protein in leaves, in order to cope with the changing environment including light, temperature and CO_2 level. Despite being an important enzyme, Rubisco is inefficient in that it is a relatively slow enzyme and cannot differentiate between CO_2 and oxygen O_2. The reaction with O_2 produces a toxic byproduct that needs to be recycled, which expends energy. Due to these inefficiencies, Rubisco has been a target to improve photosynthesis and crop productivity.

Rubisco is an enzyme composing of large subunits (LSU) and small subunits (SSU). The LSUs are where the reaction with CO_2 and O_2 occurs. The roles of SSUs are still somewhat elusive but we know that they can influence the catalytic activities of Rubisco. The production of SSUs in some plant species varies in different tissues, organs, developmental stages, and/or fluctuates with environmental conditions.

In this study, the model plant *Arabidopsis thaliana* (Arabidopsis) was used to decipher the functional roles of SSUs. Arabidopsis has four SSU genes (1A, 1B, 2B and 3B) that are produced differentially. 1A is responsible for about 50% of total SSU pool, followed by 3B (35%), 2B (10%) and 1B (5%). In order to assess if these individual SSUs are important to growth and survival, we generated knockout mutants for each and a combination of SSU genes using a gene editing method called CRISPR/Cas9. A suite of mutants was generated and grown under different environmental conditions. Firstly, we

found that knocking down SSU production down to 40% had no adverse effects on plant growth under standard growth condition of Arabidopsis (200 µmol m^{-2} s^{-1}, 21^{o}C). However, when grown under highlight (1000 µmol m^{-2} s^{-1}, i.e. higher demand for Rubisco), at least 60% of SSUs was needed so that growth is not affected. Secondly, the production of 2B and 3B increased under high temperature (30^{o}C) and decreased under low temperature (10^{o}C). These two genes are the main temperature mediators in Arabidopsis and may play important roles when plants are grown at elevated temperature. Lastly, triple mutant lacking 1A, 2B and 3B (given the name "BigBoi") generated in this study could be exploited to test the activity of Rubisco. This mutant is ideal because it has only one SSU supporting photosynthetic growth and grows very slowly. As a proof of concept, an SSU gene from green algae *Chlamydomonas reinhardtii* was put in BigBoi and a 40% increase in growth was observed compared to BigBoi. A hybrid Rubisco between the native LSU and other foreign SSUs could be made and re-engineered to improve the catalytic properties of Rubisco.

Abstract

Rubisco is the enzyme responsible for the net photosynthetic carbon fixation in plants. The enzyme consists of chloroplast-encoded large subunits and a family of nuclear-encoded small subunits (SSUs). SSUs are essential for the assembly of the Rubisco enzyme in higher plants and have been shown to influence catalytic activities of Rubisco (Atkinson *et al*., 2017; Laterre *et al*., 2017). This study aims to characterise the roles of SSUs in the model plant *Arabidopsis thaliana* (Arabidopsis). Arabidopsis contains four SSU (*RbcS*) genes, *RbcS1A* (1A hereafter) on chromosome 1, and *RbcS1B*, *RbcS2B* and *RbcS3B* (1B, 2B, 3B, respectively hereafter) located in tandem on chromosome 5. To characterise the roles of SSU, I have i) generated SSU knock-out mutants using CRISPR/Cas9 editing and analyse the impact of single and multiple SSU knock-outs on plant growth and fitness; ii) measured *RbcS* expression under different light qualities, quantities and temperatures; iii) performed growth analyses under different environmental conditions using CRISPR/Cas9 *rbcs* mutants; and iv) complemented the triple mutant *1a2b3b* (BigBoi) with SSU from *Chlamydomonas reinhardtii* (Chlamydomonas) and performed growth analyses on the complemented lines.

To generate SSU knock-out mutants via CRISPR/Cas9, two pairs of gRNAs were designed to target each *RbcS* gene. The efficiency of the gRNAs pairs was evaluated in mesophyll protoplasts and it was found that at least one pair for each gene was able to induce large deletions of 96-180 bp in *RbcS*. Constructs containing Cas9 nuclease and gRNAs were stably transformed in Arabidopsis by floral dipping. The T1 progeny containing the transgene were screened for large deletions by PCR and small

insertions/deletions (indels) by Sanger sequencing. PCR screening showed that large deletions were induced *in planta*, but they were chimeric deletions and not transmittable to the T2 progeny. On the other hand, indels of 1-7 bp occurred at a higher rate (12% and 7%, respectively) and were heritable. Analyses of the T2 progeny revealed that heterozygous mutation was the most common type of mutation in 1B and 2B but chimeric mutation was the most common in 1A and 3B. The heritability rates for *1a*, *1b*, *2b* and *3b* were 4%, 20%, 8% and 6%, respectively.

To measure the *RbcS* expression under different environmental conditions, the arrhythmic clock mutant *prr5/7/9* mutant was grown under constant light for 14 d. The mutant was kept in darkness for 24 h before exposing to white light for 12 h. Transcript analysis was performed and the result showed that i) all *RbcS* genes were induced by light and the total transcript abundance increased when light was turned on and decreased after light was turned off; and ii) each *RbcS* had different induction and degradation rates. 1A was induced the most quickly and degraded most rapidly while 1B was induced the most slowly and 2B was the most stable transcript after light was turned off. The experiment was repeated but with different light qualities (blue, red, and far-red), light quantities (high (1000 µmol photon $m^{-}2\ s^{-1}$), medium (200 µmol photon $m^{-}2\ s^{-1}$) and low (50 µmol $m^{-}2\ s^{-1}$) light), and temperatures (high (30^{o}C) and low (10^{o}C), white light at 200 µmol $m^{-2}\ s^{-1}$). Transcript analyses showed that blue light induced the highest level of increase among light qualities followed by red light and far-red light. High light induced the highest level of transcript abundance followed by medium light and low light. Under high temperature, the expression of 2B and 3B increased significantly and 3B was the major isoform. On

the other hand, the expression of 2B and 3B were suppressed under low temperature and 1A was the major isoform. This suggested that 2B and 3B were the most sensitive temperature mediators of the *RbcS* gene family.

Based on the transcript analyses, the high light, high temperature and low temperature conditions were chosen for growth experiments. WT, T-DNA and CRISPR/Cas9 mutants were used to test the following hypotheses: i) under the light saturating condition (high light), Rubisco becomes limiting and plants with reduced Rubisco content (*1a*, *3b*, *2b3b* and *1a2b*) would grow more slowly than WT; ii) under high temperature where 3B is the major isoform, plants lacking 3B (*3b*, *2b3b*) would suffer a reduced growth rate relative to WT; iii) under low temperature where 1A is the major isoform, plants lacking 1A (*1a*, *1a2b*) would suffer a reduced growth rate relative to WT. Growth under high light was able to differentiate the areas of *1a*, *2b3b* and *1a2b* mutant in comparison to WT, but not *3b* mutant. However, the weight of *3b* mutant was significantly lower than that of WT, suggesting the leaves of *3b* were thinner. Under high temperature, *3b* and *2b3b* mutants were not significantly different from WT. This was due to 3B accounting for *ca* 50% of the transcript abundance under high temperature and growth was found to be unaffected at this level of *RbcS* decrease. Under low temperature, the areas of *1a* and *1a2b* were not significantly different from that of WT, but weights were significantly lower. This was similar to *3b* under high light and suggested that leaves of plants with significant Rubisco reduction become thinner first and further decrease in Rubisco resulted in the loss of leaf area. Altogether, this study showed that *RbcS* genes

collectively contribute to the overall transcript abundance and 2B and 3B genes are most susceptible to the changes in temperature.

The triple mutant *1a2b3b* generated in this study was used as a model to study the effects of heterologous SSUs to growth. After complementation with Chlamydomonas SSU, seven independent complemented lines were identified and the slow-growing phenotype was rescued in all lines. The area of complemented plants ranged from 8-34% of WT compared to 1% of the triple mutant on day 28. This study showed that the triple mutant could be used as an Arabidopsis platform to study the effects of heterologous SSUs to Rubisco catalytic activities.

Table of content

Published reviewed article “CRISPR/Cas in Arabidopsis: overcoming challenges to accelerate improvements in crop photosynthetic efficiencies” in Physiologia Plantarum

Chapter 1 - Literature review

Introduction

Ribulose-1,5-bisphosphate carboxylase/oxygenase (Rubisco) is the enzyme complex responsible for photosynthetic carbon uptake in plants. Rubisco fixes carbon dioxide (CO_2) through carboxylation of ribulose-1,5-bisphosphate (RuBP) to produce two molecules of 3-phosphoglycerate (3PGA), which is subsequently converted in to sugars and starch. Rubisco is a relatively slow catalyst for carboxylation with a turnover rate (k_{cat}^{c}) of ~1-15 s^{-1} (Badger *et al.,* 1998; Dodd *et al.,* 2002; Von Caemmerer and Furbank, 2003; Flamholz *et al.,* 2019). Carboxylation efficiency is further compromised by a competing side reaction with oxygen (O_2). Instead of producing two molecules of 3PGA, the oxygenic reaction produces a single 3PGA and 2-phosphoglycolate (2PGA), a toxic compound that needs to be recycled via photorespiration. Photorespiration expends ATP and results in a loss of previously fixed carbon and nitrogen that must be recaptured through the photorespiratory salvage pathway. Competitive oxygenation can reduce the efficiency of photosynthetic carbon assimilation by 25% in C3 plants and thus limits the productivity of C3 crops (Smith *et al.,* 2010). Increasing the yield of C3 crops through improving photosynthetic efficiencies is a key approach to ameliorate food security (Ingram and Porter, 2015; Long *et al.,* 2015). Various strategies, including the introduction of a carbon concentrating mechanism (CCM) into C3 plants, photorespiratory bypass mechanisms and directed mutation of the Rubisco complex are currently being explored (Whitney *et al.,* 1999; Dalal *et al.,* 2015; Atkinson *et al.,* 2016; South *et al.,* 2019).

Rubisco biogenesis and activation

Rubisco in plants and algae is an L8S8 complex composed of eight large subunits (LSUs), encoded by an *RbcL* gene on the chloroplastic genome, and eight small subunits (SSUs) encoded by a family of *RbcS* genes in the nuclear genome. Biogenesis of plant Rubisco requires coordination between chloroplastic and cytosolic translation because the LSUs are synthesised in the chloroplast stroma while SSUs are synthesised in the cytosol. Furthermore, assembly of Rubisco requires a suite of proteins needed for folding and assembly (chaperones), all of which are nuclear-encoded (Onizuka *et al.*, 2004; Emlyn-Jones *et al.*, 2006; Aigner *et al.*, 2017). After the translation on the ribosome, the chaperones and SSUs are transported to the chloroplast in the unfolded state and the chloroplast signal peptide is cleaved. The chaperones (currently eight are known) and SSUs are then folded into a functional state in the stroma where the folding and assembly of Rubisco occurs (Aigner *et al.*, 2017; Bracher *et al.*, 2017). Chaperonin cpn60α, cpn60β, cpn 10 and cpn 20 facilitate appropriate folding of LSUs, which subsequently dimerise into L2 complex with the assistance of Raf1 and RbcX. Four dimers of L2 are then oligomerised into the L8 conformation, which is believed to be mediated by Raf2 and BSD2. The L8 assembly is held together by eight BSD2 proteins, which are then displaced by eight SSUs to form a functional L8S8 Rubisco enzyme (Aigner *et al.*, 2017; Wilson and Hayer-Hartl, 2018).

Activation of RuBP-bound Rubisco (inactive form) is essential to switch Rubisco to an active form (i.e. a form that is capable of CO_2 fixation). Activation is facilitated by the enzyme Rubisco activase, which physically interacts with and changes the

conformation of Rubisco to release the bound inhibitor RuBP (Lorimer *et al.,* 1976; Perchorowicz *et al.,* 1981; Portis, 1995). Disassociation of RuBP from the active site allows for carbamylation (covalent modification of the amino group) of the active site by an activator CO_2 and subsequent binding of Mg^{2+} (Stec 2012). The active form of Rubisco, denoted by the bound activator CO_2 and Mg^{2+}, is capable of catalysis using the substrates RuBP and CO_2. Activation of Rubisco by Rubisco activase is an ATP-dependent process and therefore depends on the amount of ATP produced from the light reactions of photosynthesis (Portis 1995). The activity of Rubisco activase is also influenced by external environmental factors, such as light, temperature and CO_2 levels (Crafts-Brandner and Salvucci 2000; Salvucci and Crafts-Brandner 2004). Therefore, the pool of active Rubisco at a given time can vary depending on the activity of Rubisco activase.

Structure and functions of Rubisco

Rubisco evolved *ca.* 2.4 billion years ago from a symbiotic event (Nisbet *et al.,* 2007; Robinson *et al.,* 2012). The ancestral form of Rubisco has since diverged into four forms categorised based on differences in sequences of the ~50-55 kDa LSU (Tabita, 1999; Tabita *et al.,* 2008). Form I is the most abundant and found in all plants, algae and cyanobacteria while Form II are found in proteobacteria. Form I is further classified into Form IA found in some marine cyanobacteria and proteobacteria, and IB found in plants (Shih *et al.,* 2015). Forms III and IV (also known as Rubisco-like protein) are found in anaerobic prokaryotes (Tabita *et al.*, 2008). For the purpose of and relevance to this study, only Form I will be reviewed.

The functional unit of Rubisco is comprised of a dimer of LSUs which is repeated four times to form the L8 core of the LSU (Andersson *et al.,* 1989; Andersson and Backlund, 2008). The distinctive feature of Form I Rubisco is the presence of the eight ~12-18 kDa SSU capping both ends of the L8 core, forming the ~530-550 kDa L8S8 Rubisco enzyme (**Figure 1.1 A, B**) (Knight *et al.*, 1990; Andersson, 1996). The sequences of Form I LSU are more conserved while those of SSUs are are more diverse (Spreitzer, 2003; Pottier et al., 2018). Crystal structure studies of LSU revealed the shorter N-terminus (NT) domain is composed of five strands of β-sheets and α-helices and the larger C-terminus (CT) domain contains eight α/β-units arranged as α/β barrel structure (**Figure 1.1 C, D**). The active site is located at β-strand of the CT end and the adjoining residues of the NT domain of the adjacent LSU of the dimer (**Figure 1.1 C, D**). Therefore, a catalytically active LSU dimer contains two active sites (Andersson and Taylor 2003). The common core structure of the SSU consists of four β-sheets and two helices. Two distinct regions of the SSU are the loop between the βA and βB strands (the βA-βB loop) and the CT, which differ in length depending on lineage (**Figure 1.1 C, D**). The βA-βB loop of higher plants and green algae contains 22 and 28 residues, respectively, and a shorter CT. In contrast, prokaryotes and non-green algae have a CT extension (βE-βF loop) that displaces the space that is occupied by the longer βA-βB loop in higher plants and green algae. Prokaryotes and non-green algae also have a shorter 10-residue βA-βB loop (Spreitzer 2003; Andersson 2008).

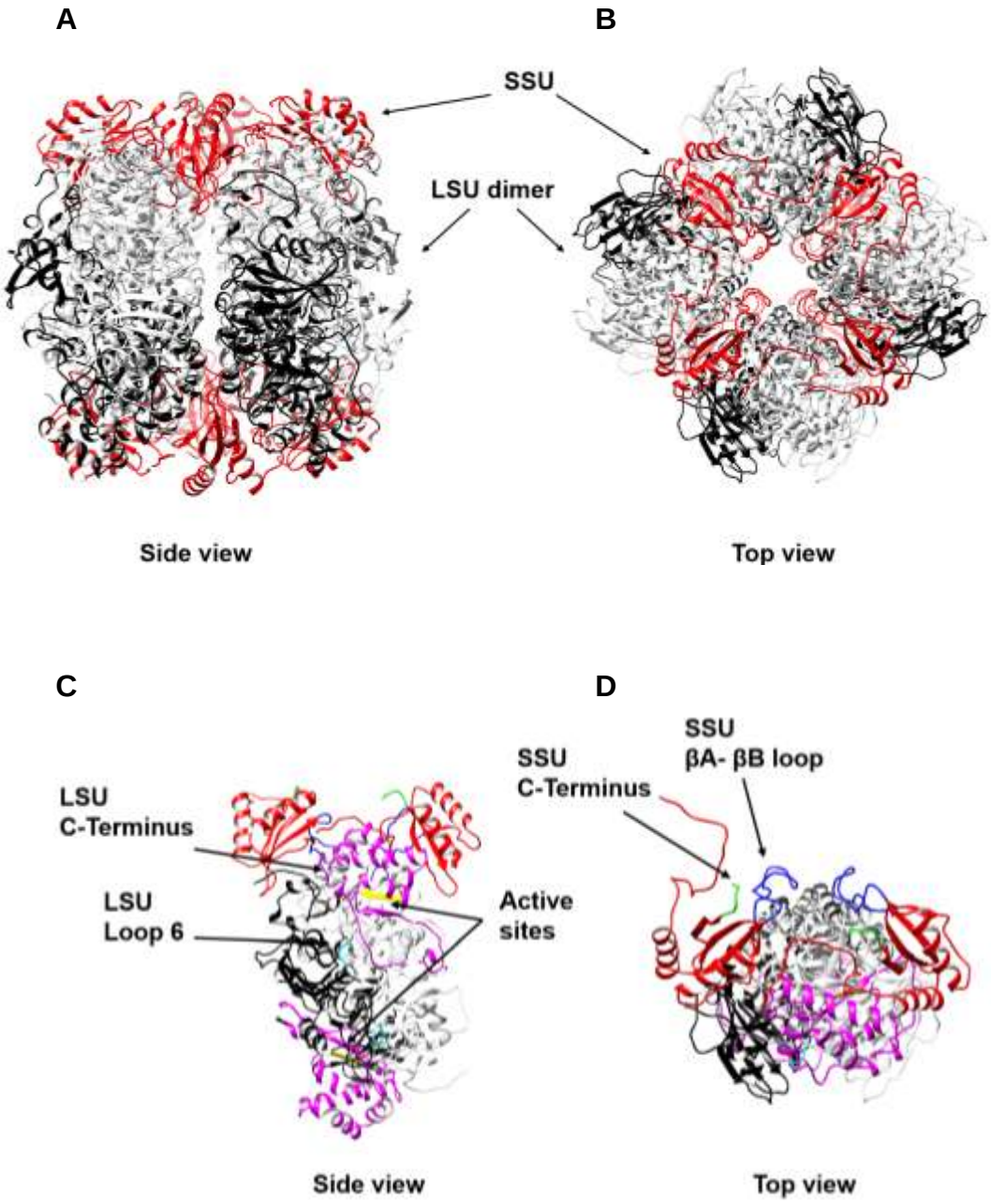

Figure 1.1. Crystal structure of Spinach Rubisco L8S8 unit and L2 dimer with two SSUs. A) Side view and B) top view of Rubisco enzyme. C) Side view and D) top view of the L2 dimer with two SSUs. SSUs are shown in red and dimers of LSU are in black and grey. The C-Terminus (CT) of the LSU CT is highlighted in magenta, the active sites are in

yellow and loop 6 is in cyan. SSU CT's are highlighted in green and βA-βB loops in blue. Crystal structure of Rubisco was obtained from Protein Data Bank (PDB) with the PBD code 1AUS.

Regions both close and distal to the active sites have been investigated and shown to influence the catalysis of Rubisco. The CT of the LSU forms a part of the catalytic site and is also responsible for the open and closed conformation of Rubisco active site (Schneider *et al*. 1990; Taylor and Andersson 1996). The crystal structure of tobacco LSU revealed that the CT may serve as a "latch" to hold and pack against loop 6 in the closed state, which in turn, stabilizes the active site by its polar interaction with the side chain of Asp473 (**Figure 1.1 C**) (Duff *et al.,* 2000). Directed mutagenesis of Asp473 disrupted the polar interaction between CT and loop 6 and destabilized the closed state (Karkehabadi *et al.,* 2007), which resulted in an 87% decrease in carboxylation catalytic efficiency and 16% decrease in CO_2/O_2 specificity ($S_{c/o}$) (Satagopan and Spreitzer 2004). Removal of the last α-helix of the CT caused a significant shift in quaternary structure of Rubisco, resulting in formation of an LSU octomer instead of a dimer, resulting in an enzyme that was inactive (Ranty *et al.,* 1990).

Interacting with the CT is loop 6 (residues 331 – 338) of the LSU, which connects the β-strand 6 with the α-helix 6 in the CT α/β-barrel. Loop 6 is responsible for the open (active site unbounded to ligands) or the closed (bounded to substrate or inhibitor) states of the Rubisco active site (Duff *et al.,* 2000). The sequence of this loop is well conserved in higher plants and it has been shown to influence $S_{c/o}$, as it forms a part of the catalytic mechanism (Karkehabadi *et al.,* 2007). Loop 6 constitutes a "flexible hinge" that contains

the two highly conserve residues Val331 and Lys334 (part of the active site) in plants and green algae. A replacement of Val331 by Ala decreased $S_{c/o}$ by 37% due to the altered flexibility of the loop. Lys334 has been shown to interact with CO_2 and O_2 and amino acid residues in the adjacent NT during catalysis. Site-directed mutagenesis of Lys334 abolished the carboxylation capacity or caused a significantly decreased the maximum rate of Rubisco carboxylation ($V_{c,max}$). These amino acids were found to affect the interaction with the RuBP and assist in stabilizing the intermediates following the reaction with CO_2 or O_2 (Gutteridge *et al.*, 1993).

Amino acid residues in the LSU that are distant from the active site can influence the catalysis and $S_{c/o}$ of Rubisco. In Chlamydomonas, a mutant strain with substitution of Leu290, which is located at the bottom of the α/β -barrel, by Phe resulted in a 13% decrease in $S_{c/o}$. The mutation also had an negative effect on the enzyme assembly and thermal stability as Rubisco was non-functional at 35^{o}C (Chen *et al.*, 1988). Subsequent structural analysis indicated that the conserved Leu290 residue forms a van der Waal interaction at the interface between the LSUs that influence temperature sensitivity (Karkehabadi *et al.*, 2005). This suggests that long-range interactions between or within subunits influence protein dynamics and catalysis.

The longer βA-βB loop of land plant and green algae extends to the bottom side of the α/β barrel of the LSU and also interacts with the LSU helices 2 and 8 and the βA-βB loops of the adjacent SSUs (Wasmann *et al.*, 1989). Transformation of βA-βB loops from a spinach SSU (22 residues) or a *Synechococcus* (*Aspergillus nidulans*) SSU (10 residues) into *Chlamydomonas reinhardtii* (Chlamydomonas hereafter) resulted in an

enzyme with a decrease in $V_{c,max}$ (50%) when containing a spinach βA-βB loop, and both $V_{c,max}$ (46%) and $S_{c/o}$ (11%) for that of *Synecchoccus* loop (Karkehabadi *et al.,* 2005). However, the mutant Rubisco was still photosynthetically competent, implying that altering the βA-βB loop length was not absolutely essential for the assembly of the enzyme but could potentially be a target to modify the catalytic activity.

The CT is another site of the SSU that is divergent. Truncation of the last nine residues in the CT of Chlamydomonas did not perturb $S_{c/o}$, but $V_{c,max}$ was reduced by 68% (Genkov and Spreitzer 2009). Furthermore, the enzyme was no longer active at 55^{o}C as compared to WT. This suggests that although these residues on the CT are not essential for Rubisco catalysis and assembly, it is required for thermal stability.

The small subunit of Rubisco

Members of the *RbcS* gene family vary in number in different eukaryotic species, ranging from two in the green alga Chlamydomonas (Goldschmidt-Clermont and Rahire 1986) to as many as 22 in wheat (Galili *et al.,* 1992). *RbcS* genes in higher plants are divided into subfamilies depending on their sequence similarity and arrangement. The number of genes within each SSU subfamily varies and those that are arranged in clusters within the genome are usually the product of gene duplication and conversion (Meagher *et al.,* 1989; Derocher *et al.,* 1993; Schwarte and Tiedemann, 2011). Genes within the same subfamily are usually identical or nearly identical, while sequence similarity decreases between different subfamilies. For instance, SSUs in petunia are encoded by

eight *RbcS* genes that are divided into three subfamilies (51, 71, 117) (Dean *et al.,* 1987). Subfamily 51 contains six genes, five of which are arranged in tandem within a 25 kb region. Within this subfamily, the nucleotide similarity (excluding introns) is between 97-100%. The other two subfamilies are located on different chromosomes and contain one gene each. The sequence of the other two subfamilies are more divergent and the similarity of mature mRNA among these three subfamilies is 89.8% (Dean *et al.,* 1989) . In Arabidopsis, the four *RbcS* isoforms are divided into two subfamilies – A and B. The A subfamily contains one gene called *RbcS1A* (1A hereafter) located on chromosome 1 while the B subfamily contains three genes – *RbcS1B, RbcS2B* and *RbcS3B* (1B, 2B and 3B hereafter) located on chromosome 5 (Krebbers *et al.,* 1988). The B subfamily genes are more than 97% similar in nucleotide sequence (excluding introns). The mature protein sequences of 2B and 3B are identical while that of 1B differs by 2 amino acid residues. However, the amino acid sequence of 1A is more divergent and is 180 amino acid residues in length as opposed to 181 amino acid residues of the B-subfamily mature protein (**Figure 1.2**).

Figure 1.2: Amino acid sequence alignment of Arabidopsis SSUs. The first 55 amino acids (italicised) constitute the chloroplast signal peptide which is cleaved out once the transcript is transported into the chloroplast. The mature mRNA starts with a methionine residue (M, bold). Amino acids in red represent α-helices and those in blue represent β-sheets. Asterisk (*) indicates identical amino acid among the four SSUs, colon (:) indicates conserved substitution between groups of strongly similar properties, full-stop (.) indicates conserved substitution between groups of weakly similar properties, and space ( ) indicates that the substitution is not conserved.

Functional roles of the small subunit

Although the SSU is distant to the active sites of Rubisco, several lines of evidence suggest that the sequence of the SSU may contribute to phylogenetic differences in the catalytic activity of Rubisco, including turnover rate ($k_{cat,c}$) and $S_{c/o}$ (Andrews and Lorimer, 1985; Read and Tabita, 1992; Kostov *et al.*, 1997; Kanevski, 1999; Du *et al.*, 2003; Karkehabadi *et al.*, 2005). Moreover, the presence of SSU in higher plants indicates that SSU may assist in binding and concentrating LSU. Sequence analysis of SSU shows that the βC-βD loop (**Figure 1.3**) is highly similar to that of the CcmM protein which mediates carboxysome formation and CO_2 concentrating mechanism in the cyanobacterium *Synechococcus* (Price *et al.*, 1993; Kaplan and Reinhold, 1999). This evidence suggests that SSU may have evolved from the carboxysomal protein that was eventually incorporated with the LSU. Binding of the SSU also allows for a more compact form of Rubisco, which increases the enzyme concentration in a cell, and thereby increases the net CO_2 fixation (Spreitzer 2003).

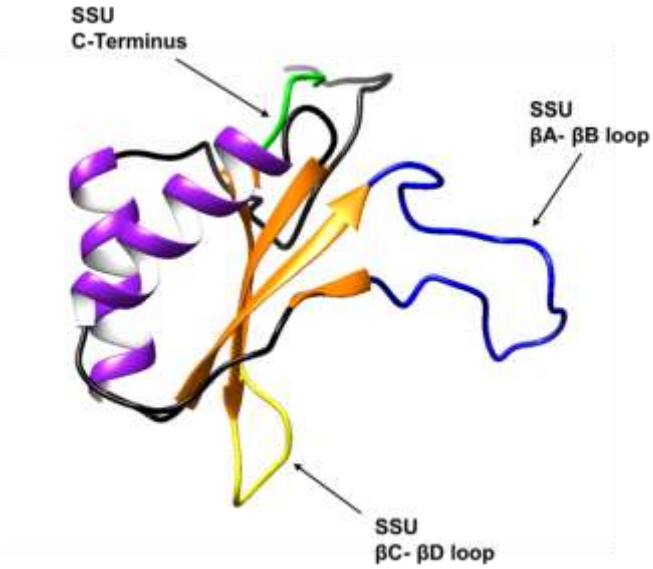

Figure 1.3. Structure of spinach Rubisco SSU. Four β-sheets (orange) are lined by two α-helices (purple). The CT is shown in green, βA-βB loop is blue and βC-βD is yellow. Crystal structure of Rubisco was obtained from Protein Data Bank (PDB) with the PBD code 1AUS.

SSU significantly affects the activity of Form I Rubisco enzyme (Morell *et al.*, 1997). A truncation study in cyanobacterium *Synechococcus* sp. PCC 6310 demonstrates the importance of the first 20 residues in the NT of SSU and their influence over Rubisco assembly and catalytic properties (Paul *et al.,* 1991). The deletion of the first 13 and 14 residues significantly decreased $k_{cat,c}$ to 2.7 s^{-1} and 5.2 s^{-1}, respectively, from 12.1 s^{-1} for WT. Deletion of the first 20 residues completely abolished the activity of the enzyme

In rice, a single native SSU isoform has been shown to have a significant impact on that catalytic characteristics of Rubisco (Morita *et al.,* 2014). Of the five *RbcS* genes

in the rice SSU family, *OsRbcS1* is more genetically distant from other four. Furthermore, *OsRbcS1* is expressed in the developing leaf sheath, culm, anther and root, but not in the photosynthetic leaf blade. Transgenic lines over expressing *OsRbcS1* in the leaf blade showed that *OsRbcS1* was able assemble into a functional Rubisco that exhibited an increased $k_{cat,c}$ (by up to 1.46-fold), a 3-fold higher K_c and a slight decrease in $S_{c/o}$ compared to WT plants. Expression of tobacco trichome-specific *RbcS-T* isoform in Chlamydomonas conferred higher $V_{c,max}$ and K_m values than the isoform expressed in leaves (Laterre *et al.,* 2017). The observed changes following expression of *RbcS-T* both in rice and Chlamydomonas demonstrated that the SSU can influence the catalytic properties of Rubisco.

RbcS genes are also differently expressed in different organs in plants as SSUs regulate the abundance of Rubisco in specific tissues and in some cases, might impart a different catalytic activity in special organs. For example, tomato (*Solanum lycopersicum* L.) has five *RbcS* genes (i.e. *RbcS1*, *RbcS2*, *RbcS3A*, *RbcS3B*, *RbcS3C*) that are expressed in leaves. However, only *RbcS1* and *RbcS2* are expressed in unripe fruits, although expression declines during fruit maturation (Wanner and Gruissem 1991). In maize (*Zea mays* L.), *ZmRbcS1* transcripts are relatively more abundant in the husks than the other four isoforms, while both *ZmRbcS1 and ZmRbcS2* accumulate to high levels in the bundle sheath cells (Ewing *et al.,* 1998). Recently, a phylogenetically distinct SSU isoform has been identified in several monocot and dicot species that contain glandular trichomes (Laterre *et al.,* 2017). In tobacco, the isoform was called *NtRbcS-T* and was found to be exclusively expressed in trichomes. It was postulated that SSU expression in specific

organs, such as *OsRbcS1* in rice and *NtRbcS-T* in tobacco, may play a specialised role in recycling of CO_2 generated by the metabolism in organs that are less permeable to gas exchange. In Arabidopsis leaves, 1A and 3B genes are uniformly expressed throughout the leaf while 2B is predominantly expressed on the base of the leaf and 1B on the abaxial side of the leaf (Sawchuk *et al.*, 2008). Since the upper side of the leaf is specialized in photosynthesis while the lower side is involved in gas exchange, Sawchuk *et al.*, (2008) suggested the differences in expression may contribute to an effect on the catalytic properties of Rubisco in these regions. However, this is unlikely as 1B differs by only 2 amino acid from 2B and 3B. Together with evidence of the role of SSUs in Rubisco catalysis, these studies suggest that the *RbcS* gene family may play an important function during organ development.

RbcS gene expression is also affected by temperature. When WT Arabidopsis (Col-0 ecotype) plants were grown under 14 h light/10 h dark with 100 µmol m^2 s^{-1} at three different temperatures, differential expression of *RbcS* genes was observed (Yoon *et al.*, 2001). At 10^{o}C and 20^{o}C, 1A contributed to the majority of the *RbcS* mRNA pool, and was especially dominant at 10^{o}C (*ca.* 68%). The expression of 3B was relatively low at 10^{o}C (*ca.* 15%) but increases to 40% at 30^{o}C. The combined expression of 1A and 3B were dominant at all three temperatures and always made up more than 70% of the total *RbcS* mRNA pool. At 10^{o}C the expression of 1B and 2B made up about 12% and 5%, respectively, while at 30^{o}C both 1B and 2B were 10% (Yoon *et al.*, 2001). 2B and 3B responded similarly to the change in temperature.

A large number of plant genes related to photosynthesis and photomorphogenesis are regulated by light (Petrillo *et al.,* 2014; Ido *et al.,* 2016). Members of the Arabidopsis *RbcS* family also respond differently to light conditions. The expression 1A, 2B, and 3B have been shown to be regulated by light of differing quality and quantity (Dedonder *et al.,* 1993). 1A expression was less sensitive to blue light compared to 3B but very receptive to white, red and, to a lesser extent, far red light. 1A was also found to be more strongly induced than 2B and 3B under higher fluence of white light (Ido *et al.,* 2016). In contrast, 1B essentially showed no response to light (Dedonder *et al.,* 1993). Thus, the expression of each *RbcS* gene in Arabidopsis responds differently to light of different quality and quantity.

CRISPR/Cas9 editing

The clustered regularly interspaced short palindromic repeats (CRISPR) and CRISPR associated protein (Cas9) system (CRISPR/Cas9) is a relatively new tool that can induce DNA mutation after a double strand break at specific locations in the genome (Cong *et al.,* 2013; Jiang *et al.,* 2013a). CRISPR/Cas9 is comprised of two major components: a guide RNA (gRNA) and the Cas9 endonuclease. The gRNA is a short sequence of nucleotide of 19-22 bp that complements a gene of interest. The gRNA recognises the gene of interest through a binding of the protospacer adjacent motif (PAM) sequence, which is NGG if using the Cas9 from *Streptococcus pyogenes* (SpCas9, the Cas protein still most commonly used) (Jiang and Doudna 2017). The binding of the gRNA-Cas9 complex to the PAM sequence initiates a double strand break (DSB) three bp

upstream of the PAM sequence. DSBs are repaired by either non-homologous end joining (NHEJ) or homology-directed repair (HDR) mechanisms. NHEJ repairs DSBs through an error-prone mechanism, which causes small deletions or insertions (**Figure 1.4**) (Li *et al.*, 2013; Knoll *et al.*, 2014). HDR integrates an exogenously supplied DNA template at the DSB site and can be utilised to induce gene insertion (Barrangou and Marraffini, 2014; Miki *et al.*, 2018; Wolter *et al.*, 2018). Due to the relative ease of use compared to other targeted DNA editing methods, such as zinc finger nucleases (ZFNs) and TAL effector nucleases (TALENs), the CRISPR/Cas9 system has been utilised widely in both animals and plants.

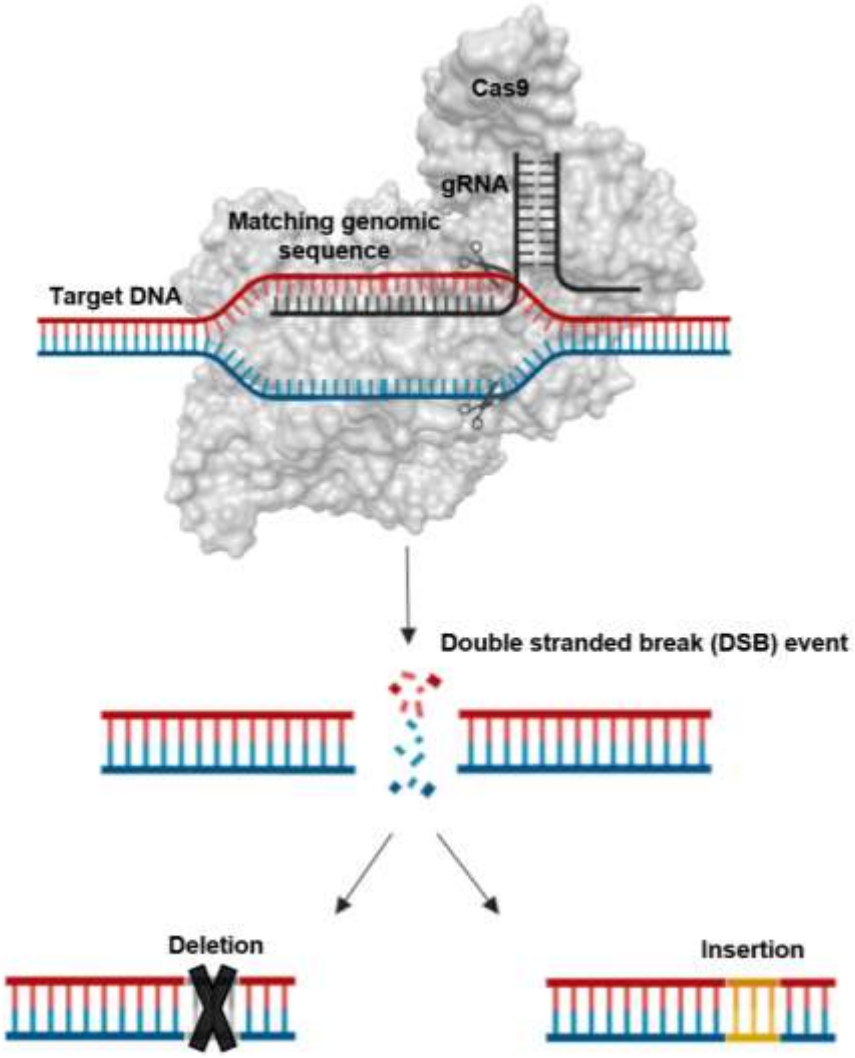

Figure 1.4: Mechanism of CRISPR/Cas9 editing. Cas9-gRNA complex unwinds the double helix, binds to the matching genomic sequence and Cas9 induces a double stranded break 3-bp upstream of the PAM sequence. The error-prone NHEJ repairs the break and often results in base-pair deletions and/or insertions (indels). Small indels lead to a frame-shift mutation which effectively knocks out the target gene.

The CRISPR/Cas9 system has been exploited to induce targeted mutagenesis in several plant species, including Arabidopsis, maize, barley and wild tomato (Xing *et al.,* 2014; Lawrenson *et al.,* 2015; Zsögön *et al.,* 2018; Ordon *et al.,* 2019). CRISPR/Cas9 is versatile as it enables simultaneous editing of multiple genes (multiplex editing). For example, three genes were simultaneously edited by two gRNAs in hexaploid wheat with an efficiency of ~5% and edited heterozygous progeny was recovered in the T2 generation (Howells *et al.,* 2018). Large genomic deletions of up to 100 kb can also be induced at a rate of 0.1% by using two gRNAs in Arabidopsis (Ordon *et al.,* 2017). The versatility of CRISPR/Cas9 system has now extended beyond gene editing as further engineering of Cas9 and/or discovering of new Cas orthologs has introduced novel functions to the CRISPR/Cas approach, including RNA editing by Cas13b, modulation of transcript levels by dCas9, and precise nucleotide base-pair editing and gene targeting (Tan *et al.,*; Wolter and Puchta, 2018; Wolter *et al.,* 2018; Papikian *et al.,* 2019)

CRISPR/Cas9 editing in Arabidopsis

Arabidopsis was one of the first plants that served as a platform for CRISPR/Cas9 editing (Feng *et al.,* 2013; Li *et al.,* 2013). studies in Arabidopsis protoplasts showed that CRISPR/Cas9 was able to induce mutations with high specificity (Jiang *et al.,* 2013b; Fauser *et al.,* 2014). Unlike other model species, such as tobacco and rice, initial applications of CRISPR/Cas9 in Arabidopsis was focused to protoplast studies as initial reports had shown low transformation efficiencies and heritability (Feng *et al.,* 2014; Mao *et al.,* 2016). Generating stable mutations in Arabidopsis required a localised expression

of Cas9 in germ-cells or during an early embryonic stage. However, the Cauliflower mosaic virus (CaMV35S) promoter was often used and has been shown to have low activity during such stages resulting in a low rate of heritable mutations *in planta* in the T1 generation (Hyun *et al.,* 2015; Wang *et al.,* 2015). Therefore, the majority of mutations induced by Cas9 driven by CaMV35S promoter was chimeric mutations in somatic cells (Feng *et al.,* 2014).

Localised expression of Cas9 to improve the heritability rate was achieved by using germ-line-specific promoters or constitutive promoters that display higher activity during embryogenesis. To date, 13 germ-line specific promoters have been reported and successfully applied to increase the rate of heritable mutations in the T1 generation in Arabidopsis (Hyun *et al.,* 2015; Wang *et al.,* 2015; Yan *et al.,* 2015; Eid *et al.,* 2016; Mao *et al.,* 2016; Osakabe *et al.,* 2016). One outstanding example of these promoters is the fused EC1.1/EC1.2 promoter that yielded a 17% rate of heritable mutation compared to 0% by CaMV35S in the T1 generation (Wang *et al.,* 2015). Since the activity of Cas9 is localised, using germ-line specific promoter reduces the requirement for multi-generational analyses and number of sample size needed for screening as chimeric mutation was less frequent.

The editing efficiency of CRISPR/Cas9 could be further enhanced by optimising the CRISPR/Cas9 construct and the architecture. Ordon *et al.,* (2019) tested combinations of promoter-terminator pairs and identified the *RPS5a* promoter and *RbcSE9* terminator as most effective to induce mutations. Cas9 driven by the promoter-terminator pair, combining with the paired gRNAs, was able to generate a 70 kb deletion at a 30% rate

(Ordon *et al.,* 2019). Editing efficiency can also be enhanced by optimising the T-DNA architecture, for example, by expression Cas9 and gRNA in a head-to-head divergent orientation to enhance the transcription of the gRNA (Castel *et al.*, 2019). This suggested that the CRISPR/Cas9 components in addition to their arrangement contribute to the editing activity.

Periodic heat stress of Arabidopsis also has been shown to increase the editing efficiency of SpCas9. LeBlanc *et al.,* (2018) subjected Arabidopsis to four heat stress treatments at 37^{o}C for 30 h before the transition to the reproductive stage and found that there was a higher level of Cas9 expression in germ-cells. Exposure to heat stress led to a 42% homozygous editing rate compared to 8% in the untreated plants (LeBlanc *et al.*, 2017). This study suggested that the optimal temperature for Cas9 activity is higher than the Arabidopsis standard growth temperature, since SpCas9 is derived from bacteria that typically grow at 37^{o}C. However, reproductive development of Arabidopsis is adversely affected at 37^{o}C and therefore it is important to limit the heat stress exposure to the vegetative stage (Warner and Erwin 2005).

Cas9 derived from different bacterial system have been successfully applied in Arabidopsis gene editing. Cas9 from *Streptococcus thermophiles* and *Staphylococcus aureus* have been reported to have similar editing efficiency as SpCas9 (Steinert *et al.*, 2015). Moreover, SaCas9 was shown to be more efficient for *in planta* gene targeting than SpCas9 (Wolter *et al.,* 2018). Other Cas orthologs, including Cas12a derived from *Acidaminococcus* sp. *BV3L6* and *Lachnospiraceae bacterium ND2006,* have also been used in Arabidopsis (Tang *et al.,* 2017). The main advantage of Cas12a over Cas9 is its

ability to process multiple gRNAs, which enables simpler CRISPR/Cas9 construct with a single promoter driving multiple gRNAs (Hu *et al.*, 2017; Wang *et al.*, 2017). Since these Cas orthologs require different PAM sequences, they offer different avenues to targeting regions that are limited by the requirements of SpCas9.

Aims of this study

This study aimed to elucidate the functions of *RbcS* gene family in Arabidopsis. To characterise the functions of *RbcS* genes, I have i) characterised the available *rbcs* T-DNA mutants and cleaned up second-site mutations in one of the mutant lines; ii) generated single and novel double and triple SSU KO mutants using CRISPR/Cas9 editing and performed molecular and physiological characterisations of new mutants against the T-DNA lines; iii) performed transcript analysis of *RbcS* genes under different environmental conditions including different light qualities, quantities and temperature, as well as growth experiments under different environmental conditions to study the effects on growth; iv) complemented a triple SSU KO mutant with a Chlamydomonas SSU to generate hybrid Rubisco and study the effects of heterologous SSUs on Arabidopsis.

Chapter 2 - Materials and methods

Chapter 3

Plant material and growth conditions

Arabidopsis (Arabidopsis thaliana (L.) Heyn. Col-0) seeds were sown on soil and stratified for 3d at 4ºC and grown at 21ºC, ambient CO_2, 70% relative humidity and 200 µmol photons m^{-2} s^{-1} in 12 h of light/dark cycle (standard conditions) unless otherwise specified. Arabidopsis T-DNA insertion lines *1a* (GABI_608F01), *1b* (SAIL_755_D09), *2b* (GABI_324A03), *3b* (SALK_117835) were used. Double mutant *1a2b* was generated in our laboratory by crossing T-DNA insertion lines GABI_608F01 and GABI_324A03, and was previously described (Atkinson *et al*., 2017). Crossing *1a2b* back to WT was performed to clean up background mutations and the "new 1a2b" was recovered in F2 generation. The *1a3b* mutant was generated by crossing GABI_608F01 with SALK_117835, and was provided by Hiroyuki Ishida, Department of Applied Plant Science, Tohoku University, Japan. The crossing between *1a* (GABI_608F01) and *1b* (SAIL_755_D09) was performed and F2 and F3 plants were screened to in an attempt to find homozygous *1a1b*.

DNA extraction

DNA was extracted from a mature leaf as described in Li and Chory (1998). Plants were screened using specific primers for each *RbcS* gene and T-DNA insertion.

Chlorophyll quantification

Leaf discs (*c.* 20 mm^2) were frozen in liquid nitrogen, powdered and then mixed with 1 mil of ice-cold 80% (v/v) acetone, 10 mM Tris-HCl. The extract was centrifuged at 17,200 g for 10 min and chlorophyll was quantified according to Porra *et al.* (1989).

Construction of RT-qPCR standard

A DNA fragment containing regions matching the target loci for the *RbcS* for RT-qPCR primers were synthesised with overhangs compatible with the Golden Gate Level 0 acceptor vector (pAGM9121) (Gblock, IDT) (**Supplemental Figure 3.1**). The synthesised DNA fragment was cloned into the acceptor vector as described in Engler *et al*. (2014). In the Golden Gate one pot digestion/ligation reaction, 100 ng of the synthesised DNA fragment and 100 ng of Level 0 acceptor vector were added to a reaction containing 10 units of BpiI (ThermoFisher) 2 µl of Buffer G (ThermoFisher), 400 units of T4 DNA ligase (ThermoFisher) and 2 µl of 10 mM ATP. The reaction was placed in a thermocycler and the "Golden Gate" program was applied: 3 cycles of [10 min at 37ºC, 10 min at 16ºC], 10 min 37ºC at and 20 min at 65ºC.

RT-qPCR analysis

Total RNA was isolated from leaves using the RNeasy plant mini kit (Qiagen, USA). Isolated RNA was treated with DNase (Qiagen, USA) and reverse transcribed with random primers (Promega, USA). Gene-specific primers amplifying the unique 3' region of the transcript were used for RT-qPCR (Izumi *et al*., 2012). Calibration curves were constructed with synthesized serially diluted standard plasmid (0.976–125 picograms) for

quantifications of each *RbcS* mRNA levels. For quantitative analysis, an aliquot of cDNA derived from 4 ng of RNA was used (total volume 10 µl) with SYBR Green Master Mix (Eurogentec, Belgium).

Chapter 4

Construction of CRISPR/Cas9 constructs

The vectors were assembled using the Golden Gate modular cloning method (Engler *et al*., 2014). To construct Level 1 Cas9 expression cassette, UBI10 promoter, SpCas9 coding sequence and heat shock protein (HSP) terminator were used. In the Golden Gate one pot digestion/ligation reaction, 100 ng of each part and Level 1 Position 2 acceptor plasmid (pICH47742) were added to the reaction containing 10 units of BsaI (ThermoFisher), 2 ul of Buffer G (ThermoFisher), and 400 units of T4 DNA ligase (ThermoFisher) and 2ul of 10 mM ATP. The reaction was placed in a thermocycler and the "Golden Gate" program was applied: 3 cycles of [10 minutes at 37^{o}C, 10 minutes at 16^{o}C], and 10 min at 37 ^{o}C and 20 min at 65 ^{o}C.

The gRNA expression cassettes were constructed by amplifying the synthesized gRNA flanked with BsaI restriction site with the U6 terminator. The amplicon was assembled with the U6 promoter in Level 1 positions 3 or 4 (pICH47751 or pICH47761) acceptor vectors using the Golden Gate protocol and BsaI enzyme (ThermoFisher). The Level 2 expression cassettes (pICSL4723) were assembled by combining Level 1 vector containing pFAST selectable marker (pICH11015), a Cas9 expression cassette, and two gRNA expression cassettes using BpiI enzyme and the Golden Gate protocol. All plasmids

were prepared using ThermoFisher GeneJet miniprep kit on *Escherichia coli* Top10 cells selected on antibiotic and X-gal.

Expression of Cas9 and gRNA and Chlamydomonas SSU in Arabidopsis

Binary vectors were transformed into *Agrobacterium tumefaciens* (AGL1) for stable insertion in Arabidopsis by floral dipping (Clough and Bent, 1998). For the CRISPR/Cas9 work, T1 plants were screened for the presence of a transgene by the FAST marker and for the presence of mutations by Sanger sequencing (Shimada *et al*. 2010). Stable mutations in transgene-free T2 plants were identified by Sanger sequencing. For the Chlamydomonas SSU work, BASTA was sprayed on 10-d-old plants on days 10, 12, 14 and 17. Plants that survived the selection were checked for the presence of the transgene insertion by PCR using primers specific to Chlamydomonas SSU.

SDS-PAGE

Arabidopsis leaf tissue (39.3 mm^2) collected from fully expanded seventh or eighth leaf of 35-d-old plants were snap frozen in liquid nitrogen. The tissues were extracted with the 5 times weight/volume of leaf tissue using the extraction buffer (100 mM Tris-HCl [pH 7.5], 10 mM DTT, 2 mM sodium iodoacetate, 5% [v/v] glycerol in H2O). Triton X-100 (10% [v/v]) was added to a final concentration of 0.1% (v/v) and the samples were vortexed for 30 s and centrifuged at 5,000 g for 5 min at 4ºC. The supernatant was transferred to a new tube where LDS and β-mercaptoethanol were added to a final

concentration of 1% (w/v) and 1% (v/v), respectively. Samples were then briefly vortexed, heated to 100ºC for 1 min, and used for SDS PAGE.

Prior to SDS PAGE, protein extracts (10 µl) were treated 0.6 µl of DTT (500 mM) and 5 µL Native Tris-Glycine Sample Buffer (2X), then heated to 85ºC for 2 min. Protein extracts (13 µL) were run on 12% (w/v) NuPAGE Bis-Tris polyacrylamide gels (Thermo Fisher Scientific) in Tricine SDS Running Buffer (Life Technologies) at 125 V. Gels were either stained with Coomassie Brilliant Blue R-250 Staining Solution (Bio-Rad) for 30 min, and destained with a destaining solution (10% glacial acetic acid, 40% MeOH, 50% H_2O [v/v]) or used to perform Western blot.

Western blot

Samples that were subjected to SDS-PAGE were transferred onto polyvinylidene fluoride (PVDF) membrane using the wet transfer method. The transfer was performed in Mini Trans-Blot Electrophoretic Transfer Cell (Bio-Rad) at 100 V for 1 h at 4ºC in ice-cold transfer buffer (25 mM Tris, pH 8.3, 192 mM glycine, 0.1% [w/v] SDS, 20% [v/v] methanol). Membranes were blocked in 5% (v/v) milk in TBST for 1 h then probed with rabbit-raised anti-Rubisco primary antibody at 1:10,000 dilution (Howe *et al*. 1982) followed by LI-COR IRDye 800CW goat anti-rabbit IgG also at a 1:10,000 dilution (Li-Cor Inc.). The membranes were imaged with LI-COR Odyssey CLx imager and processed with ImageStudioLite (Li-Cor Inc.).

Total soluble protein and Rubisco content analysis

Leaf samples of 59 mm^2 were collected, snap frozen and stored at -80 °C prior to extraction. The extraction buffer contained 50 mM Bicine-NaOH pH 8.2, 20 mM $MgCl_2$, 1 mM EDTA, 2 mM benzamidine, 5 mM ε-aminocaproic acid, 50 mM 2-mercaptoethanol, 10 mM dithiothriotol, 1% (v/v) protease inhibitor cocktail (Sigma-Aldrich, Mo, USA), and 1 mM phenylmethylsulphonyl fluoride. Samples were ground rapidly in an ice-cold mortar and pestle in 200 µL of extraction buffer for *ca*. 1 min followed by 1 min centrifugation at 4 °C, 14700 *g*. 90 µL of the supernatant was then mixed with 100 µL of CABP binding buffer which contained 100 mM Bicine-NaOH pH 8.2, 20 mM $MgCl_2$, 20 mM $NaHCO_3$, 1.2 mM (37 kBq/µmol) [^{14}C]CABP (carboxyarabintol-1,5-bisphosphate), incubated at RT for 25 min, and Rubisco content determined via [^{14}C]CABP binding (Sharwood *et al*., 2016). Bradford assay (Bradford, 1976) was used to determine total soluble protein in the same supernatant as prepared for Rubisco content analysis.

Measurements of photosynthetic parameters

Gas exchange was determined using a Li-Cor LI-6400 portable infra-red gas analyser with a 6400-40 leaf chamber. The measurements were performed on either fully expanded sixth or seventh leaf of non-flowering 37- to 47-d old rosettes of WT and mutants and 80-d-old nonflowering rosette for BigBoi. For all gas exchange measurements, leaf temperature was kept at 25^{o}C and chamber relative humidity was at *c.* 65%. The light response curve (0-1800 µmol photon m^{-2} s^{-1}) for net photosynthetic CO_2

assimilation (*A*) was generated at ambient CO_2 (400 µmol mol^{-1}). The response of *A* to varying sub-stomatal CO_2 concentration (C_i) was measured at 1800 µmol photon m^{-2} s^{-1}). Maximum rate of Rubisco carboxylation ($V_{c,max}$), maximum photosynthetic electron transport rate (J_{max}), respiration in the dark (R_d) were calculated using the A/C_i data fitted to the C3 photosynthesis model as in Ethier & Livingston (2004).

Chapter 5

Growth conditions under different environmental conditions

Arabidopsis (*Arabidopsis thaliana* (L.) Heyn. Col-0) seeds were sown on soil and stratified for 3d at 4ºC and grown under the high light (1,000 µmol m^{-2} s^{-1}, 21ºC), high temperature (200 µmol m^{-2} s^{-1}, 30ºC) and low temperature (200 µmol m^{-2} s^{-1}, 10ºC) conditions. The photoperiod was 12 h light/12 h dark. For the high light growth experiment, WT and all of the available TDNA and CRISPR/Cas9 *rbcs* mutants were used and grown in the Percival cabinet (AR-41L3). For the high temperature and low temperature growth experiments, WT and TDNA and CRISPR/Cas9 *1a, 3b, 2b3b, 1a2b, 1a3b* and BigBoi mutants were used and grown in the Percival cabinet (AR-36L3).

Growth conditions of circadian-dampened WT plants and prr5/7/9 mutant

Arabidopsis (*Arabidopsis thaliana* (L.) Heyn. Col-0) seeds were sown on soil and stratified for 3d at 4ºC and grown under the 200 µmol m^{-2} S^{-1}, 21ºC, 12 h light/12 h dark photoperiod for 7 d. The seedlings were transferred to a constant light photoperiod for 7 d (200 µmol m^{-2} s^{-1}, 21ºC, 25 h light). The *prr5/7/9* mutant seeds were sown on soil and

stratified for 3d at 4ºC and grown under the 200 µmol m^{-2} s^{-1} and constant light for 14 d. On day 15, both WT and *prr5/7/9* mutant seedlings were transferred to a dark cabinet and the trays were covered with aluminium foil. For the time course experiment, plants were exposed to white light at 200 µmol m^{-2} s^{-1} for 12 h and harvested at ZT -2, 4, 8, 14, and 16. For other environmental conditions, seedlings were exposed to different environmental condition including blue light (80 µmol m^{-2} s^{-1}), red light (µmol m^{-2} s^{-1}), far red light (50 µmol m^{-2} s^{-1}); white light at 1000, 200 and 50 µmol m^{-2} s^{-1} all of which the temperature was kept at 21ºC; 30ºC and 10ºC both of which the light level was kept at 200 µmol m^{-2} s^{-1} for 8h. Samples were collected in the dark for dark time points and snap frozen in liquid N_2. Three biological replicates were presented for each data point and each biological replicate consisted of 25-30 seedlings.

Chapter 6

Construction of Chlamydomonas RbcS2 for BigBoi complementation plasmid

The vectors were assembled using the Golden Gate modular cloning method (Engler *et al*., 2014). To construct Level 1 *RbcS2* expression cassette, either 1A promoter or 1B promoter, RbcS2 coding sequence and heat shock protein (HSP) terminator were used. In the Golden Gate one pot digestion/ligation reaction, 100 ng of each part and Level 1 Position 2 acceptor plasmid (pICH47742) (for 1A promoter) or Level 1 positions 3 (pICH47751) (for 1B promoter) were added to the reaction containing 10 units of BsaI (ThermoFisher), 2 ul of Buffer G (ThermoFisher), and 400 units of T4 DNA ligase (ThermoFisher) and 2ul of 10 mM ATP. The reaction was placed in a thermocycler and

the “Golden Gate” program was applied: 3 cycles of [10 minutes at 37^{o}C, 10 minutes at 16^{o}C], and 10 min at 37 ^{o}C and 20 min at 65 ^{o}C.

The Level 2 expression cassettes (pICSL4723) were assembled by combining Level 1 vector containing BASTA selectable marker (pICH11017) and both L1 cassettes of *RbcS2* driven by 1A or 1B promoters using BpiI enzyme and the Golden Gate protocol. All plasmids were prepared using ThermoFisher GeneJet miniprep kit on *Escherichia coli* Top10 cells selected on antibiotic and X-gal.

Chapter 3 - Characterisation of *rbcs* T-DNA insertion mutants and their effects on growth

Introduction

Arabidopsis transfer-DNA (T-DNA) insertion mutants have been key to understanding gene functions. The process involves random insertion of T-DNA through transformation mediated by *Agrobacterium tumefaciens* after which the T-DNA is mapped to identify a gene (or genes if more than one insertions occurred) that has been disrupted (Qu and Qin, 2014). The availability of large libraries of gene knockout mutants in addition to complete genome sequences of Arabidopsis have fuelled opportunities to pursue reverse genetics in an exhaustive manner (Krysan *et al.*, 1999; Alonso *et al.*, 2003).

We initially screened for on T-DNA express database (http://signal.salk.edu/cgi-bin/tdnaexpress) to identify T-DNA insertion lines for each of the *RbcS* gene. Based on the availability of homozygous and exon or near-exon insertions, two alleles were selected for 1A (GABI_083C04 and GABI_608F01) and one allele for 1B (SAIL_755D09), 2B (GABI_324A03) and 3B (SALK_117835) (**Figure 3.1**). While the insertion sites for 1A and 2B are located in exons, the insertion site for 1B and 3B is in the 5'UTR. Previous work has shown that the expression levels of 3B in SALK_117835 is reduced to *ca.* 5% of WT (Izumi *et al.*, 2012; Atkinson *et al.*, 2017). In addition to single mutants, previous studies have generated double mutants *1a2b* and *1a3b* by crossing the single T-DNA insertion lines (Izumi *et al.*, 2012; Atkinson *et al.*, 2017).

This chapter outlines a characterisation of the *rbcs* T-DNA insertion lines by PCR for homozygous insertions and examination of the absolute abundance of each *RbcS* transcript in each mutant line by RT-qPCR. The growth of these mutants was also characterised to assess their impact on growth. In addition, crossing between the *1a* and *1b* T-DNA insertion lines was attempted and challenges to generate the *1a1b* double mutant were described.

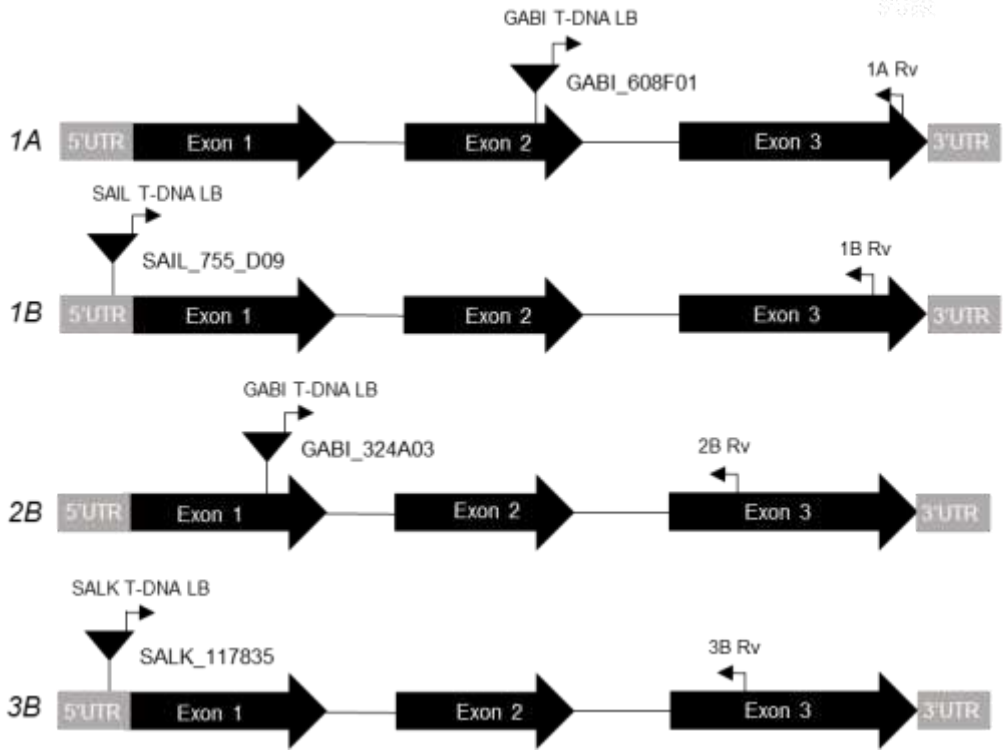

Figure 3.1. Diagram representing single and homozygous T-DNA insertion sites for the four *RbcS* genes available from the SALK library. For this study, *1a* (GABI_608F01), *1b* (SAIL_755_D09), *2b* (GABI_324A03), *3b* (SALK_117835) were used. Specific primers (indicated by arrows) were used to amplify each *RbcS* gene and T-DNA insertion (**Supplemental Table 3.1**).

Results

Characterisation of the T-DNA insertion mutants by PCR

Initial characterisation of *rbcs* T-DNA insertion lines was performed using PCR to confirm the zygosity and sites of T-DNA inserts in the *RbcS* genes. Primers specific to each of the *RbcS* gene were used to amplify the WT band. The forward left border (LB) primer specific to the T-DNA insertion and the specific *RbcS* reverse primer were used to amplify the insertion (**Figure 3.1 and Supplemental table 3.1**). PCR images of WT and T-DNA insertion for each gene are shown in **Figure 3.2**.

The PCR results showed that the primers used were specific to the *RbcS* genes. In addition, the absence of the WT band in the T-DNA insertion lines suggested that the insertion was homozygous for all *rbcs* T-DNA insertion lines. This confirms that the T-DNA insertion was homozygous and in the *RbcS* genes. RT-qPCR was performed to confirm the reduction in transcript levels of *RbcS* genes.

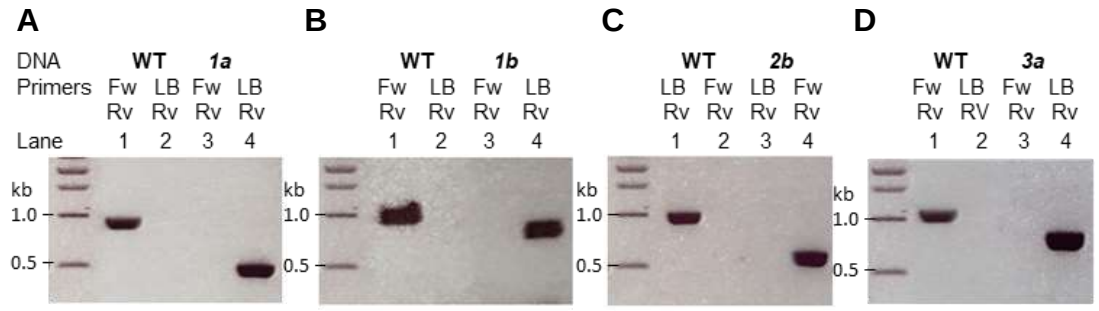

Figure 3.2. PCR confirmation of T-DNA insertion in the four *RbcS* genes. Amplicons of A) *1a* T-DNA insertion line (GABI_608F01), B) *1b* T-DNA insertion line (SAIL_755_D09), C) *2b* T-DNA insertion line (GABI_324A03), D) *3b* T-DNA insertion line (SALK_117835) are shown in comparison to WT control. The first two lanes are DNA extract of WT control and the last two are that of T-DNA insertion line. Specific forward (Fw) and reverse (Rv) primers were used to amplify the WT band (lanes 1 and 3), and the T-DNA insertion left border (LB) primer and reverse primer specific to each *RbcS* gene were used to amplify the T-DNA insertion band (lane 2 and 4) (**Supplemental table 3.1**).

Transcript expression of RbcS genes in rbcs mutants

Two set of primers were sourced for RT-qPCR analysis of *RbcS* gene expression. The first primer set ("Iz" hereafter) was sourced from Izumi *et al.*, (2012) and the second set from Cavanagh (2016) ("Ca" hereafter) (**Supplemental table 3.2**). Both sets target the 3'UTR regions of each *RbcS* gene as designing RT-qPCR primers that target exon-exon junctions was not possible due to high sequence homology among the *RbcS* genes. The

difference between the two sets of primer is both forward (Fw) and reverse (Rv) primers of the Iz set bind to specific region within each *RbcS* 5'UTR. The Ca primer set utilises a common Fw primer that binds to a homologous region in exon 3 of all four *RbcS* genes and Rv primers that bind to unique sequences of individual *RbcS* 5'UTR. These two sets of primers were tested on cDNA reverse-transcribed from total RNA pool from an Arabidopsis leaf to ensure their specificity to the target (**Figure 3.3A, B**).

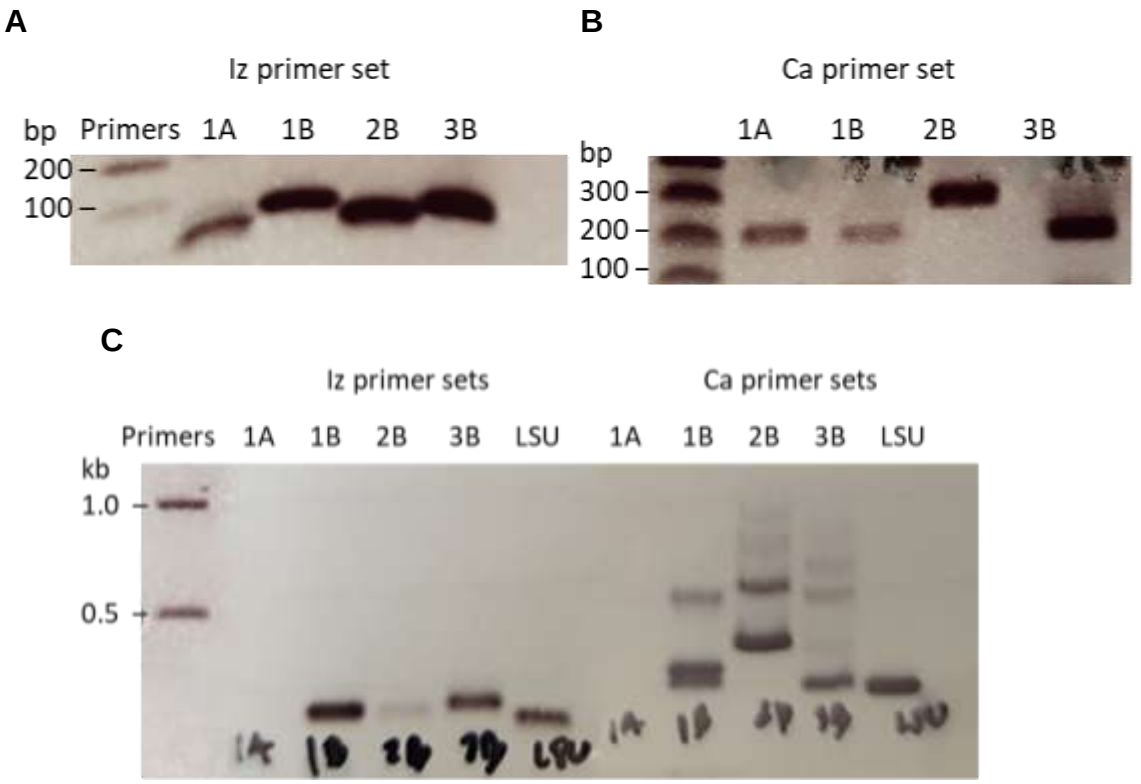

Figure 3.3. Comparison of the Iz and Ca RT-qPCR primer sets for specificity to the *RbcS* cDNA and the standard plasmid. A) PCR amplicons (69 bp, 83 bp, 80 bp, 99 bp for *1A*, *1B*, *2B* and *3B* respectively) of the Iz primer sets using cDNA as template. B) PCR amplicons (217 bp, 205 bp, 329 bp, 196 bp for *1A*, *1B*, *2B* and *3B* respectively) of Ca

primer sets using cDNA as template. C) PCR amplicons of the two primer sets using the internal standard plasmid as template (**Supplemental Figure 3.1**).

PCR results of the two primer sets showed that all primers were specific to their respective *RbcS* when using cDNA as template (**Figure 3.3A, B**). The lower intensity of the 1A and 1B bands in the Ca primer set was possibly due to lower primer efficiencies. To determine the absolute abundances of individual *RbcS* and *RbcL* transcripts, a plasmid containing sequences of the *RbcS* and *RbcL* genes matching the target loci for both sets of RT-qPCR primers was constructed and used as an internal standard (hereafter called the "standard plasmid" (**Figure 3.4**). PCR amplification of the standard plasmid using both sets of primers were performed again to ensure specificity to the cloned fragments (**Figure 3.3C**). The PCR results showed that the 1A fragment was not cloned properly as 1A bands were not present for both Iz and Ca primers. Sequencing of the plasmid revealed that two fragments that in the regions of both Fw primers were missing. In addition, multiple bands were present in 1B, 2B and 3B for Ca primers. The presence of these bands was due to the use of the Fw primer that targets homologous sequence in the *RbcS* genes. Multiple bands that appeared on the PCR resulted from the Fw primer that was bound to different Fw sequences on the plasmid and the specific Rv primer for each gene. For example, the expected amplicon size for 2B at 329 bp (the lower band) was the correct size for the 2B primer pair. The non-specific 550 bp band for 2B was likely the product of the primers binding to the common forward sequence in the 1B fragment and the specific 2B sequence in the 2B fragment. Due to the latter specificity issue, the Ca primers were deemed

unsuitable for absolute quantification with the standard plasmid and the Iz primers were used for the remainder of this study. A plasmid containing RT-qPCR amplicons of each *RbcS* and *RbcL* genes were synthesised because of the difficulty in construction by cloning (**Supplementary Figure 3.1**). The Iz primer pairs were used to amplify the standard plasmids and the band sizes similar to those in **Figure 3.3A** were produced. The synthesised standard plasmid is used for the remainder of this study.

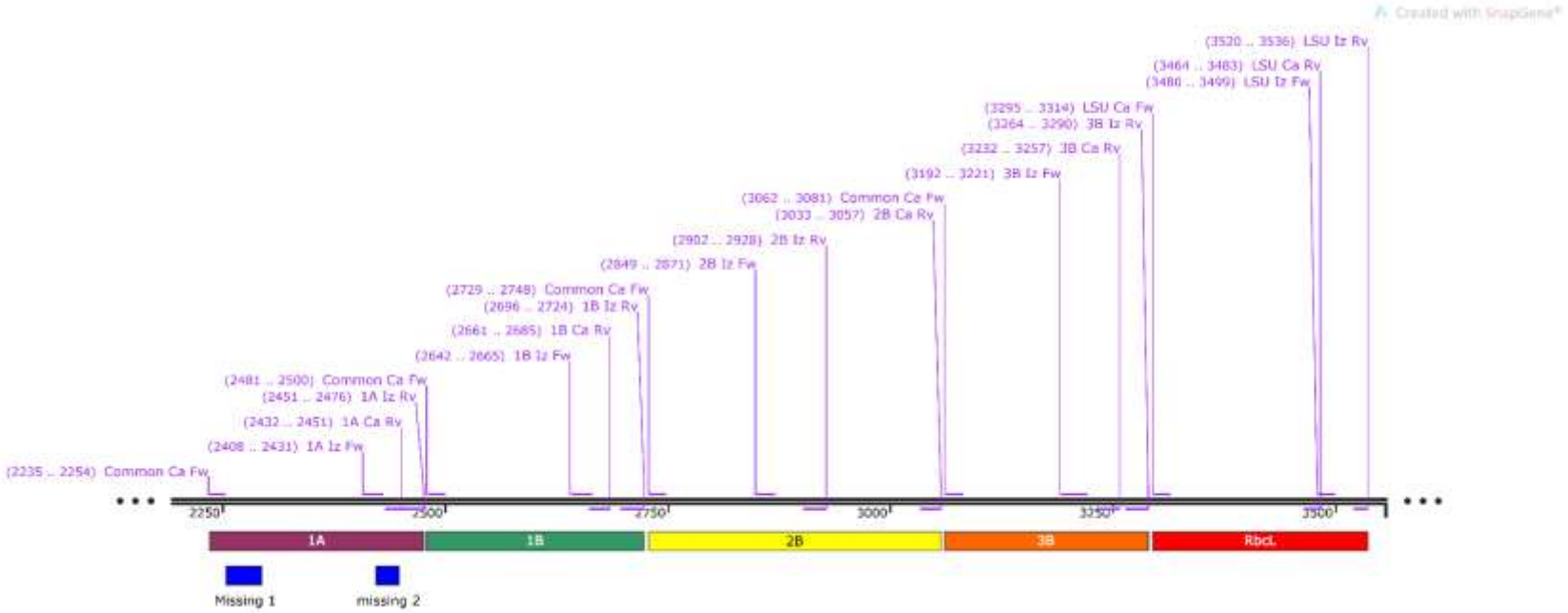

Figure 3.4. Standard plasmid containing target fragments for Iz and Ca primer sets. The Fw and Rv primers for both sets of primers are labelled on the map. The two blue regions denoted “missing 1” and “missing 2” are the sequences that were not clone properly into the plasmid.

To construct a standard curve for quantification of the expression of the *RbcS* and *RbcL* genes, the standard plasmid was serially diluted and amplified to match Ct values with the concentration of each amplicon (**Figure 3.5 A-E**). The melting curve showed a single peak for each of the RT-qPCR amplicon, indicating that the primer pairs were specific to their respective *RbcS* gene targets on the standard plasmid (**Figure 3.5F**). The most efficiency primer pair was that of the *RbcL* (94.8%) followed by 2B (94.1%), 1B (89.3%, 1A (87.6%) and 3B (81.6%).

A

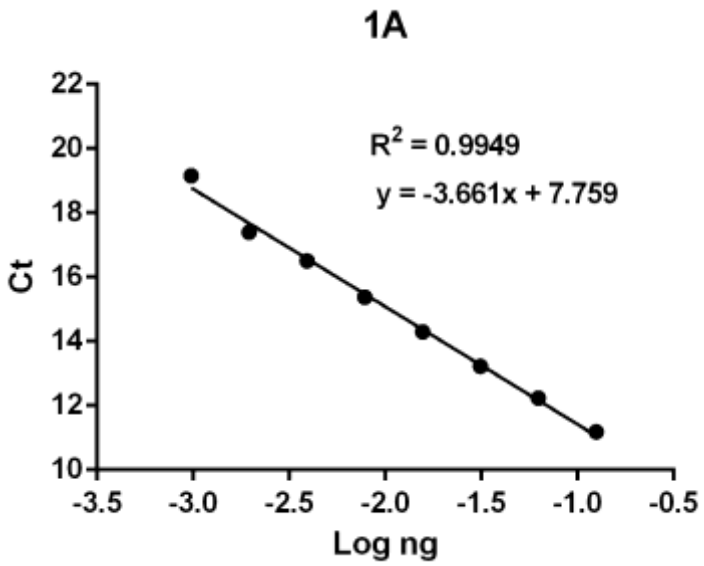
1A
R^2 = 0.9949
y = -3.661x + 7.759
Ct
Log ng
22
20
18
16
14
12
10
-3.5
-3.0
-2.5
-2.0
-1.5
-1.0
-0.5

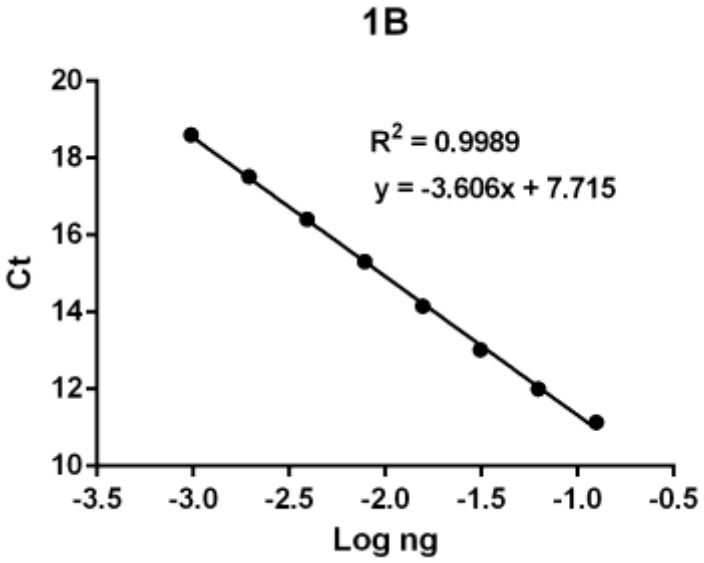
1B
R^2 = 0.9989
y = -3.606x + 7.715
Ct
Log ng
20
18
16
14
12
10
-3.5
-3.0
-2.5
-2.0
-1.5
-1.0
-0.5

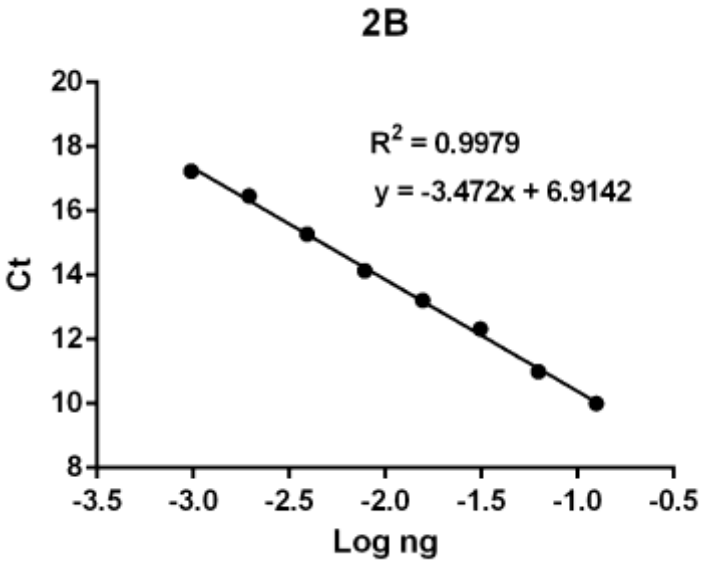
2B
20
18
16
14
12
10
8
Ct
R2 = 0.9979
y = -3.472x + 6.9142
-3.5
-3.0
-2.5
-2.0
-1.5
-1.0
-0.5
Log ng

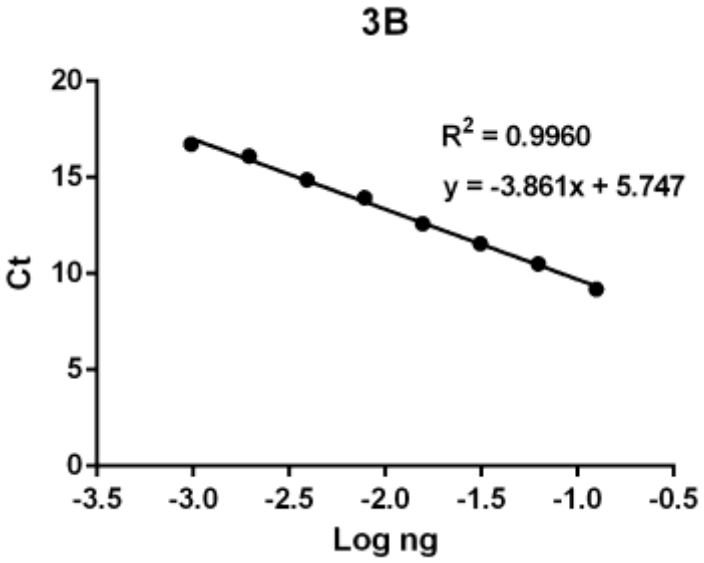
3B
20
15
10
5
0
Ct
R2 = 0.9960
y = -3.861x + 5.747
-3.5
-3.0
-2.5
-2.0
-1.5
-1.0
-0.5
Log ng

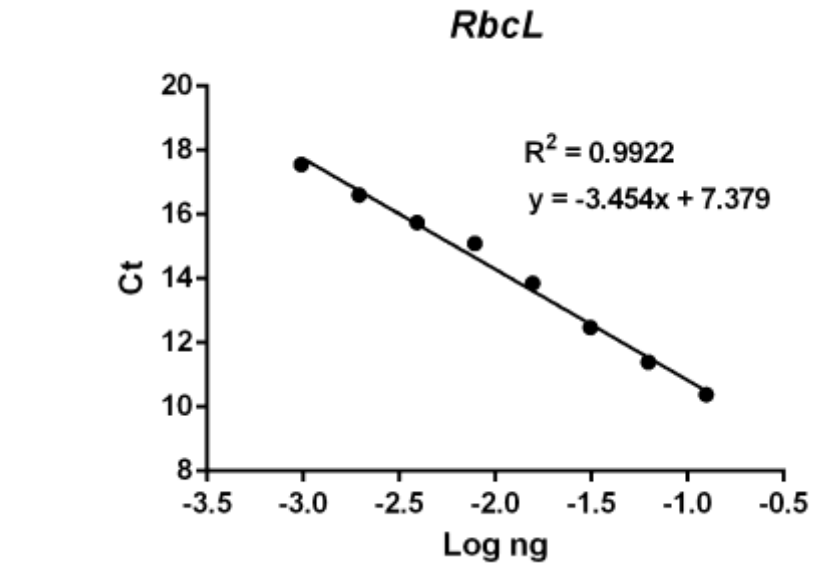

F

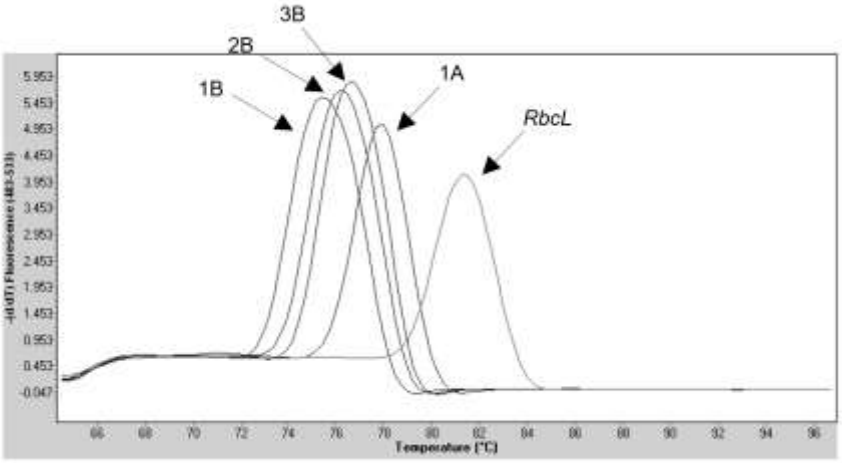

Figure 3.5. Construction of standard curves for absolute quantification of *RbcS* and *RbcL* gene expression using Iz primers and the standard plasmid. A) The linear regression equation and R^2 value is show for A) 1A, 1B, 2B, 3B and *RbcL*. The synthesised standard plasmid was serially diluted to the concentrations ranging from 0.976–125 picograms (presented as log ng). F) Representative melt curves of *RbcS* and *RbcL* amplicons performed after 35 cycles of RT-qPCR. Ct is cycle threshold.

The transcript abundances of *RbcS* and *RbcL* genes was initially determined from 20 days after germination (DAG) WT plants grown under standard growth conditions (200 µmol photons m^{-2} s^{-1} white light, 22ºC, 12 hr light : 12 hr dark cycle). Consistent with previous studies (Izumi *et al.*, 2012; Atkinson *et al.*, 2017), the major isoform 1A accounted for 54.0 pmol/g total mRNA (57.2 ± 4.4% of the total *RbcS* transcript pool), followed by 3B (34.8 pmol/g total mRNA, 36.8 ± 3.3%), 2B (3.5 pmol/g total mRNA, 3.7 ± 0.70%) and 1B (2.1 pmol/g total mRNA, 2.3 ± 0.4%) (**Figure 3.6A**). The three *rbcs* T-DNA insertion mutants for 1A, 1B and 2B showed a reduction in transcript abundance below detectable levels, consistent with a knockout of the relevant transcript. As expected, the T-DNA insertion mutants for 3B was reduced but still detectable (*ca*. 3% of WT levels). A reduction of an individual *RbcS* transcript did not lead to a change of other transcripts. A reduction in *RbcL* transcript was observed for each mutant line, but the reduction was smaller relative to the observed *RbcS* transcript decrease (**Figure 3.6B**).

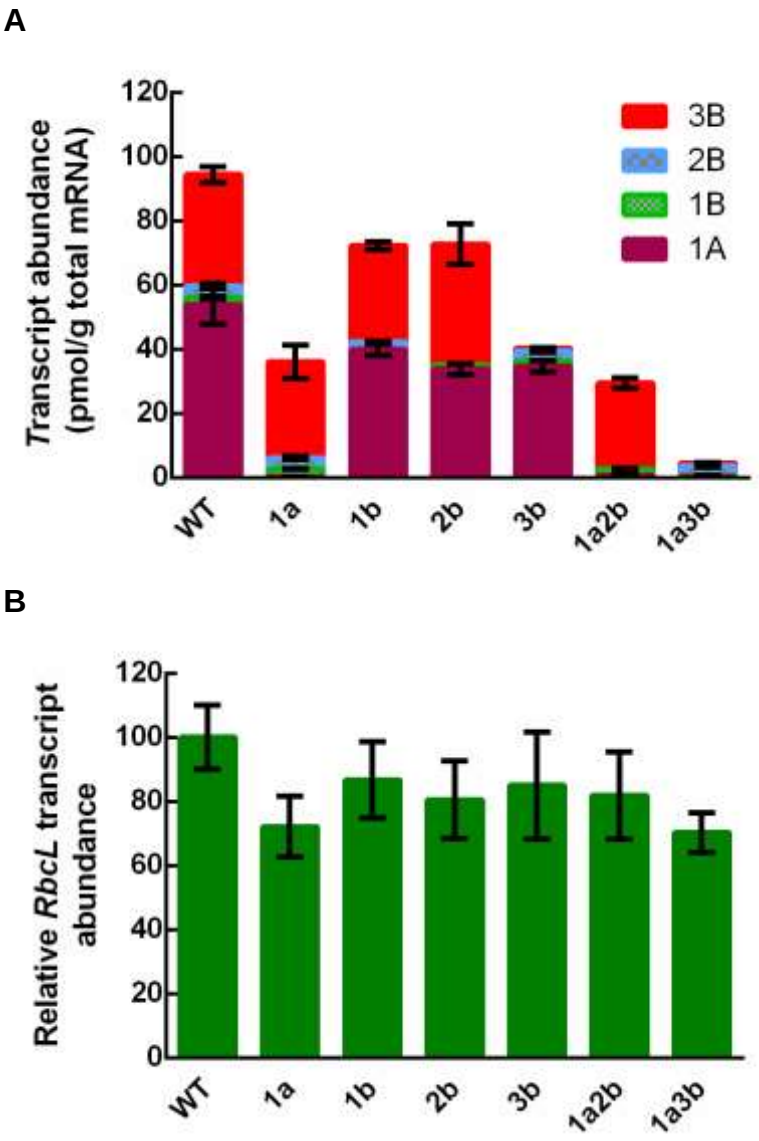

Figure 3.6. Transcript measurements of WT and *rbcs* T-DNA insertion lines. A) *RbcS* transcript abundance and B) Relative *RbcL* transcript abundance. Quantification was performed and transcript abundance was calculated using the standard curves obtained from the plasmid (**Figure 3.5A**). The values are means ± SE of measurements made on three individual 20 DAG rosettes.

Growth analysis of T-DNA insertion mutants under standard conditions

The growth analysis under standard conditions was performed to monitor the effect of *RbcS* gene knockout (or knockdown for *3b*) on growth. WT plants and *rbcs* T-DNA insertion mutants were grown and imaged daily for 32 days. The results showed that the disruption of a single *RbcS* gene did not significantly affect growth. However, significantly slower growth rate was observed in double mutants *1a2b* and *1b3b* where the *RbcS* content was reduced to 30% and 6% of WT, respectively (**Figure 3.7A, B)**. As a result of decreased growth rate, the double mutants also had significantly lower weight and higher specific leaf area (SLA) (**Figure 3.8A, B**). The chlorophyll content and maximum quantum efficiency of PSII (F_v/F_m) of the *1a2b* mutant were not significantly different from WT and single mutants. However, the *1a3b* mutant exhibited a pale leaf phenotype, had significantly less chlorophyll per area and a lower F_v/F_m value (**Figure 3.8C, D**).

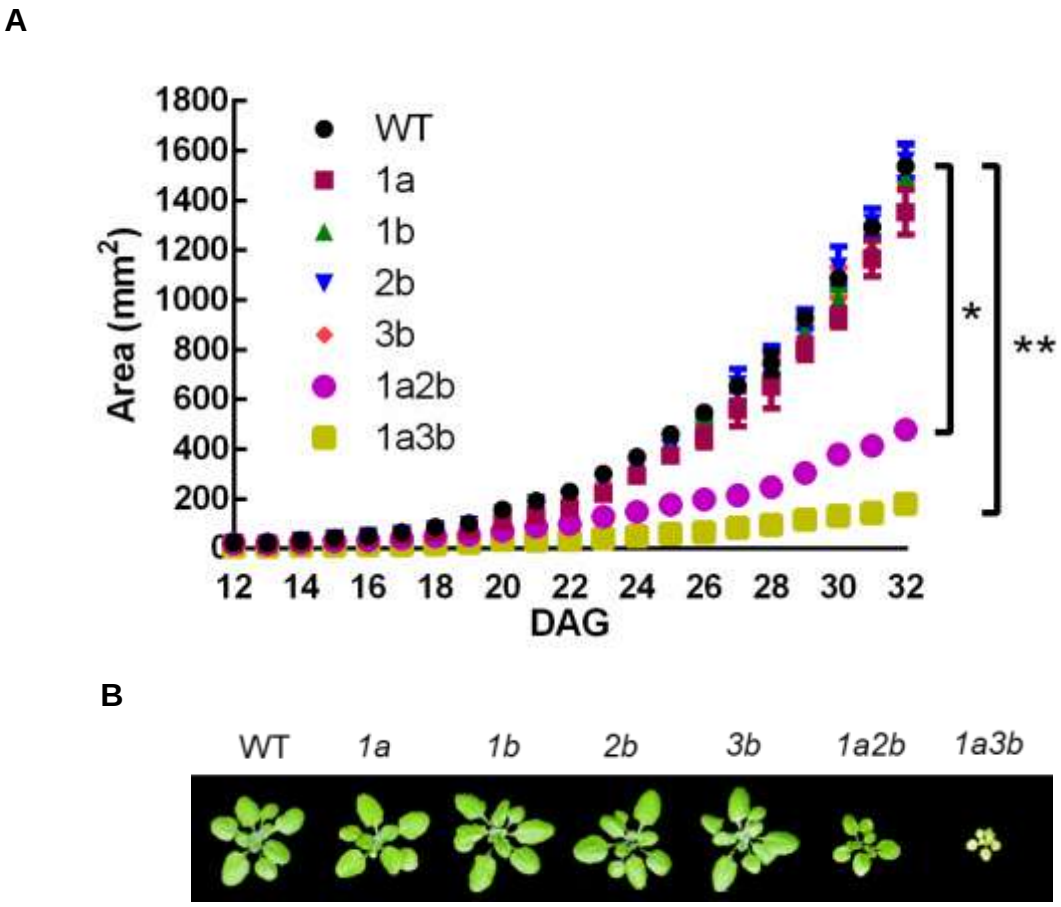

Figure 3.7. Growth analysis of *rbcs* T-DNA insertion mutants. A) Rosette expansion of T-DNA single and double mutants in comparison to WT monitored from 12-32 days after germination (DAG). The values are means ± SE of measurements made on 8-15 individual rosettes. One (*) and two (**) asterisks denote significant difference between groups. Significant difference ($P < 0.05$) was determined by ANOVA followed by Tukey's HSD tests. B) Representative images of 25-d-old rosettes of WT and *rbcs* T-DNA insertion mutants.

A

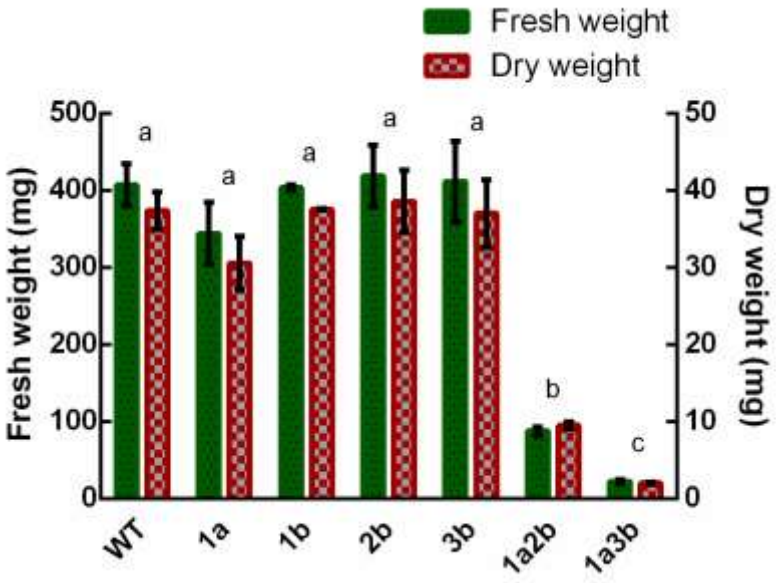
Fresh weight
Dry weight
Fresh weight (mg)
Dry weight (mg)
500
400
300
200
100
0
50
40
30
20
10
0
a
a
a
a
a
b
c
WT
1a
1b
2b
3b
1a2b
1a3b

B

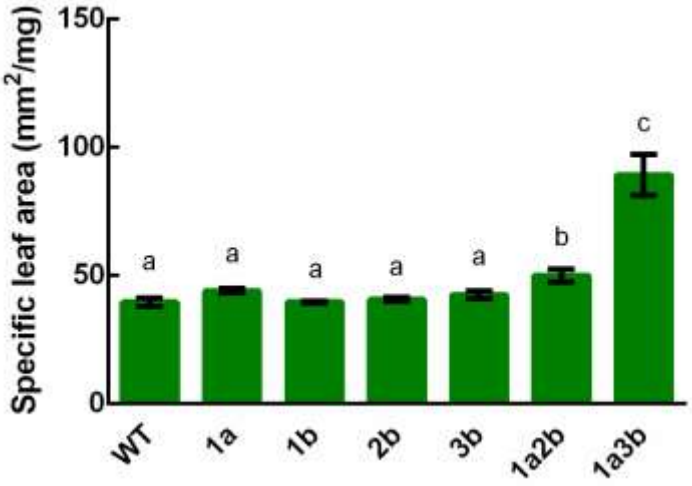
Specific leaf area (mm²/mg)
150
100
50
0
a
a
a
a
a
b
c
WT
1a
1b
2b
3b
1a2b
1a3b

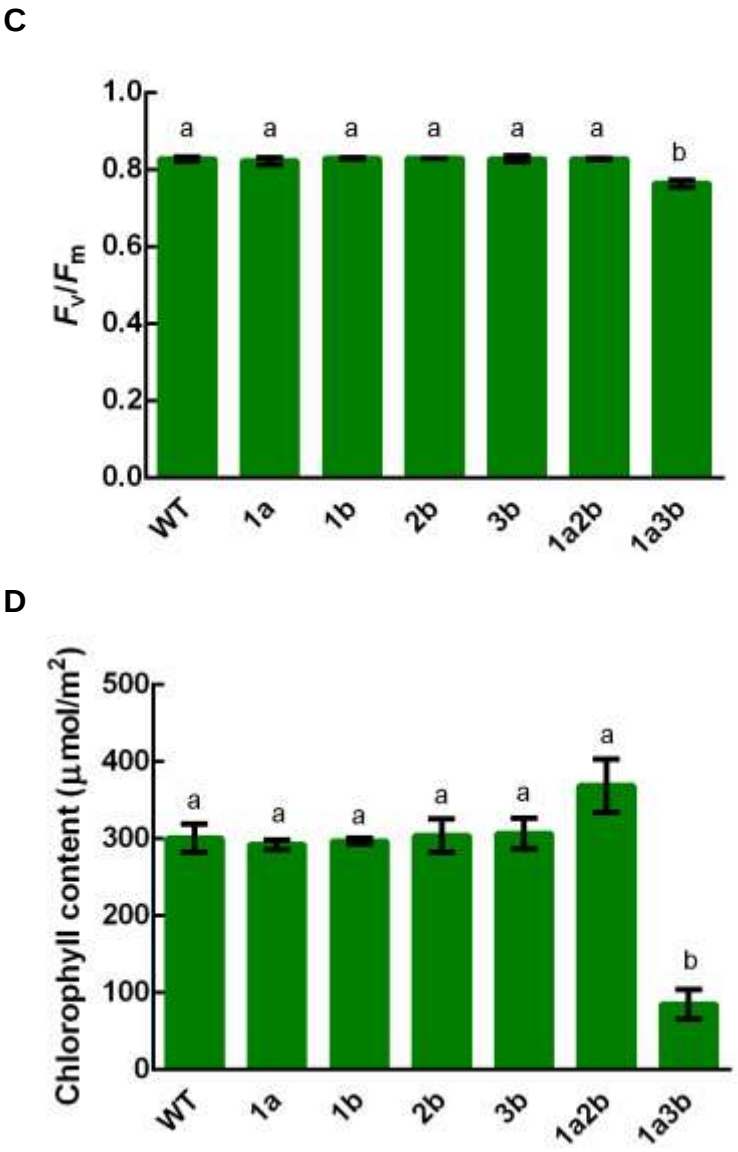

Figure 3.8. Phenotype of *rbcs* T-DNA insertion mutant plants. A) Fresh and dry weight, B) specific leaf area, C) maximum potential quantum efficiency of PSII (F_v/F_m) and D) chlorophyll content per area. The values represent mean ± SEM of measurements made on 8-15 samples for fresh weight, dry weight and specific leaf area and four samples for chlorophyll content and F_v/F_m. Different letters above the bars indicate significant difference ($P < 0.05$) as determined by ANOVA followed by Tukey's HSD tests.

Second site mutation in 1a2b mutant caused the silique phenotype

Based on the growth measurements and observation during reproduction, the double mutant *1a2b* exhibited unique phenotypes including shorter silique length and lower seed yield (**Figure 3.9A, B**). Further investigation was conducted to measure other phenotypes during different developmental stages (**Table 3.1**). Phenotypes that were significantly different include days until bolting and days until first flower open, which were five days later than WT in both *1a2b* and *1a3b*. These phenotypes were likely attributed to lower Rubisco content and therefore more time was required to accumulate biomass to enter the reproductive stage. However, silique size and seed yield issues were more severe in *1a2b* than *1a3b* despite having more biomass (**Figure 3.8A**). The fresh silique length of *1a2b* (10.7 ± 0.3 mm) was shorter than that of WT (18.0 ± 0.1 mm) and *1a3b* (16.9 ± 0.1 mm) and seed count per silique of *1a2b* (9.9 ± 1.3) was significantly lower than *1a3b* (26.6 ± 0.8) or WT (29.8 ± 0.4). Two hypotheses were proposed from this observation: i) 1A and 2B genes in conjunction play a role in silique and seed development and knocking out these genes caused detrimental effects on the reproductive ability; or ii) the observed phenotype was caused by second-site mutations that were not reported. To ensure that the phenotype was not linked to second-site mutations, the *1a2b* mutant was backcrossed to WT and the "new *1a2b*" was selected in the F2 generation (note that the new *1a2b* was used for transcript measurement in the previous section). The growth analysis was performed to characterise the new *1a2b* in comparison to two lines of WT segregant and the original *1a2b* (**Figure 3.10**).

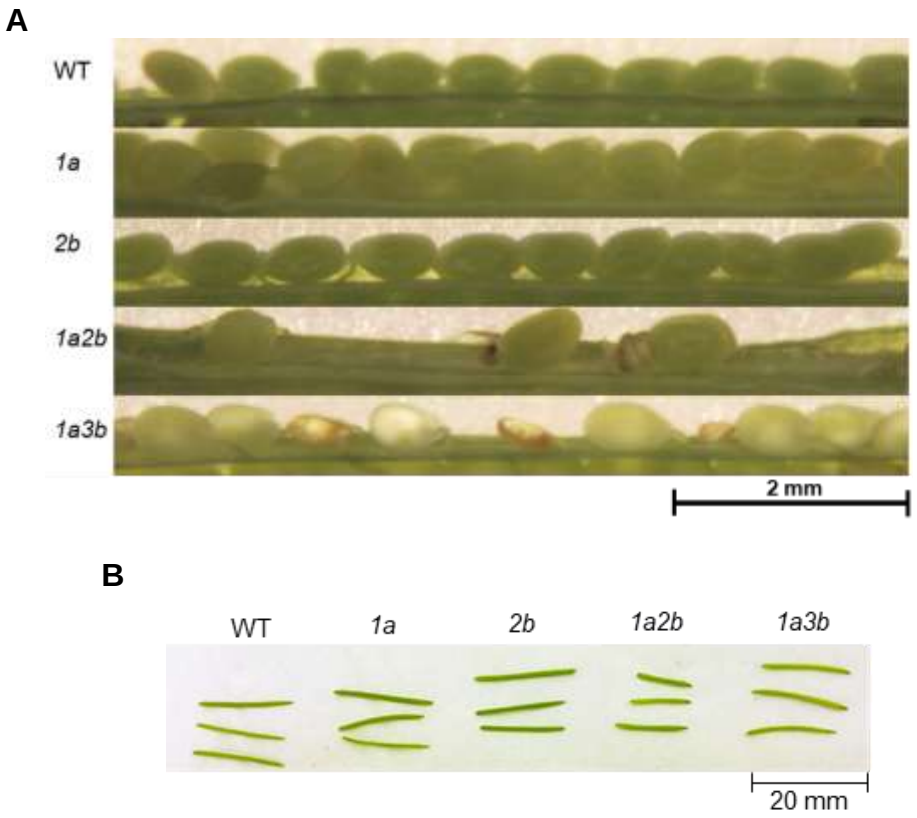

Figure 3.9. Representative images of Arabidopsis seeds and siliques in fully grown green siliques of WT and *rbcs* mutants. A) Seed count of WT, *1a*, *2b*, *1a2b* and *1a3b* T-DNA insertion mutants under 10x magnification. B) Representative images of siliques of WT, *1a*, *2b*, *1a2b* and *1a3b* T-DNA insertion mutants.

Table 3.1. Measurements performed during phenotypic analysis of Arabidopsis WT and *1a*, *2b*, *1a2b* and *1a3b* mutants to investigate the short silique and low seed yield phenotypes of *1a2b*. The numbers represent mean ± SEM of 15 plants. For distance across face of open flowers and fresh silique length, five flowers and siliques were measured per plants. For seed count per silique, seeds of 15 siliques were counted from five randomly chosen plants. Different letters indicate significant difference ($P < 0.05$) as determined by ANOVA followed by Tukey's HSD tests.

Phenotypes/Genotypes	WT	*1a*	*2b*	*1a2b*	*1a3b*
Days until bolting	30.3 ± 0.1 [a]	31.0 ± 0.1 [a]	30.8 ± 0.2 [a]	35.6 ± 1.0 [b]	34.9 ± 0.8 [b]
Days until first flower open	33.5 ± 0.3 [a]	34.7 ± 0.4 [a]	34.4 ± 0.3 [a]	39.5 ± 0.3 [b]	38.8 ± 0.3 [b]
Leaf number at bolting time	10 ± 0.3 [a]	10.4 ± 0.3 [a]	10.3 ± 0.2 [a]	10.7 ± 0.3 [a]	10.6 ± 0.3 [a]
Number of stem branches on main bolt	3.0 ± 0.7 [a]	2.7 ± 0.6 [a]	2.5 ± 0.5 [a]	2.9 ± 0.5 [a]	2.8 ± 0.7 [a]
Number of side bolts	5.3 ± 0.2 [a]	5.2 ± 0.2 [a]	4.9 ± 0.1 [a]	5.9 ± 0.1 [a]	6.1 ± 0.2 [a]
Distance across face of open flower (mm)	3.5 ± 0.3 [a]	3.5 ± 0.4 [a]	3.2 ± 0.2 [a]	3.6 ± 0.3 [a]	3.1 ± 0.2 [a]
Fresh silique length (mm)	18.0 ± 0.1 [a]	17.5 ± 0.1 [a,b]	17.8 ± 0.1 [a]	10.7 ± 0.3 [c]	16.9 ± 0.1 [b]
Seed count per silique	29.8 ± 0.4 [b]	33.0 ± 0.7 [a]	33.2 ± 1.0 [a]	9.9 ± 1.3 [c]	26.6 ± 0.8 [b]
Seed length (mm)	0.51 ±0.01 [a]	0.50 ±0.01 [a]	0.50±0.01 [a]	0.51 ±0.01 [a]	0.50 ±0.01 [a]

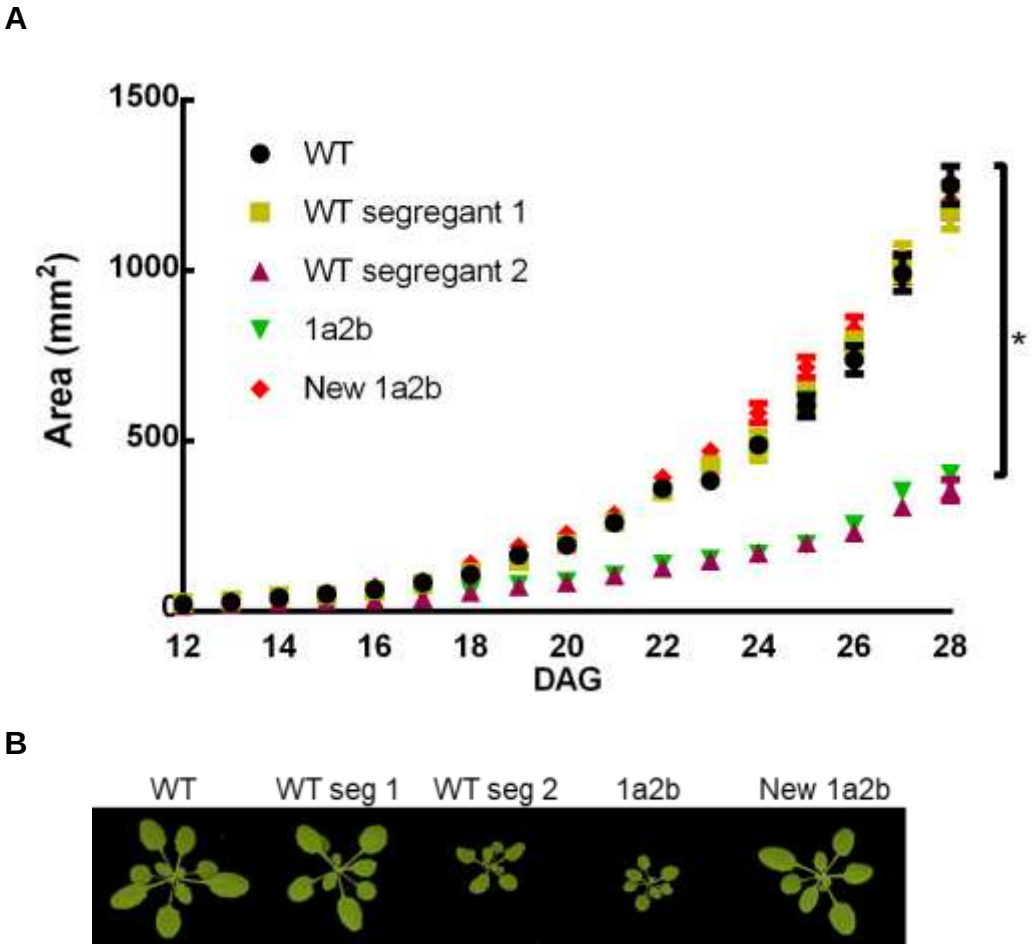

Figure 3.10. Growth analysis of T3 generation of new *1a2b* mutant and a WT segregant with the small-rosette phenotype. A line of WT segregant and original *1a2b* were used as controls (300 µmol photon m^{-2} s^{-1}, 12 h light : 12 h dark cycle, 21°C)). A) Rosette expansion of WT, mutants and segregants over a 28-day period. Each value represents means ± SE of measurements made on 8-12 rosettes. Asterisk (*) denotes significant difference between groups. Significant difference ($P < 0.05$) was determined by ANOVA followed by Tukey's HSD tests. B) Representative examples of 25-d-old rosettes.

The growth analysis revealed that the growth rates and weights of the new *1a2b* and WT were not significantly different (**Figure 3.10 and Figure 3.11A**). In addition, the new *1a2b* no longer exhibited the short silique phenotype and the seed yield was comparable to that of WT. (**Figure 3.11E, F**). There was also no significant difference in chlorophyll content, F_v/F_m, and specific leaf area between the new *1a2b* and WT (**Figures 3.11B, C, D)**. However, the WT segregant 2 exhibited the small rosette phenotype observed in the original *1a2b* although it had comparable silique length and seed count to that of WT. This suggests that at least two second-site mutations were responsible for the phenotypes of the original *1a2b*.

A

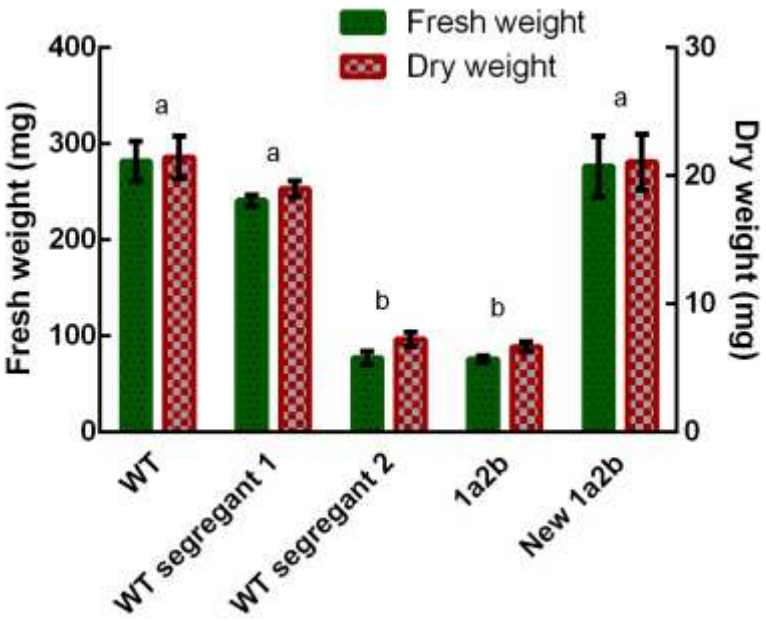
Fresh weight
Dry weight
Fresh weight (mg)
Dry weight (mg)
400
300
200
100
0
30
20
10
0
a
a
b
b
a
WT
WT segregant 1
WT segregant 2
1a2b
New 1a2b

B

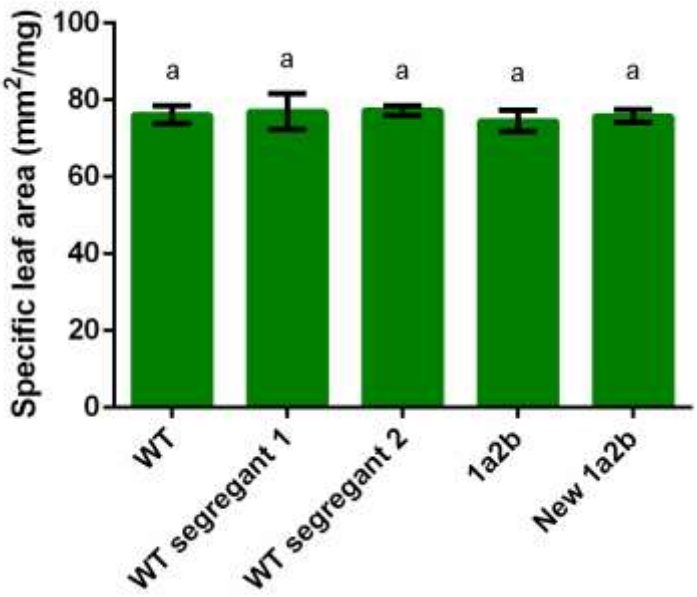
Specific leaf area (mm²/mg)
100
80
60
40
20
0
a
a
a
a
a
WT
WT segregant 1
WT segregant 2
1a2b
New 1a2b

C

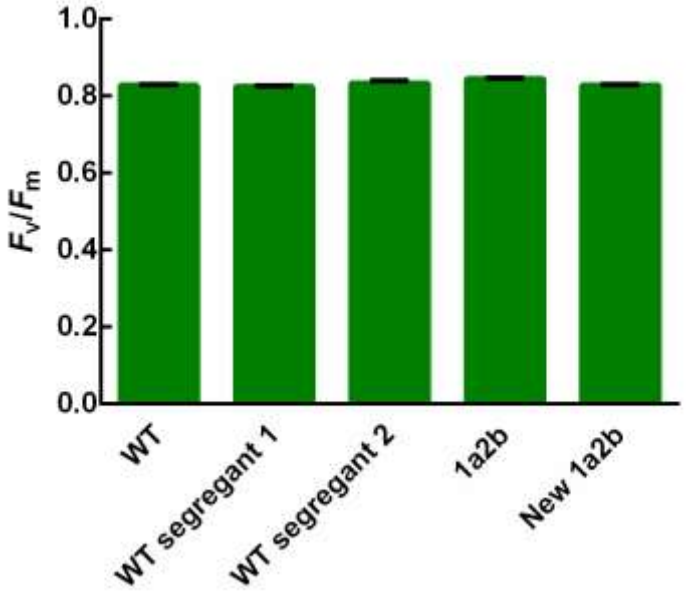
1.0
0.8
0.6
0.4
0.2
0.0
F_v/F_m
WT
WT segregant 1
WT segregant 2
1a2b
New 1a2b

D

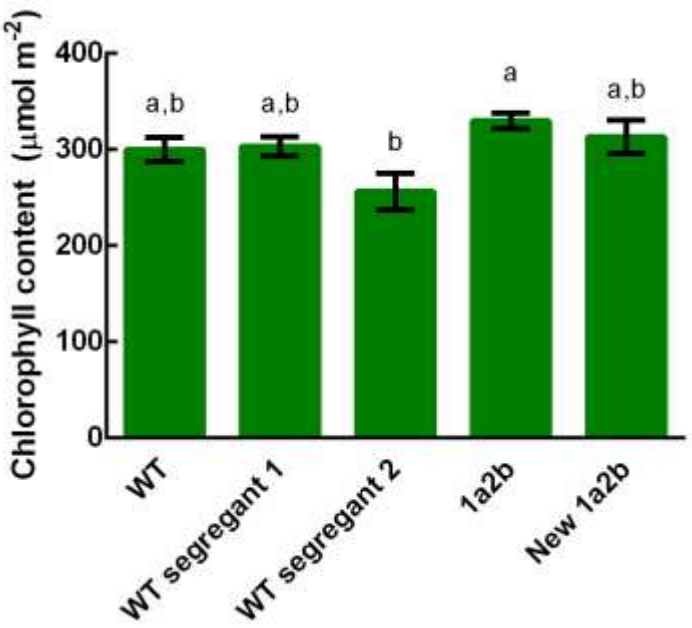
Chlorophyll content (μmol m^{-2})
400
300
200
100
0
a,b
a,b
b
a
a,b
WT
WT segregant 1
WT segregant 2
1a2b
New 1a2b

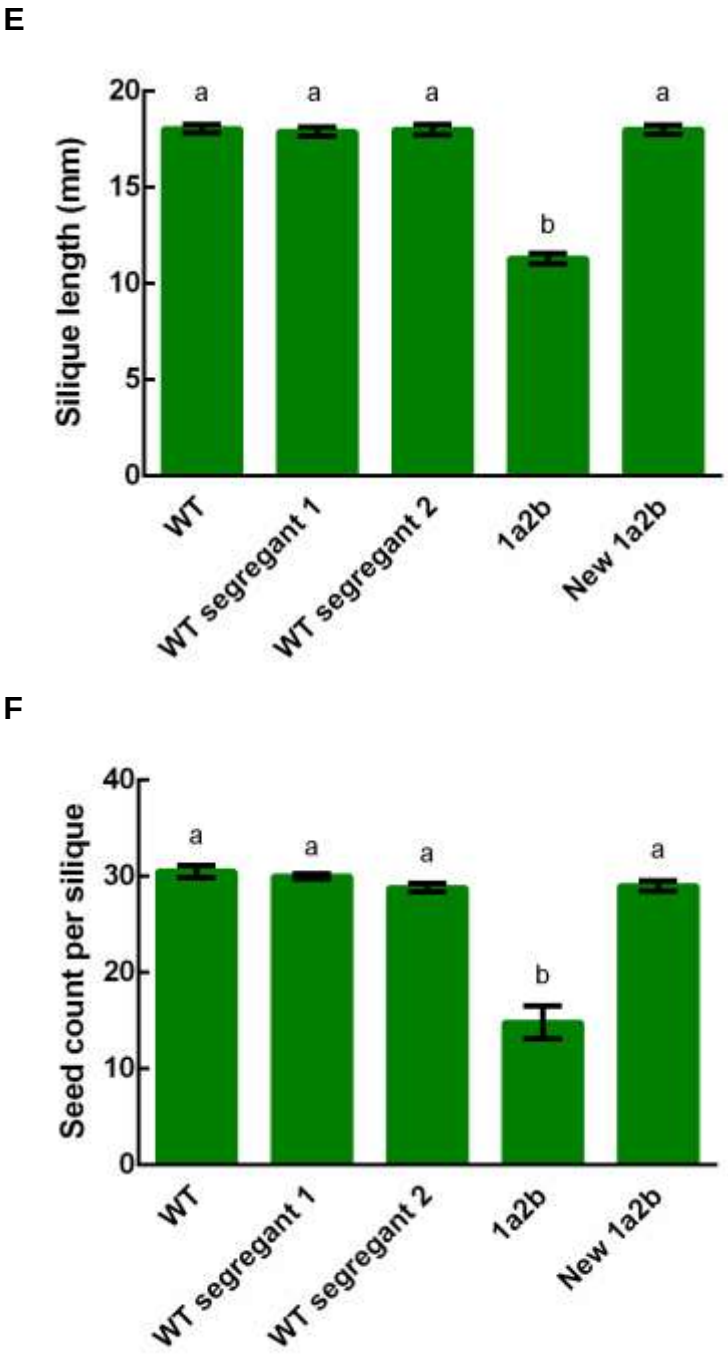

Figure 3.11: Phenotypic measurements of the new *1a2b* mutant in comparison to the original *1a2b* and a WT segregant with the small-rosette phenotype. A) Fresh and dry weight, B) specific leaf area, C) maximum potential quantum efficiency of PSII (F_v/F_m),

D) chlorophyll content per area E) Silique length and F) seed count per silique. The values represent mean ± SEM of measurements made on 8-15 samples for fresh weight, dry weight and specific leaf area, four samples for chlorophyll content and F_v/F_m. For silique length and seed count per silique, 15 siliques were measured and their seeds were counted from five randomly chosen plants. Different letters above the bars indicate significant difference ($P < 0.05$) as determined by ANOVA followed by Tukey's HSD tests.

Challenges in generating the 1a1b double mutant

T-DNA insertions that are located on different chromosomes like those 1A and the B-subfamily genes can be crossed to generate double mutants. Previous works have crossed *1a* and *2b* lines to produce the *1a2b* mutant (Atkinson *et al.*, 2017), and *1a* and *3b* lines to produce *1a3b* mutant (Izumi *et al.*, 2012), but the *1a1b* mutant was still lacking. This study also aimed to generate the *1a1b* double mutant for further functional studies of the *RbcS* genes.

The F0 single mutants *1a* and *1b* were crossed to generate the heterozygous F1 (**Figure 3.12B**), which was selfed to identify the homozygous *1a1b* mutant in the F2 generation. Screening of 125 F2 plants showed that the segregation ratio was non-Mendelian. Out of 125 plants, only one plant was homozygous for *1a* with a 1B WT. No *1a* homozygous with *1b* homozygous (*1a1b*) was recovered (**Figure 3.12A**). Further attempt to obtain the *1a1b* homozygous was made by selfing the heterozygous *1a* and homozygous *1b* plant (1A*1a1b1b*) and screen the F3 generation. Screening of 15 plants

did not identify any homozygous *1a1b* as the segregation ratio was 1:1:0 instead of the Mendelian 1:2:1.

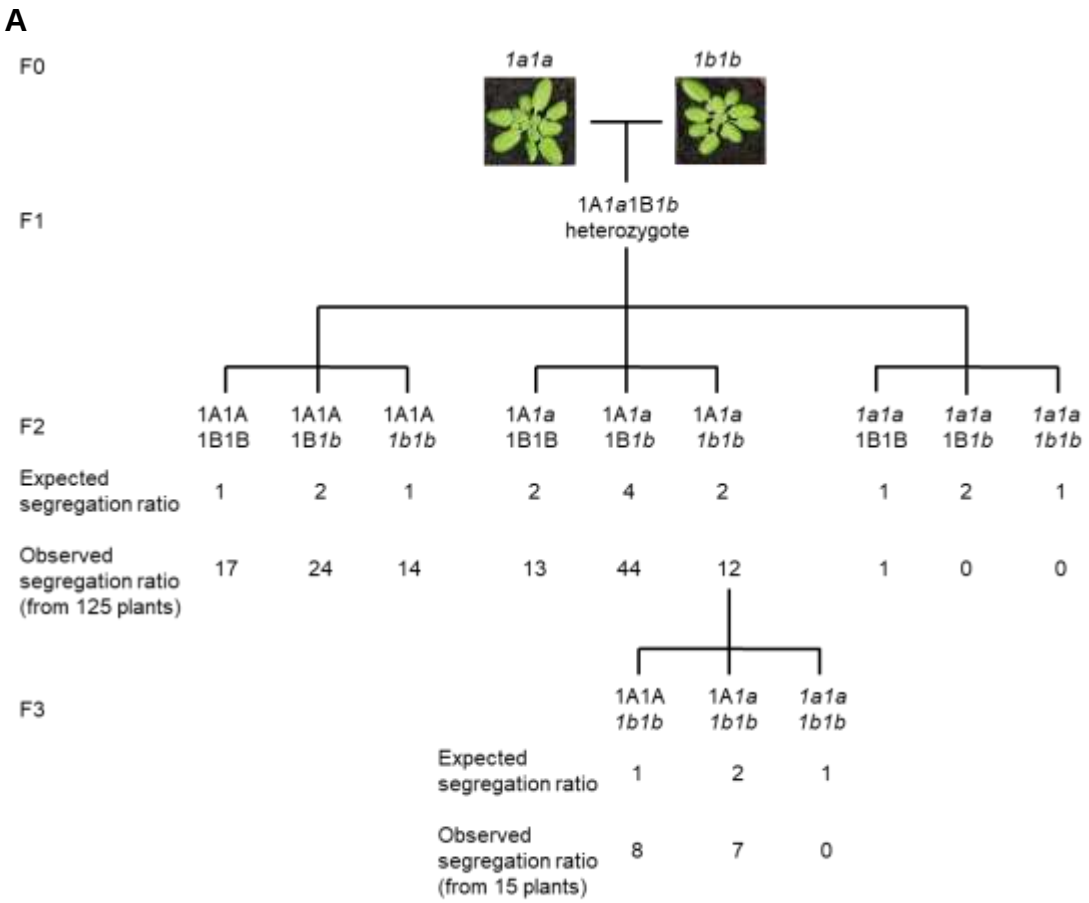

Figure 3.12. Crossing of the *1a* and *1b* T-DNA insertion mutants A) Workflow of the screening process. Single mutants *1a* and *1b* were crossed to obtain the heterozygous F1 generation. 125 F2 and 15 F3 plants were screened to find the homozygous *1a1b*. Specific primers were used to for the screening (**Supplemental table 3.1**). B) PCR example of heterozygous F1 1A*1a*1B*1b* plant.

Discussion

T-DNA insertion mutants have been used to characterise the functions of the *RbcS* genes in Arabidopsis (Izumi *et al.,* 2012; Atkinson *et al.,* 2017). This study confirmed that the T-DNA was inserted in the *RbcS* genes which effectively knocked out 1A, 1B, 2B and reduced the expression of 3B to *ca.* 3% of WT (**Figure 3.6A**). The reduction of the *RbcL* transcript was observed in these mutants compared to WT but not to the same extent as the decrease in *RbcS* level, as Arabidopsis *RbcL* transcript is controlled post-transcriptionally at the translation initiation process (Rodermel et al., 1996). The smaller decrease of *RbcL* transcript relative to *RbcS* transcript was observed in other studies in Arabidopsis and tobacco, which showed that *RbcL* was partially independent of the *RbcS* transcript level and LSU production was subject to assembly state-dependent regulation that operated at the translational level (Wostrikoff and Stern, 2007; Izumi et al., 2012). In contrast, a study in rice showed a greater decrease in *RbcL* relative to decreasing *RbcS* in senescent leaves (Suzuki and Makino, 2013). Although rice *RbcL* is also regulated at the level of translation, other factors such as *RbcL* mRNA stability may contribute to the decrease of *RbcL*.

Under the standard growth condition for Arabidopsis, the decrease in *RbcS* level to 30% (in *1a2b*) caused no detrimental effects to growth. Slow-growth and pale-leaf phenotypes were observed in *1a3b* upon further reduction of *RbcS* level to *ca* 6%. A significant reduction of Rubisco was needed to elicit the growth phenotype and affect photosynthesis because Rubisco in C3 plants is usually produced in excess while a fraction is activated at a time (Quick *et al.,* 1991; Andrews, 1996). The over-investment of Rubisco

underlines how plants respond to changing environment and the buffering system of Rubisco is important to modulate photosynthesis (Krapp *et al.,* 1993; Lauerer *et al.,* 1993).

The observation that the homozygous *1a1b* was not recovered in both F2 and F3 generations was unexpected as both the double mutants *1a2b* and *1a3b* have been generated and both *1a* and *1b* single mutants can survive and propagate. Therefore, generating *1a1b* should theoretically be possible especially when 1B is the minor isoform and contributes *ca*. 3% to the *RbcS* pool. However, generating *1a1b* homozygous from crossing the currently available T-DNA lines proved challenging. The absence of *1a1b* homozygote may be due to background mutations in the *1a* and/or *1b* T-DNA lines that may have prevented successful generation of the *1a1b* double KO mutant. Confirming this hypothesis could be achieved by crossing other *1a* and *1b* lines generated via other gene-editing methods and comparing the segregation ratios between the two crossing events. Alternatively, the absence of *1a1b* homozygote may allude to specialised functions of 1A and 1B and knocking out both genes may be lethal. Localised expression of *RbcS* has been reported in many species including tomato, maize and Arabidopsis (Wanner and Gruissem, 1991; Ewing *et al.,* 1998; Sawchuk *et al.,* 2008). In Arabidopsis, 1B was reported to be expressed exclusively on the abaxial side while 1A were expressed ubiquitously in leaves and the only isoform that is expressed in roots (Sawchuk *et al.,* 2008). Tissue- or organ-specific expression may suggest other important specialised functions of 1A and 1B genes like that of the *RbcS-T* which is expressed only in tobacco trichomes (Laterre *et al.,* 2017). Therefore, knocking out 1B in conjunction with 1A may pose survival or reproductive difficulty in Arabidopsis.

Although T-DNA insertion mutants have been used to characterised the functions of SSUs, these mutants also carry some shortcomings. Firstly, second-site mutations may be present and not annotated. These mutations are sometimes not characterised and may contribute to a phenotype that is not caused by the knock-out of the gene of interest (Yoshida *et al.*, 2018). In this study, the *1a2b* mutant was originally found to exhibit phenotypes that were assumed to be caused by T-DNA insertions of the *RbcS* genes. However, after crossing back with WT, those phenotypes disappeared, suggesting that the observed phenotypes were linked to the disruption of other genes. Another limitation of T-DNA insertion mutants is that knocking out closely-linked genes is not easily achieved by simply crossing two mutant lines, hence posing challenges for generating double or triple mutants within the B-subfamily genes. Overcoming this inherent difficulty may be achieved by a gene editing method such as CRISPR/Cas editing as the method allows for specific sites to be targeted regardless of the location (Raitskin and Patron, 2016). Double and triple mutants generated via gene editing would serve as useful models for further characterisation of *RbcS* genes and provide a platform for the study for Rubisco.

Chapter 4 - Generating *rbcs* mutants with CRISPR/Cas9 and characterisation

Introduction

Arabidopsis T-DNA insertion mutants have served as tools to characterise the function of the *RbcS* genes (Izumi *et al.,* 2012; Atkinson *et al.,* 2017). However, T-DNA insertion lines have intrinsic limitations, for example, generating double or multiple knockout mutants by crossing is typically unfeasible for closely-linked genes (e.g. the 1B, 2B and 3B genes). In addition, the availability of T-DNA insertion lines for specific genes can be limited (See chapter 3). The background of T-DNA lines may also contain additional unknown mutations. For example, a second-site mutation was found in a previously generated *1a2b* mutant (Atkinson *et al.,* 2017) that elicited a significant phenotypic impact (see chapter 3). Due to limited alleles and types of multiple mutants of the *rbcs* T-DNA insertion lines, the availability of more mutant alleles, ideally lacking in background mutations, would assist in the studies of *RbcS* genes.

The advent of CRISPR/Cas9 has allowed for a relatively simpler and faster avenue to generate knock-out (KO) lines (Belhaj *et al.,* 2015). Moreover, the method is able to overcome limitations of the T-DNA lines as single and multiple genes can be targeted at higher specificity irrespective of proximity (Nekrasov *et al.,* 2013). This chapter aimed to generate single and novel multiple SSU KO mutants using CRISPR/Cas9 editing. Molecular and physiological characterisations was performed to determine the effects of SSU knockout to plant growth.

Results

Generating rbcs single mutants using CRISPR/Cas9

To generate CRISPR/Cas9 KO mutants, constructs containing Cas9 endonuclease and a two gRNAs specific to each *RbcS* gene were assembled (**Supplemental table 4.1**). Two pairs of gRNAs were designed for each gene (**Figure 4.1A**). Some gRNA pairs target introns to ensure high target specificity. Using two gRNAs (paired gRNA method) that target introns adjacent to the exon (for example, 2B Pair 1) could potentially remove the exon if a large deletion between two gRNAs occurred. The method has been successfully utilised to knock out genes in rice (Xie *et al.,* 2015).

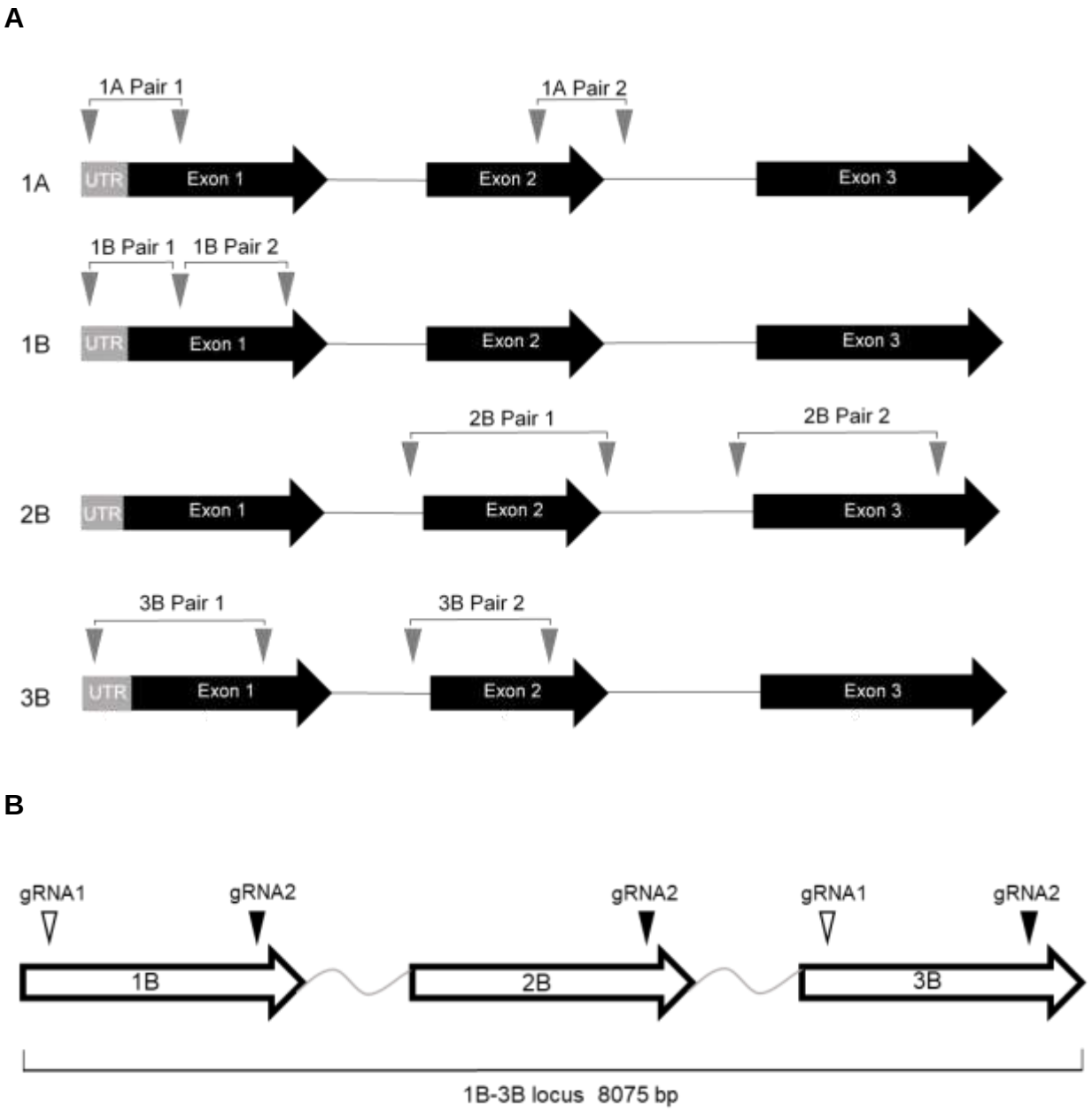

Figure 4.1. Target sites of gRNAs that target regions of *RbcS* genes. A) gRNA target sites for pairs designed to knock out each of the four *RbcS* genes. B) gRNA target sites of homologous regions within the 1B-3B locus.

To assess the effectiveness of the CRISPR/Cas9 constructs to induce mutations, a transient expression in Arabidopsis protoplasts was performed. After 24 h of protoplast transfection with CRISPR/Cas9 constructs, DNA was extracted for PCR (**Figure 4.2A**). Amplification of the WT locus for each SSU produced smaller "deletion bands" indicative of a deletion between the gRNA pair. Deletion bands were observed for both gRNA pairs for 1A and 1B, but only one pair each for 2B and 3B. Sanger sequencing indicated that deletions occurred 3-4 bp upstream of the PAM sequence, which is consistent with the cleavage site for Cas9 (**Figure 4.2B**). For gRNA pairs that produced deletion bands, the deletion efficiency, indicated by the ratio of deletion to WT, was calculated by comparing the intensity of the deletion band to the respective WT band (**Figure 4.2A**). The deletion efficiency in protoplasts was used as a proxy to guide the focus on the mutation screening *in planta*.

A

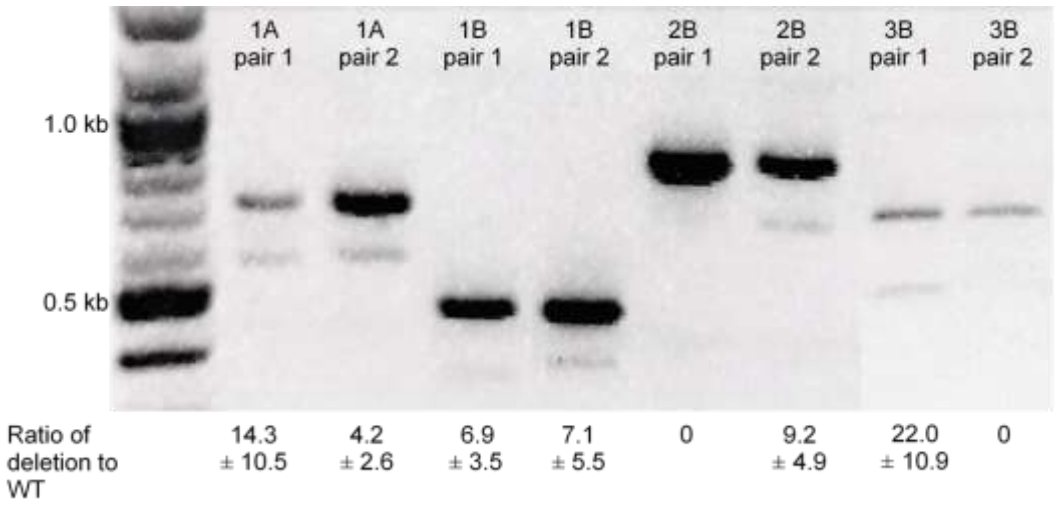

B

1A pair 1

TGTATCCT**AGACCCTCCGATCACTCCAA** **[130 bp]** **TATGCTCTCTTCCGCTACTA**TGGTTGCCT

TGTATCCT**AGA**----------**CTA**TGGTTGCCT

1A pair 2

TCTTACCT**TCCTGACCTTACCGATTCCG** **[126 bp]** **ATATAAACTAGCTAGATCTT**AGGAAAATT

TCTTACCT**TCC**----------**TCTT**AGGAAAATT

1B pair 1

GCTCTCCT**CTGCCGCTGTGGTTACCTCC** **[119 bp]** **TTACTTCCATCACAAGCAAT**GGGGGAAG

GCTCTCCT**CTG**----------**AAT**GGGGGAAG

1B pair 2

TTTTGCCT**CTTACGGTTCTCACTATATA** **[96 bp]** CCT**CTGCCGCTGTGGTTACCTCC**CCGGC

TTTTGCCT**CTTA**----------**CCGCTGTGGTTACCTCC**CCGGC

2B pair 2

CAATA**TATATATCAATTGTATTGAA**TGG **[168 bp]** CCC**TGGCGCCTTCATTAGGATCA**TCGGA

CAATA**TATATATCAATTGTATT**----------**CGCCTTCATTAGGATCA**TCGGA

3B pair 1

ATTAT**ATAAAGATGACAACACCAGT**AGG **[180 bp]** **GGTCACCCGCAAGACCAACA**AGGACATC

ATTAT**ATAAAGATGACAACACC**----------**AACA**AGGACATC

Figure 4.2. PCR amplification of protoplasts transfected with CRISPR/Cas9 constructs targeting individual *RbcS* genes and sequencing of the deletion bands. A) CRISPR/Cas9

editing was able to induce large deletions in protoplasts. Specific primers were used to amplify each *RbcS* (**Supplemental table 4.2**). The top bands represent the WT bands. The lower bands were the results of a deletion induced by gRNA pairs (i.e. "deletion bands"). The ratio of deletion to WT was quantify by comparing the intensity of the deletion band to the respective WT band. Ratios are the means ±SE of three separate protoplast transfections. B) Sequence alignment of deletion bands (bottom sequence) in comparison to WT bands (top sequence) showed SpCas9-induced deletion events at predicted locations 3-4 bp upstream of the PAM sequence (underlined). The gRNAs are shown in bold. The paired gRNAs approach produced deletions of 96 bp to 180 bp in size.

Stable transformation in Arabidopsis was performed by floral dipping. T1 seeds containing CRISPR/Cas9 construct were visually selected using the red fluorescent seed coat marker (pFAST selection). Mutation screening of T1 plants was performed initially by PCR to identify large deletions. Almost all gRNA pairs (with the exception of 1B pairs) that produced deletions detectable by PCR in protoplasts were able to induce such deletions *in planta* (**Table 4.1**). For gRNAs pairs that did not produce deletions in protoplasts, deletions were also not detected by PCR *in planta* (2B pair 1 and 3B pair 2). For those that produced deletions in plants, the deletion efficiency ranged from 1-14%. (**Table 4.1**). However, for all deletions that were detected, the WT bands were always present. This indicated that the deletions were not homozygous and likely chimeric because the intensity of the deletion bands were significantly less than that of the WT band (**Figure 4.3A**).

Table 4.1. Mutation frequency of gRNA pairs that targeted specific *RbcS* genes in the T1 and T2 generations. Red T1 seeds (i.e. transformants carrying the pFAST cassette, Cas9 and a gRNA pair) were screened for large deletions by PCR using *RbcS* specific primers (**Supplemental table 4.2**). Indels and point mutations (PMs) were detected by Sanger sequencing. Transgene-free T2 plants were screened as for T1 plants.

Target	gRNA pair	T1 (with transgene)		T2 (Transgene-free)	
		Large deletion	Indels/PM	Large deletion	Indels/PM
1A	1	1/70 (1 %)	8/53 (15%)	0/1 (0%)	1/9 (11%)
	2	8/92 (9%)	26/106 (25%)	0/8 (0%)	4/26 (15%)
1B	1	0/31 (0%)	N/A	N/A	N/A
	2	0/112 (0%)	11/35 (31%)	N/A	7/11 (63%)
2B	1	0/21 (0%)	N/A	N/A	N/A
	2	1/69 (1%)	12/63 (19%)	0/1 (0%)	5/12 (41 %)
3B	1	10/70 (14%)	1/32 (3%)	0/11 (0%)	4/11 (36%)
	2	0/33 (0%)	0/24 (0%)	N/A	N/A

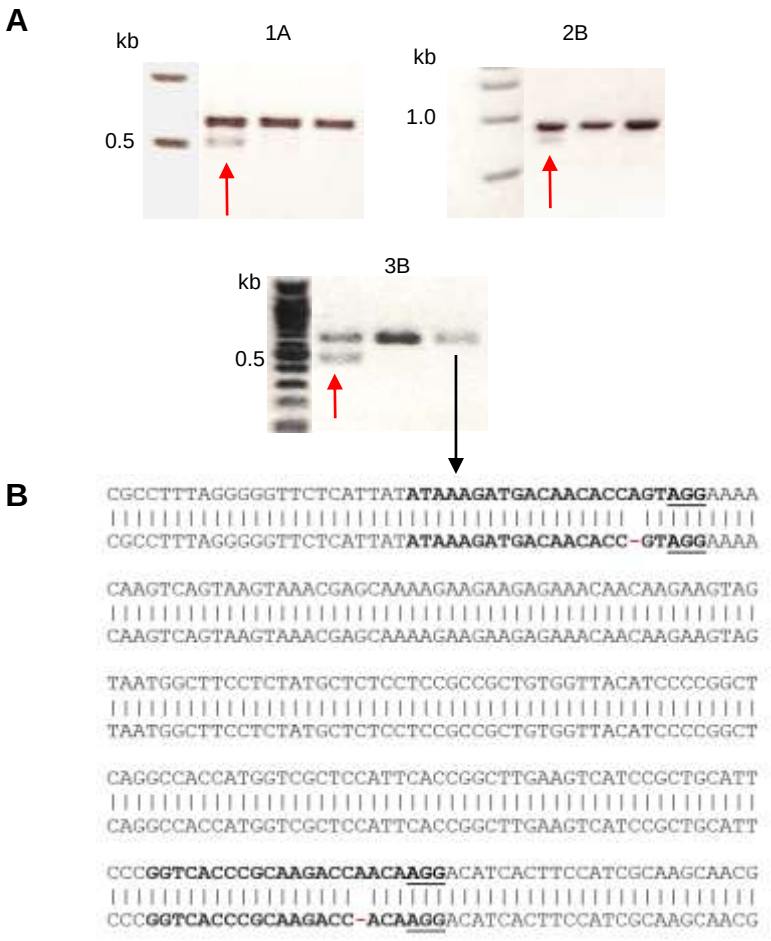

Figure 4.3. PCR screening of deletion bands and Sanger sequencing screening of indels T1 generation A) Large deletions gRNA pairs in 1A, 2B and 3B in representative T1 transformants (indicated by red arrows). The top bands are WT bands. No large deletions were detected for 1B. B). Plants with no large deletions were sequenced to find indels or PMs (indicated by the black arrow). Representative sequence alignment of the 3B gene showing an indel induced by two gRNAs. The top sequence is WT and bottom is sequencing of a plant containing 1-bp deletion (red) in the 3B genes. Bold nucleotides indicate gRNAs and unlined are PAM sequence.

The occurrence of large deletions depends on both gRNAs inducing a DBS. Thus, screening for large deletions by PCR alone overlooks potential indels induced by a single gRNA. Sanger sequencing was performed to detect indels, and showed that indels occurred at a higher frequency than large deletions with gRNA 1B pair 2 induced mutations at the highest rate (31%) (**Table 4.1, Figure 4.4A**). 3B pair 1 is the only pair that produced more deletions (14%) than indels/PMs as the frequency of indels/PMs were 3%.

A

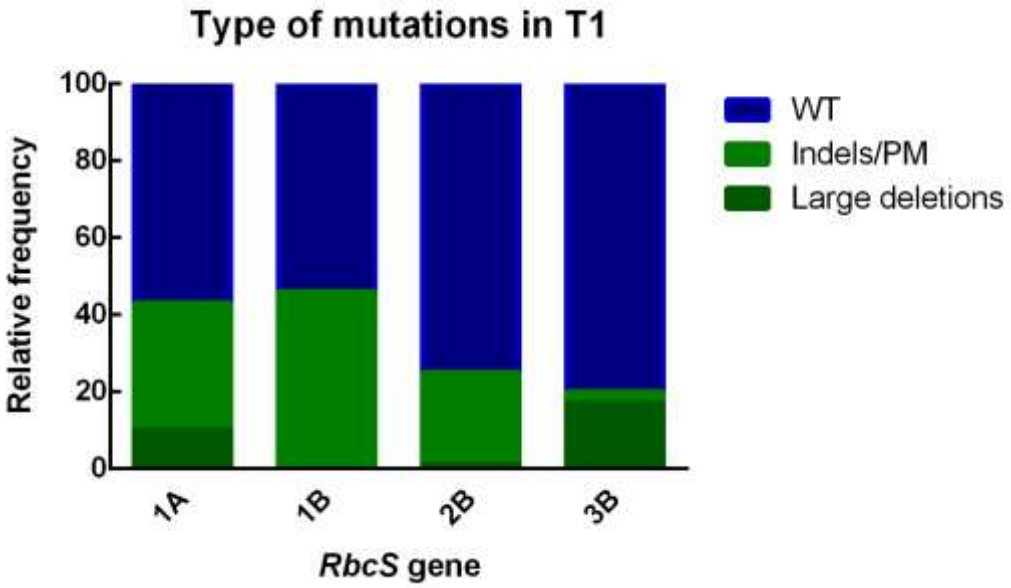
Type of mutations in T1
Relative frequency
100
80
60
40
20
0
1A
1B
2B
3B
RbcS gene
WT
Indels/PM
Large deletions

B

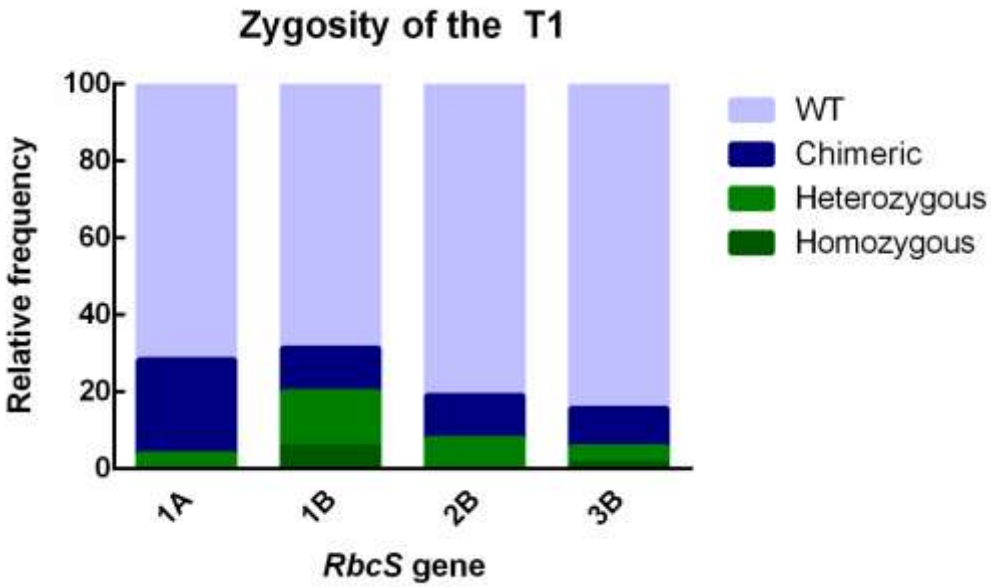
Zygosity of the T1
Relative frequency
100
80
60
40
20
0
1A
1B
2B
3B
RbcS gene
WT
Chimeric
Heterozygous
Homozygous

C

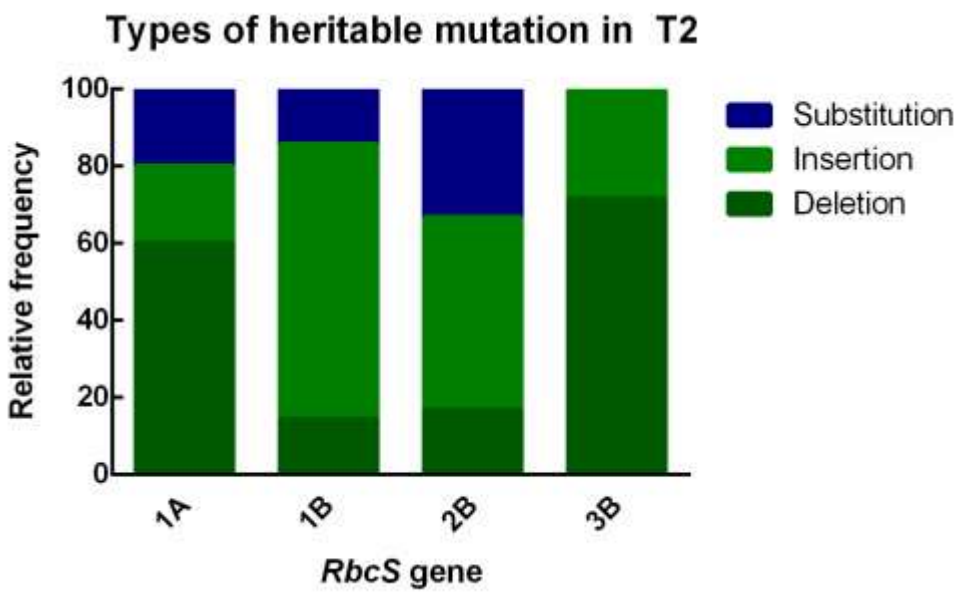

Figure 4.4. Mutation characterisations in the T1 and T2 generations. A) Frequency of different types of mutations and non-mutated plants (WT) in T1. B) Frequency of different types of zygosity in the T1 generation. All heritable mutations were indels and/or PMs. The number of T1 plants screened were 106 for 1A, 35 for 2B, 63 for 2B and 102 for 3B. C) Frequency of different types of heritable mutation in T2 plants. The number of T2 plants screened were 352 for 1A, 88 for 1B, 96 for 2B and 88 or 3B.

Plants showing Cas9-induced mutations (both large deletions and indels/PMs) were taken to the T2 generation to screen for heritable mutations. For those plants that contained large deletions in the T1 (9 plants for 1A, 1 for 2B and 11 for 3B), eight transgene-free T2 progeny per line were screened by PCR. No large deletions were detected in the T2 generation for any gRNA pair, indicating that large deletions were

chimeric mutations. T2 plants that showed evidence of indels and large deletions in T1 were screened by sequencing. A total of 352 (1A), 88 (1B), 96 (2B) and 88 (3B) T2 plants (eight plants per T1 line that showed evidence of mutations) were sequenced to find indels/PMs. Stable mutations in forms of homozygous or heterozygous indels were identified in all *RbcS* genes (**Figure 4.4 B, C and 4.5**). These indels led to an emergence of frame-shift mutation which gave rise to an early stop codon. In addition, two larger deletions of 23 and 45 bp induced by the first gRNA of 1A pair 2 were found in the 1A gene. Since most heritable mutations in the T1 generation were heterozygous, a 1:2:1 segregation occurred in T2 and homozygous KO mutants were identified in the T2 generation. Plants containing homozygous mutations were taken to T3 generation and three plants from each line (4 lines of 1A, 7 lines of 1B, 5 lines of 2B and 4 lines of 3B) were sequenced to confirm the mutations. A library of stable mutant *rbcs* lines are listed in **Figure 4.5**. Note the same mutation was counted as one line although they arose from independent mutation events and therefore 5 lines of 1B and 4 lines of 2B are shown.

1a mutants

```
WT     GAAGTTTGAGACTCTCTTCTTACCTTCCTGACCTTACCGATTCCGAAT
1aCC1  GAAGTTTGAGACTCTCTTCTTACCTTCCTTGACCTTACCGATTCCGAAT              +1
1aCC2  GAAGTTTGAGACTCTCTTCTTACC-----GACCTTACCGATTCCGAAT               -5
1aCC3  GAAGTGAGAGACTCTCTT-TTTCC---------- 22bp --------               -23, S
1aCC4  GAAGTTTGAGACTCTCTTCTTACCTTC------- 45bp --------               -45
```

1b mutants

```
WT     CTTCTTACGGTTCTCACTATATAAAG--97bp--CCTCTGCCGCTGTGGTTACCTCCCCG
1bCC1  CTTCTTACGGTTCTCACTATATAAAG--97bp--CCTCTGCCCGCTGTGGTTACCTCCCCG  +1
1bCC2  CTTCTTACGGTTCTCACTATATAAAG--97bp--CCTCTGACCGCTGTGGTTACCTCCCCG  +1
1bCC3  CTTCTTAACGGTTCTCACTATATAAAG-97bp--CCTCTGACCGCTGTGGTTACCTCCCCG  +1, +1
1bCC4  CTTCTTACGGTTCTCACTATATAAAG--97bp--------CCGCTGTGGTTACCTCCCCG   -6
1bCC5  CTTCTTACGGTTCTCACTATATAAAG--97bp--CCTCTGCCGCTGTGGGTACCTCCCCG    S
```

2b mutants

```
WT     AAGTTGAAGAATGCAAGAAGGAGTACCCTGGCGCCTTCATTAGGATCATCGG
2bCC1  AAGTTGAAGAATGCAAGAAGGAGTACCCTGGGCGCCTTCATTAGGATCATCGG          +1
2bCC2  AAGTTGAAGAATGCAAGAAGGAGTACCCTGGGCGCCTTCATTAGGATCATCGG          +1
2bCC3  AAGTTGAAGAATGCAAGAAGGAGTACCCTGGGGATCGACTTCATTAGGATCATCGG       +4, S
2bCC4  AACGAAGAAGAATGCAA----GTGTTC---GGATGCCTTCATTAGGATCATCGG         +2, -7, S
```

3b mutants

```
WT     TATATAAAGATGACAACACCAGTAGG--154bp--CCCGGTCACCCGCAAGACCAACAAGG
3bCC1  TATATAAAGATGACAACACCAGTAGG--154bp--CCCGGTCACCCGCAAGACC-ACAAGG  -1
3bCC2  TATATAAAGATGACAACACCCAGTAGG-154bp--CCCGGTCACCCGCAAGACC-ACAAGG  +1, -1
3bCC3  TATATAAAGATGACAACACCAGTAGG--154bp--CCCGGTCACCCGC-------ACAAGG  -7
3bCC4  TATATAAAGATGACAACACC-GTAGG--154bp--CCCGGTCACCCGCAAGACC-ACAAGG  -1, -1
```

Figure 4.5. The CRISPR/Cas9 approach produced a library of single *rbcs* KO mutants. Mutations were confirmed by Sanger sequencing of the T2 and T3 generations. The PAM sequences are underlined, gRNA sequences are in bold and nucleotides in red denote mutations (+ is insertion, - is deletion and s is substitution).

Generating rbcs CRISPR/Cas9 triple KO mutants based on T-DNA lines

CRISPR/Cas9 editing can be utilised to edit closely-linked genes, which allowed for the possibility to edit multiple *RbcS* genes of the B-subfamily. Generating double or triple mutants within the 1B-3B locus was attempted by i) using promiscuous gRNAs or ii) targeting B-subfamily gene(s) in available T-DNA double knockout mutants *1a2b* (generated in chapter 3) and *1a3b* (Izumi *et al.*, 2012). In the *1a2b* mutant, triple mutants *1a1b2b* or *1a2b3b* could be obtained by targeting 1B or 3B, respectively. Similarly in the *1a3b* mutant, 1B or 2B could be targeted to generate *1a1b3b* or *1a2b3b*, respectively. After transformation of *1a2b* with gRNAs 3B pair 1 and *1a3b* with gRNAs 2B pair 2, T1 generations were screened for mutations. For the *1a2b* T-DNA line targeted with 3B gRNAs, 30 T1 transformants were grown. Three putative triple *1a2b3b* KO mutants were identified in the T1 generation due to a distinctive slow-growing and pale phenotype (**Figure 4.6**). Sanger sequencing showed small indels in 3B, thus three *1a2b3b* triple knockout lines were confirmed. For the *1a3b* T-DNA line targeted with 2B gRNAs, 45 T1 transformants were grown. Similarly to the *1a2b*-based triple mutant, slow-growing and pale phenotype was observed in two T1 plants. Sanger sequencing confirmed that CRISPR/Cas9 editing induced indels in 2B, thus generating *1a2b3b* KO mutant. The five triple mutant plants were taken to the T2 generation to confirm mutations. Altogether, three alleles of *1a2b*-based and two alleles of *1a3b*-based triple mutant were obtained (hereafter BigBoi or BB and BigGurl or BG, respectively (**Figure 4.7**). Since *1a2b* mutant shows complete absence of 1A and 2B, the interruption of 3B in BigBoi indicates that only a single SSU gene (1B) was involved in Rubisco production in this line. In contrast

to targeting 2B or 3B, targeting the 1B gene in either *1a2b* or *1a3b* T-DNA line did not result in a growth phenotype. This was not unexpected as 1B is a minor isoform. Therefore, Sanger sequencing was performed to identify mutations in 1B. Out of 78 plants, only a single and silent substitution mutation was identified (**Table 4.2**).

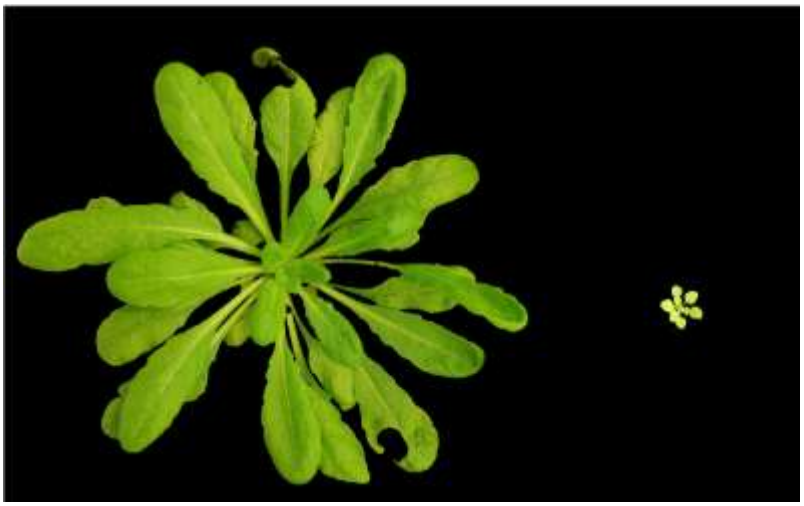

Figure 4.6. Comparison of 7-weeks old rosettes of WT (left) and BigBoi (*1a2b3b*, right). Plants were grown under 200 µmol photon m^{-2} s^{-1} of white light, under 12 hr (light) /12 hr (dark) cycles at 21ºC**.**

1a2b3b mutant or BB

```
WT                  CCCGGTCACCCGCAAGACCAACAAGG
BB1 (Biallelic)     CCCGGTCACCCGCAAGACC--CAAGG      -2
BB1 (Biallelic)     CCCGGTCACCCGCAAGACCA-CAAGG      -1
BB2                 CCCGGTCACCCGCAAGACCAAACAAGG     +1
BB3                 CCCGGTCACCCGCAAGACCA-CAAGG      -1
```

1a2b3b mutant or BG

```
WT                  CCCTGGCGCCTTCATTAGGATCATCGG
BG1                 CCCTGG-GCCTTCATTAGGATCATCGG     -1
BG2                 CCCTGGTCGCCTTCATTAGGATCATCGG    +1
```

Figure 4.7. The CRISPR/Cas9 approach produced *1a2b3b* triple KO mutants. Mutations were confirmed by Sanger sequencing of the T2 generation. The PAM sequences are underlined, gRNA sequences are in bold and nucleotides in red denote mutations (+ is insertion and - is deletion).

Table 4.2. Mutation frequency of gene targeting using specific gRNAs to edit *1a2b* or *1a3b* T-DNA lines to generate triple mutants. The analysis was performed in the T1 generation.

Target Mutant	Background	Target gene	T1 editing rate	Type of mutations observed in transgene-free T2
1a2b3b	*1a2b*	3B	3/30 (10%)	Indels
1a2b3b	*1a3b*	2B	2/45 (4%)	Indels
1a1b2b	*1a2b*	1B	8/33 (24%)	Substitution
1a1b3b	*1a3b*	1B	1/45 (2%)	Substitution

Targeting B-subfamily using promiscuous gRNAs

One of the main strengths of CRISPR/Cas9 editing is the ability to edit multiple genes simultaneously by targeting homologous regions. Taking advantage of high

sequence homology among the *RbcS* genes, a pair of promiscuous gRNAs were designed to target the B-subfamily genes as shown in **Figure 4.1B**. After floral dipping, seeds were screened using the pFAST selection and 76 T1 plants were grown. Plants were screened by PCR and two showed a *ca.* 800 bp deletion band induced by gRNA 1 in 1B and gRNA 2 in 3B (Lines 15 and 20). Six showed a *ca*. 1.4 kb deletion band induced by gRNA 1 in 1B and 3B (one plants, Line L1) or gRNA 2 in 1B and 3B (five plants, Lines 4, 5, 8, 12, and 23) (**Table 4.3**, **Figure 4.8A and 4.9**). The presence of smaller bands at 800 bp in four of the plants in the latter group indicated that these plants contained the deletion induced by gRNA 1 in 1B and gRNA 2 in 3B, and were likely chimeric (**Figure 4.8B**). Bands for each deletion event were gel purified and sequenced. The sequencing result confirmed the deletion regions (**Figure 4.9**).

Table 4.3: Editing efficiency of promiscuous gRNAs targeting the 1B3B locus. Plants were screened for deletions by PCR using specific primers to amplify the 1B-3B locus. Indels were screened by Sanger sequencing. Seventy-six T1 plants were screened for large deletions. In the T2 generation, eight plants from each T1 that showed large deletions were grown (64 plants in total) and screened for deletions by PCR and four plants were screened by Sanger sequencing.

	T1	T2 (transgene-free)	
Target	Deletion	Deletion	Indels
1B3B locus	8/76 (11%)	0/64(0%)	2/36 (6%)

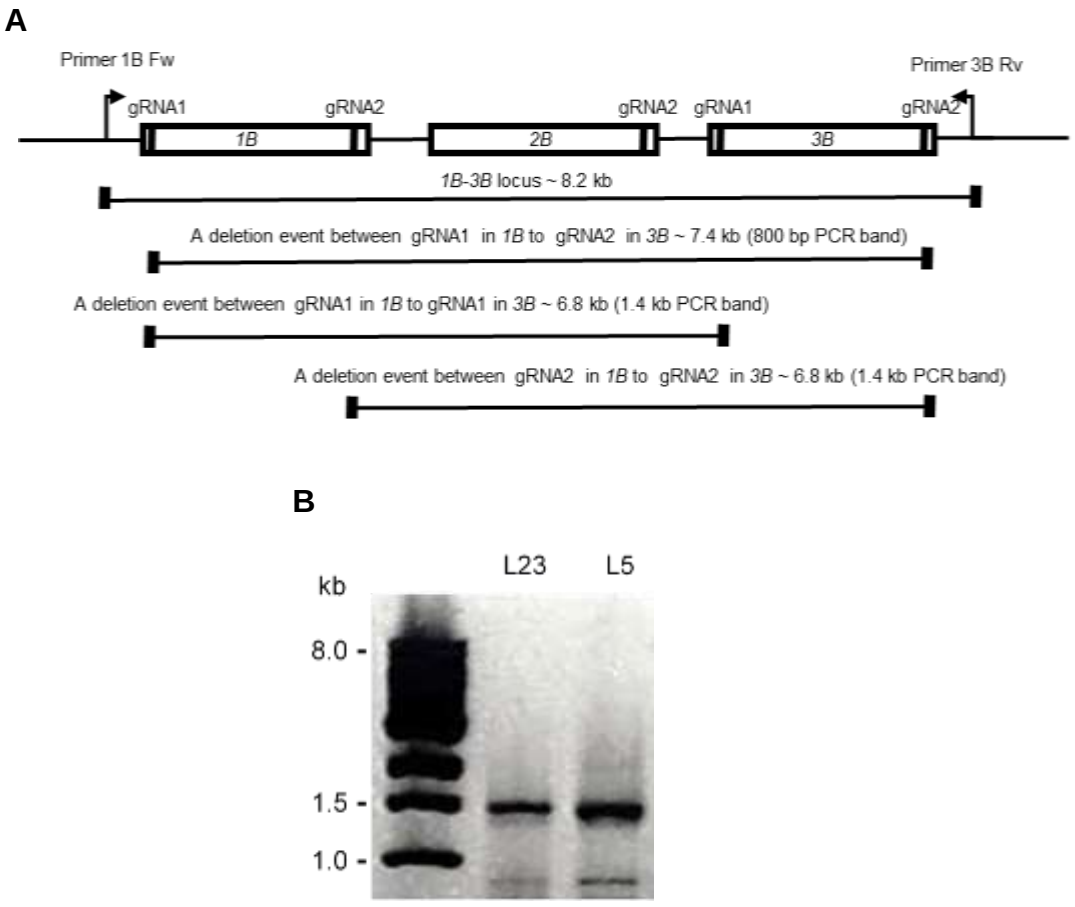

Figure 4.8. CRISPR/Cas9 editing induced large deletions in the B-subfamily genes. A) Graphic representation of deletion induced by a paired gRNA targeting strategy. A PCR amplification from 1B Fw primer and 3B Rv primer produces an 8.2 kb WT amplicon. Depending on the deletion location, two different band sizes of 800 bp and 1.4 kb can be produced from PCR. A deletion between gRNA1 in 1B and gRNA2 in 3B induces a 7.4 kb deletion, which results in a 800 bp band in PCR. A deletion between gRNA1 pairs or gRNA2 pairs in 1B and 3B induces a 6.8 kb deletion, which results in a 1.4 kb band in PCR. B) PCR products using specific primers to amplify the 1B-3B locus (**Supplemental**

table 4.2). The representative deletion bands from two biological samples are approximately 1.4 kb and 800 bp.

gRNA 1 on 1B and gRNA 2 on 3B

```
WT      AATGGGGGAAGAGTTAGCTGCATGAAGGTAATG----- 8kb -----TGAAGGAAGTTGAAGAATGCAAGAAGGAGTAC
L15     AATGGGGGAAGAGTTAGCTGCATGAAGGTAATG----- 8kb -----TGGAGGAAGTTGAAGAATGCAAGAAGGAGTAC
L20     AATGGGGGAAGAGTTGGCTGCATCAAGGTAATG----- 8kb -----TGGAGGAAGTTGAAGAATGCAAGAAGGAGTAC
```

gRNA 2 on 1B and gRNA 2 on 3B

```
WT      TTGAAGGAAGTTGAAGAATGCAAGAAGGAGTAC----- 6kb -----TTGAAGGAAGTTGAAGAATGCAAGAAGGAGTAC
L4      TTGAAGGAAGTTGAAGAATGCAAGAATGG--------- 6kb ----------------GAAGAATGCA-AAGGAGTAC
L5      TAGAA----------------------------------- 6kb -----TTGAAGGAAGTTGAAGAATGCAAGAAGGAGTAC
L8      TTGAAGGAAGTTGAAGAATGCAGAAAGGAG-------- 6kb -----TGGAAGGAAGTTGAAGAATGCAAGAAGGAGTAC
L12     TTGAAGGAAGTTGAAGAATGCAAGAAGGA--------- 6kb ----------------GAAGAATGCAAGAAGGAGTAC
L23     TTGAAGGAAGTTGAA-ATGCAAGAGAGA---------- 6kb -----TTGAAGGAAGTTGAAGAATGCAAGAAGGAGTAC
```

gRNA 1 on 1B and sRNA 1 on 3B

```
WT      AATGGGGGAAGAGTTAGCTGCATGAAGGTAATG----- 6kb -----TTGAAGGAAGTTGAAGAATGCAAGAAGGAGTAC
L1      AATGGGGGAAGAGTTAGCTGC----------------- 6kb ----------------------------------TAC
```

Figure 4.9: Sequence alignment of the deletion bands induced by gRNAs that targeted the 1B-3B locus. The PAM sequences are underlined, gRNA sequences are in bold and sequences in red denote mutations. L stands for Line.

In the T2 generation, eight transgene-free progenies from each line that showed evidence of large deletions were screened by PCR. No large deletion was detected in 64 plants (**Table 4.3**). However, pale-rosette and slow-growing phenotypes were observed in 24% of the population of a single line (Line 4) (**Figure 4.10A**). A 1:3 phenotypic segregation ratio suggested that the T1 generation was heterozygous for mutation that

could be small indels at each gRNA site. Individual *RbcS* genes from plants with the phenotype were sequenced, but no indels were detected. The presence of a phenotype with no detected mutations in any *RbcS* genes suggested off-target mutations had occurred and that further investigation would be required to identify the cause of the phenotype. This was not pursued here.

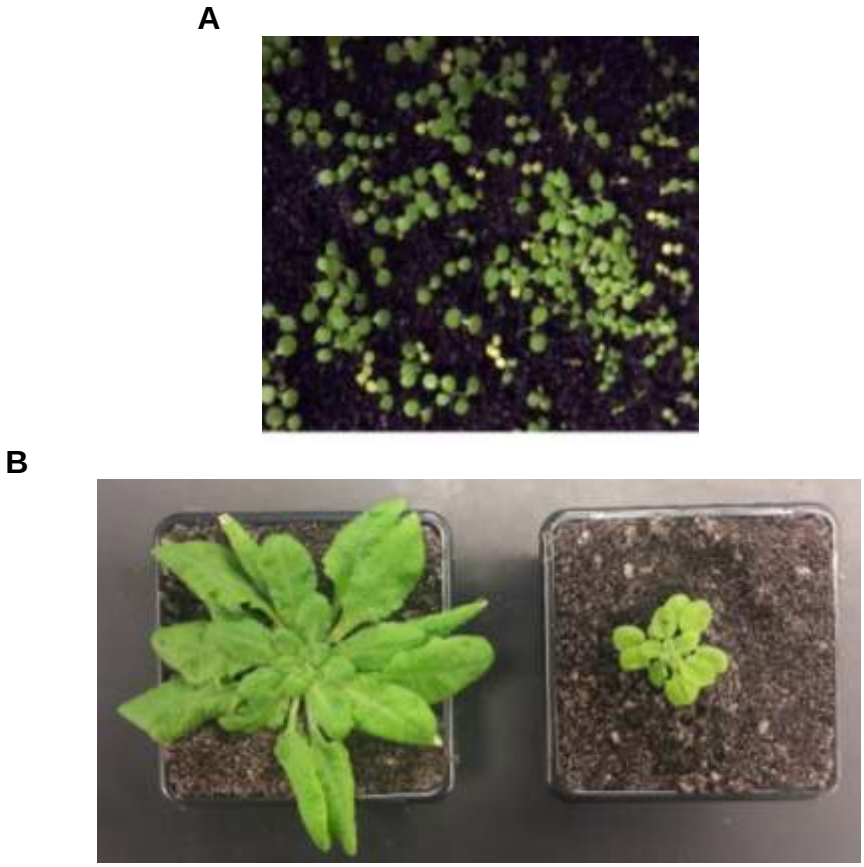

Figure 4.10. Phenotype of the T2 progeny of Line 4 targeted by CRISPR/Cas9 editing that target homologous regions in the 1B-3B locus. A) image of T2 seedlings from line 4 after seven days of sowing. 100 plants were counted and 24 seedlings appeared paler green

and grew much more slowly than green seedlings. B) Images of 6-week old rosettes of WT (left) and a pale plant (right).

As previous results suggested that small indels occurred more frequently and were more likely to be heritable, individual genes in the T2 generation were then screened for small mutations. Amplification of individual genes showed a shift of ~150 bp that was detected in the 3B gene in one transgene-free progeny of Line 5 (**Figure 4.11A**). Sequencing result showed that this plant contained a deletion of 147-bp induced by gRNA2 in exon 3 of 3B and a 4-bp deletion in exon 3 of 2B induced by the gRNA2, resulting in a *2b3b* KO mutant (**Figure 4.11B**). A total of four plants were sequenced from this line and two plants showed a 4-bp deletion in 3B and one other had no mutation, suggesting that the parental T1 was multi-allelic. No mutation was detected in 1B in all four transgene-free T2 lines.

Identifying the triple mutant required multi-generational screening as multiple sites were targeted simultaneously. Further screening of Line 5 was performed by growing 40 red T2 seeds that still contained Cas9 and gRNAs. Some of the T2 plants showed spotted pale leaves and slower-growing phenotypes, indicating chimerism (**Figure 4.11C, D**). Eight plants with strong spotted leaves were selfed and taken to the T3 generation. Transgene-free T3 seeds were grown. Unlike the T2 parental line, T3 progeny lacked the phenotypes that were previously observed and grew similarly to WT plants. Sequencing of four plants per line showed that two plants in one line had a 4-bp deletion in 3B similar to the one in T2. Seven other lines (four plants per line) showed no mutations in 1B, 2B

or 3B. The lack of mutations in the transgene-free T3 plants may infer chimeric off-targeting effect in the T2 as seen in line 4 (**Figure 4.10**).

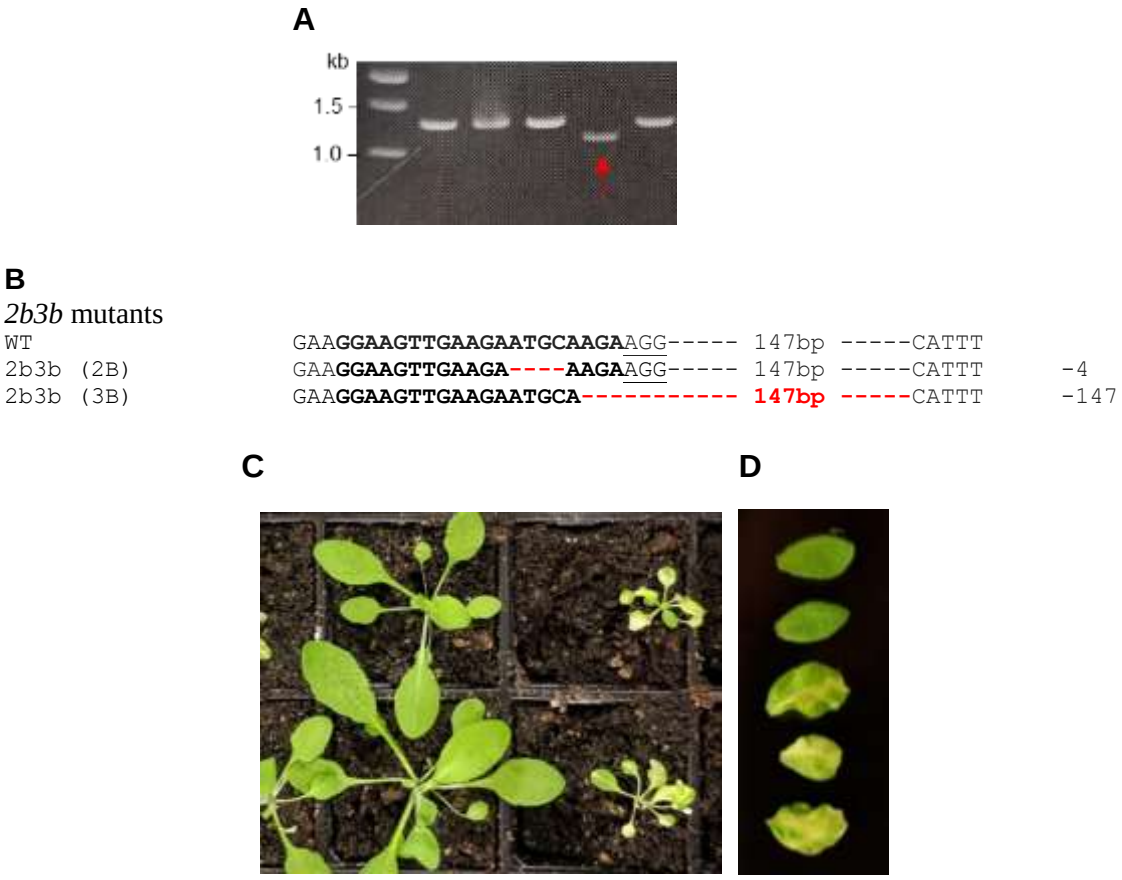

Figure 4.11: Phenotype of T2 (Line 5) generations of plants targeted by CRISPR/Cas9 editing of homologous regions in the 1B-3B locus. A) PCR products using specific primers to amplify 3B of plants lacking CRISPR/Cas9 transgene. The WT band is 1326 bp (**Supplemental table 4.2**) and sample indicated by the red arrow showed a 147 bp deletion induced by gRNA 2 in 3B. B) Sequence alignment of 2B and 3B genes of the *2b3b* KO mutant. The PAM sequences are underlined, gRNA sequences are in bold and sequences in red denote mutations. C) Representative image of Cas9-containing T2 plants

from Line 5. Plants with strong spotted leaves and slow growing phenotype were grown next to plants that grew similarly to WT. D) Images of green WT-like leaves in comparison to leaves with pale spots.

Molecular characterisation of CRISPR/Cas9 mutant

Molecular characterisation to confirm gene knockouts was performed at the transcript level by RT-qPCR (as described in Chapter 3). The RT-qPCR results indicated that there was a reduction of transcript of genes that were targeted by both T-DNA insertion and CRISPR/Cas9 editing (**Figure 4.12A**). The knockout of genes led to a decrease in the total *RbcS* transcript abundance in *1a*, *3b*, double mutants and BigBoi. Consequently, a decrease in Rubisco content was observed as 53% of Rubisco remained for *1a*, 85% for *3b*, 62% for *2b3b*, 79% for *1a2b*, 45% for *1a3b*, and 15% for BigBoi relative to Rubisco content of WT (**Figure 4.12D**). However, *RbcL* transcript and soluble protein content did not decrease to the same extent as that of *RbcS* (**Figure 4.12B, C**).

SDS-PAGE and Western blot were performed to confirm the absence of the SSU proteins in *rbcs* KO mutants. Since the B subfamily genes are 100 Da bigger in size than 1A, 12% Bis-Tris gel and Coomasi staining was able to separate the two subfamilies (**Figure 4.12E**). SDS-PAGE and Western blot showed that *1a* KO mutants did not express 1A protein as indicated by the absence of the lower molecular weight band (**Figure 12E, F**). A decrease in the B-subfamily protein was observed in *3b* KO mutants, but the decrease in the B-subfamily protein band was not obvious in the *1b* and *2b* KO mutants

as they are minor isoforms. The decrease in the LSU levels was distinct in double mutants and BigBoi (**Figure 12F**).

A

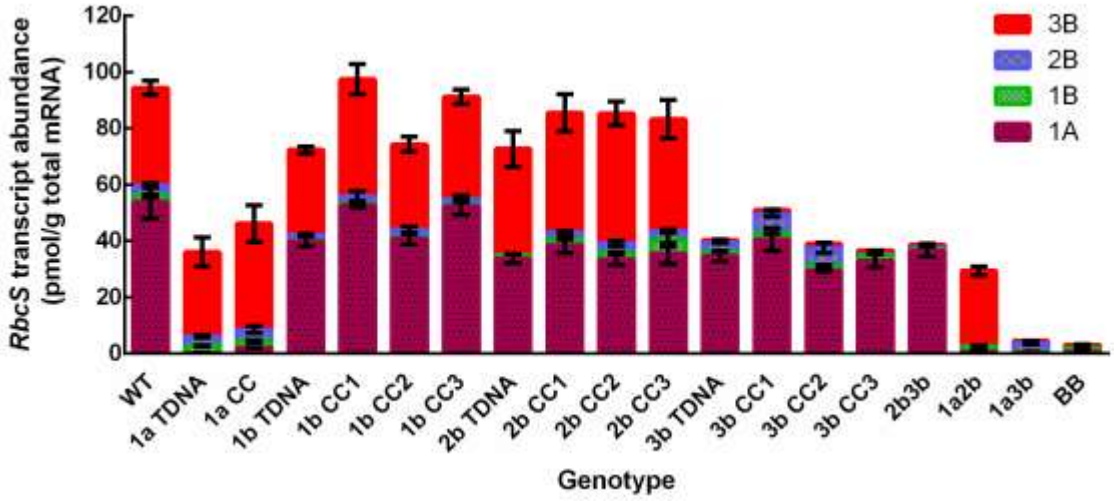

B

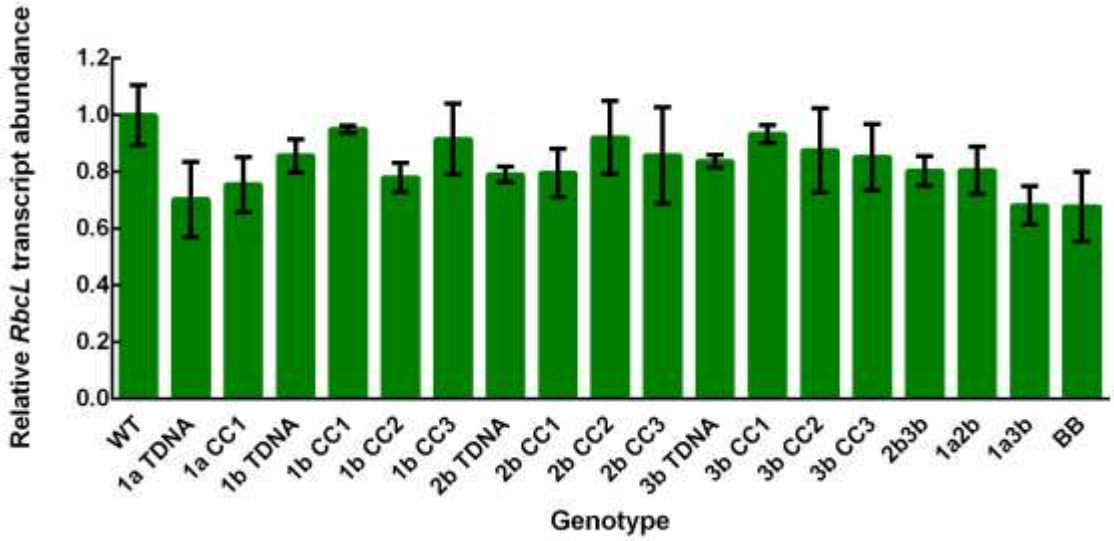

C

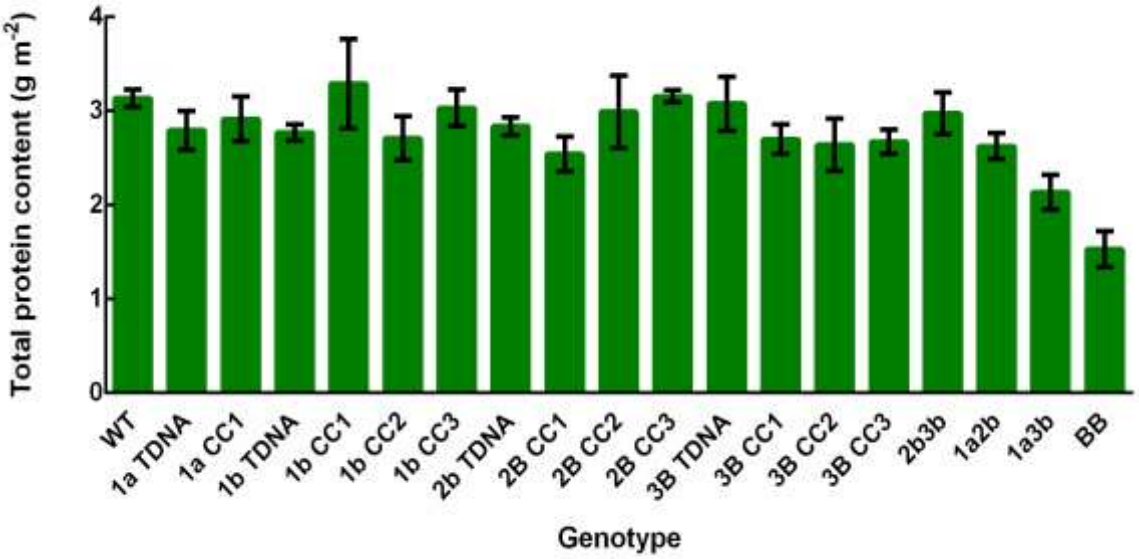
Total protein content (g m-2)
0
1
2
3
4
WT
1a TDNA
1a CC1
1b TDNA
1b CC1
1b CC2
1b CC3
2b TDNA
2B CC1
2B CC2
2B CC3
3B TDNA
3B CC1
3B CC2
3B CC3
2b3b
1a2b
1a3b
BB
Genotype

D

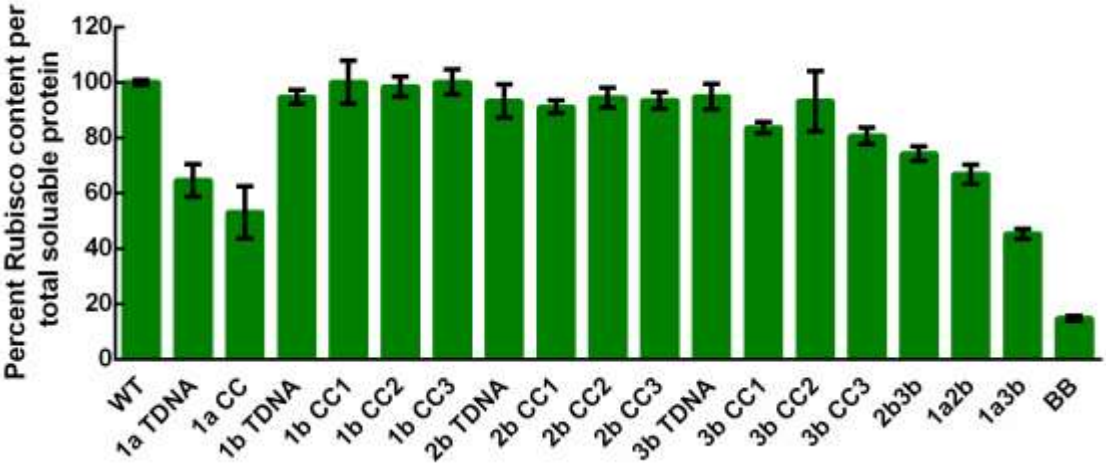
Percent Rubisco content per total soluable protein
0
20
40
60
80
100
120
WT
1a TDNA
1a CC
1b TDNA
1b CC1
1b CC2
1b CC3
2b TDNA
2b CC1
2b CC2
2b CC3
3b TDNA
3b CC1
3b CC2
3b CC3
2b3b
1a2b
1a3b
BB

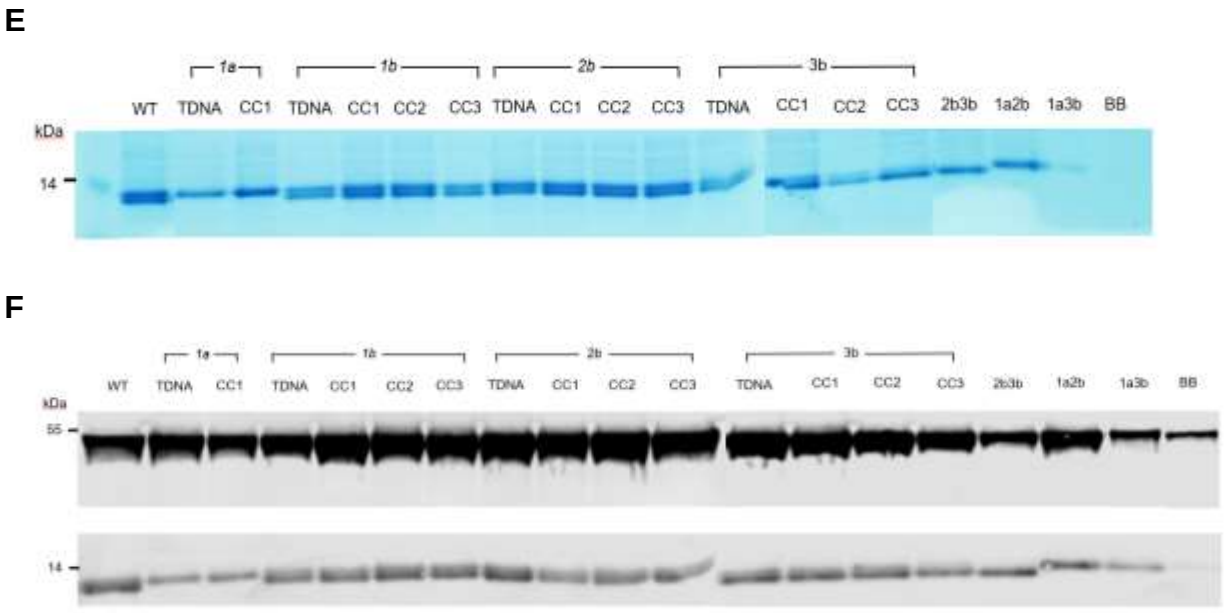

Figure 4.12. Molecular characterisation of *rbcs* KO mutants. A) Absolute *RbcS* transcript abundance and B) relative *RbcL* transcript abundance in WT and CRISPR/Cas9 (CC) mutants generated in this study compared to those of T-DNA lines. Plants of 35 days of age were used (n = 3; BB indicates BigBoi) C) Total soluble protein content for WT, CRISPR/Cas9 and T-DNA mutants were determined using leaf tissue of 35-day old rosettes by the Bradford assay (n = 4). D) Percent Rubisco content per soluble protein (n = 5). The values are mean ± SEM of measurements. E) Coomasi staining of 12% bis-tris SDS-PAGE showing the separation between the B-subfamily SSU (top band) from the A-subfamily SSU (bottom band). F) Immunoblots for WT and *rbcs* KO mutants probed with polyclonal antibodies against Rubisco. The LSU (55 kDa) and SSU (14 kDa) are shown.

Physiological characterisation of CRISPR/Cas9 mutants

An initial set of growth experiments were performed under standard conditions (200 µmol photon m^{-2} s^{-1}, 12 h light : 12 h dark cycle, 21^{o}C) to characterise the growth of the *rbcs* KO mutants (**Figure 4.13**). The rosette expansion rates of CRISPR/Cas9 KO mutants for individual *RbcS* genes (*1a*, *1b*, *2b* and *3b*) and their respective T-DNA KO mutants were not significantly different from WT plants (**Figure 4.13A, C**). Similarly, no difference was observed for fresh weight (FW), dry weight (DW), specific leaf area (SLA), chlorophyll content and maximum potential quantum efficiency of PSII (F_v/F_m) harvested at 28 days after germination (DAG) (**Figure 4.14 A-D**). The rosette expansion rates, FW and DW of double mutants *2b3b* and *1a2b* were slightly lower than but not significantly different from that of WT (**Figure 4.13 B, C** and **Figure 4.14 A-D**). However, the rosette expansion rates, FW and DW of *1a3b* and BB were significantly reduced. *1a3b* and BigBoi also had a significantly increased SLA compared to WT, with BigBoi 4-fold greater than and *1a3b* 2-fold greater than WT (**Figure 4.13 B, C** and **Figure 4.14 A-D**). Furthermore, a significant decrease in chlorophyll content and F_v/F_m were observed for *1a3b* and BigBoi (**Figure 4.14E, F**). The latter results are consistent with Izumi *et al.,* (2012) and suggest that reducing Rubisco content below 45% in Arabidopsis leads a reduction in chlorophyll investment and a corresponding decrease in the efficiency of PSII.

A

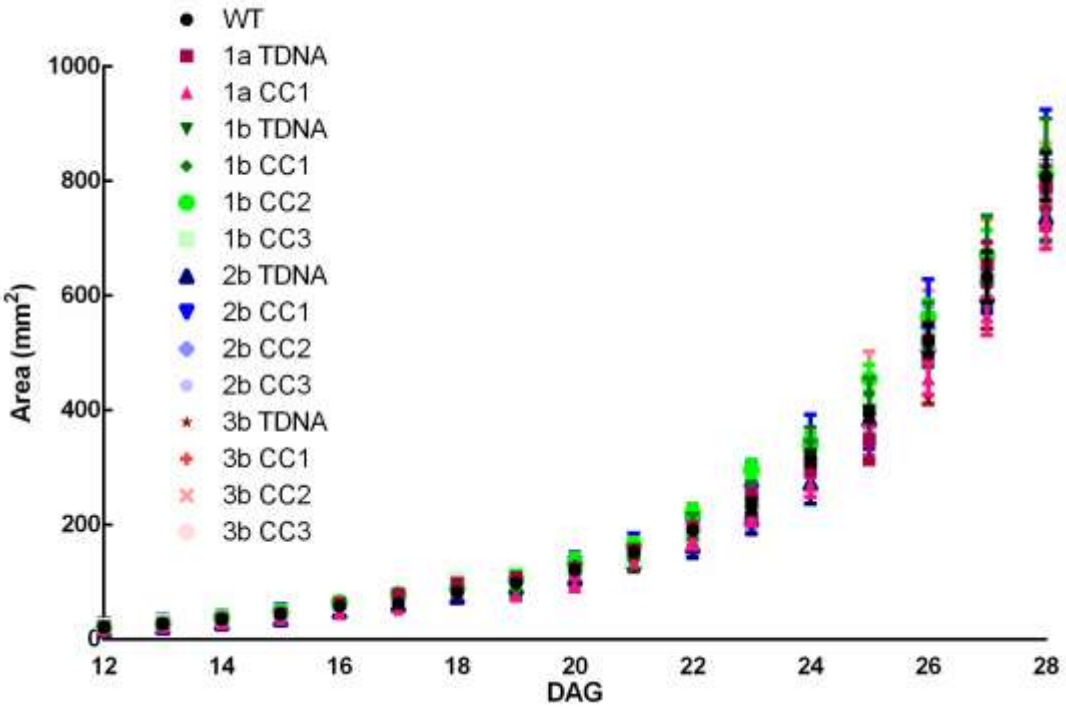
WT
1a TDNA
1a CC1
1b TDNA
1b CC1
1b CC2
1b CC3
2b TDNA
2b CC1
2b CC2
2b CC3
3b TDNA
3b CC1
3b CC2
3b CC3
Area (mm²)
DAG
0
200
400
600
800
1000
12
14
16
18
20
22
24
26
28

B

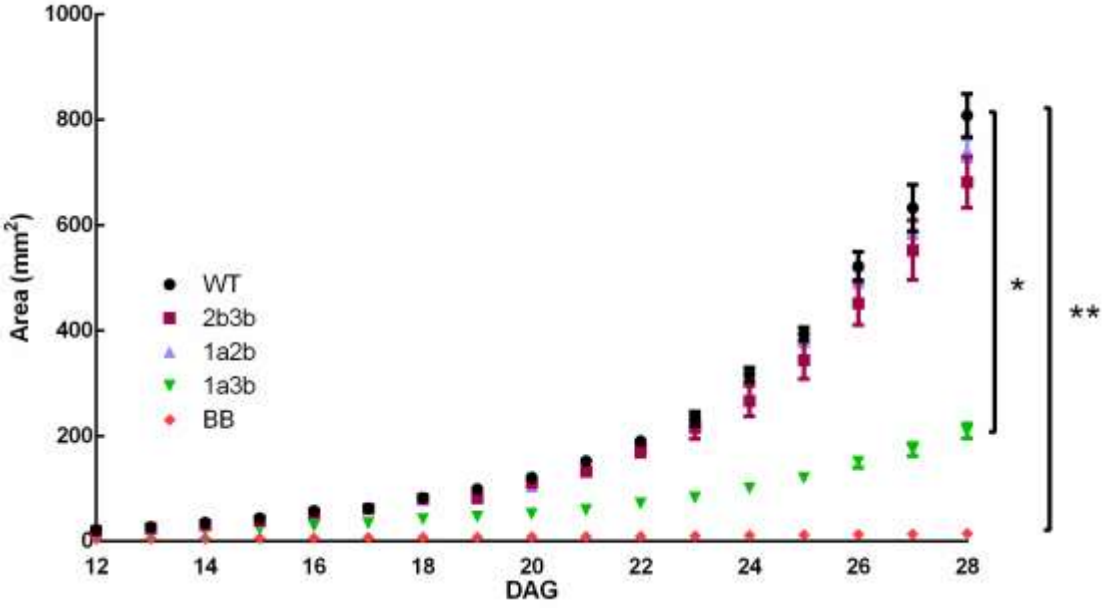
WT
2b3b
1a2b
1a3b
BB
Area (mm²)
DAG
*
**
0
200
400
600
800
1000
12
14
16
18
20
22
24
26
28

C

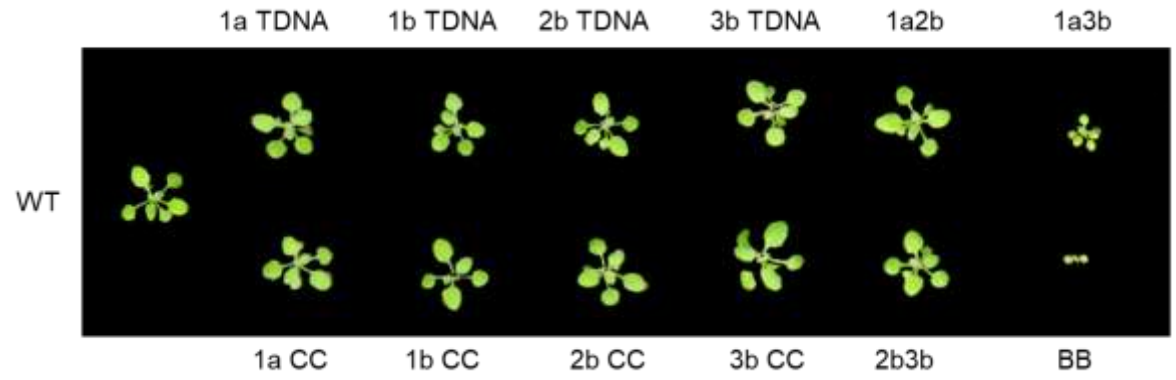

Figure 4.13. Growth analysis of *rbcs* KO mutants. A) Rosette expansion of T-DNA and CRISPR/Cas9 (CC) single KO mutants (CC1 for *1a* and CC1-3 for *1b*, *2b* and *3b*). B) Rosette expansion of double mutants and the triple mutant BigBoi (BB). The values are means ± SE of measurements made on 8-15 individual rosettes. No significant difference in area compared to WT was observed for any single *rbcs* KO mutant, *2b3b* or *1a2b*. DAG is days after germination. Asterisks denotes significant difference from WT for *1a3b* and BB. One (*) and two (**) asterisks denote significant difference between groups. Significant difference ($P < 0.05$) was determined by ANOVA followed by Tukey's HSD tests. C) Representative images of 23-d-old rosettes of WT and *rbcs* KO mutants.

A

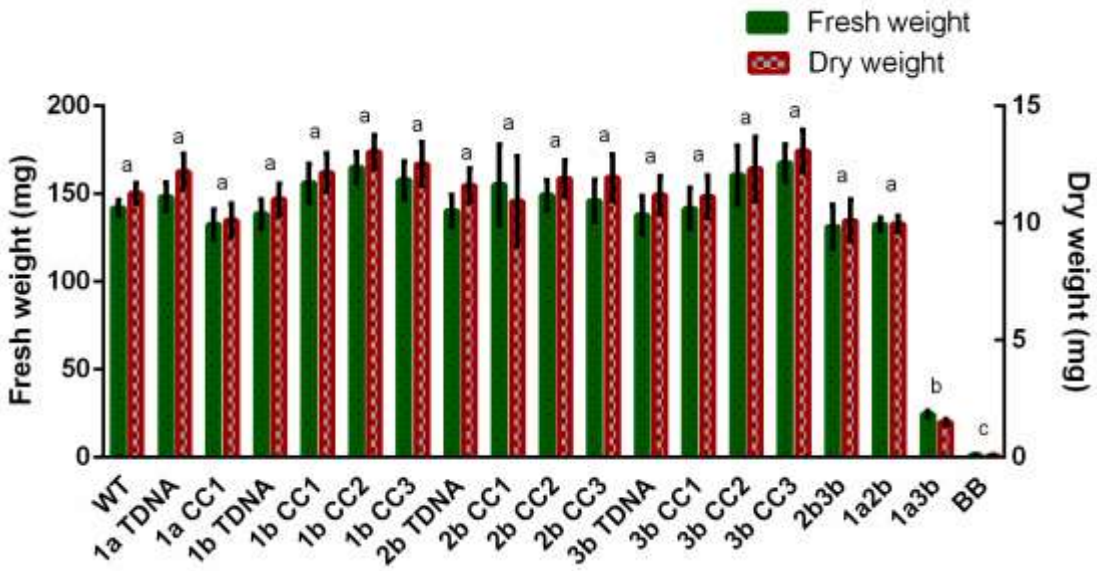
Fresh weight
Dry weight
Fresh weight (mg)
Dry weight (mg)
200
150
100
50
0
15
10
5
0
WT
1a TDNA
1a CC1
1b TDNA
1b CC1
1b CC2
1b CC3
2b TDNA
2b CC1
2b CC2
2b CC3
3b TDNA
3b CC1
3b CC2
3b CC3
2b3b
1a2b
1a3b
BB

B

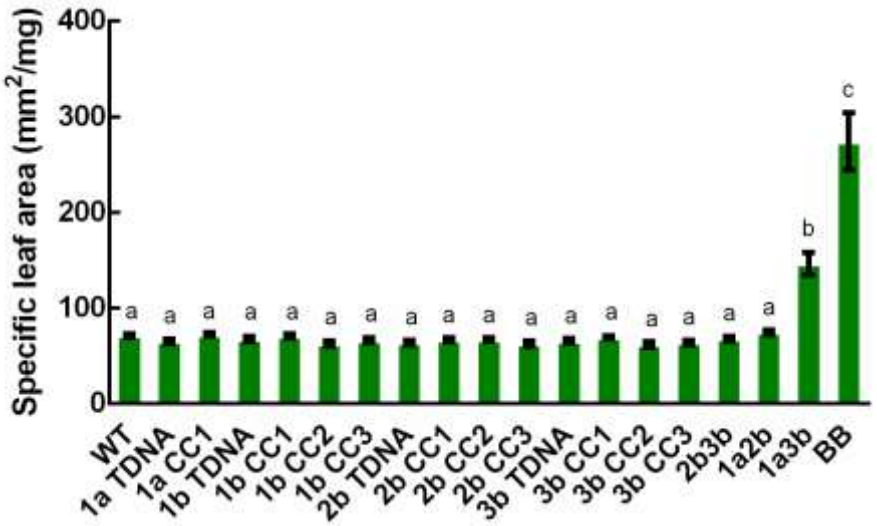
Specific leaf area (mm²/mg)
400
300
200
100
0
WT
1a TDNA
1a CC1
1b TDNA
1b CC1
1b CC2
1b CC3
2b TDNA
2b CC1
2b CC2
2b CC3
3b TDNA
3b CC1
3b CC2
3b CC3
2b3b
1a2b
1a3b
BB

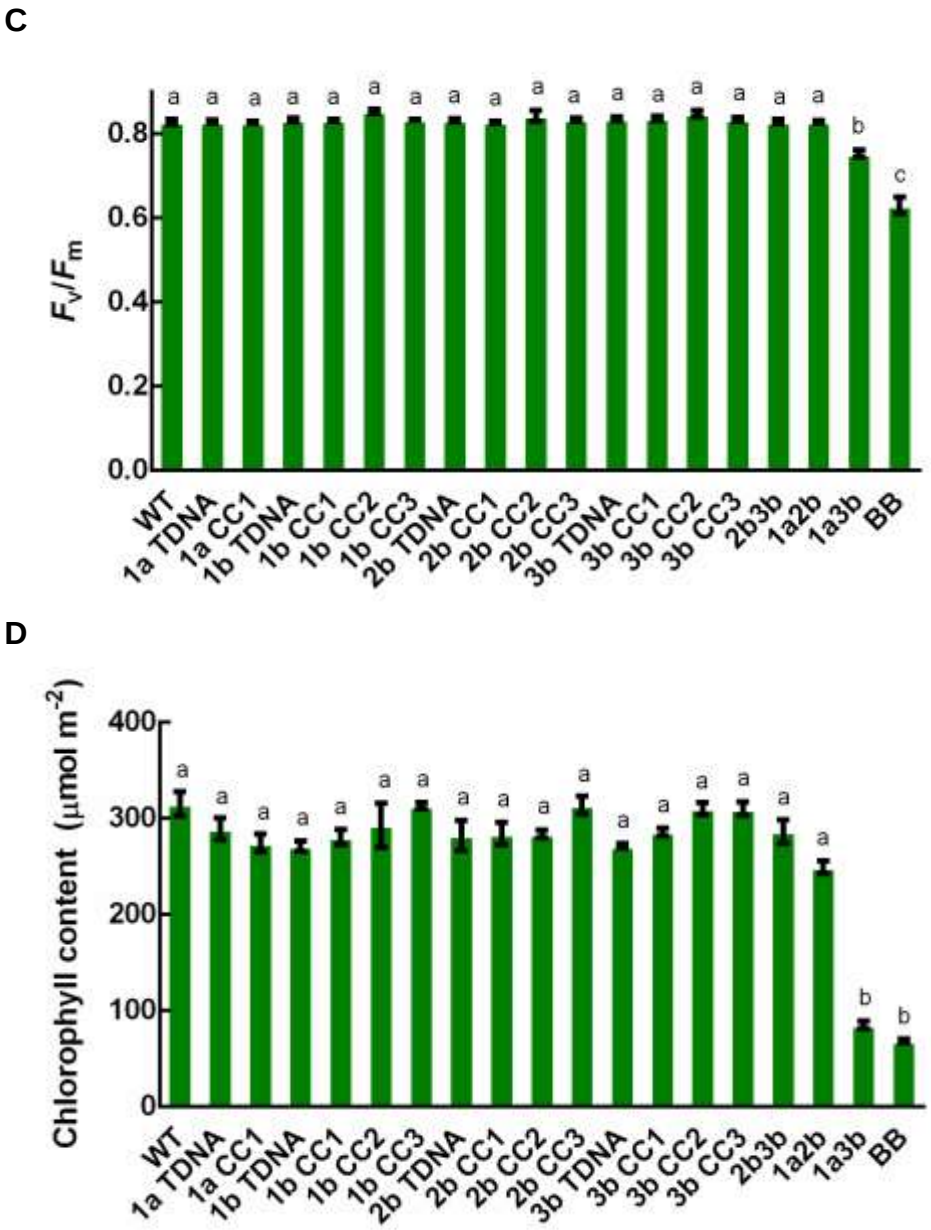

Figure 4.14. Phenotype of *rbcs* KO mutant plants. A) Fresh and dry weight, B) specific leaf area, C) maximum potential quantum efficiency of PSII (F_v/F_m) and D) chlorophyll content per area. The values represent mean ± SEM of measurements made on 8-15 samples for fresh weight, dry weight and specific leaf area and four samples for chlorophyll content and F_v/F_m. Different letters above the bars indicate significant difference ($P < 0.05$) as determined by ANOVA followed by Tukey's HSD tests.

A light response curve test (*A*/ photosynthetically active radiation (PAR) curve, ambient CO_2 and varying light levels) was performed on WT plants to determine the saturating light level for Arabidopsis grown under standard conditions. The rate of CO_2 assimilation (*A*) increased rapidly from 0-400 µmol photon m^{-2} s^{-1} and started to plateau afterwards (**Figure 4.15A**). Assimilation rates rose by less than 10% from 400-1,800 µmol photon m^{-2} s^{-1}, but showed no indication of photoinhibition. Thus, 1,800 µmol photon m^{-2} s^{-1} was chosen to as the light saturating condition for subsequent measurements.

The response of *A* and sub-stomatal CO_2 concentrations (C_i) to changing ambient CO_2 concentration (C_a) under saturating light (A/C_i curves) was measured for all KO mutant lines grown under standard conditions (**Figure 4.15 B-F**) as well as key photosynthetic variables (**Table 4.4**) and their correlation to *RbcS* content (**Figure 4.16**) were derived from these curves. Single *rbcs* KO mutants for 1A and 3B showed a significant reduction in the maximum rate of Rubisco carboxylation ($V_{c,max}$) and the maximum photosynthetic electron transport rate (J_{max}) compared to WT plants. In contrast, *1b* mutants were similar to WT. Interestingly, 2b CC lines had lower J_{max} than WT but not for the T-DNA line. Double mutants *1a2b* and *2b3b* showed similar levels for $V_{c,max}$ compared to *1a* mutants, and similar levels for J_{max} compared to *1a* and *3b* mutants. The double mutant *1a3b* showed the greatest reductions among double mutants. However, BigBoi was significantly lower than all other plant lines, with $V_{c,max}$ and J_{max} at *ca*. 10% and 5% of WT values, respectively, indicating less Rubisco activity in BigBoi. The values for mitochondrial respiration in the light (R_d) and stomatal conductance (g_s) were not significantly between WT and mutants.

A

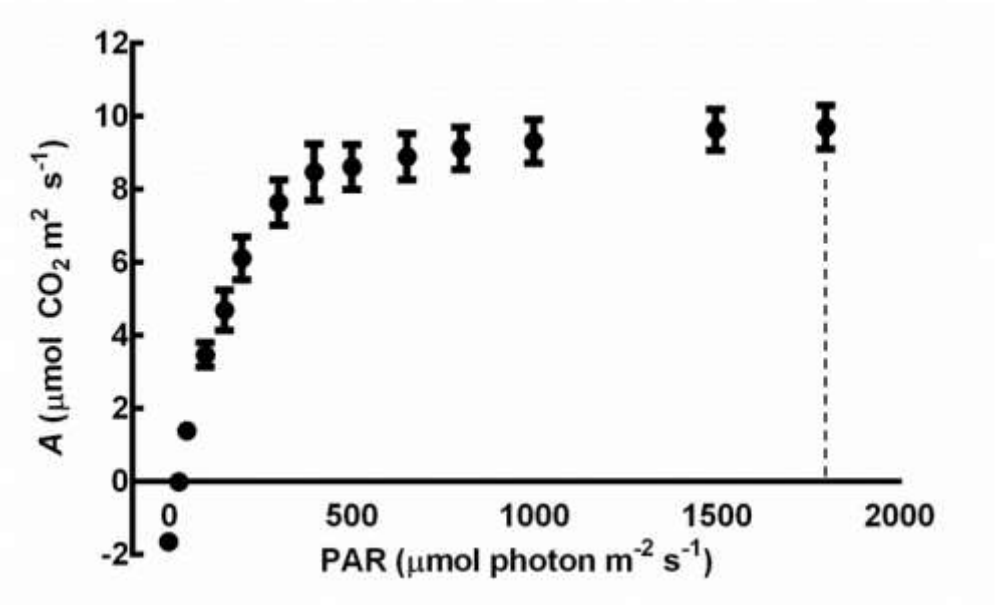
12
10
8
6
4
2
0
-2
A (μmol CO2 m2 s-1)
0
500
1000
1500
2000
PAR (μmol photon m-2 s-1)

B

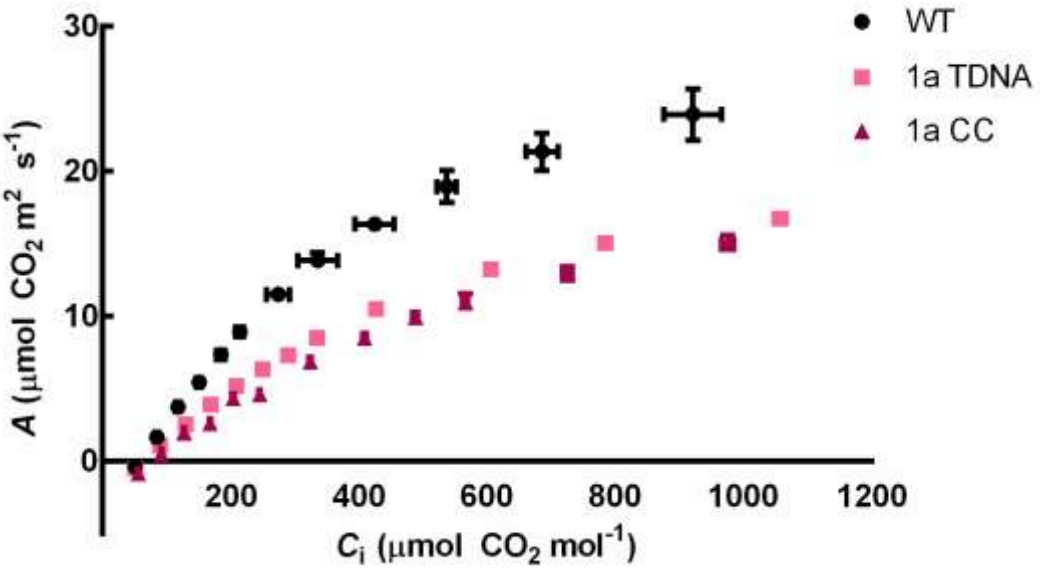
WT
1a TDNA
1a CC
30
20
10
0
A (μmol CO2 m2 s-1)
200
400
600
800
1000
1200
Ci (μmol CO2 mol-1)

C

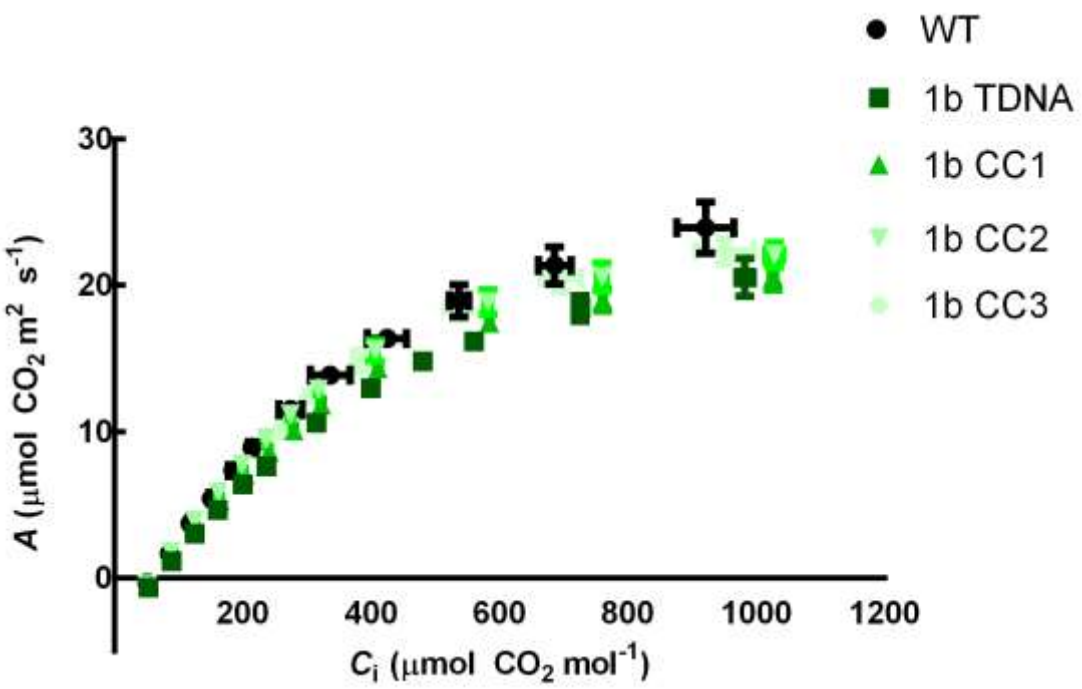
WT
1b TDNA
1b CC1
1b CC2
1b CC3
30
20
10
0
200
400
600
800
1000
1200
A (μmol CO2 m2 s-1)
Ci (μmol CO2 mol-1)

D

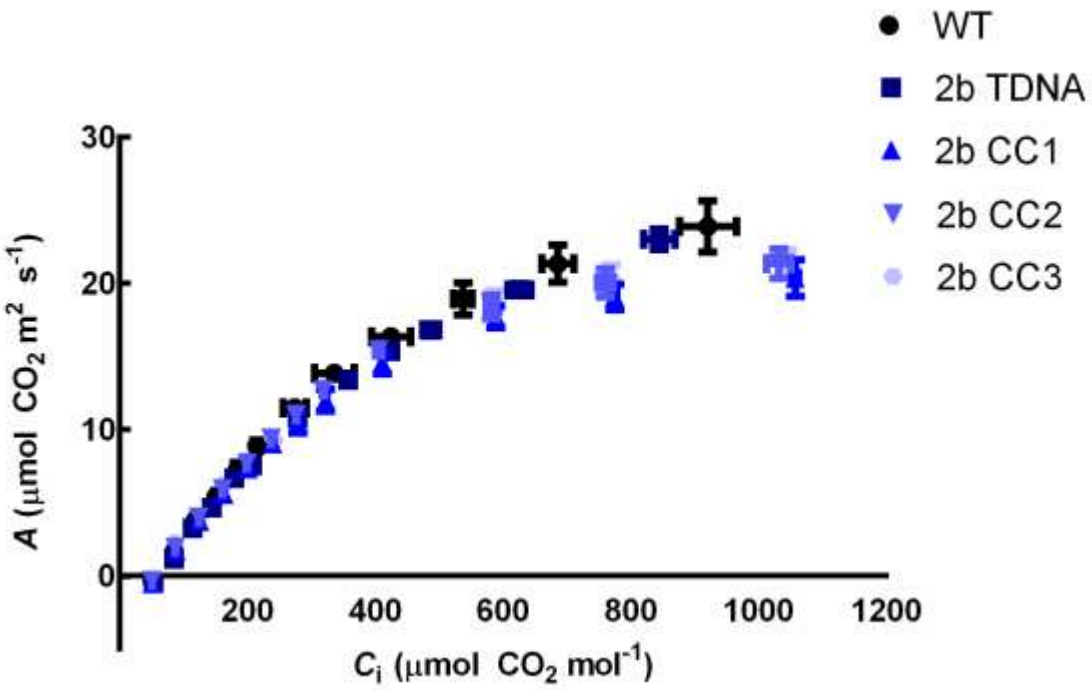
WT
2b TDNA
2b CC1
2b CC2
2b CC3
30
20
10
0
200
400
600
800
1000
1200
A (μmol CO2 m2 s-1)
Ci (μmol CO2 mol-1)

E

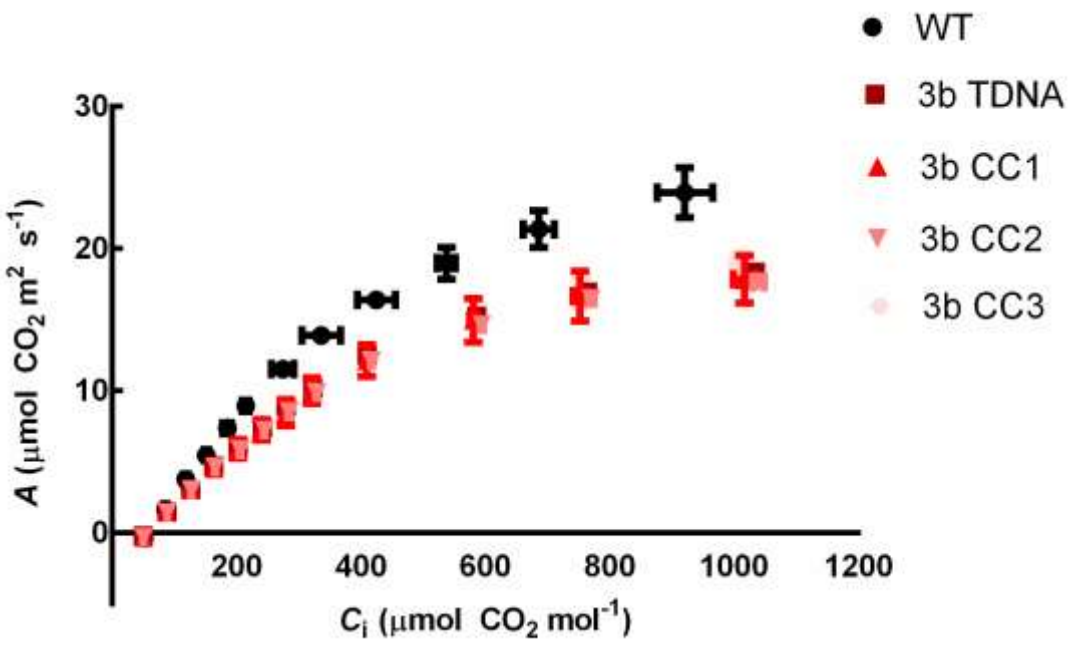
WT
3b TDNA
3b CC1
3b CC2
3b CC3
30
20
10
0
200
400
600
800
1000
1200
A (μmol CO2 m2 s-1)
Ci (μmol CO2 mol-1)

F

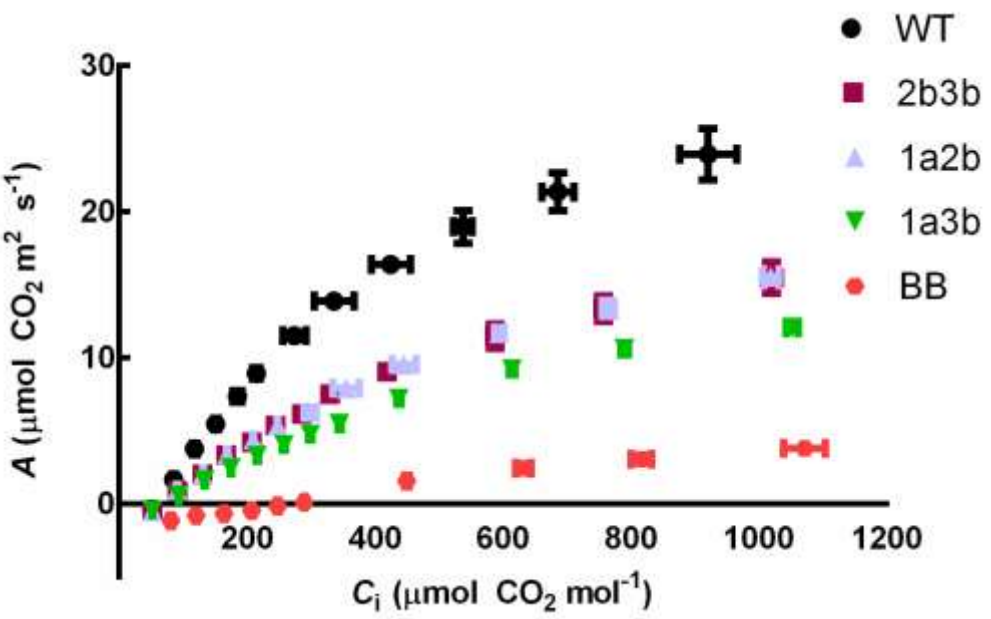
WT
2b3b
1a2b
1a3b
BB
30
20
10
0
200
400
600
800
1000
1200
A (μmol CO2 m2 s-1)
Ci (μmol CO2 mol-1)

Figure 4.15. Photosynthesis response curves for WT and *rbcs* KO mutants. Measurements were made on fully expanded sixth or seventh leaf of 37- to 47 DAG non-flowering rosettes for WT and mutants and 80-d-old nonflowering rosette for BigBoi. Relative humidity was maintained at 65 ± 3% and 25ºC. A) *A*/PAR curve showing the response of CO_2 assimilation rate to different light levels at ambient CO_2 level of 400 µmol mol^{-1} of WT plants. A/C_i curves showing the response of net CO_2 assimilation to different sub-stomatal concentration of CO_2 (C_i) under saturating light (1800 µmol photon m^{-2} s^{-1}, indicated by the dash line) for B) *1a* KO mutants, C) *1b* KO mutants, D) *2b* KO mutants, E) *3b* KO mutants and F) double KO mutants and BigBoi. Each value represents mean ± SE of measurements made on individual leaves from three to four different rosettes.

Table 4.4. Variables derived from photosynthetic response curves, based on gas exchange analysis of 37- to 47-d-old plants. Values are mean ± SE of measurements made on three or four leaves from different plants (as shown in **Figure 4.15**). Values followed by the same letters in the same column are not significantly different ($P < 0.05$) as determined by Tukey's test. $V_{c,max}$, maximum rate of Rubisco carboxylation; J_{max}, maximum electron transport rate; R_d, mitochondrial respiration in the light. G_s, Stomatal conductance at 400 ppm CO_2.

	$V_{c,max}$ (mmol e^- m^{-2} s^{-1})	J_{max} (mmol CO_2 m^{-2} s^{-1})	R_d (mmol CO_2 m^{-2} s^{-1})	g_s (mmol CO_2 m^{-2} s^{-1})
WT	53.27 ± 1.20 [a]	100.40 ± 5.66 [a]	1.08 ± 0.38 [a]	0.25 ± 0.03 [a]
1a TDNA	31.01 ± 1.96 [c,d]	66.85 ± 2.78 [c]	1.38 ± 0.19 [a]	0.21 ± 0.01 [a]
1a CC1	33.82 ± 1.05 [c,d]	73.06 ± 2.99 [b,c]	0.93 ± 0.03 [a]	0.24 ± 0.03 [a]
1b TDNA	44.15 ± 1.49 [a,b]	89.29 ± 4.70 [a,b]	1.29 ± 0.13 [a]	0.24 ± 0.01 [a]
1b CC1	45.75 ± 1.56 [a,b]	89.45 ± 4.52 [a,b]	0.91 ± 0.06 [a]	0.29 ± 0.01 [a]
1b CC2	51.37 ± 2.80 [a]	92.26 ± 3.13 [a,b]	1.07 ± 0.14 [a]	0.30 ± 0.02 [a]
1b CC3	49.07 ± 3.35 [a]	95.00 ± 3.00 [a,b]	0.72 ± 0.09 [a]	0.24 ± 0.02 [a]
2b TDNA	49.96 ± 1.76 [a]	99.71 ± 2.85 [a]	1.22 ±0.13 [a]	0.23 ± 0.07 [a]
2b CC1	47.71 ± 3.21 [a]	85.62 ± 3.64 [b,c]	0.99 ± 0.14 [a]	0.24 ± 0.04 [a]
2b CC2	49.52 ± 1.25 [a]	89.45 ± 3.66 [b,c]	0.79 ± 0.08 [a]	0.30 ± 0.01 [a]
2b CC3	49.17 ± 2.10 [a]	89.74 ± 3.09 [b,c]	0.69 ± 0.07 [a]	0.30 ± 0.04 [a]
3b TDNA	38.21 ± 3.09 [b,c]	77.96 ± 2.45 [b,c]	0.65 ± 0.07 [a]	0.26 ± 0.01 [a]
3b CC1	37.47 ± 3.53 [b,c]	76.38 ± 6.97 [b,c]	0.66 ± 0.06 [a]	0.25 ± 0.03 [a]
3b CC2	39.09 ± 1.35 [b,c]	78.62 ± 1.64 [b,c]	0.73 ± 0.01 [a]	0.27 ± 0.01 [a]
3b CC3	38.46 ± 2.63 [b,c]	79.61 ± 4.24 [b,c]	0.89 ± 0.10 [a]	0.26 ± 0.01 [a]
2b3b	29.09 ± 1.76 [d]	69.25 ± 4.37 [b,c]	0.88 ± 0.07 [a]	0.25 ± 0.02 [a]
1a2b	29.09 ± 1.31 [d]	69.25 ± 2.71 [b,c]	0.88 ± 0.11 [a]	0.26 ± 0.01 [a]
1a3b	21.33 ± 1.15 [e]	52.43 ± 2.58 [c]	0.71 ± 0.08 [a]	0.25 ± 0.01 [a]
BB	4.92 0.42 [f]	12.51 ± 0.98 [d]	1.33 ± 0.09 [a]	0.22 ± 0.04 [a]

A

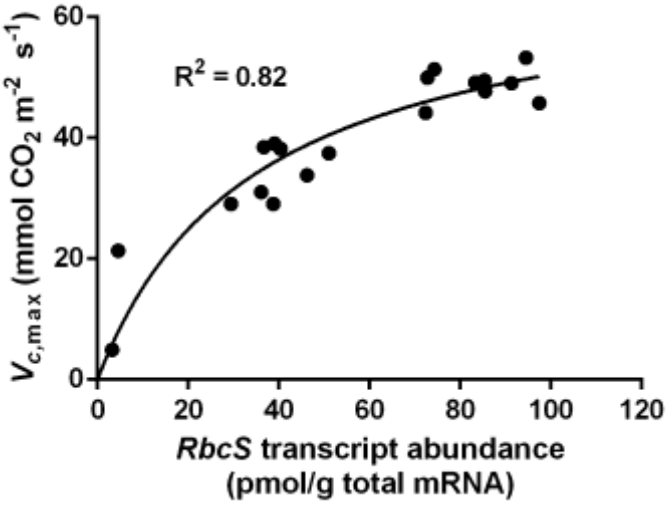

B

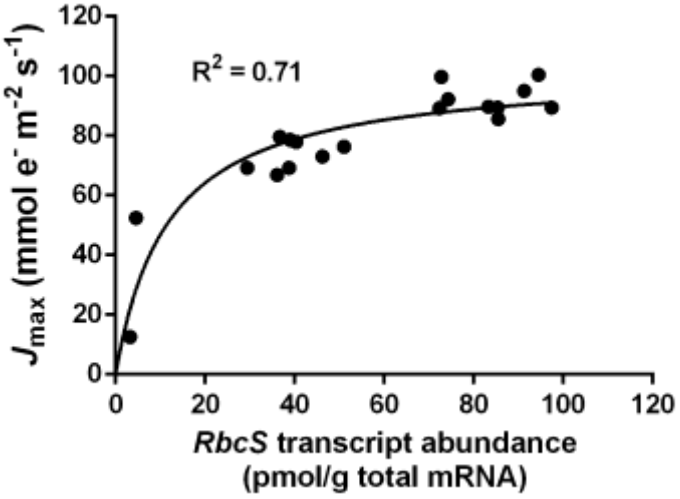

Figure 4.16.Correlations between *RbcS* transcript abundance and derived photosynthetic parameters. A) A correlation between *RbcS* transcript level and $V_{c,max}$ and B) a correlation between *RbcS* transcript level and J_{max}. A parabolic curve was fit to data points and R^2 values were calculated**.**

Further analyses were performed to determine if each SSU has different effects on Rubisco catalytic properties (**Figure 4.17)**. This was done by dividing *A* by Rubisco content for each WT and *rbcs* line. The results showed that *A* per Rubisco content was *ca* 35 µmol CO_2 m^2 S^{-1} per g m^{-2} for WT, *1b*, *2b*, *3b* and *2b3b*, but higher in *1a*, *1a2b*, *1a3b* and especially BB. The higher *A* per Rubisco content suggested that 1A and 1B may have different effects on Rubisco catalytic properties than 2B and 3B.

A

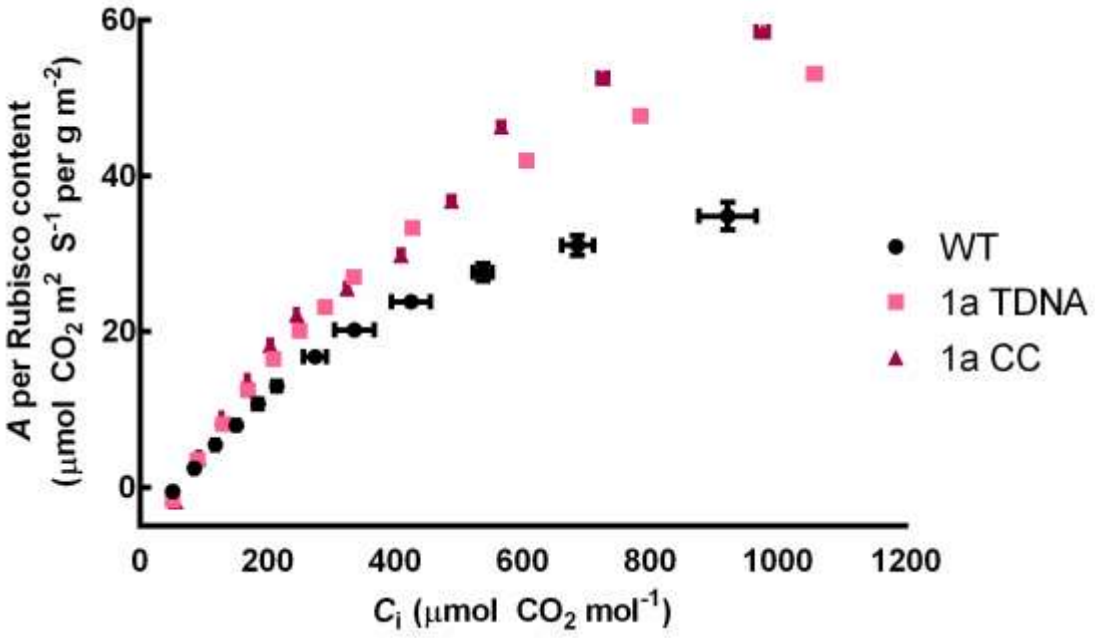

B

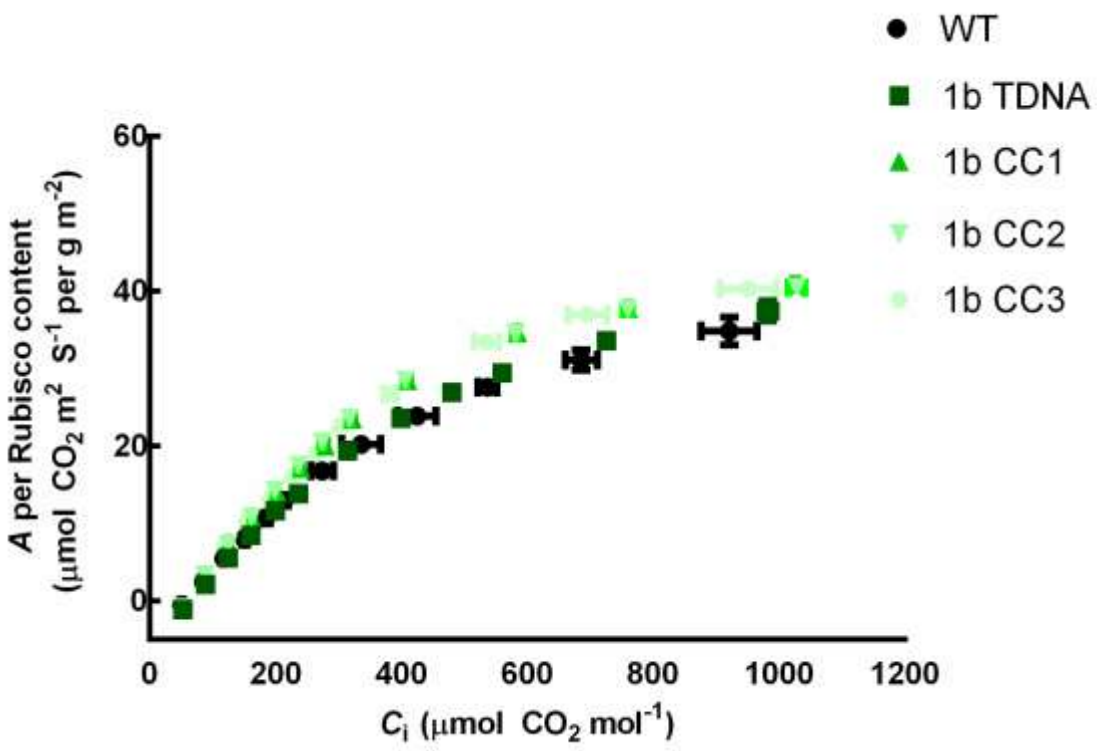
WT
1b TDNA
1b CC1
1b CC2
1b CC3
A per Rubisco content
(μmol CO2 m2 S-1 per g m-2)
60
40
20
0
0
200
400
600
800
1000
1200
Ci (μmol CO2 mol-1)

C

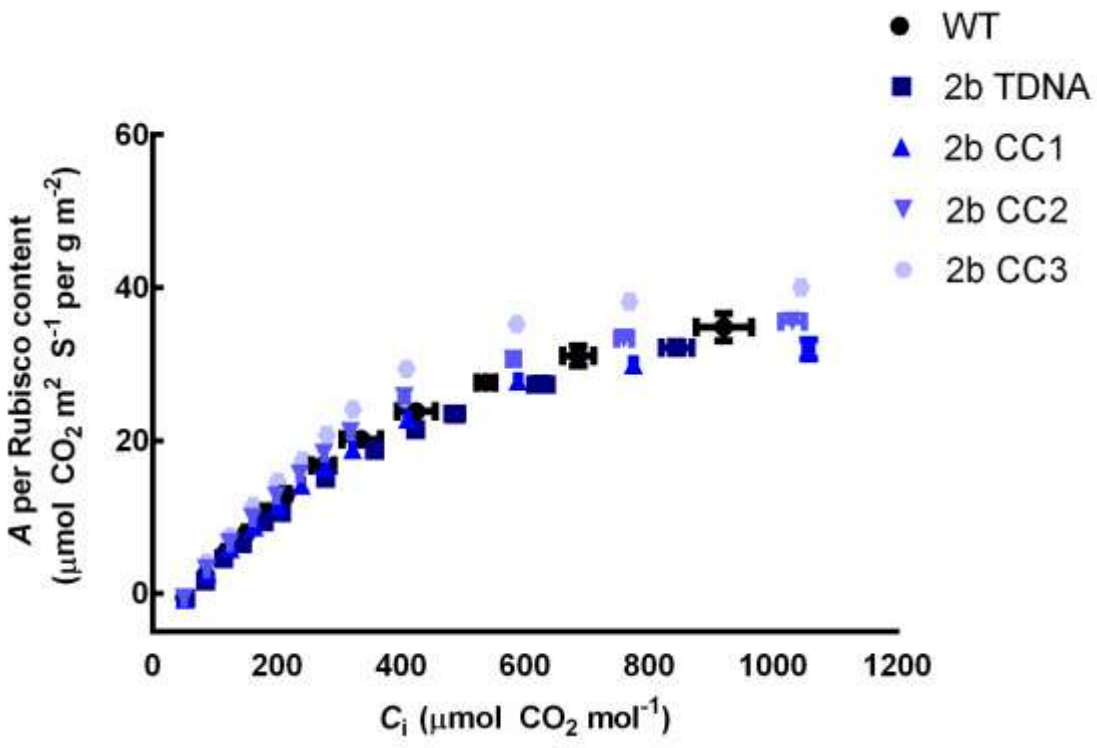
WT
2b TDNA
2b CC1
2b CC2
2b CC3
A per Rubisco content
(μmol CO2 m2 S-1 per g m-2)
60
40
20
0
0
200
400
600
800
1000
1200
Ci (μmol CO2 mol-1)

D

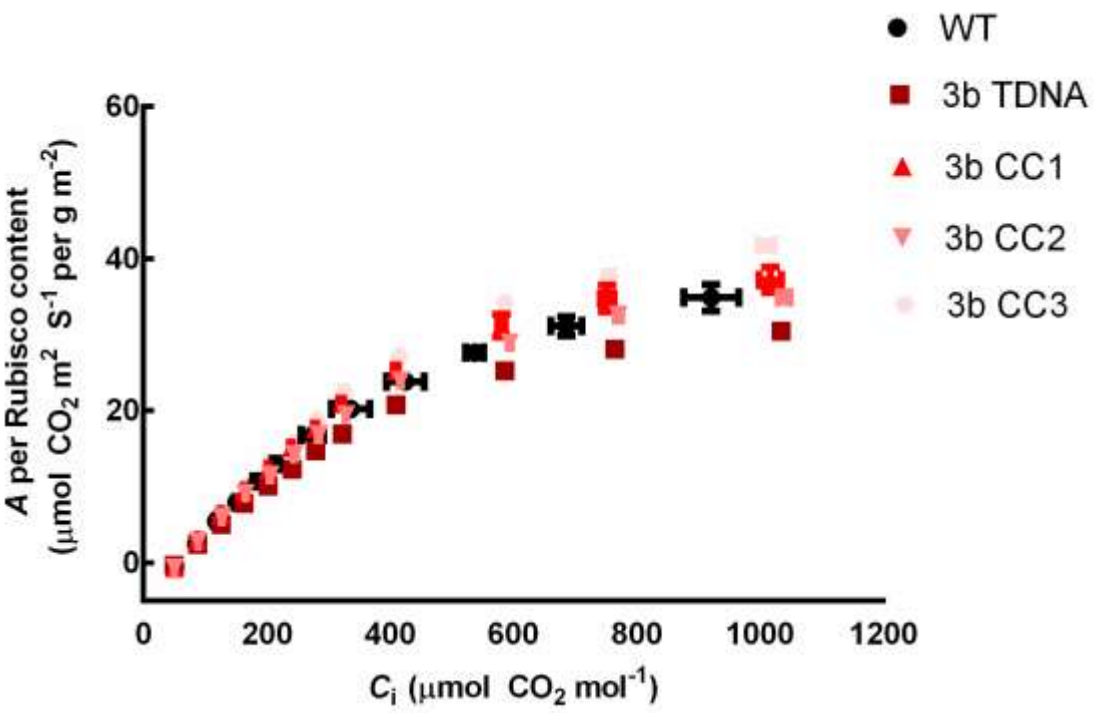
WT
3b TDNA
3b CC1
3b CC2
3b CC3
A per Rubisco content
(µmol CO2 m2 S-1 per g m-2)
Ci (µmol CO2 mol-1)
0
20
40
60
0
200
400
600
800
1000
1200

E

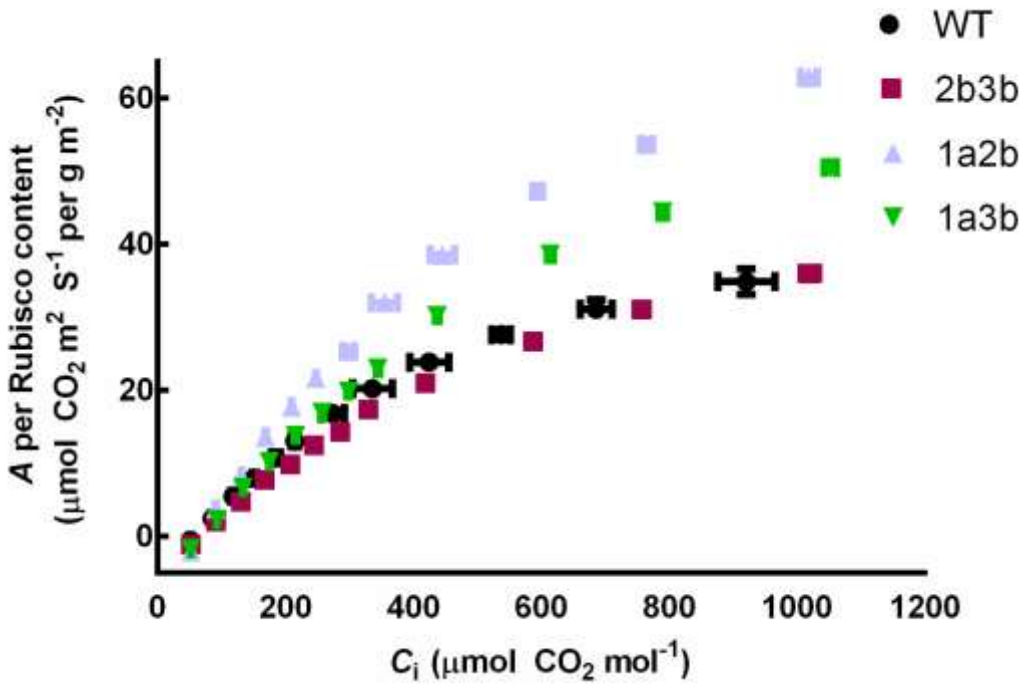
WT
2b3b
1a2b
1a3b
A per Rubisco content
(µmol CO2 m2 S-1 per g m-2)
Ci (µmol CO2 mol-1)
0
20
40
60
0
200
400
600
800
1000
1200

F

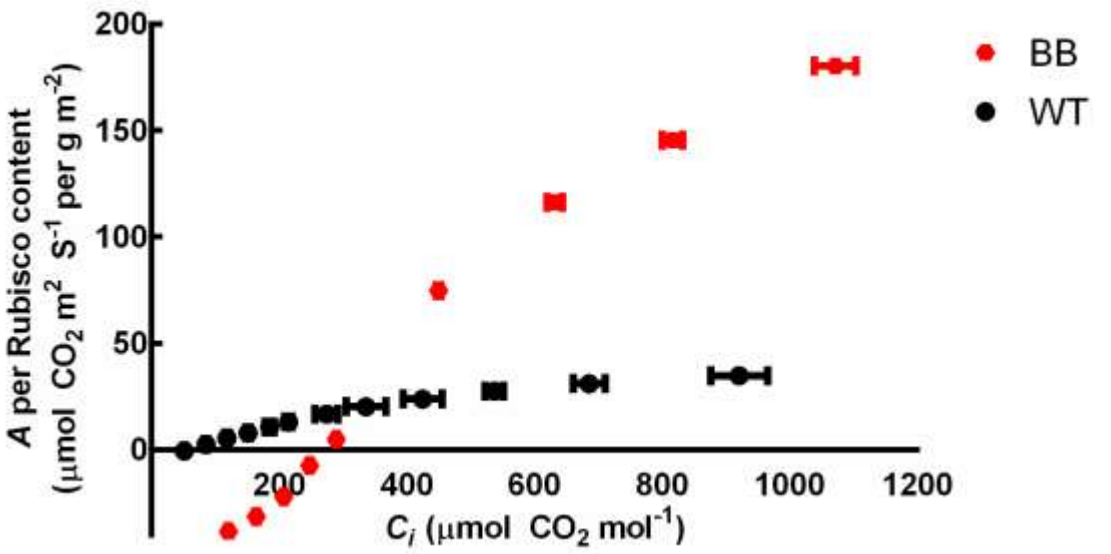

Figure 4.17. Photosynthetic response curves for WT and *rbcs* KO mutants per Rubisco content. The data were derived from the A/C_i curve divided by Rubisco content for A) *1a* KO mutants, B) *1b* KO mutants, C) *2b* KO mutants, D) *3b* KO mutants, E) double KO mutants and F) BigBoi.

Discussion

CRISPR/Cas9 is a versatile tool that has been successfully used for genetic editing in a wide variety of plant species (reviewed in Khumsupan *et al.*, 2019). Although the uptake of CRISPR/Cas9 in plant biology has increased dramatically in recent years, many aspects concerning efficiency are still unclear, especially as established guidelines for CRISRP/Cas9 for mammalian cells are not necessarily applicable to plants (Liang *et al.*,

2016; Hahn and Nekrasov 2019). For instance, 60-80% G/C content of gRNAs confers the higher rate of editing in mammalian cells but 20-80% G/C content was found to be the effective range in plants (Liang *et al.,* 2016). Since stable transformation in plants can be relatively more time-consuming, a transient system to test the gRNA efficiency would be useful to select the most effective gRNA (Li *et al.,* 2013; Durr *et al.,* 2018).

Protoplasts transient expression systems have been robust models to test the efficiency of CRISPR/Cas9 approaches (Li *et al.,* 2013; Durr *et al.,* 2018). In this study, protoplasts were used to test the efficiency of gRNA pairs and the results mostly reflected what was observed *in planta*. For most gRNA pairs that produced deletion bands except 1B pairs, deletions were observed *in planta* (**Figure 4.2**). In addition, for pairs that did not produce deletion bands in protoplasts, namely 2B pair 1 and 3B pair 2, deletion bands were not detected *in planta* and nor were indels in T1 plants (**Figure 4.2** and **Table 4.1**). Although large deletions were found in T1 progeny, they were all chimeric and were not detected in T2 plants that were screened. Since a cluster of edited chimeric cells can give rise to germ cells and therefore can be heritable, a large number of transgene-free plants needs to be screened. For example, Durr *et al.* (2018) reported a low rate heritability for a chimeric T1 parental line as only two edited plants were found out of 396 transgene-free T2 progeny.

Using two gRNAs to induce a large deletion has been used successfully in various plant species including rice, Arabidopsis, tobacco, tomato and wheat (Xie *et al.,* 2015; Ordon *et al.,* 2016; Cermak *et al.,* 2017). The main advantage of the method is the ease of detection as a large DNA region is deleted and readily detectable by PCR. However, the

efficiency of large deletions in Arabidopsis was found to be lower than 1% when the deletion size was more than 5 kb and deletion sizes of below 100 bp was found more frequently and likely to be heritable (Ordon *et al.,* 2016). Recently, Ordon *et al.,* (2019) improved the rate of heritability for large deletions in Arabidopsis by 25-fold through the use of germ-line specific promoters RPS5a and DD45. The use of these promoters to drive Cas9 may be a useful modification for the current work to improve the frequency of mutagenesis and heritability for large deletions.

This study has shown that CRISPR/Cas9 editing was able to induce stable mutations in the *RbcS* genes and a library of *rbcs* KO mutants have been generated. Moreover, the editing method was able to overcome the inherent limitations of T-DNA insertion lines as closely linked genes were successfully edited. As a result, novel mutants including *2b3b* and BigBoi were generated. In addition, the CRISPR/Cas9 KO mutants are less likely to contain background mutations or chromosomal rearrangement as found in T-DNA insertion lines (Nacry et al. 1998; Clark and Krysan 2010; Hahn and Nekrasov 2019). As outlined in Chapter 3, the *1a2b* T-DNA line contained background mutations that were rid of after back-crossing with WT. As the *1a2b* line was generated from crossing *1a* and *2b* T-DNA lines, background mutations could be present in *1a* and/or *2b*. The presence of the background mutations attributed to the previously observed phenotype of the old *1a2b* line including smaller rosette and silique size, and could be responsible for differences in measurements between the *rbcs* T-DNA lines and their respective CC lines such as the difference seen in J_{max} in the *2b* KO mutant lines.

The difficulty in knocking out 1B in the *1a2b* and *1a3b* T-DNA lines adds to a line of evidence in Chapter 3 that knocking out 1A and 1B in conjunction may be lethal. As knocking out other genes in the B-subfamily together with 1A was possible, knocking out 1B should pose no challenge especially when it is the least expressed isoform. However, the inability to knock out 1B with 1A suggests that both genes do not only contribute to the SSU pool but may also play specialised roles in development. Organ and tissue-specific *RbcS* expression has been reported in other plant species including tomato and maize although knock-out studies have yet to be performed to assess the contribution of these *RbcS* genes to survivability (Wanner and Gruissem 1991; Ewing et al. 1998). Further research in Arabidopsis may explore how the lack of 1A and 1B impacts fertility by performing a germination test to see if the *1a1b* homozygote was produced as seeds and if the seeds were viable.

The NHEJ event that follows the DBS induced by Cas9 could result in mutations in the form of PMs and/or indels. In this study, most indels were small, ranging from up to 4 bp insertions to 7 bp deletions. Small indels are prominent products of the canonical NHEJ pathway, which involves the degradation of 5' and 3' regions to generate 4-nucleotide overhangs for relegation (Chang *et al.,* 2017). The less frequent NHEJ pathway, called alternative-NHEJ, involves a larger degradation of DBS ends (>20 nucleotides) and results in a larger deletion (Pannunzio *et al.,* 2014). The larger deletions of 45 bp in the 1A gene or 147 bp in the 3B gene could be attributed to the alternative-NHEJ pathway. The higher frequency of small indels than larger deletions was due to the canonical NHEJ pathway being more active (Kozak *et al.,* 2009). Improving the rate of

alternative-NHEJ pathway, which resulted in higher frequency of larger deletions, was achieved by knocking out genes involved in the canonical NHEJ pathway such as KU70 and LIG4 (Qi *et al.,* 2013)

The resulting small and pale plants generated by the gRNA pairs that target 1B-3B locus with no apparent mutation in the *RbcS* genes implies that off-target mutagenesis had occurred. Off-target effects have been reported in mouse and human cell lines (Fu *et al.,* 2013; Hsu *et al.,* 2013; Kempton and Qi 2019), but are considered rare in plants (Hahn and Nekrasov 2019). Numerous studies in different plant species where whole genome sequencing and sequencing of potential target sites were performed have shown no occurrence of off-target activity given that gRNAs were completely specific to the target site (Xie and Yang 2013; Hahn *et al.,* 2017; Li *et al.,* 2019; Young *et al.,* 2019). The evidence of off-target activity suggests that the 1B-3B gRNA pairs may have disrupted other genes despite their specificity to that locus. Further investigation such as Sanger sequencing of highly homologous target sequences or whole genome sequencing could be performed to pinpoint the mutations.

Gene editing via CRISPR/Cas9 resulted in a decrease in mRNA abundance of the target gene (**Figure 4.12A**). For major isoforms such as 1A and 3B, the reduction in the mRNA also led to an overall decrease in the *RbcS* transcript, $V_{c,max}$ and J_{max}. The reduction of mRNA was likely due to the presence of an early stop codon emerged from frame-shift mutations, which consequently led to the degradation of mRNA through the nonsense-mediated decay process (Hug *et al.,* 2015). However, the reduction in *RbcS* transcript did not lead to the same reduction in the *RbcL* transcript. This is because Arabidopsis *RbcL*

transcript is controlled post-transcriptionally at the translation initiation process (Rodermel *et al.,* 1996). Similar to Arabidopsis, *RbcL* synthesis in tobacco was independent of the *RbcS* transcript level as LSU production was subject to assembly state-dependent regulation that operates at the translational level (Wostrikoff and Stern, 2007).

The mutants generated from this study were subject to a growth assay to characterise the phenotype under the standard conditions for Arabidopsis. Growth parameters, chlorophyll content and F_v/F_m of single mutants and *1a2b* and *2b3b* were not significantly different from WT, which is in agreement with previous reports (Izumi *et al.,* 2012; Atkinson *et al.,* 2017). A previously study in tobacco have suggested that the reduction of SSUs to 60% did not result in a growth defect because Rubisco is produced in excess in C3, but reduced growth and photoinhibition was observed when SSU was reduced to below 50% (Quick *et al.,* 1991). In that study, the reduction of Rubisco in *1a*, *3b*, *1a2b* and *2b3b* resulted in a higher activation state of the remaining Rubisco pool and growth was unaffected. Therefore, a growth analysis under a higher light under Rubisco-limiting condition would likely elicit differences in phenotypes in these KO mutants (Lauerer *et al.,* 1993).

The photosynthetic parameters $V_{c,max}$ and J_{max} for the *rbcs* KO mutants were strongly correlated with *RbcS* transcript abundance (R^2 = 0.82 and 0.71, respectively) (**Figure 4.16**). This suggests that the four *RbcS* genes cumulatively contribute to photosynthetic capacity in Arabidopsis. It was previously suggested that the change in composition of native Arabidopsis SSUs would result in the change of catalytic properties as previous studies in Arabidopsis and tobacco have shown that there was no significant

difference in photosynthetic characteristics among *rbcs* mutants (Izumi *et al.,* 2012; Atkinson *et al.,* 2017). However, upon examining localised expression of SSUs, Sawchuck *et al.* (2008) hypothesised that 1B may be able to shift the catalytic properties of Rubisco. This study provided an evidence that supported the proposed hypothesis as the *A* per Rubisco content of BigBoi is higher than that of WT. In addition, it was also found that 1A may also affect Rubisco catalytic properties differently than 2B and 3B. As 1A and 1B contain 8 and 2 substitutions, respectively, relative to 2B and 3B, this observation was not unexpected. Confirming this finding could be done by directly measuring the catalytic properties of Rubisco of BigBoi. Previous studies have shown that native SSUs can modify catalytic properties of Rubisco. For example, in rice leaf blades, an increase in the $k_{cat,c}$ and a decrease in the $S_{c/o}$ of the Rubisco pool was observed when *OsRbcS1* (*RbcS* found only in rice roots) were expressed (Ishikawa *et al.,* 2011; Morita *et al.,* 2014). These evidence suggested that SSUs contribute to the catalytic properties of Rubisco and improving Rubisco activity could be achieved through the modification of SSUs.

Chapter 5 - Effects of environmental conditions to the *RbcS* genes differential expression

Introduction

Multiple lines of evidence suggest that the SSUs not only regulate the translation initiation of the LSU and consequently the level of Rubisco, but also influence the catalytic activity of Rubisco (Khrebtukova and Spreitzer, 1996; Rodermel *et al.*, 1996; Wostrikoff and Stern, 2007; Genkov and Spreitzer, 2009; Suzuki and Makino, 2012; Laterre *et al.*, 2017). The regulation of LSU translation by SSU may be one of the key means for plants to modulate Rubisco content under changing environmental conditions as *RbcS* expression varies under different light wavelengths, temperature, sugar levels and CO_2 concentration, and is under the control of circadian rhythm (Dedonder *et al.*, 1993; Pilgrim and McClung, 1993; Cheng *et al.*, 1998; Gesch *et al.*, 1998; Nielsen *et al.*, 1998; Yoon *et al.*, 2001; Song *et al.*, 2014). In Arabidopsis, the transcript abundance of 1A dominates at low temperatures (10^{o}C) while 3B is reduced. However, at high temperature (30^{o}C), the 3B is the most abundant isoform. The expression pattern of 1B and 2B are similar to that of 3B under different temperatures (Yoon *et al.*, 2001). In terms of light responses, 1A and 3B are the most responsive red and blue light, followed by 2B and 1B is the least responsive to light stimulus (Dedonder *et al.*, 1993). 3B saw the greatest reduction in expression under high CO_2 concentration (1000 µL L^{-1} CO_2) in comparison to ambient CO_2 concentration (400 µL L^{-1} CO_2), followed by 1A, 2B and 1B (Cheng *et al.*, 1998). In addition, *RbcS* expression indirectly correlates with the leaf sugar levels (Nielsen *et al.*, 1998). Altogether, the dynamic transcriptional responses of the SSU family

to various environmental condition results in changes in Rubisco content, which can ultimately affect plant growth.

This chapter aimed to determine the expression of Arabidopsis *RbcS* genes under different environmental conditions and characterise the impact on their absence on growth using *rbcs* KO mutants isolated in Chapter 4. In addition to external environmental conditions, circadian clock was also found to be a major contributor that affects *RbcS* expression (Pilgrim and McClung, 1993). Circadian rhythm anticipates light/dark oscillation within the 24 h period and adjusts the *RbcS* expression to optimise Rubisco production. As the circadian-controlled expression of *RbcS* genes persists through changing environments, we first aimed to abolish the the expression influenced by circadian clock in order to accurately quantify the transcriptional responses of *RbcS* genes under different environmental conditions. This chapter also explored the effects of different environments, namely high light, high temperature and low temperature conditions, on Arabidopsis growth.

Results

Differential expression of RbcS gene family under different environmental conditions

Apart from environmental and metabolic factors, the expression of *RbcS* genes is also controlled by an internal circadian clock (Pilgrim and McClung, 1993). *RbcS* genes oscillates during the 24 h period independent of other factors. To disable the clock and remove circadian rhythm, plants were grown in constant light for seven days to induce

arrhythmicity. After dark adaption for 24 h, plants were exposed to light for 12 h and the changes in expression were quantified (**Figure 5.1**).

A

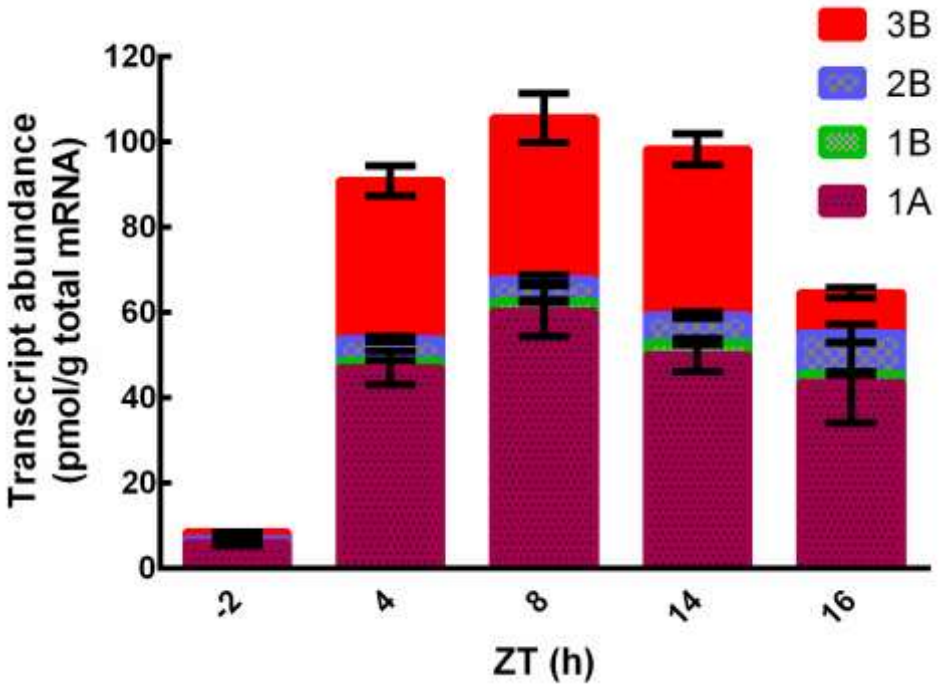

B

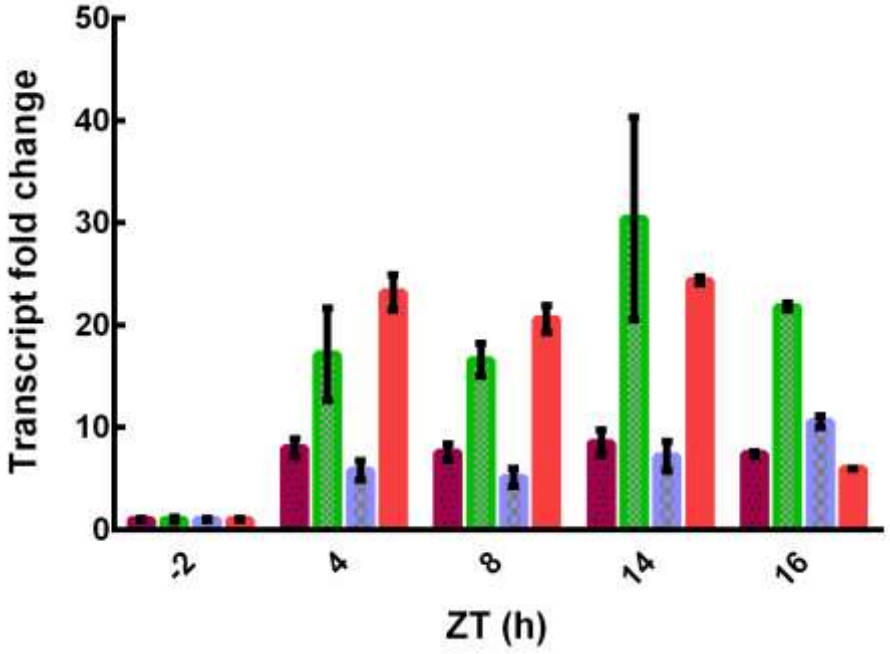
Transcript fold change
50
40
30
20
10
0
2
4
8
14
16
ZT (h)

C

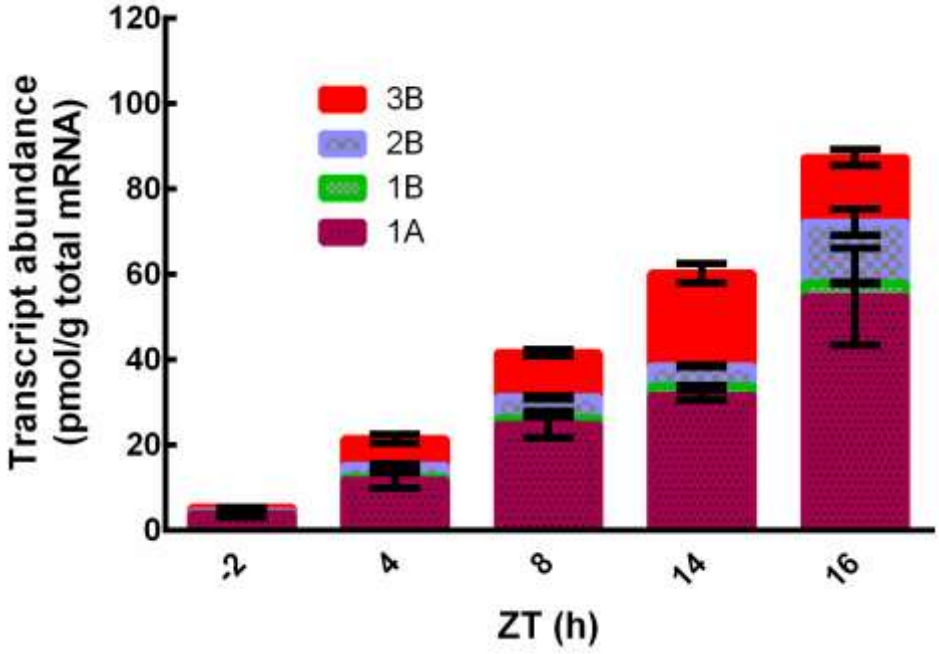
Transcript abundance
(pmol/g total mRNA)
120
100
80
60
40
20
0
3B
2B
1B
1A
2
4
8
14
16
ZT (h)

D

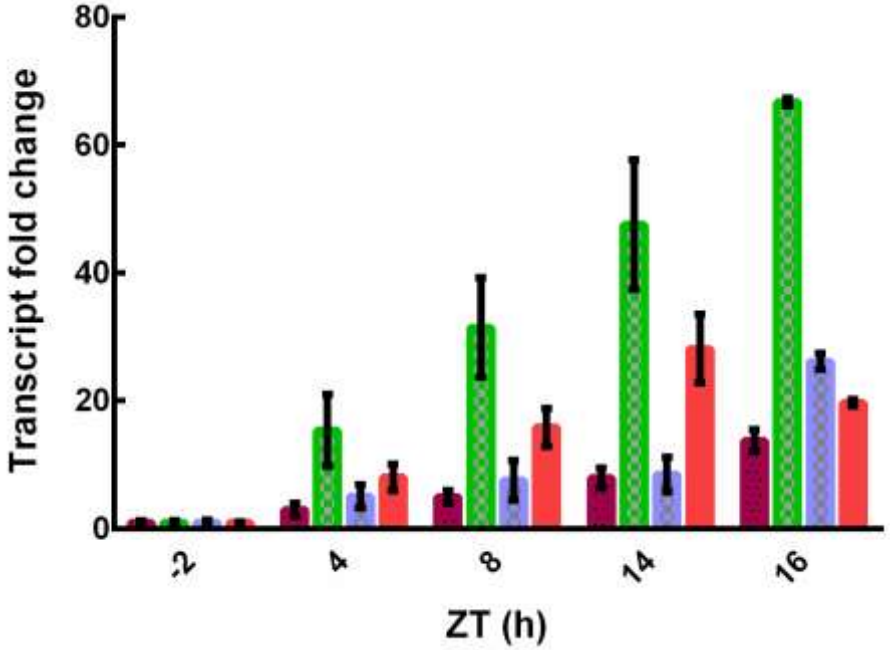
Transcript fold change
80
60
40
20
0
2
4
8
14
16
ZT (h)

E

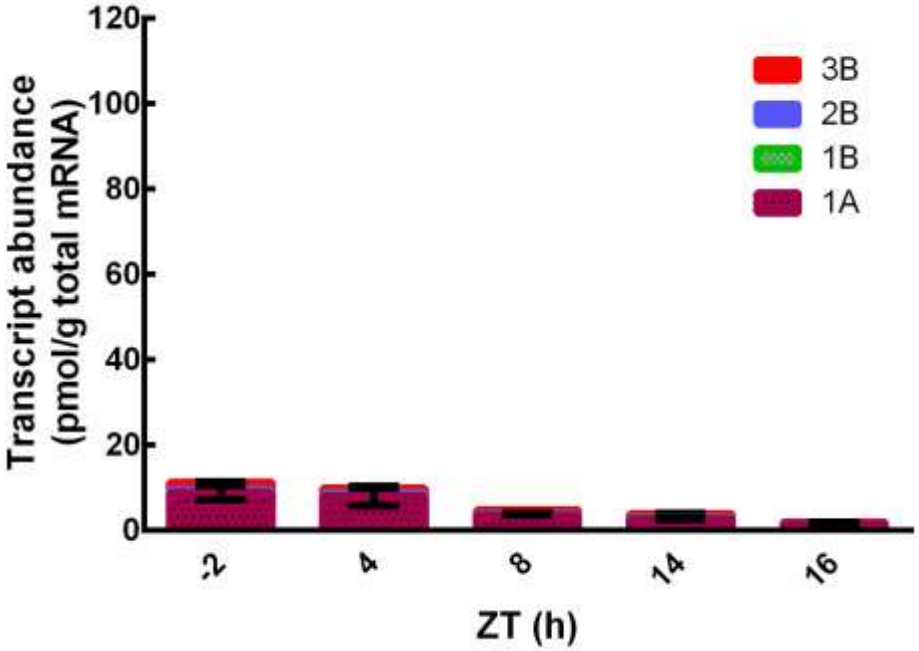
Transcript abundance
(pmol/g total mRNA)
120
100
80
60
40
20
0
3B
2B
1B
1A
2
4
8
14
16
ZT (h)

F

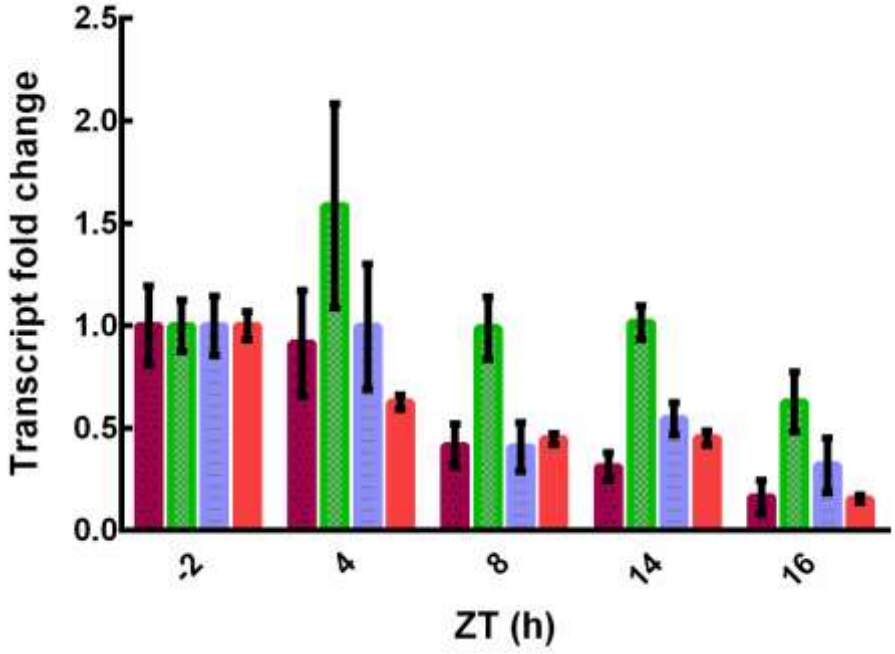

Figure 5.1. Total *RbcS* transcript abundance and fold change in Arabidopsis plants grown under different conditions. Transcript abundance was measured using the synthesised standard plasmid as described in Chapter 3. A) *RbcS* transcript abundance and B) transcript fold change relative to ZT -2 of plants grown under 12 h light : 12 h dark cycle for 15 days (light control). C) *RbcS* transcript abundance and D) transcript fold change relative to ZT -2 of plants grown under 12 h light : 12 h dark cycle for seven days and constant light for additional seven days. Plants were kept in the dark for 24 h before light exposure (experimental group). E) *RbcS* transcript abundance and F) transcript fold change relative to ZT -2 of plants that grown under 12 h light : 12 h dark cycle for seven days and constant light for additional seven days, but were kept in the dark through the experimental period (dark control). Plants in A, B, C and D were exposed to white light at 200 µmol photon m^{-2} s^{-1} and 21ºC for 12 h on day 16 and collected at five time points

shown in zeitgeber time (ZT). Each data point consisted of three biological replicates and each biological replicate contained 25-30 seedlings.

In the control group (i.e. plants with normal circadian oscillation grown under a 12 h light : 12 h dark cycle), the total expression of *RbcS* genes increased to 90 pmol/g after 4 h of light exposure (**Figure 5.1A**). Expression levels appeared to remain relatively constant during the light period and 2 h into the dark period, but showed a decrease after 6 h of darkness. The latter decrease was primarily attributed able to 3B that decreased by 75% followed by 1A, which decreased by 13% relative to the expression at 14 h (**Figure 5.1B**). In contrast to the control group, the increase in expression of *RbcS* genes in the experimental group (i.e. plants grown under constant light) was slower and more linear over time (**Figure 5.1C**). Moreover, the overall levels of expression continued to increase even during the dark period. The observed expression levels were due in part to the continued increase of 1A, 1B and 2B. In contrast, the expression levels of 3B decreased after 6 h of darkness (**Figure 5.1D**). *RbcS* gene 1B showed the largest relative increases in expression in response to white light in both groups (1B had a 66-fold increase at 16 h in the control group and 28-fold increase at 14 h in the experimental group) (**Figure 5.1B, D**) The levels of *RbcS* gene expression in the dark control group (i.e. plants grown under constant light then kept in dark) were significantly lower than in the other two groups (**Figure 5.1E, F**). However, the basal levels of expression observed suggested that circadian rhythm could still be active. To validate that circadian rhythm has been removed in the experimental group, circadian genes (*CCA1*, *PRR7* and *TOC1*) were probed at 4 h, 8 h and 14 h (**Figure 5.2**).

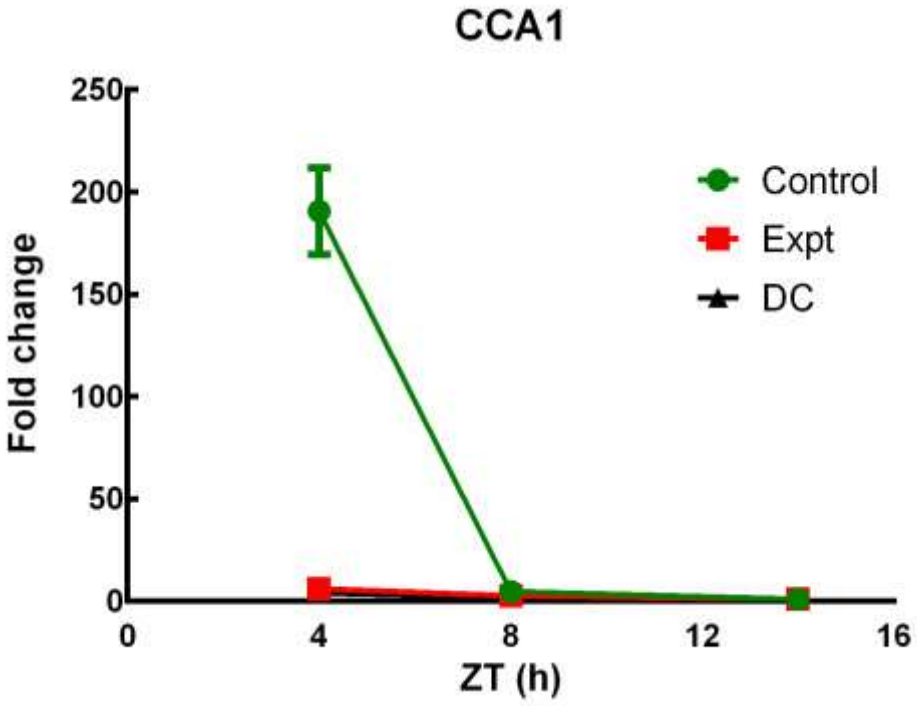
CCA1
250
200
150
100
50
0
Fold change
0
4
8
12
16
ZT (h)
Control
Expt
DC

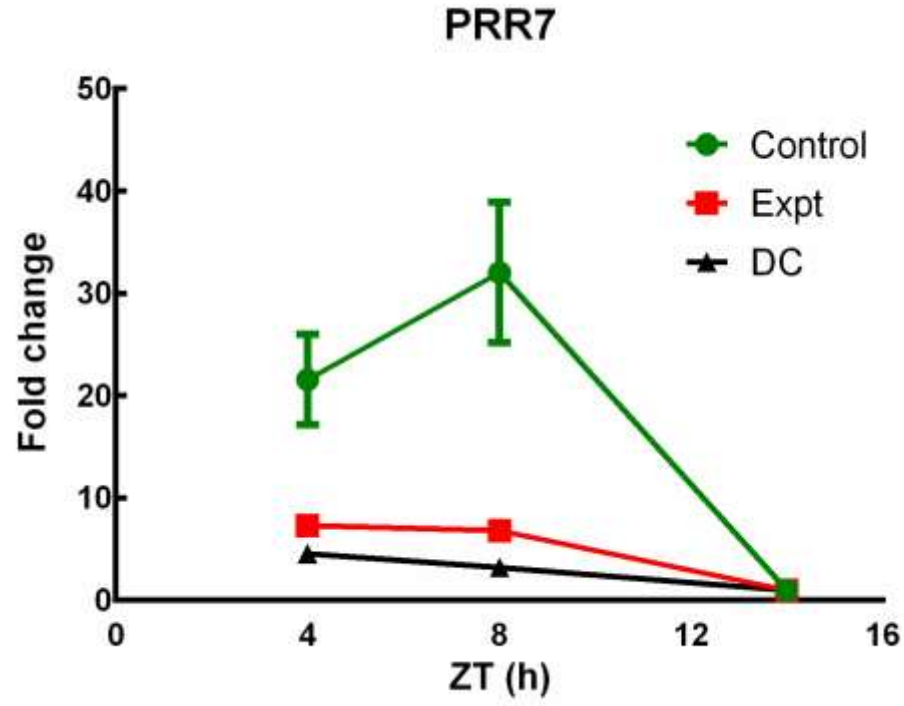
PRR7
50
40
30
20
10
0
Fold change
0
4
8
12
16
ZT (h)
Control
Expt
DC

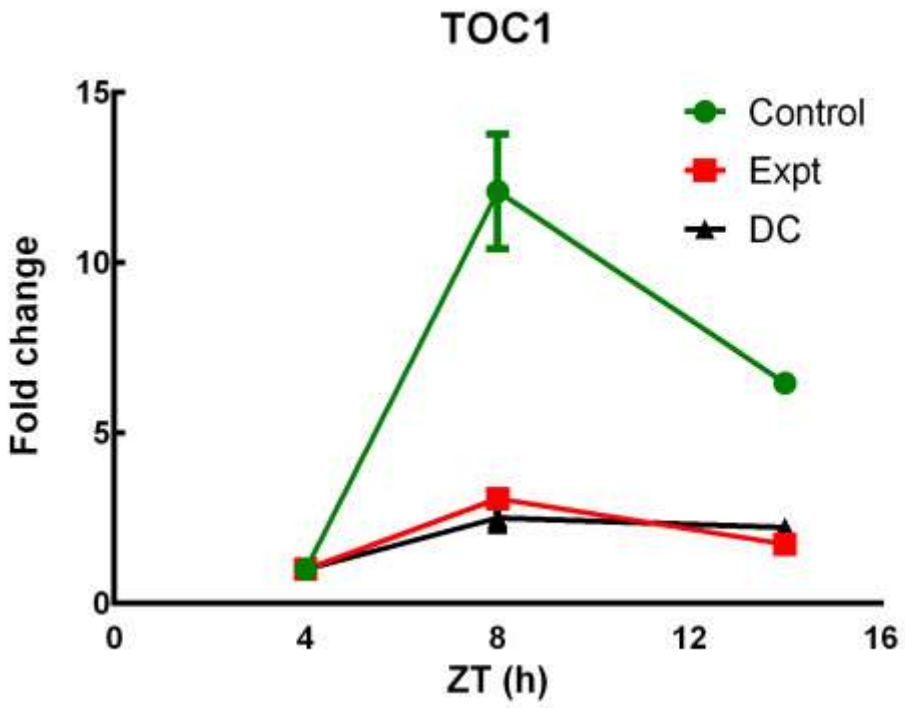

Figure 5.2. Expression profiles of clock genes *CCA1*, *PRR7* and *TOC1*. Transcript abundance was measured using gene-specific primers and relative abundance to the lowest time point (14 h for CCA1 and PRR7, and 4h for TOC1) was calculated. Control plants with normal circadian oscillation were grown under 12 h light : 12 h dark cycle for 15 d. Experimental plants (Expt) were grown under 12 h light : 12 h dark cycle for seven days and constant light for additional seven days. Control and Expt plants were exposed to white light at 200 µmol photon m^{-2} s^{-1} and 21ºC for 12 h. Dark control (DC) plants were grown under 12 h light : 12 h dark cycle for seven days and constant light for additional seven days, but were kept in the dark through the experimental period. Results are shown in over zeitgeber time (ZT). Each data point consisted of three biological replicates and each biological replicate contained 25-30 seedlings.

Quantification of the three clock genes suggested that circadian rhythm in the experimental and dark control groups was significantly dampened, but not completely abolished (**Figure 5.2**). The expressions of *CCA1* (peak expression at dawn), *PRR7* (peak expression in the afternoon) and *TOC1* (peak expression in the late afternoon) were 190-, 32- and 12-fold higher, respectively, in the control group than the experimental group (**Figure 5.2 A, B, C**). Nevertheless, an oscillation of these genes still occurred in both the experimental and dark control groups despite being significantly lower. The continued rhythmicity of these circadian genes suggested that the 7 d light adaption was not sufficient to get rid of circadian rhythm and that *RbcS* expression in the experimental group could still be influenced by circadian clock. Therefore, the arrhythmic clock mutant *prr5/7/9* (Nakamichi *et al.*, 2005) was used to quantify the expression level of *RbcS* genes in response to light (**Figure 5.3**).

A

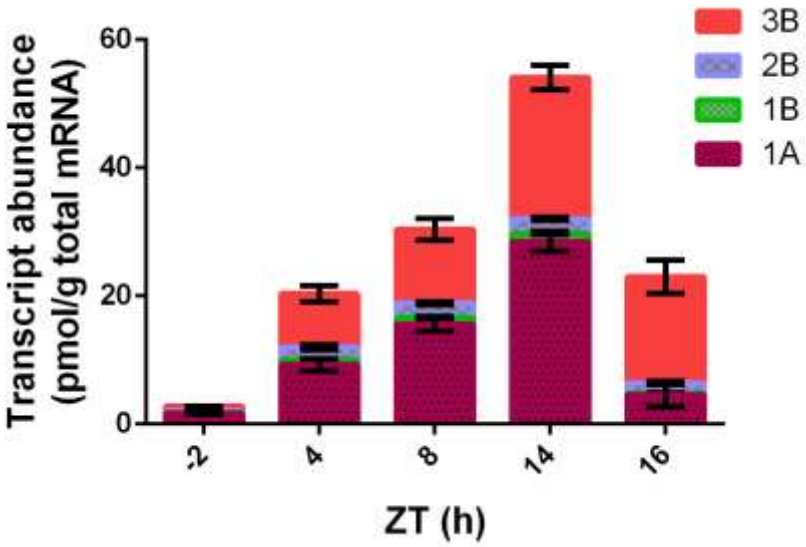
Transcript abundance
(pmol/g total mRNA)
60
40
20
0
3B
2B
1B
1A
:2
4
8
14
16
ZT (h)

B

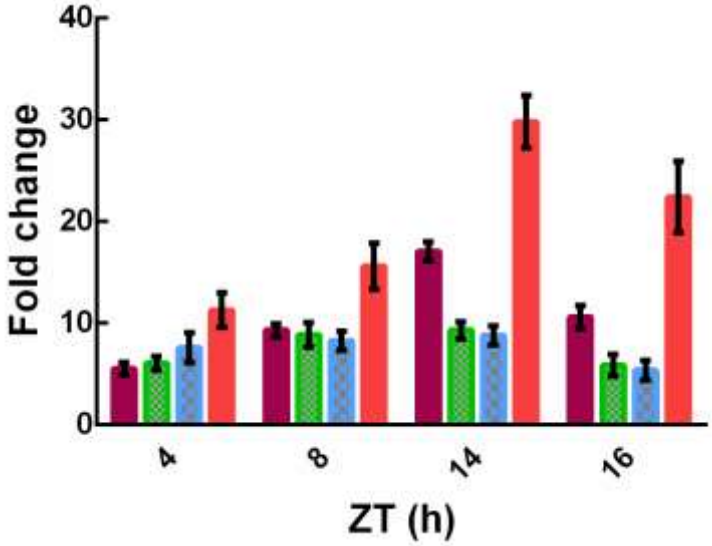
Fold change
40
30
20
10
0
4
8
14
16
ZT (h)

C

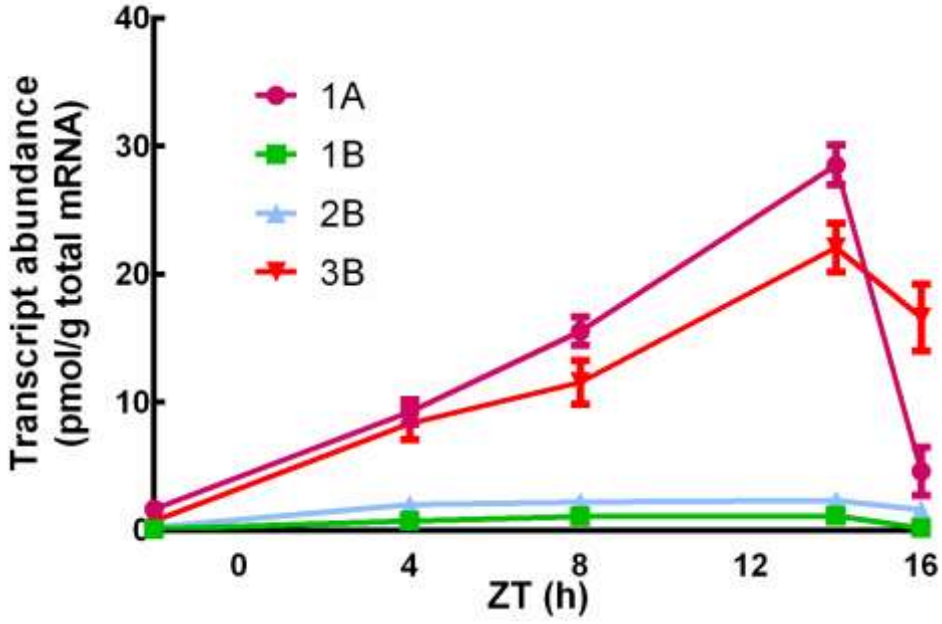

Figure 5.3. Expression of *RbcS* genes in the *prr5/7/9* mutant. Transcript abundance was measured using the synthesised standard plasmid as described in Chapter 3. The mutant was grown under constant light for 14 days, kept in the dark for 24 h and exposed to white light at 200 µmol photon m^{-2} s^{-1} and 21ºC for 12 h. Results are shown in zeitgeber time (ZT). A) Total transcript abundance for *RbcS* genes. B) Transcript fold changes relative to ZT -2 for *RbcS* genes. C) Transcript abundance of individual *RbcS* genes. Each data point consisted of three biological replicates and each biological replicate contained 25-30 seedlings.

In the *prr5/7/9* mutant, the expression of the *RbcS* genes showed a gradual increase over time followed by a decrease in expression at 16 h (**Figure 5.3A**). The latter data trend was similar to the experimental group (plants with dampened circadian rhythm) in the

previous experiment (**Figure 5.2B**), with the exception of the decline at the last time point. The total expression of *RbcS* genes in the dark at time point -2 was only 2.8 pmol/g total mRNA (2 fold lower than the experimental group) and gradually increased through the period of light exposure. The expression of the minor isoforms 1B and 2B reached maximum levels at 4 h of light exposure, whereas 1A and 3B continued to increase until 14 h (**Figure 5.3C**). All four *RbcS* genes were sensitive to white light. 3B showed the highest relative increase in expression (29-fold increase), followed by 1A (17-fold increase) and 1B (9-fold increase) and finally 2B (8-fold) at 14 h. (**Figure 5.3B**). The gene that was most rapidly induced was 1A and 3B and 1A reached the highest maximum expression at 14 h. 1B was the slowest to induce. 1A was also the quickest to degrade (**Figure 5.3C**). The most stable transcript was 2B as it showed the least changed over the measured period (**Figure 5.3C**). The observed decline in *RbcS* transcript abundances at 16 h contrasted that of the control group in **Figure 5.1A**, where 1A decreased more slowly than 3B after light was turned off. We hypothesise that the latter effect was due to the influence of circadian rhythm still present in the control group.

Based on these time course experiments, 8 ZT was chosen as the best time point to measure the impact of different environmental treatments on *RbcS* transcript abundances. Plants with dampened circadian rhythm and *prr5/7/9* mutant were used to measure the effects of environmental treatment to transcript abundance to compare and contrast the outcome. Both *prr5/7/9* and circadian-dampened WT were grown and exposed to different light qualities (blue, red and far-red, temperature was kept at 21^{o}C), quantities (1000, 200 and 50 µmol photon m^{-2} s^{-1}, temperature was kept at 21^{o}C) and

temperatures (30ºC and 10ºC, white light 200 µmol photon m^{-2} s^{-1}) for 8 h and transcript abundance was quantified (**Figure 5.4**). Overall, the trends between the two groups were similar – blue light induced the highest expression among the light quality group, followed by red light and far-red light (**Figure 5.4 A, D**). In the light quantity group, high light induced the highest level of expression, followed by medium light and low light (**Figure 5.4 C, F**). For the temperature group, exposing plants to high temperature resulted in an increase in expression, while low temperature reduced the *RbcS* gene expression relative to the expression at 20ºC. The change in temperature also dramatically altered differential expression of *RbcS* gene as the expression of 2B and 3B increased significantly and 3B became the dominant isoform under high temperature. On the other hand, low temperature suppressed the expression of 2B and 3B and the overall transcript abundance was decreased. Under low temperature, the 1A isoform became the major contributor to the total mRNA pool and accounted for 70% of the transcript abundance in both groups (**Figure 5.4 B, E**). Comparing the total expression level between the *prr5/7/9* mutant and the circadian-dampened plants, the total transcript abundance under all environmental treatments was higher in the latter group.

A

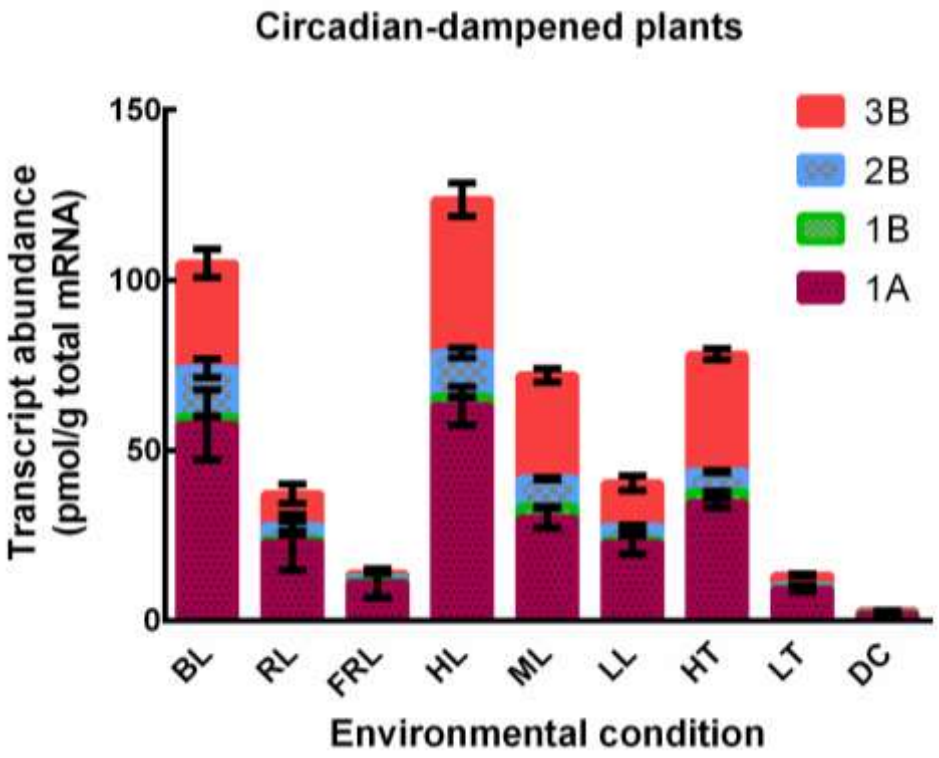
Circadian-dampened plants
Transcript abundance (pmol/g total mRNA)
150
100
50
0
3B
2B
1B
1A
BL
RL
FRL
HL
ML
LL
HT
LT
DC
Environmental condition

B

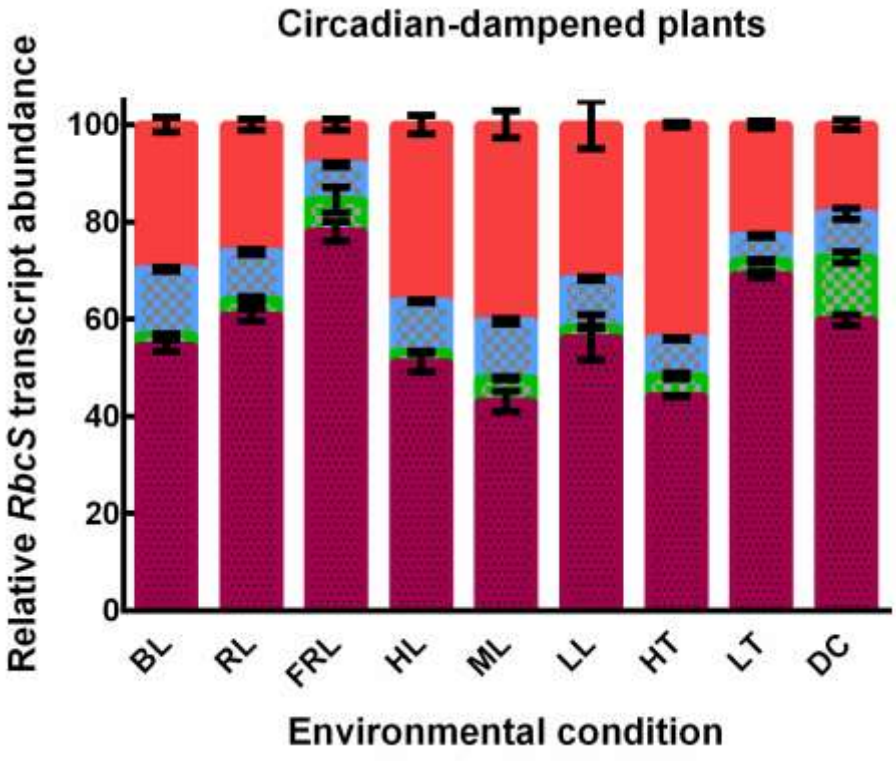
Circadian-dampened plants
Relative RbcS transcript abundance
100
80
60
40
20
0
BL
RL
FRL
HL
ML
LL
HT
LT
DC
Environmental condition

C

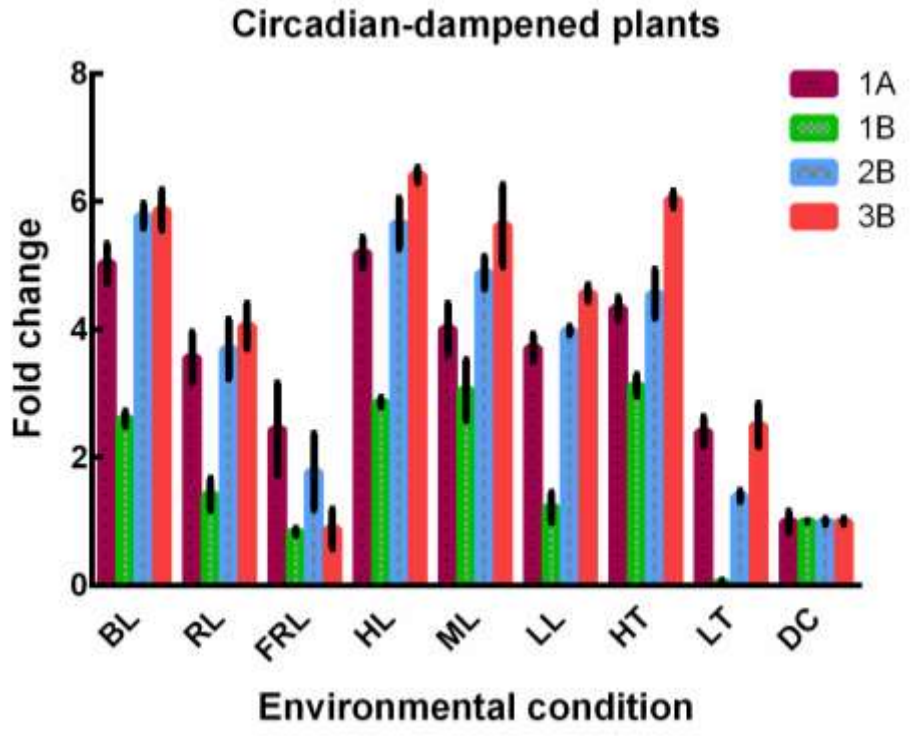
Circadian-dampened plants
1A
1B
2B
3B
Fold change
0
2
4
6
8
BL
RL
FRL
HL
ML
LL
HT
LT
DC
Environmental condition

D

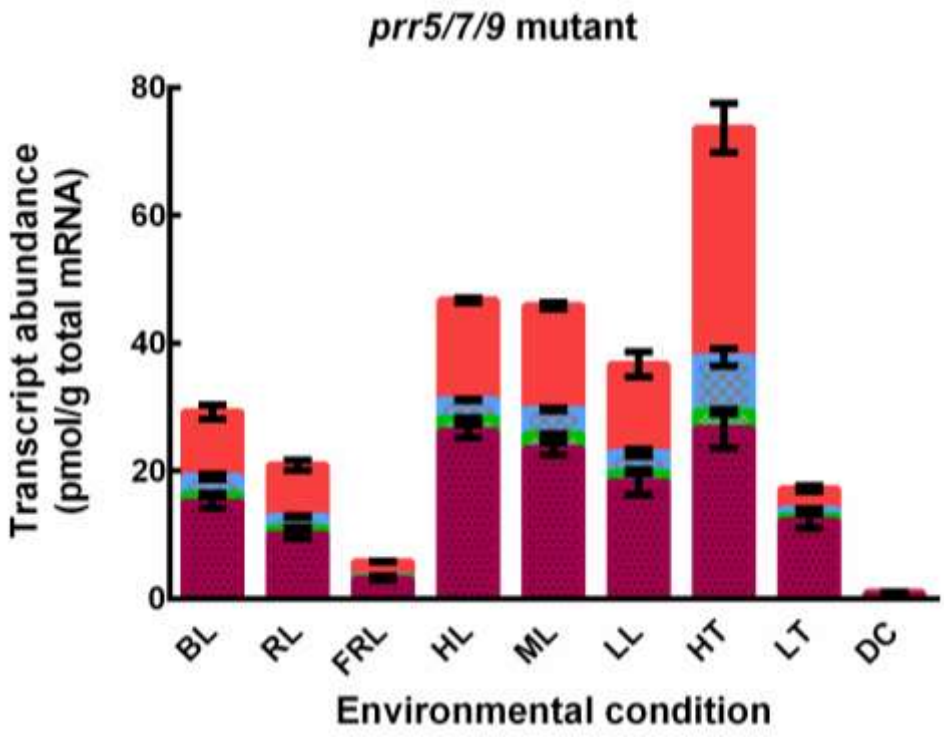
prr5/7/9 mutant
Transcript abundance
(pmol/g total mRNA)
0
20
40
60
80
BL
RL
FRL
HL
ML
LL
HT
LT
DC
Environmental condition

E

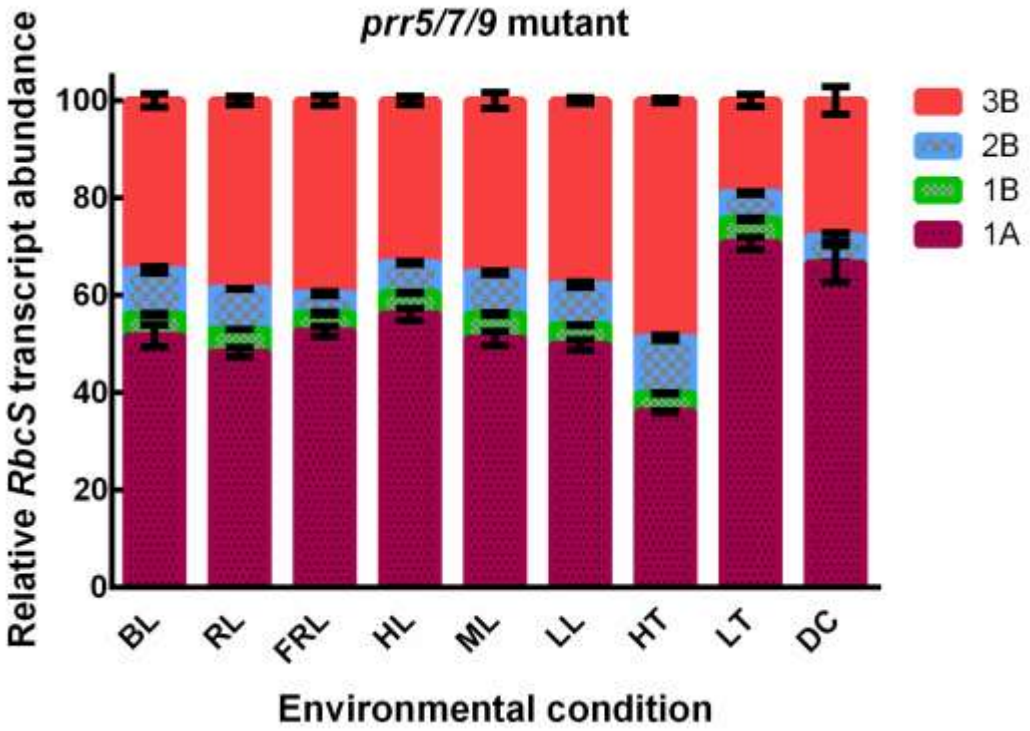
prr5/7/9 mutant
Relative RbcS transcript abundance
100
80
60
40
20
0
3B
2B
1B
1A
BL
RL
FRL
HL
ML
LL
HT
LT
DC
Environmental condition

F

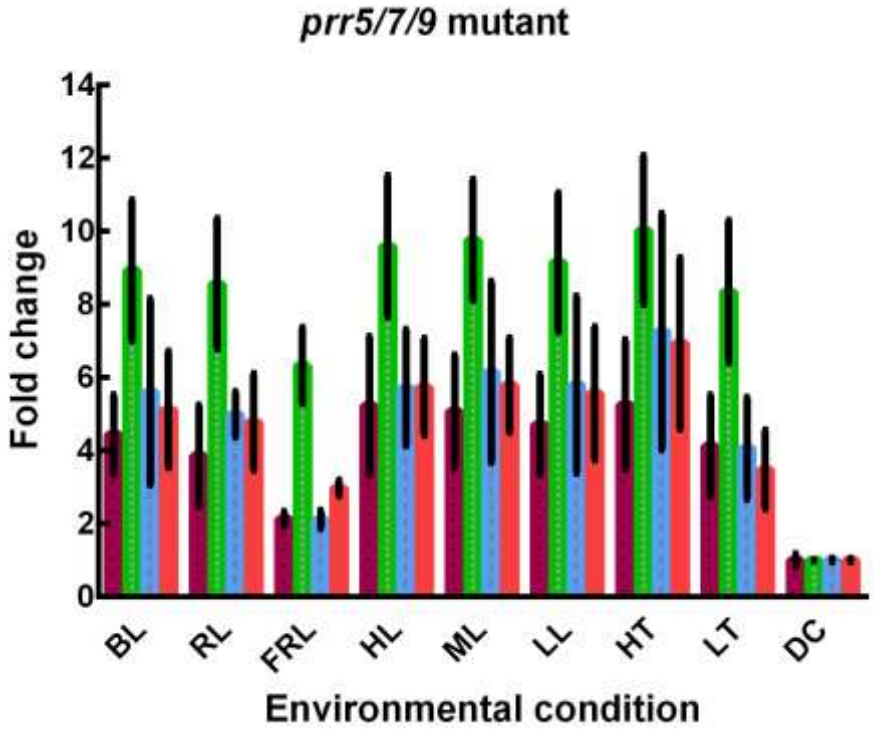
prr5/7/9 mutant
Fold change
14
12
10
8
6
4
2
0
BL
RL
FRL
HL
ML
LL
HT
LT
DC
Environmental condition

Figure 5.4. Expression of *RbcS* genes of circadian-dampened plants and *prr5/7/9* mutant exposed to different environmental conditions. Transcript abundance was measured using the synthesised standard plasmid as described in Chapter 3. A) total transcript abundance; B) transcript fold change relative to dark control (DC); and C) relative transcript abundance of circadian-dampened plants to -2 ZT. Expression of *RbcS* genes of *prr5/7/9* mutant represented as D) total transcript abundance; E) transcript fold change relative to DC; and F) relative transcript abundance -2 ZT. Both groups of plants were exposed to blue light (BL) at 80 µmol photon m^{-2} s^{-1}, red light (RL) at 80 µmol photon m^{-2} s^{-1}, far-red light (FRL) at 50 µmol photon m^{-2} s^{-1}, white light at 1000 µmol photon m^{-2} s^{-1} (HL), 200 µmol photon m^{-2} s^{-1} (ML) or 50 µmol photon m^{-2} s^{-1} (LL). Temperature was kept at 21ºC for different light conditions. White light at 200 µmol photon m^{-2} s^{-1} was used for the 30ºC high temperature (HT) and 10ºC low temperature (LT) exposures. Plants were exposed to each condition for 8 h. Each data point consisted of three biological replicates and each biological replicate contained 25-30 seedlings.

Physiological analysis of plants grown under high light

Based on the results obtained from the RT-qPCR screening experiments, three environmental conditions - high light, high temperature and low temperature were selected to analyse the potential impact of SSU knockout on growth. We aimed to test the following hypotheses: i) under the light saturating condition (high light), Rubisco becomes limiting and plants with significantly reduced Rubisco content (i.e. *1a*, *3b*, *2b3b* and *1a2b*) would

grow more slowly than WT; ii) under high temperature where 3B is the major isoform, plants lacking 3B (*3b*, *2b3b*) would suffer a reduced growth rate relative to WT and other mutants; iii) under low temperature where 1A is the major isoform, plants lacking 1A (*1a*, *1a2b*) would suffer a reduced growth rate relative to WT and other mutants.

A high light growth experiment (1000 µmol photon m^{-2} s^{-1}, 21ºC) was performed to examine the impact of Rubisco-limiting conditions on the growth phenotype of *rbcs* mutants generated by CRISPR/Cas9 or T-DNA insertions in Chapter 4. Under high light, both WT plants and almost all mutants grew at a faster rate than those in standard conditions, with the exception of BigBoi which suffered severe bleaching and did not survive past 15 DAG. All plant lines showed increased leaf area at 28 DAG compared to those in standard conditions (200 µmol photon m^{-2} s^{-1}, 21ºC) (**Figure 4.13C**, **5.5 and 5.6**). The area and weight (FW and DW) of WT rosettes under high light was approximately three-fold and 11-fold higher, respectively, than those under standard conditions at 28 DAG (**Figure 5.6 and 5.7A**). Notably, high light elicited a significant difference between the area and weight (FW and DW) between WT plants and *1a*, *1a2b* and *2b3b* (**Figure 5.6A, D, and 5.7A**). This difference was not observed under standard conditions (**Figure 4.14A**). No significant differences were seen for *1b* and *2b* mutants (**Figure 5.6B, C**). A slight decrease in rosette area relative to WT was noted for *3b* mutants, but this was not significant. However, the FW and DW of *3b* mutants were significantly lower than that of WT and therefore resulted in a significantly higher SLA (**Figure 5.7A, B**). The area, FW and DW of *1a3b* were significantly lower than those of WT, although they were higher than *1a3b* grown in standard conditions.

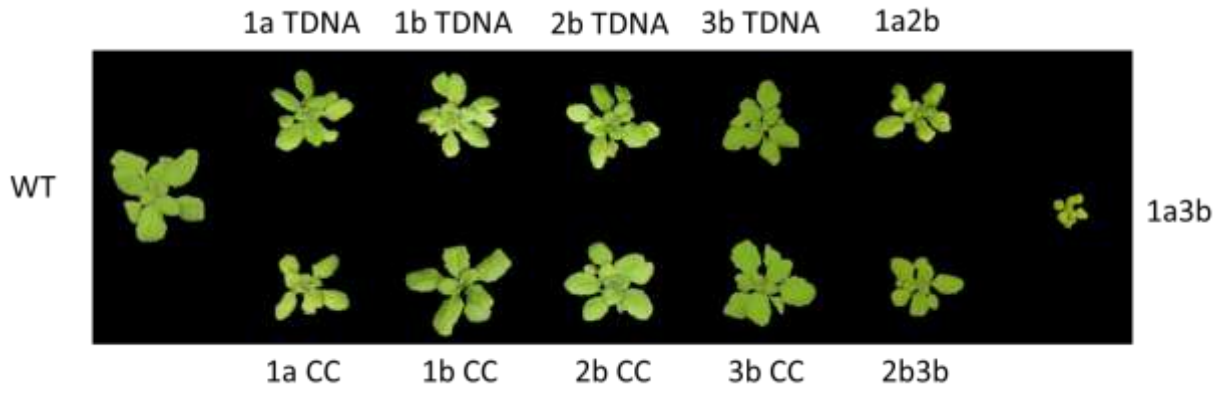

Figure 5.5. Representative images of 23-d-old rosettes of WT, T-DNA and CRISPR/Cas9 (CC) *rbcs* KO mutants grown under high light (1000 µmol photon m^{-2} s^{-1}, 21ºC).

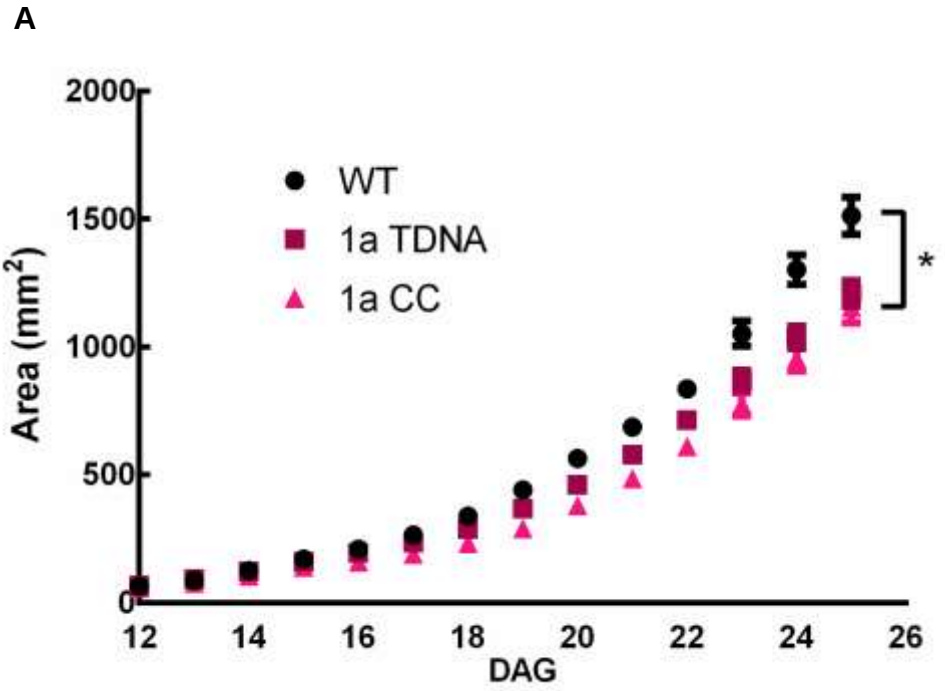

B

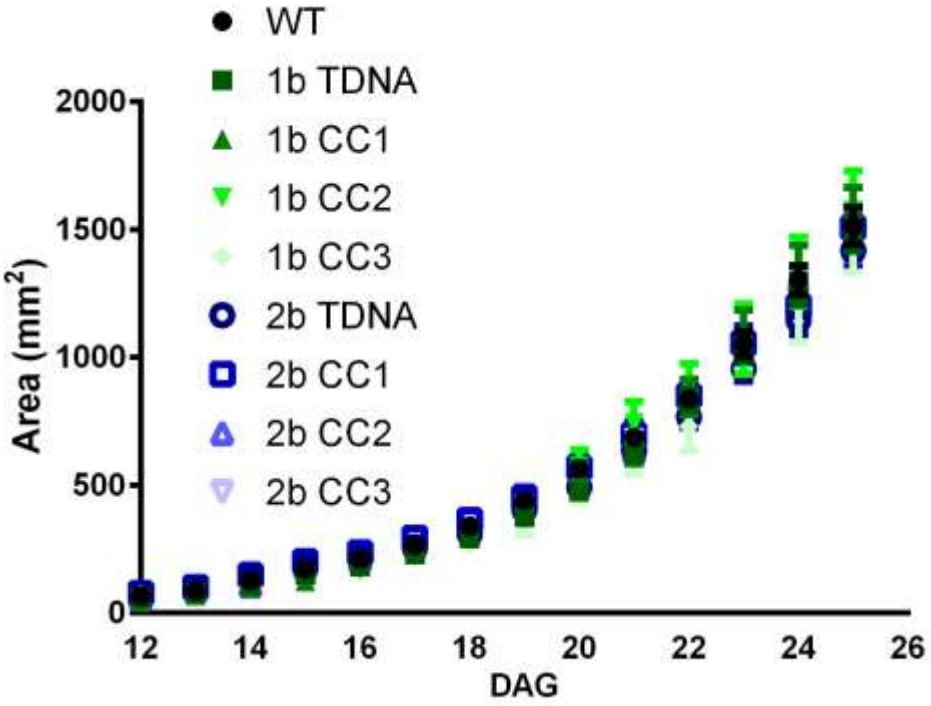
WT
1b TDNA
1b CC1
1b CC2
1b CC3
2b TDNA
2b CC1
2b CC2
2b CC3
Area (mm²)
2000
1500
1000
500
0
12
14
16
18
20
22
24
26
DAG

C

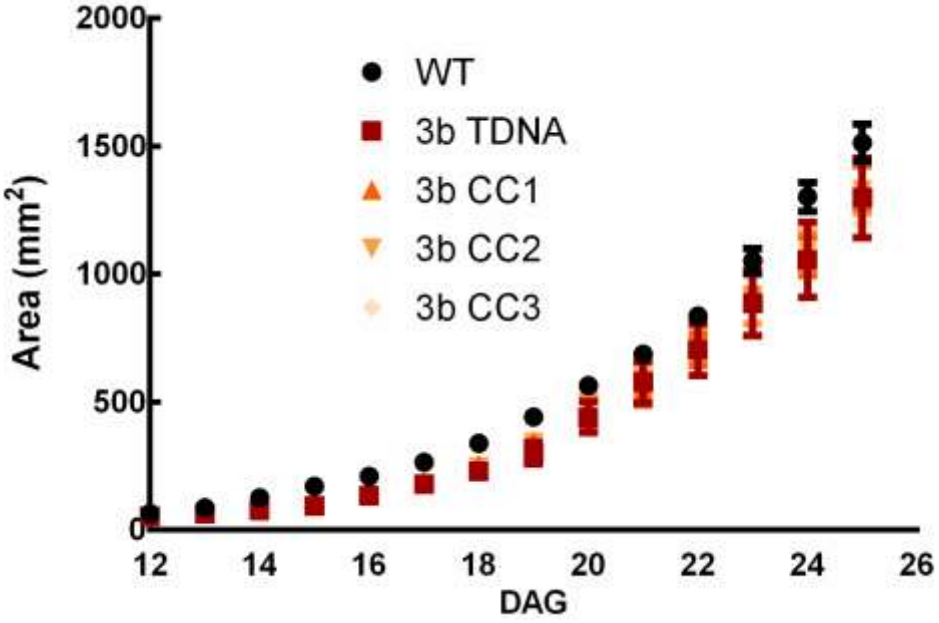
WT
3b TDNA
3b CC1
3b CC2
3b CC3
Area (mm²)
2000
1500
1000
500
0
12
14
16
18
20
22
24
26
DAG

D

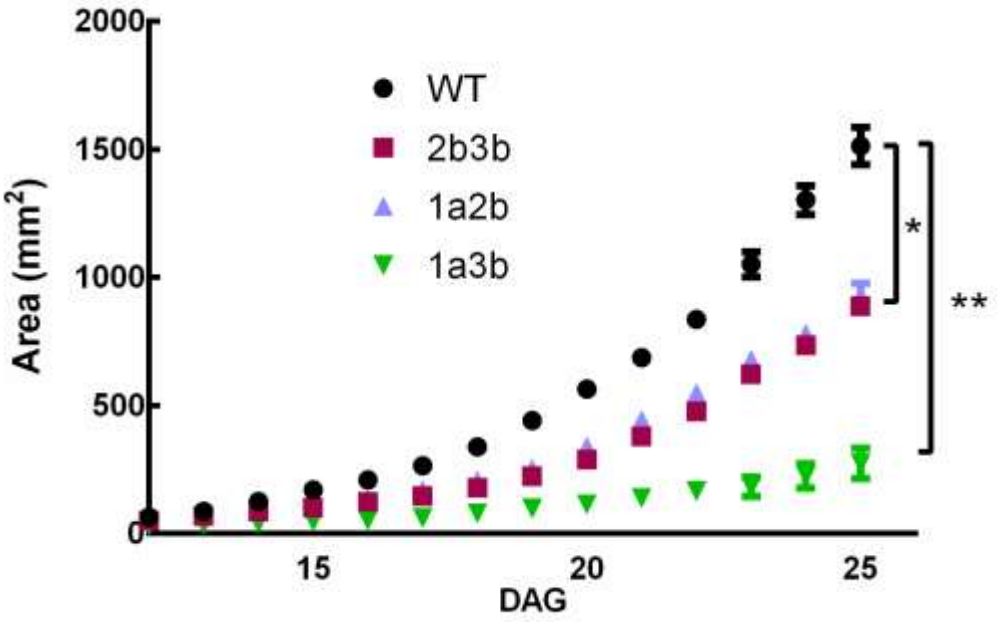

Figure 5.6. Growth analysis of *rbcs* KO mutants under high light (1000 µmol photon m^{-2} s^{-1}, 21°C). A) Rosette expansion of T-DNA and CRISPR/Cas9 (CC) *1a* single KO mutants. B) Rosette expansion of T-DNA and CRISPR/Cas9 (CC) *1b* and *2b* single KO mutants. C) Rosette expansion of T-DNA *3b* knockdown mutant and CRISPR/Cas9 (CC) *3b* single KO mutants. D) Rosette expansion of double mutants *2b3b*, *1a2b* and *1a3b*. Values are mean ± SE of measurements made on 8-15 rosettes. DAG is days after germination. Asterisks denotes significant difference from WT for *1a3b* and BB. One (*) and two (**) asterisks denote significant difference between groups. Significant difference ($P < 0.05$) was determined by ANOVA followed by Tukey's HSD tests.

A

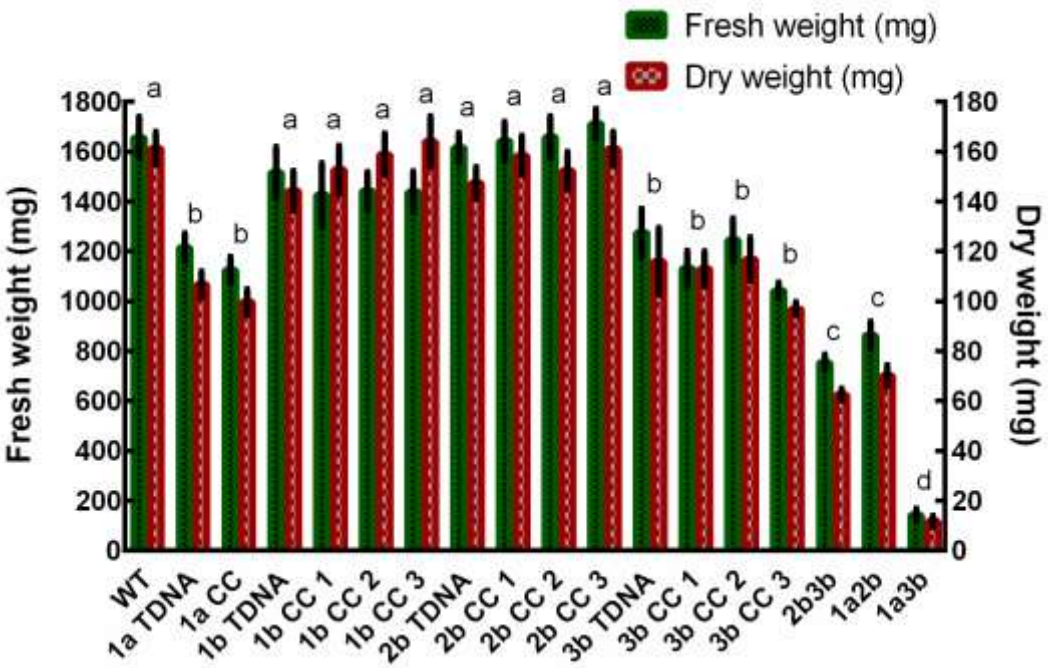
Fresh weight (mg)
Dry weight (mg)
Fresh weight (mg)
Dry weight (mg)
0
200
400
600
800
1000
1200
1400
1600
1800
0
20
40
60
80
100
120
140
160
180
a b b a a a a a a a a b b b b c c d
WT
1a TDNA
1a CC
1b TDNA
1b CC 1
1b CC 2
1b CC 3
2b TDNA
2b CC 1
2b CC 2
2b CC 3
3b TDNA
3b CC 1
3b CC 2
3b CC 3
2b3b
1a2b
1a3b

B

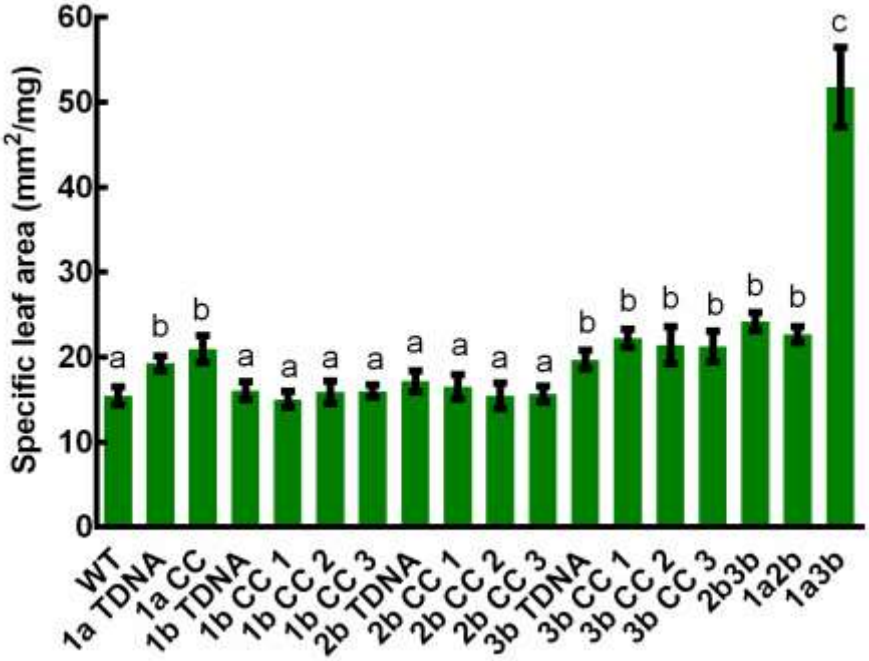
Specific leaf area (mm2/mg)
0
10
20
30
40
50
60
a b b a a a a a a a a b b b b b b c
WT
1a TDNA
1a CC
1b TDNA
1b CC 1
1b CC 2
1b CC 3
2b TDNA
2b CC 1
2b CC 2
2b CC 3
3b TDNA
3b CC 1
3b CC 2
3b CC 3
2b3b
1a2b
1a3b

C

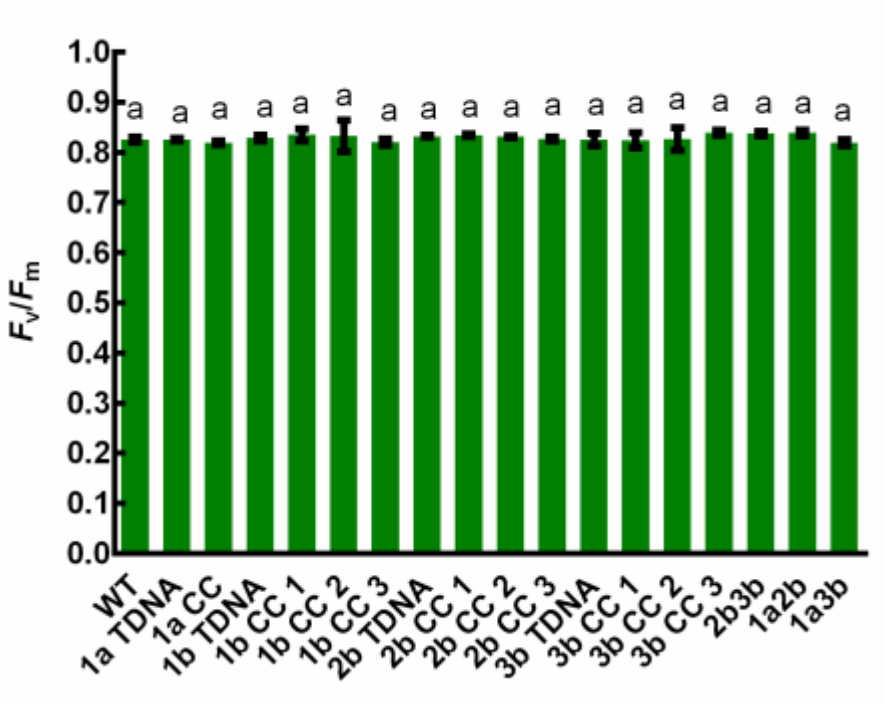
1.0
0.9
0.8
0.7
0.6
0.5
0.4
0.3
0.2
0.1
0.0
F_v/F_m
a a a a a a a a a a a a a a a a a a
WT
1a TDNA
1a CC
1b TDNA
1b CC 1
1b CC 2
1b CC 3
2b TDNA
2b CC 1
2b CC 2
2b CC 3
3b TDNA
3b CC 1
3b CC 2
3b CC 3
2b3b
1a2b
1a3b

D

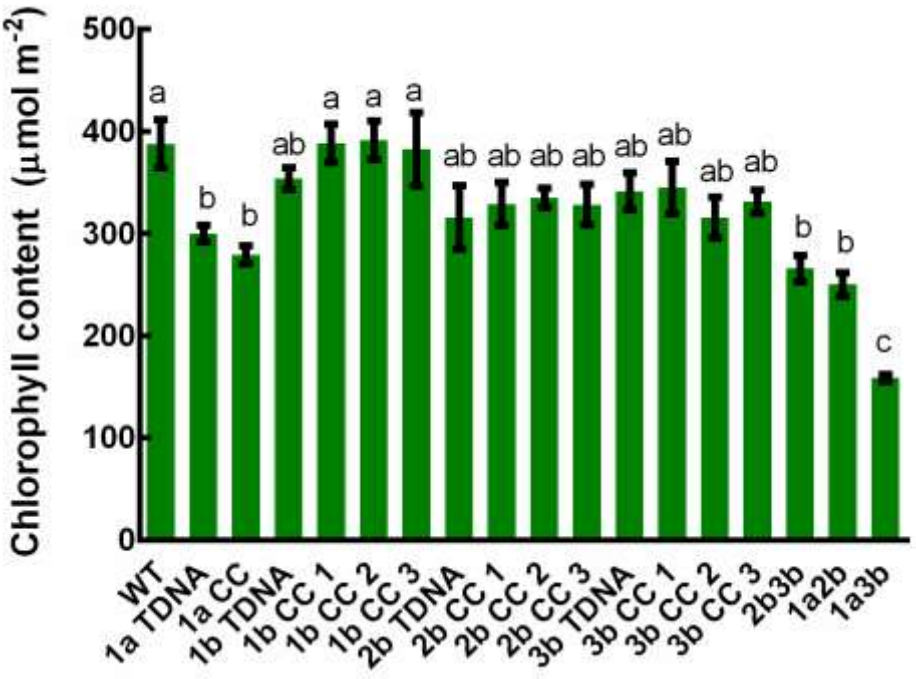
500
400
300
200
100
0
Chlorophyll content (μmol m^{-2})
a b b ab a a a ab ab ab ab ab ab ab ab b b c
WT
1a TDNA
1a CC
1b TDNA
1b CC 1
1b CC 2
1b CC 3
2b TDNA
2b CC 1
2b CC 2
2b CC 3
3b TDNA
3b CC 1
3b CC 2
3b CC 3
2b3b
1a2b
1a3b

E

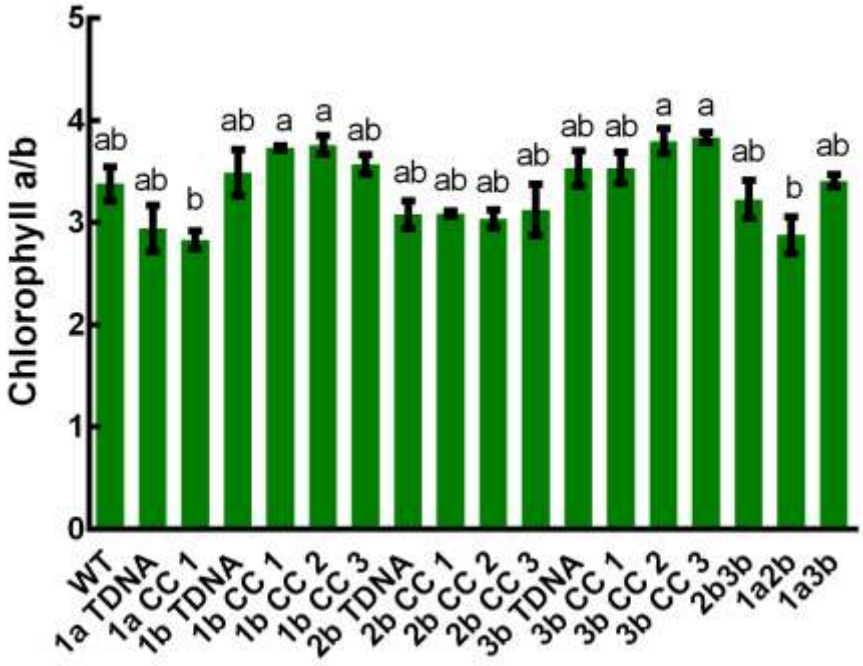

Figure 5.7. Growth analysis of WT, T-DNA and CRISPR/Cas9 (CC) *rbcs* KO mutants grown under high light (1000 µmol photon m^{-2} s^{-1}, 21ºC). A) Fresh and dry weights of 28-d old plants; B) Specific leaf area; C) F_v/F_m; D) chlorophyll content; E) Chlorophyll *a/b* ratio. Values are mean ± SE of measurements made on 8-15 rosettes. Values followed by the same letters are not significantly different ($P < 0.05$) as determined by Tukey's HSD test.

No significant differences in F_v/F_m were observed between plant lines grown under high light. However, a decrease in chlorophyll content relative to WT was observed in a subset of mutants, specifically *1a*, *2b3b*, *1a2b* and *1a3b* (**Figure 5.7D**). Additionally,

the pale-leaf phenotype of *1a3b* observed under standard conditions was less obvious under high light.

Physiological analysis of plants grown under high temperature

Previous RT-qPCR results showed that plants exposed to high temperature had increased expression levels for 2B and 3B, and 3B was the major isoform at 30^{o}C (**Figure 5.4B, E**). To test whether mutants lacking 3B would result in a reduced growth rate, WT, *1a*, *3b*, *2b3b*, *1a2b*, *1a3b* and BigBoi were grown and monitor for 28 days under 30^{o}C and 200 µmol photon m^{-2} s^{-1} of white light.

Plants grown under high temperature grew more quickly than those under standard conditions (**Figure 4.13 and 5.9**). In addition, all plants had a higher ratio of petiole to leaf blades and higher leaf insertion angle (hyponasty, from a qualitative assessment) (**Figure 5.8**). No significant difference in area, FW, DW or SLA were observed between WT and *1a*, *1b*, *2b3b* or *1a2b* mutants. However, the area, FW and DW of *1a3b* and BigBoi were significantly reduced (**Figure 5.9, 5.10A, B**). Chlorophyll content, chlorophyll *a/b* ratio and F_v/F_m value of the *1a3b* mutant were slightly but not significantly lower than that of WT. On the other hand, chlorophyll content, chlorophyll *a/b* ratio and F_v/F_m of BigBoi were significantly reduced relative to WT (**Figure 5.10 C, D, E**).

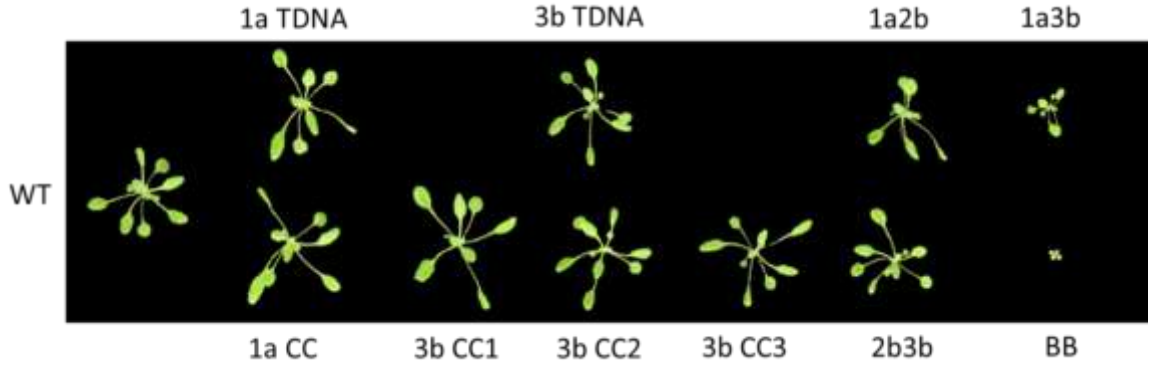

Figure 5.8. Representative images of 23-d-old rosettes of WT, T-DNA and CRISPR/Cas9 (CC) *rbcs* KO mutants grown under high temperature (200 µmol photon m^{-2} s^{-1}, 30ºC). BB is BigBoi.

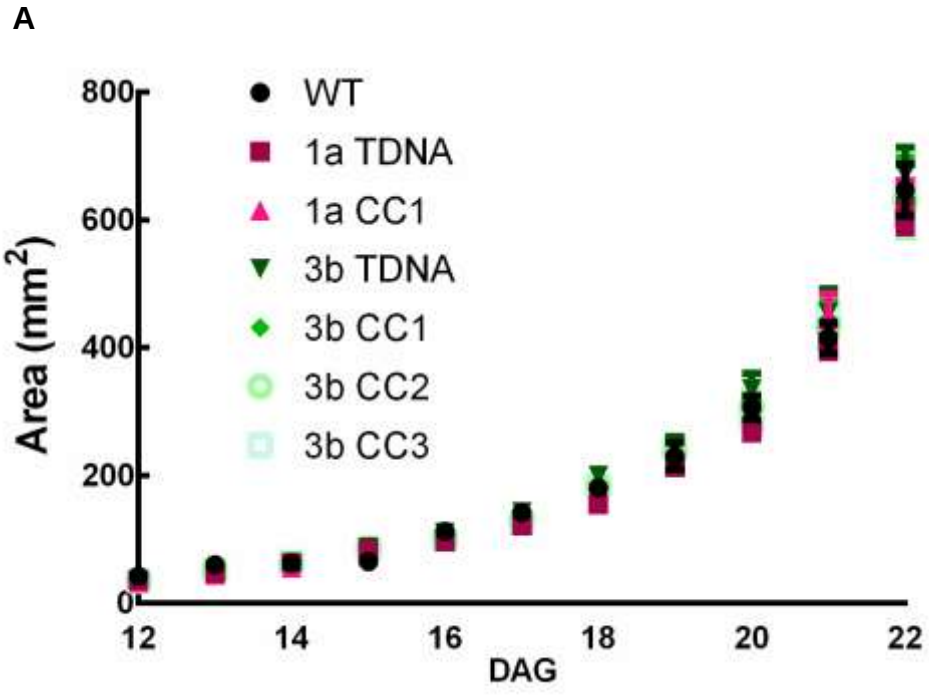

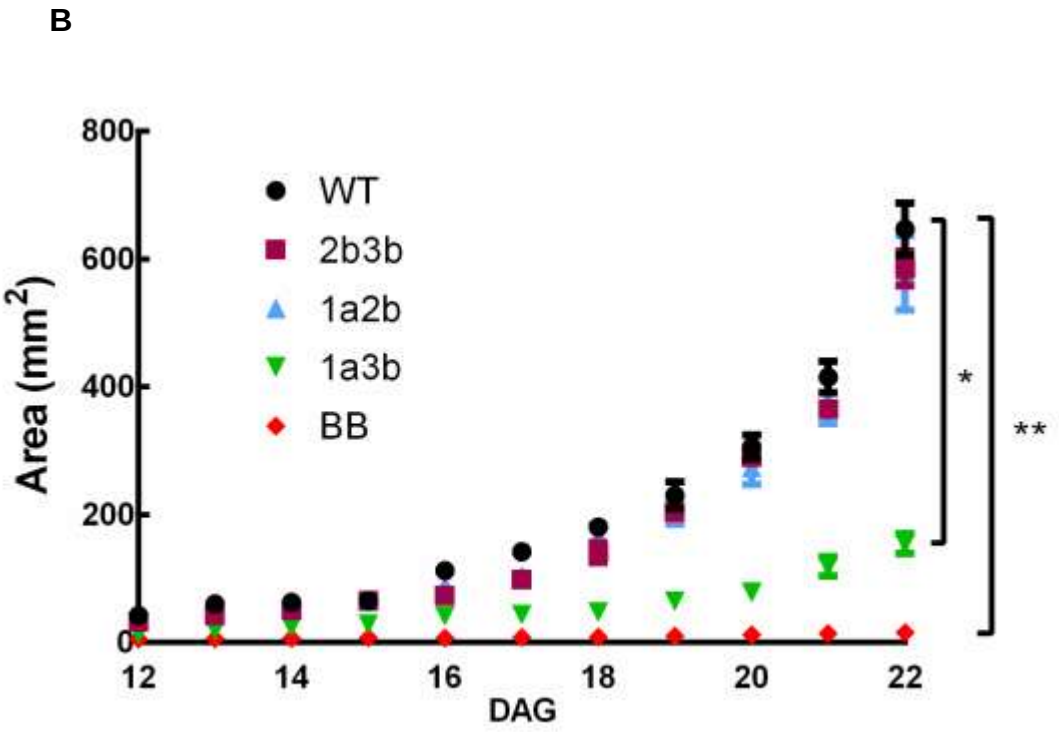

Figure 5.9. Growth analysis of *rbcs* T-DNA and CRISPR/Cas9 (CC) KO mutants under high temperature (200 µmol photon m^{-2} s^{-1}, 30°C). A) Rosette expansion of *1a and 3b* single KO mutants (*3b* T-DNA is a knockdown). B) Rosette expansion of double mutants *2b3b*, *1a2b* and *1a3b* and the triple mutant BigBoi (BB). Values are mean ± SE of measurements made on 8-15 rosettes. DAG is days after germination. One (*) and two (**) asterisks denote significant difference between groups. Significant difference ($P < 0.05$) was determined by ANOVA followed by Tukey's HSD tests.

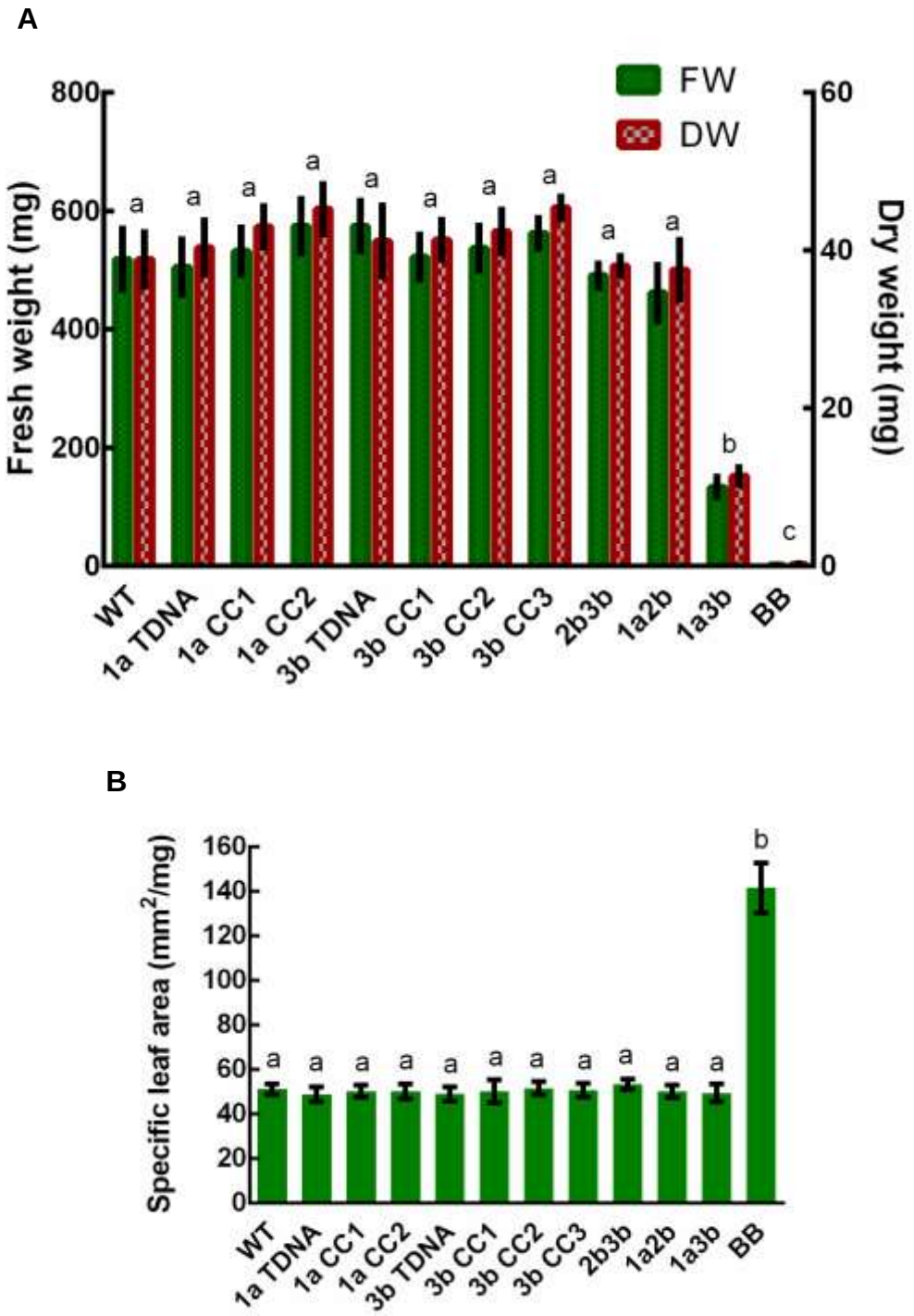
A
FW
DW
Fresh weight (mg)
Dry weight (mg)
800
600
400
200
0
60
40
20
0
a
a
a
a
a
a
a
a
a
a
b
c
WT
1a TDNA
1a CC1
1a CC2
3b TDNA
3b CC1
3b CC2
3b CC3
2b3b
1a2b
1a3b
BB
B
Specific leaf area (mm2/mg)
160
140
120
100
80
60
40
20
0
a
a
a
a
a
a
a
a
a
a
b
WT
1a TDNA
1a CC1
1a CC2
3b TDNA
3b CC1
3b CC2
3b CC3
2b3b
1a2b
1a3b
BB

C

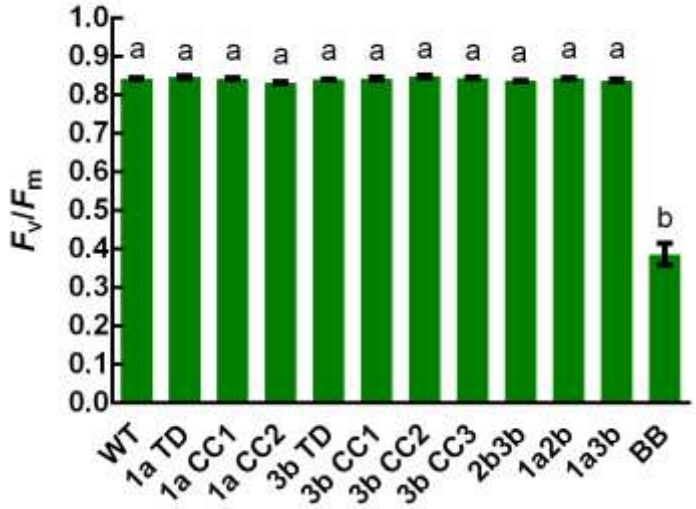
1.0
0.9
0.8
0.7
0.6
0.5
0.4
0.3
0.2
0.1
0.0
F_v/F_m
a a a a a a a a a a a
b
WT
1a TD
1a CC1
1a CC2
3b TD
3b CC1
3b CC2
3b CC3
2b3b
1a2b
1a3b
BB

D

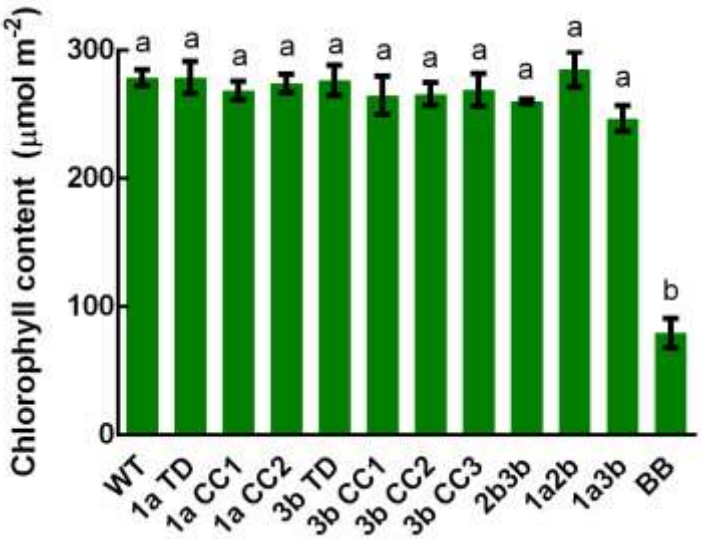
Chlorophyll content (μmol m^{-2})
300
200
100
0
a a a a a a a a a a a
b
WT
1a TD
1a CC1
1a CC2
3b TD
3b CC1
3b CC2
3b CC3
2b3b
1a2b
1a3b
BB

E

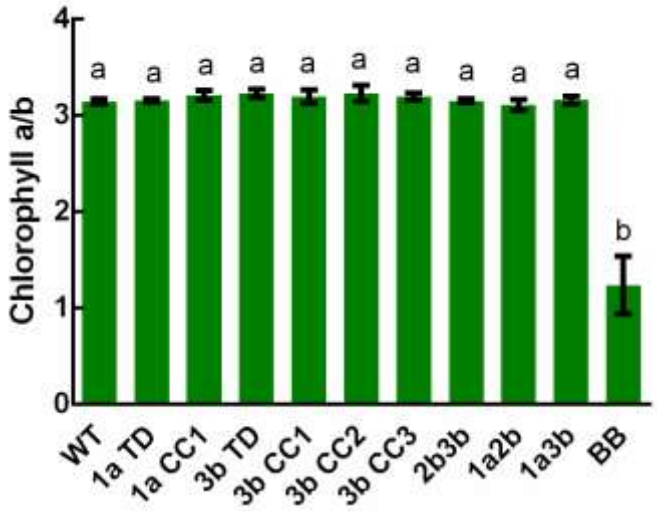

Figure 5.10. Growth analysis of WT, T-DNA and CRISPR/Cas9 (CC) *rbcs* KO mutants grown under high temperature (200 µmol photon m^{-2} s^{-1}, 30ºC). A) Fresh and dry weights of 28-d old plants; B) Specific leaf area; C) F_v/F_m; D) chlorophyll content; E) Chlorophyll *a/b* ratio. Values are mean ± SE of measurements made on 8-15 rosettes. Values followed by the same letters are not significantly different ($P < 0.05$) as determined by Tukey's HSD test.

Physiological analysis of plants grown under low temperature

Previous transcript abundance data showed that plants exposed to low temperature had reduced transcript abundance and suppressed 3B expression (**Figure 5.4B, E**). The major isoform under low temperature was 1A. To test whether plants lacking 1A would

suffer reduced growth, WT, *1a*, *3b*, *2b3b*, *1a2b*, *1a3b* and BigBoi were grown and monitored for 28 days under 10^{o}C and 200 µmol photon m^{-2} s^{-1} of white light.

Growing plants under low temperature inhibited rosette expansion, resulting in plants that were smaller than those grown under standard conditions (**Figure 5.11**). No significant differences were observed between the area of WT, *1a*, *3b*, *2b3b* and *1a2b*. However, *1a3b* and BigBoi was significantly smaller than WT and other mutants (**Figure 5.12A, B**). Although the area of *1a* and *1a2b* mutants was not significantly different to WT, the FW and DW were significantly reduced, resulting in a small but significantly increased SLA (**Figure 5.13A, B**). Chlorophyll content of *1a* and *1a2b* was also significantly lower than that of WT although the chlorophyll *a/b* ratio was not significantly different (**Figure 5.13D, E**). The F_v/F_m values of *1a* and *1a2b* were not significantly different from that of WT. For *1a3b* and BigBoi, the chlorophyll content, chlorophyll *a/b* ratio and F_v/F_m values were significantly lower than all other plant lines (**Figure 5.13C, D, E**).

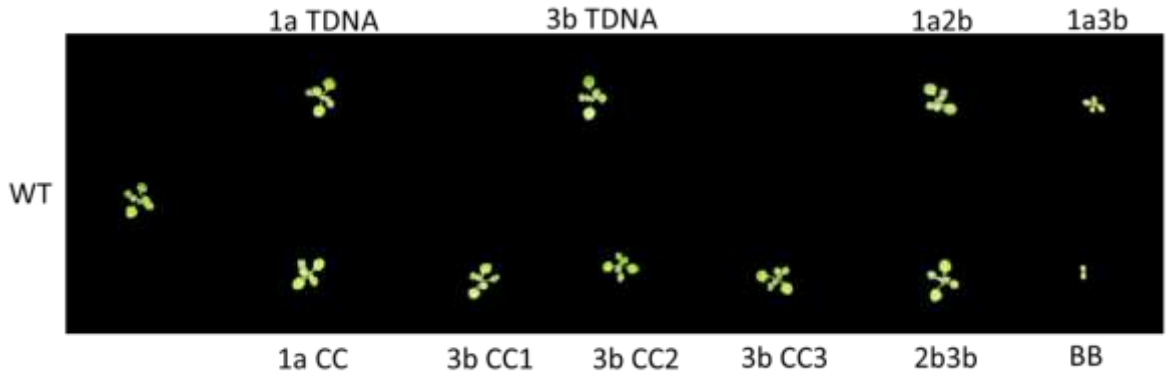

Figure 5.11. Representative images of 23-d-old rosettes of WT, T-DNA and CRISPR/Cas9 (CC) *rbcs* KO mutants grown under low temperature (200 µmol photon m^{-2} s^{-1}, 10ºC). BB is BigBoi.

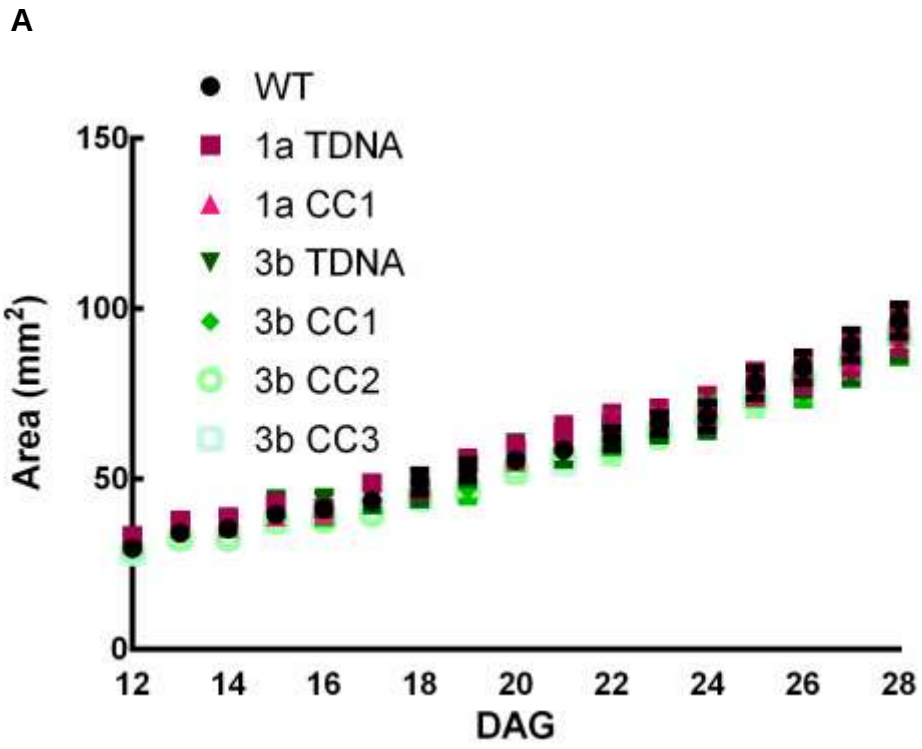

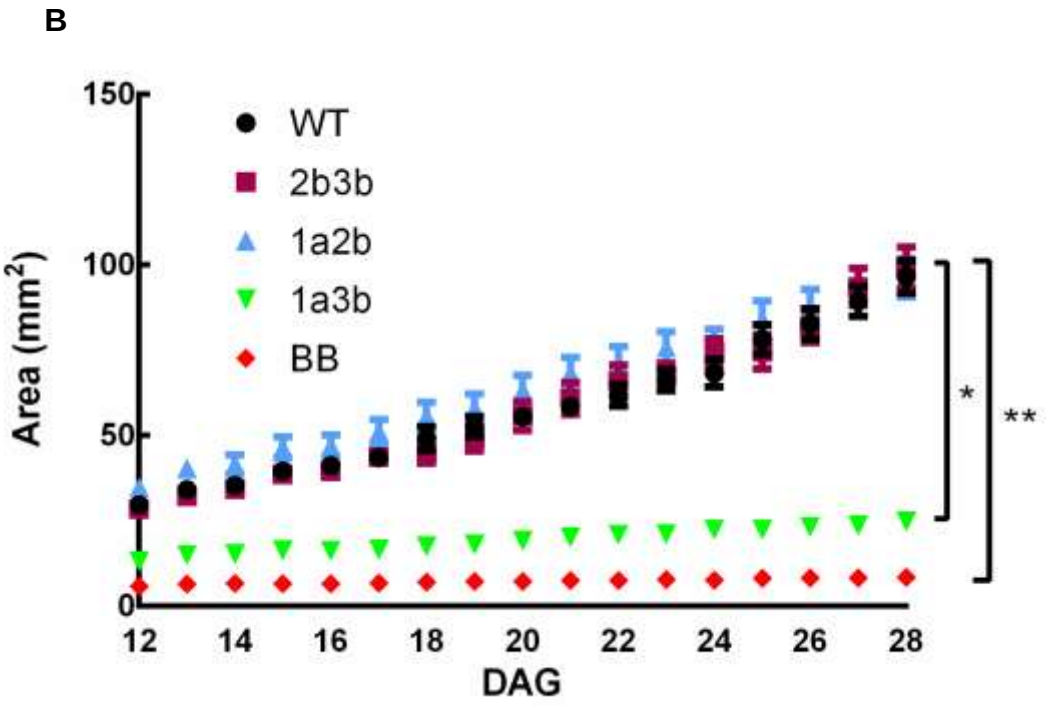

Figure 5.12. Growth analysis of *rbcs* T-DNA and CRISPR/Cas9 (CC) KO mutants under low temperature (200 µmol photon m^{-2} s^{-1}, 10°C). A) Rosette expansion of *1a and 3b* single KO mutants (*3b* T-DNA is a knockdown). B) Rosette expansion of double mutants *2b3b, 1a2b* and *1a3b* and the triple mutant BigBoi (BB). Values are mean ± SE of measurements made on 8-15 rosettes. DAG is days after germination. One (*) and two (**) asterisks denote significant difference between groups. Significant difference ($P < 0.05$) was determined by ANOVA followed by Tukey's HSD tests.

A

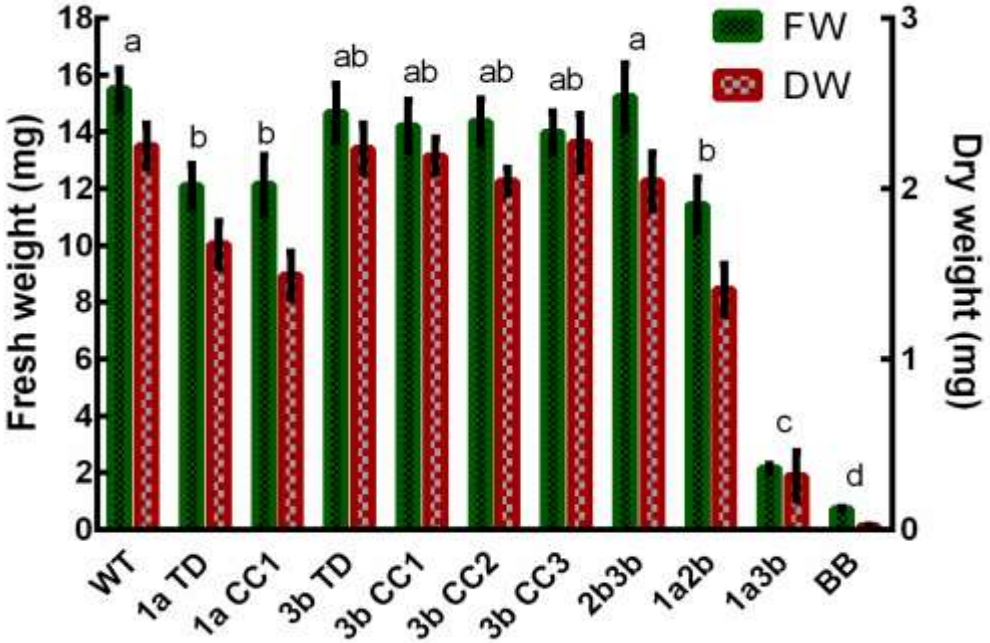
FW
DW
Fresh weight (mg)
Dry weight (mg)
0
2
4
6
8
10
12
14
16
18
0
1
2
3
a
b
b
ab
ab
ab
ab
a
b
c
d
WT
1a TD
1a CC1
3b TD
3b CC1
3b CC2
3b CC3
2b3b
1a2b
1a3b
BB

B

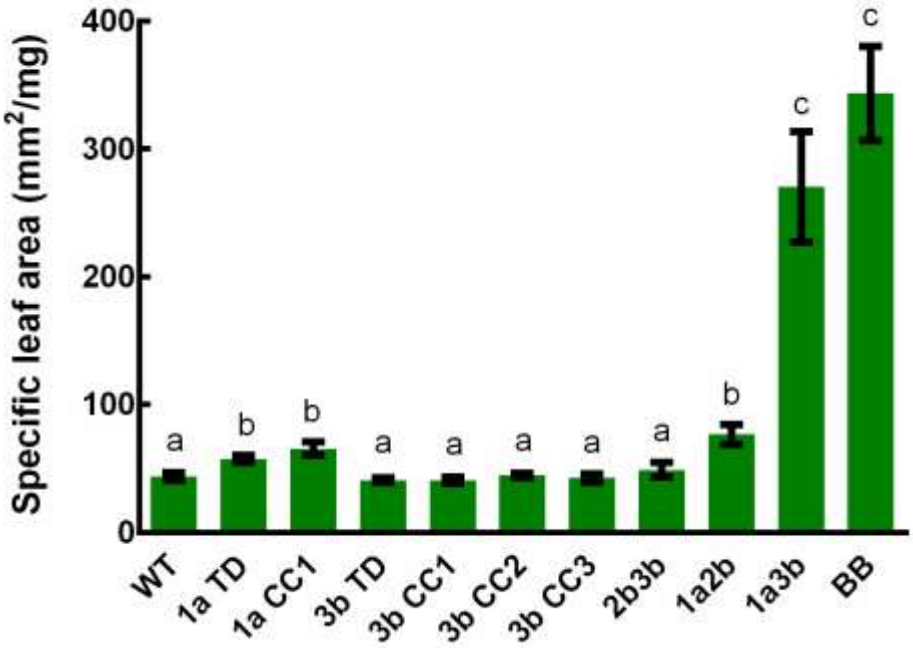
Specific leaf area (mm²/mg)
0
100
200
300
400
a
b
b
a
a
a
a
a
b
c
c
WT
1a TD
1a CC1
3b TD
3b CC1
3b CC2
3b CC3
2b3b
1a2b
1a3b
BB

C

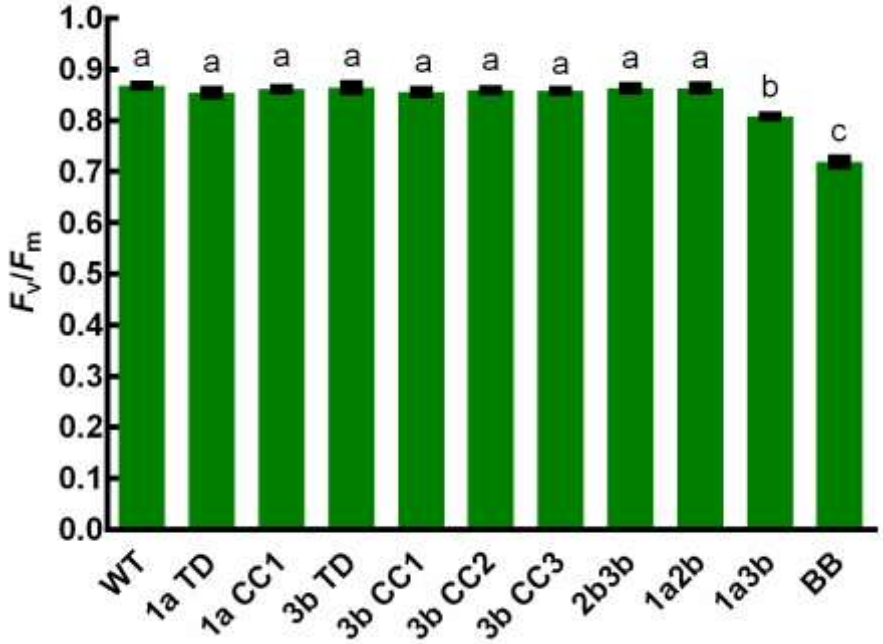
1.0
0.9
0.8
0.7
0.6
0.5
0.4
0.3
0.2
0.1
0.0
F_v/F_m
a a a a a a a a a b c
WT
1a TD
1a CC1
3b TD
3b CC1
3b CC2
3b CC3
2b3b
1a2b
1a3b
BB

D

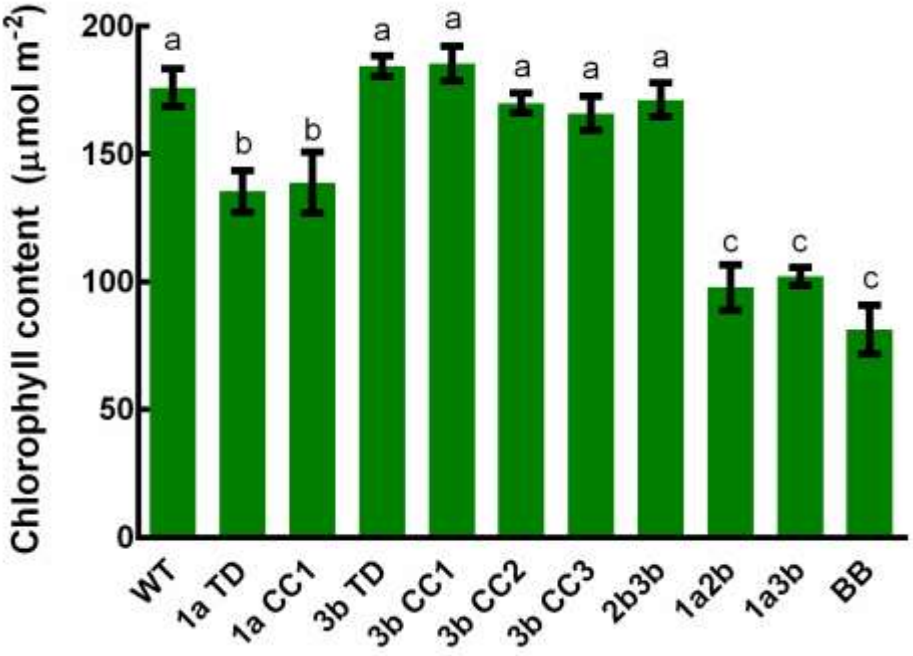
Chlorophyll content (μmol m^{-2})
200
150
100
50
0
a b b a a a a a a c c c
WT
1a TD
1a CC1
3b TD
3b CC1
3b CC2
3b CC3
2b3b
1a2b
1a3b
BB

E

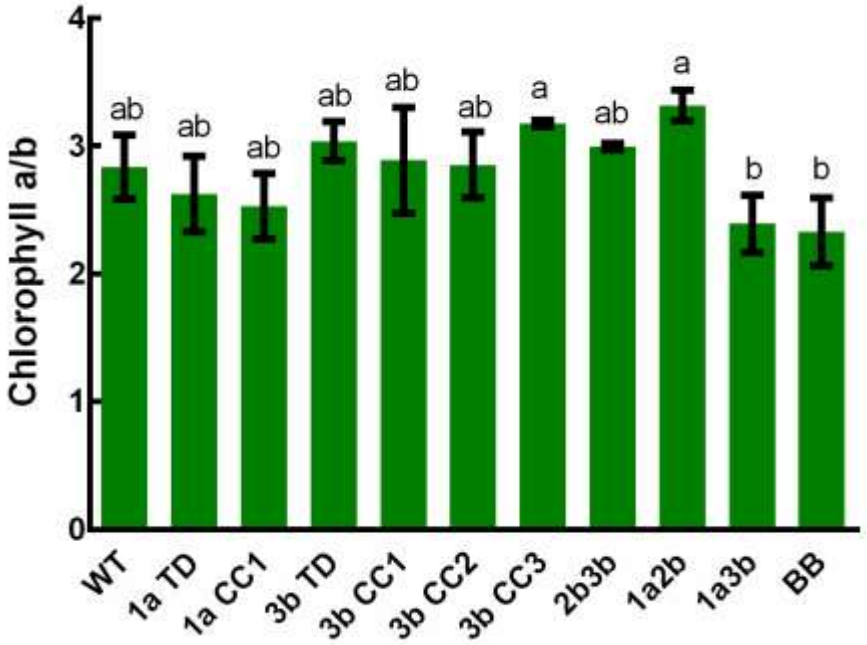

Figure 5.13. Growth analysis of WT, T-DNA and CRISPR/Cas9 (CC) *rbcs* KO mutants grown under low temperature (200 µmol photon m^{-2} s^{-1}, 10ºC). A) Fresh and dry weights of 28-d old plants; B) Specific leaf area; C) F_v/F_m; D) chlorophyll content; E) Chlorophyll *a/b* ratio. Values are mean ± SE of measurements made on 8-15 rosettes. Values followed by the same letters are not significantly different ($P < 0.05$) as determined by Tukey's HSD test.

Compound analysis of the four growth experiments under different growth conditions

The previously described growth experiments were presented as a comparison against plants grown under standard conditions, which was useful to describe the impact of a given growth environment on the SSU mutants. Here, the data from all four growth

experiments has been plotted against each other for a more direct comparison (**Figure 5.14**).

Growing plants under high light or high temperature generally promoted rosette expansion resulting in an increased area at 28 DAG compared to standard conditions (**Figure 5.14A**). WT plants grown under high light or high temperature had a four-fold and three-fold enhancement in rosette area, respectively. However, mutants with more than 40% decrease in *RbcS* transcript (*1a*, *3b*, *2b3b*, *1a2b*, *1a3b* and BigBoi) grew more slowly under high light but not in high temperature. In contrast to faster growth under high light and high temperature, growth was significantly slower under low temperature. The rosette sizes of WT was three times less than those grown under standard conditions (**Figure 5.14A**).

Growing plants under high light or high temperature also resulted in higher FW and DW. WT plants grown in high light or high temperature weighed eleven and four times more than WT grown under standard conditions, respectively (**Figure 5.14B, C**). Unlike for the area data, where *1a*, *3b*, *2b3b*, *1a2b*, *1a3b* and BigBoi were comparable under high light and high temperature, the FW and DW of mutants grown under high light were always higher than those grown under high temperature (**Figure 5.14B, C**). This resulted in a lower SLA for plants grown under high light, suggesting that their leaves were thicker (**Figure 5.14D**).

A

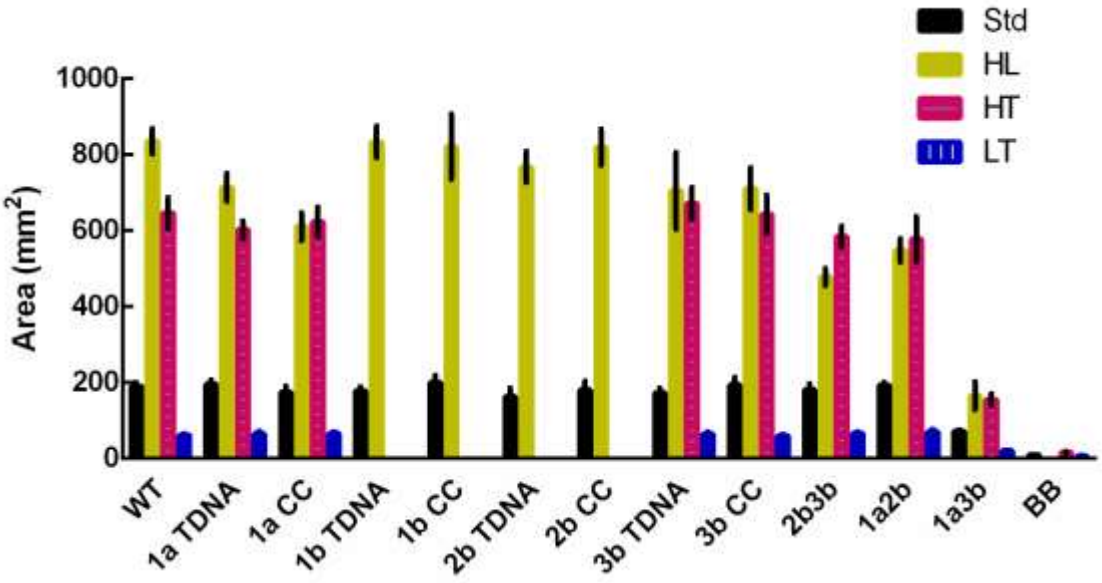
Std
HL
HT
LT
Area (mm²)
1000
800
600
400
200
0
WT
1a TDNA
1a CC
1b TDNA
1b CC
2b TDNA
2b CC
3b TDNA
3b CC
2b3b
1a2b
1a3b
BB

B

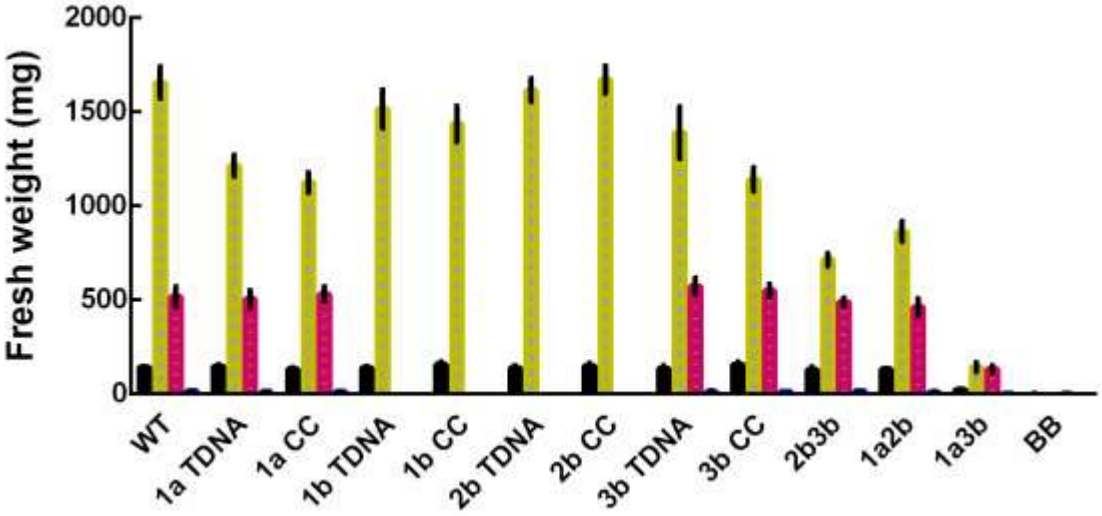
Fresh weight (mg)
2000
1500
1000
500
0
WT
1a TDNA
1a CC
1b TDNA
1b CC
2b TDNA
2b CC
3b TDNA
3b CC
2b3b
1a2b
1a3b
BB

C

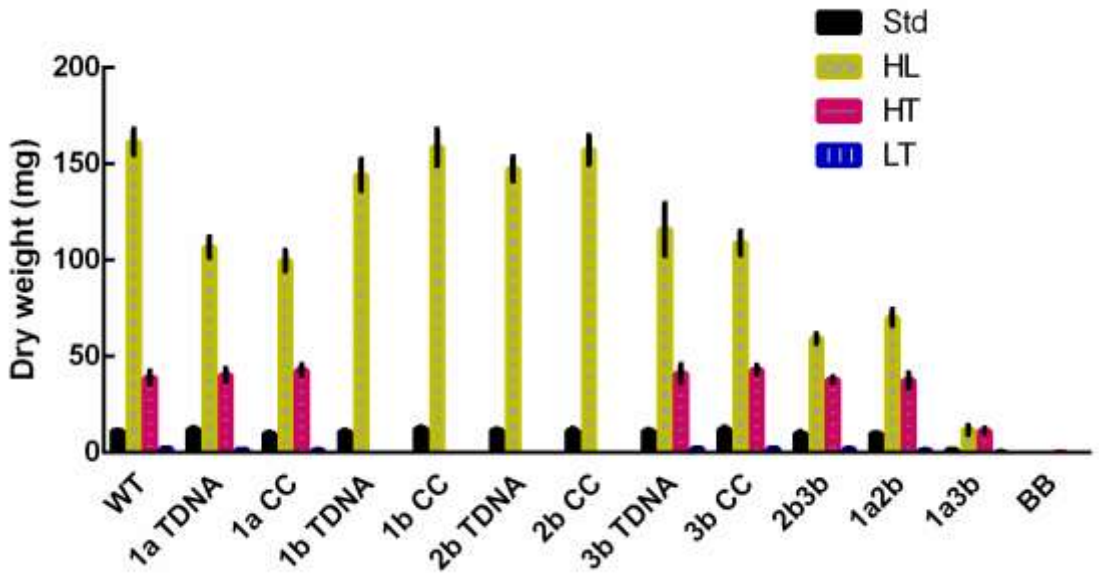
Std
HL
HT
LT
Dry weight (mg)
200
150
100
50
0
WT
1a TDNA
1a CC
1b TDNA
1b CC
2b TDNA
2b CC
3b TDNA
3b CC
2b3b
1a2b
1a3b
BB

D

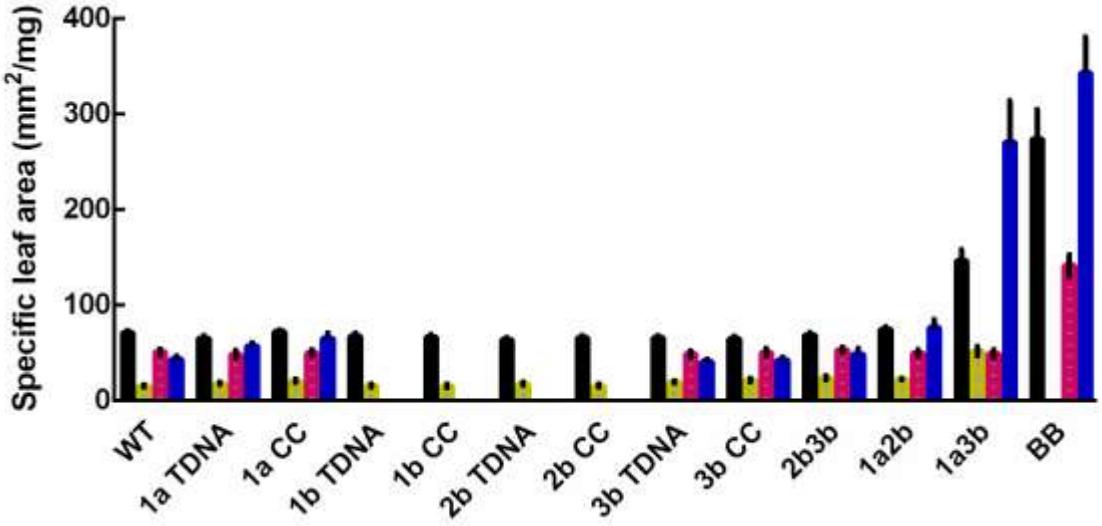
Specific leaf area (mm²/mg)
400
300
200
100
0
WT
1a TDNA
1a CC
1b TDNA
1b CC
2b TDNA
2b CC
3b TDNA
3b CC
2b3b
1a2b
1a3b
BB

E

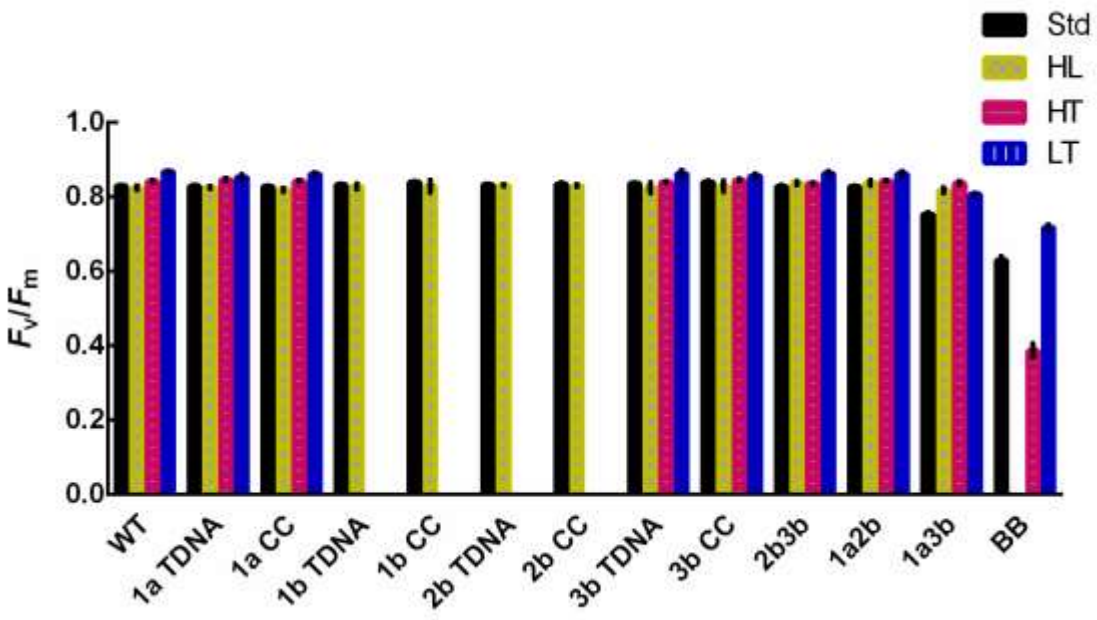
Std
HL
HT
LT
1.0
0.8
0.6
0.4
0.2
0.0
F_v/F_m
WT
1a TDNA
1a CC
1b TDNA
1b CC
2b TDNA
2b CC
3b TDNA
3b CC
2b3b
1a2b
1a3b
BB

F

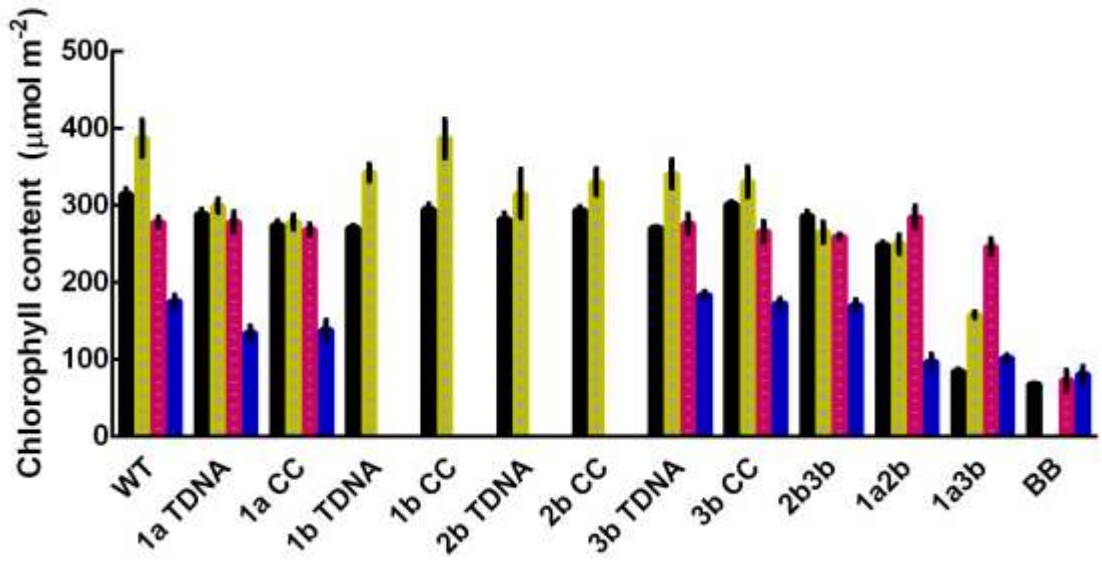
Chlorophyll content (μmol m^{-2})
500
400
300
200
100
0
WT
1a TDNA
1a CC
1b TDNA
1b CC
2b TDNA
2b CC
3b TDNA
3b CC
2b3b
1a2b
1a3b
BB

G

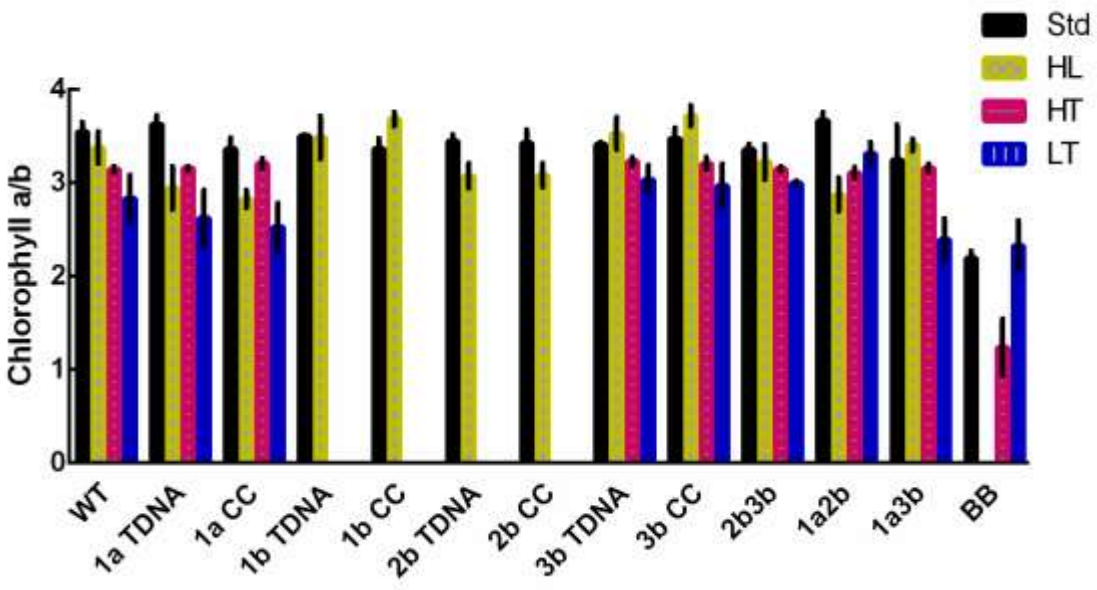

Figure 5.14: Comparison of growth of WT, TDNA and CRISPR/Cas9 (CC) *rbcs* mutants grown under standard conditions (Std, 200 µmol photon m^{-2} s^{-1}, 21^{o}C), high light condition (HL, 1000 µmol photon m^{-2} s^{-1}, 10^{o}C), high temperature condition (HT, 200 µmol photon m^{-2} s^{-1}, 30^{o}C) and low temperature condition (LT, 200 µmol photon m^{-2} s^{-1}, 10^{o}C). A) Area; B) FW; C) DW; D) Specific leaf area; E) F_v/F_m; F) chlorophyll content; G) Chlorophyll *a/b* ratio. BB is BigBoi mutant. Values are mean ± SE of measurements made on 8-15 rosettes.

The values for F_v/F_m remained unchanged in WT, *1a*, *3b*, *2b3b* and *1a2b* under the standard, high light and high temperature conditions but were increased under low temperature (**Figure 5.14E**). Unlike WT and other mutants, F_v/F_m values for *1a3b* was low under standard conditions but enhanced to near WT level under other conditions.

Measurements of F_v/F_m could not be taken for BigBoi at high light as the plants did not survive. However, BigBoi was dissimilar to other mutants in that high temperature yielded reduced F_v/F_m values, while low temperature increased the F_v/F_m values relative to standard conditions.

High light condition increased the chlorophyll content of WT, *1b*, and *1a3b* compared to standard conditions, but not for other mutants (**Figure 5.14F**). High temperature did not change chlorophyll content significantly except for *1a3b* where chlorophyll content was the highest among the growth conditions. Lowering the temperature resulted in reduced chlorophyll content compared to standard conditions in all mutants except for *1a3b* and BigBoi. This likely represented the minimum amount of chlorophyll required for photosynthesis. Unlike other mutants, chlorophyll content in BigBoi was unaffected by different growth environments. The chlorophyll *a/b* ratio followed the same trend as chlorophyll content in that standard conditions and high light promoted the highest chlorophyll *a/b* ratio and decreased under high and low temperature. In contrast, the chlorophyll *a/b* ratio for BigBoi was highest under standard conditions and low temperature and lowest under high temperature.

Discussion

Photoregulation of *RbcS* transcript has been shown in different plant species including pea, lemna, soybean, rye and Arabidopsis (Tobin and Silverthorne, 1985; Fluhr and Chua, 1986; Sasaki *et al.*, 1987; Ido *et al.*, 2016). In Arabidopsis, a study in dark-

grown seedlings suggested that the four *RbcS* genes responded differently to different light qualities and quantities (Dedonder *et al.,* 1993). For example, exposing dark-grown seedlings to continuous white light of 10 µmol photon m^{-2} s^{-1} for 24 h induced the increase in relative expression of the 1A, 1B, 2B and 3B genes by 8-, 13-, 12, and 14-fold, respectively. Higher fluence rate of 1000 µmol photon m^{-2} red light was needed to increase the expression of 2B suggesting that 2B was less responsive to red light. Dedonder *et al.* (1993) also reported that 2B was the most stable transcript. The result from this study agreed with Dedonder *et al.* (1993) in that 1A and 3B were highly expressed after light exposure while 2B and 1B expressions were significantly lower. Moreover, the RT-qPCR method used in this study was able to give quantitative data in regards to individual *RbcS* gene expression and total transcript abundance under different environmental conditions.

The quantitative transcript abundance data was useful in interpreting dynamic expressions of *RbcS* genes. For instance, Yoon *et al.* (2001) reported that the expression of 2B and 3B increased and 3B became the major isoform at 30^{o}C, while 1A was the major isoform at 10^{o}C. Consistent with Yoon *et al.* (2001), the present study found Arabidopsis exposed to high temperature had elevated expression levels of 2B and 3B, and 3B was the major isoform. However, 1A was the major isoform under 10^{o}C not because the expression of 1A was increased under low temperature, but the expression of 2B and 3B were more suppressed than that of 1A, which resulted in 1A accounting for 70% of to the total transcript (**Figure 5.4B, E**). Moreover, the total transcript abundance was six times lower under low temperature, which correlated with slower growth at 10^{o}C and faster growth and increased rosette areas for plants grown at 30^{o}C.

The regulation of *RbcS* genes can be exercised at the level of transcript stability (Ernst *et al.,* 1987; Wanner and Gruissem, 1991) or at the translational level (Rodermel *et al.,* 1996). The four *RbcS* genes in Arabidopsis were shown to have different induction and degradation rates – 1A had the highest level of induction after light exposure followed by 3B, 2B and 1B (**Figure 5.3C**). The transcript degradation of 1A was the most rapid, followed by 3B, 1B and 2B. The result is in agreement with the previous study of transcript stability of dark-grown seedlings (Dedonder *et al.,* 1993). However, the degradation rate was different in plants with circadian rhythm as 3B was the fastest to degrade after dark. While Dedonder *et al.* (1993) did not take circadian control into account, this study has compared the *RbcS* expression under circadian control and when circadian control was effectively separated out. The results from this study inferred that the difference in the rate of degradation between the two groups was attribute to circadian rhythm and further highlighted the influence of circadian rhythm over *RbcS* transcript abundance (**Figure 5.1A and 5.3A**). This complex pattern of expression also adds to many lines of evidence that the *RbcS* gene family exists not only to amplify the *RbcS* transcript abundance but is also differentially regulated with respect to various parameters including light, darkness and temperature (Coruzzi *et al.,* 1984; Dedonder *et al.,* 1993; Yoon *et al.,* 2001; Cen and Sage 2005).

The changes in the *RbcS* transcript abundance directly correlates with the changes in Rubisco level (Izumi *et al.,* 2010; Atkinson *et al.,* 2017). Although we were not able to quantify Rubisco content for all the different lines under the different growth experiments, exposing plants to high light led to an elevated level of *RbcS* transcript and likely an

increased active state of the Rubisco pool, thus resulting in the observed increases in area and biomass. Plants grown under high light also had thicker leaves (lower SLA) due to the increased size of mesophyll cells (Terashima *et al.,* 2011). The observed increase in photosynthetic capacity under high light was accompanied by increase in chlorophyll content in WT, *1b, 2b, 3b* and *1a3b* while chlorophyll content remained unchanged in *1a, 2b3b* and *1a2b* mutants relative to those in standard conditions. The increase in chlorophyll content of the former group suggests that those plants were able to invest more in light harvesting components.

Decreasing the *RbcS* content down to 30% such that in the *1a2b* KO mutant did not result in the difference in size and weight relative to WT under standard conditions (**Figure 4.12A**). The lack of apparent difference was likely due to a higher activation level of the Rubisco pool in the mutants (Quick *et al.,* 1991). However, a significant reduction in area and weight was observed in *1a, 2b3b* and *1a2b* and in weight for *3b* under the high light condition as hypothesised. Thus under high light, the available Rubisco pool likely was limiting in the latter mutants. It was expected that these mutants would have reduced growth rates compared to WT under high light as they have reduced $V_{c,max}$ and J_{max} under saturating light (**Table 4.4**). A reduction in rosette area was not observed in *3b* mutants under high light even though they also had lower $V_{c,max}$ and J_{max}. However, *3b* mutants weighed significantly less than WT, suggesting that the leaves were thinner (higher SLA) and this is in line with mutants (*1a, 2b3b, 1a2b* and *1a3b*) that had lower photosynthetic capacity. A reallocation of resources to expand leaf area and reduce thickness when

photosynthetic capacity is limiting has been observed previously in Arabidopsis antisense lines with reduced Rubisco activase grown under high light (Eckardt *et al.,* 1997).

The decrease in *RbcS* expression under low growth temperatures correlated with the decrease in Arabidopsis growth. The decrease in biomass correlates with the *RbcS* content which likely resulted in lower Rubisco content and photosynthetic rate as found in rose grown at 10^{o}C (Ushio *et al.,* 2008). However, the decrease in growth was not observed in the *1a* and *1a2b* KO mutants as hypothesised. Despite having no significant difference in rosette area compared to WT, *1a* and *1a2b* KO mutants had lower weight despite no significant decrease in rosette area, which was similar to *3b* mutants grown under high light. As the plants grown at 10^{o}C were still small at the end of 28 days relative plants grown under standard conditions, a longer experimental period may be able to discern the differences in rosette areas of *1a* and *1a2b*.

Studies have shown that a higher growth temperature increased the growth rate of Arabidopsis which was mediated by faster cell elongation (Gray *et al.,* 1998; Ghannoum *et al.,* 2010). However, growth under high temperature is also accompanied lower photosynthetic rate due to reduced activation of Rubisco by Rubisco activase (Crafts-Brandner and Salvucci, 2000; Salvucci and Crafts-Brandner, 2004). Growing Arabidopsis under high temperature did not result in differences in weights and area between WT and *3b* mutants as hypothesised. This was surprising, and could be due to the experimental design. For example, the RT-qPCR data showed that 3B accounted for *ca.* 50% of total transcript abundance in high temperature and under 200 µmol photons m^{-2} s^{-1} white light (with 1A, 1B, and 2B accounting for the remaining 50%). Similar light conditions were

used for the standard conditions growth experiment. Thus in the absence of 3B where 50% of *RbcS* transcripts were still available, the light conditions used were unlikely to result in an observable reduction in growth. This was evident in *1a2b* where 53% reduction in *RbcS* transcript did not result in reduction in growth (**Figure 5.4 and 5.9**). Previous work in in tobacco has shown that Rubisco content can be reduced to *ca*. 50% before a growth phenotype is observed under standard growth conditions (Quick *et al.,* 1991). Tobacco also reportedly adjusts to high temperature by increasing stomatal conductance to enhance the internal CO_2 concentration, which consequently compensated for the decrease in Rubisco (Krapp *et al.,* 1993). Future work could improve the experimental design to measure growth under higher light (Rubisco limiting conditions) and higher temperatures.

Chapter 6 - BigBoi as a platform to study the impact of heterologous SSUs in Arabidopsis: complementation of a triple *rbcs* mutant with a Chlamydomonas SSU

Introduction

Rubisco SSUs have been shown to influence catalytic activities of Rubisco enzyme (Fukayama *et al.,* 2019; Lin *et al.,* 2019). Modification of Rubisco performance was achieved by expressing a phylogenetically distinct native isoform of SSU or heterologous SSU in leaves (Morita *et al.,* 2014; Atkinson *et al.,* 2017). However, in a plant system where heterologous SSU was expressed, native SSUs have always been present and a confounding factor because it has been challenging to knockout all native SSUs in plants. A more common method to generate hybrid Rubisco was to switching out the single LSU gene in the chloroplast (Sharwood *et al.,* 2008; Whitney and Sharwood, 2008; Genkov *et al.,* 2010; Zhang *et al.,* 2011). Nevertheless, robust and well-established protocols for chloroplast transformation are limited to tobacco and model algae such as Chlamydomonas (Bock 2015).

In chapter 4, the generated triple *rbcs* mutant BigBoi was characterised. BigBoi is the first reported Arabidopsis mutant with only one native SSU isoform supporting photosynthetic growth. This novel mutant has two main advantages as a platform for the study of heterologous SSUs. Firstly, BigBoi can be used to generate a fully hybrid Rubisco (heterologous SSU, native LSU) in two steps: i) complementation with heterologous SSUs and ii) removal of 1B via an established CRISPR/Cas9 editing approach (Chapter 4 - Generating *rbcs* single mutants using CRISPR/Cas9). Secondly, identifying a complemented BigBoi T1 line is straightforward, as any improvement in growth

phenotype is easily visible. Therefore, BigBoi could be exploited as a model plant platform to re-engineer Rubisco and study the impact on Rubisco activity. This chapter outlines a preliminary 'proof of principle' study to complement BigBoi with a heterologous SSU from the green algae Chlamydomonas. Due to time constraints, subsequent knockout of the remaining 1B isoform was not done. Nevertheless, growth analysis showed that BigBoi was transformable and complemented by an algal SSU.

Results

Following transformation of BigBoi with a Chlamydomonas *RbcS2* expression cassette (**Supplemental Figure 6.2**), successfully transformed T1 plants were selected visually based on their greener colour and enhanced growth rates (**Figure 6.1A)** In total, seven T1 complemented lines were identified. PCR screening confirmed the presence of the Chlamydomonas SSU insert (**Figure 6.1B**). Protein extraction followed by SDS-PAGE and Coomasie staining showed a band of similar size to Chlamydomonas SSU expressed in the complemented plants (**Figure 6.2C**). Notably, the band was also of similar size to the *RbcS2* band in an Arabidopsis *1a3b* mutant previously complemented with the Chlamydomonas SSU (R2) (Atkinson *et al.*, 2017). Western blot was performed following SDS-PAGE but Chlamydomonas SSU was not detected possibly due to the low expression level. In addition, the levels of expression were much reduced compared to R2 in complemented BigBoi lines. The lower levels of Chlamydomonas SSU observed may be due to heterozygosity in the T1 generation.

In the T2 generation, segregation ratio of 1:2:1 were visibly evident for four of the seven complemented lines. For lines 1-4, putative T2 homozygous plants were more green and grew faster while putative T2 heterozygous plants were almost as pale as but bigger than the segregated BigBoi (**Figure 6.1D**). Lines 5-7 showed no differences in hypocotyl colour compared to BigBoi. Although complemented plants were bigger in size, putative homozygous and heterozygous could not be distinguished based on size. A growth analysis of T2 plants was performed (300 µmol m^{-2} s^{-1} photon, 12 h light : 12 h dark cycle, 21^{o}C) to assess the impact of Chlamydomonas SSU complementation on growth (**Figure 6.2**).

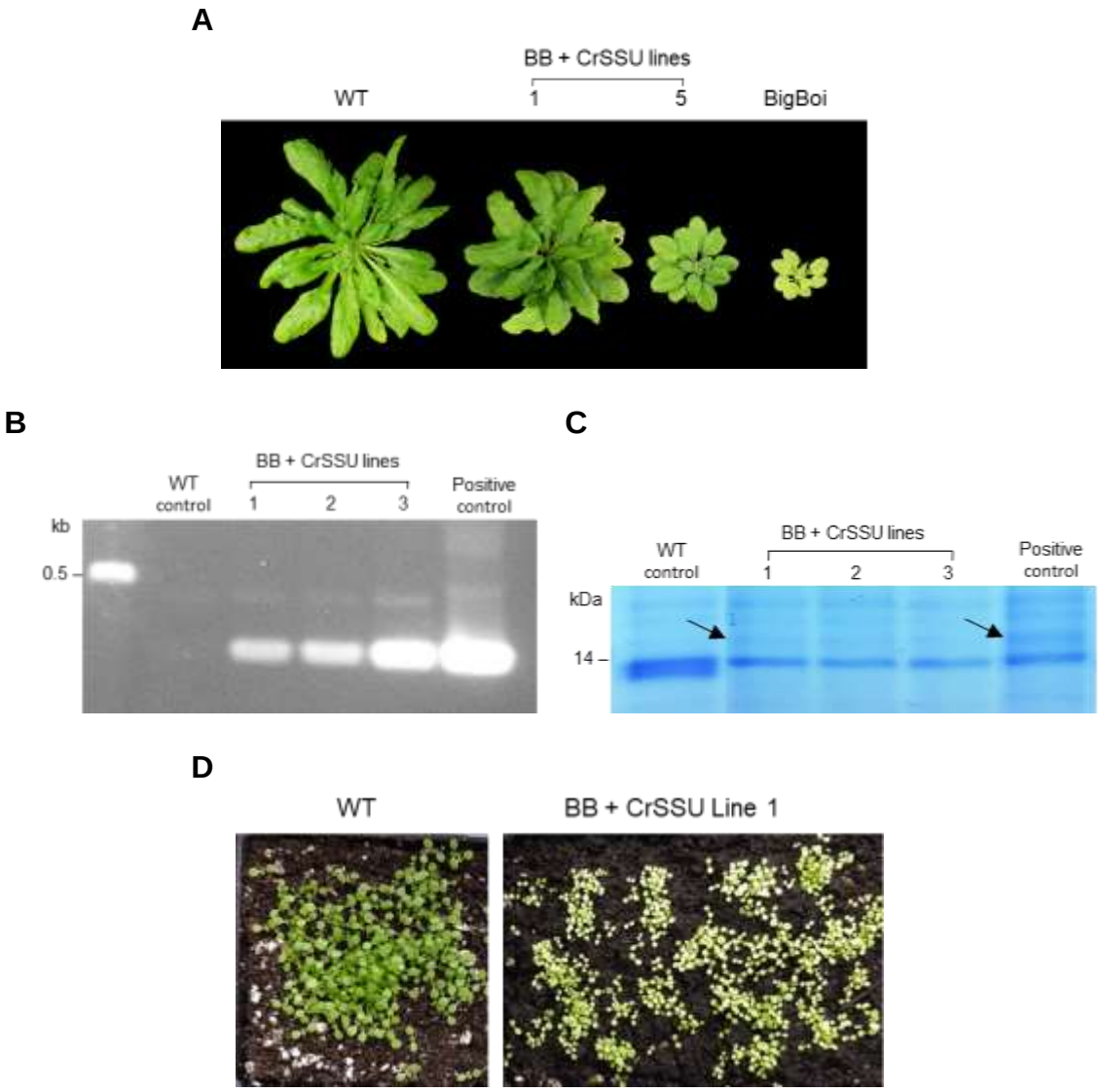

Figure 6.1A. Characteristics of Chlamydomonas SSU complemented BigBoi. A) Images of 8 weeks old biggest (Line 1) and smallest (Line 5) T1 BigBoi complemented with Chlamydomonas SSU. B) Representative image of PCR confirmation of the Chlamydomonas SSU insertion of Lines 1-3 using Chlamydomonas SSU-specific primers (**Supplemental table 6.1**). C) Representative image of Coomasi staining of 12% bis-tris SDS-PAGE showing the presence of a band of similar size to the Chlamydomonas SSU.

R2 line (Atkinson *et al.,* 2017) was used as positive control. D) Representative image of T2 segregation of Line 1 in comparison to WT.

All seven complemented lines showed improved growth phenotype compared to BigBoi (**Figure 6.2**). Putative homozygous plants in Lines 1-4 showed greener and bigger cotyledons than the segregated BigBoi while putative heterozygous was less green and smaller than putative homozygous but bigger than segregated BigBoi. In Lines 5-7, putative homozygous and heterozygous were distinguished based on the difference in sizes as there was obvious difference in colour. Putative homozygous plants for all lines had increased rosette area and biomass compared to putative heterozygous plants (**Figure 6.2 and 6.3A, D)**. Line 1 grew the fastest, while Line 5 grew the slowest. The rosette area of putative homozygous plants on 28 DAG for Lines 1 and 5 were 34% and 9% of WT plants, respectively, while FW was 18% and 4% of WT, respectively (**Figure 6.3 D, E**). In contrast, the area of BigBoi was 1.4% and FW was 0.3% of WT. The SLA values of all seven complemented lines were significantly higher than that of WT but were all lower than that of BigBoi (**Figure 6.3B**) Furthermore, F_v/F_m was restored to WT levels for all complemented lines (**Figure 6.3C**).

A

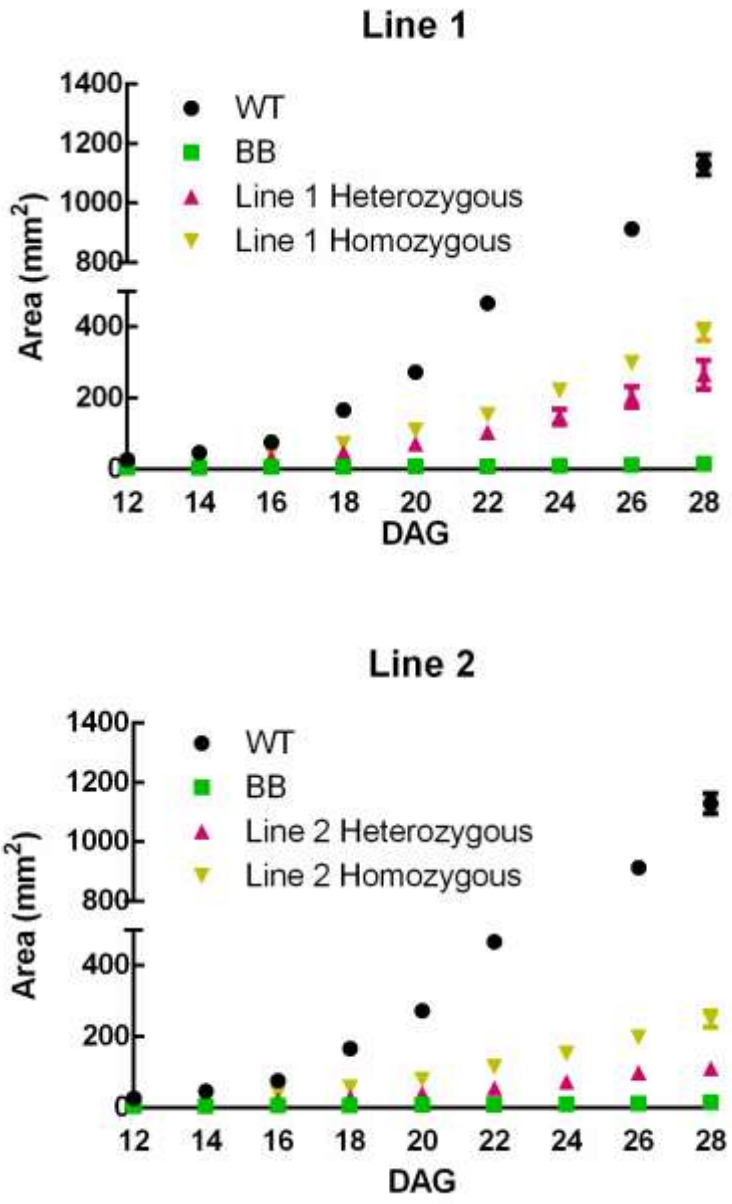
Line 1
WT
BB
Line 1 Heterozygous
Line 1 Homozygous
Area (mm2)
1400
1200
1000
800
400
200
0
12
14
16
18
20
22
24
26
28
DAG
Line 2
WT
BB
Line 2 Heterozygous
Line 2 Homozygous
Area (mm2)
1400
1200
1000
800
400
200
0
12
14
16
18
20
22
24
26
28
DAG

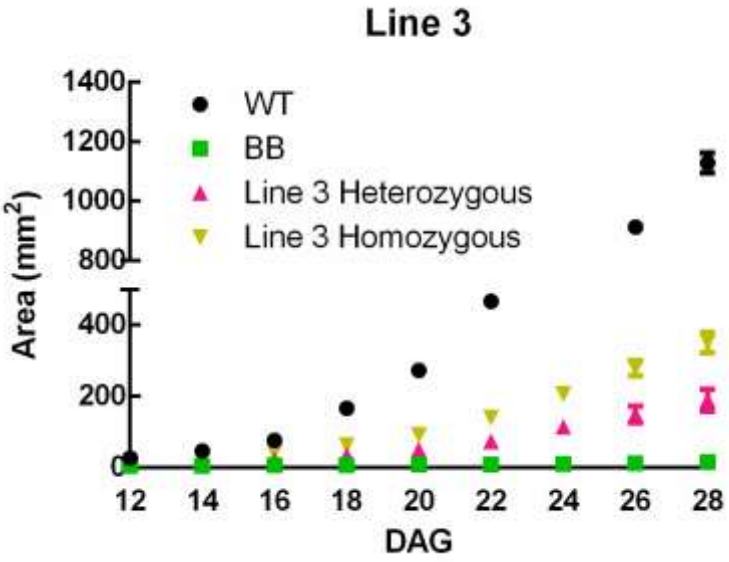
Line 3
1400
1200
1000
800
400
200
0
Area (mm2)
WT
BB
Line 3 Heterozygous
Line 3 Homozygous
12
14
16
18
20
22
24
26
28
DAG

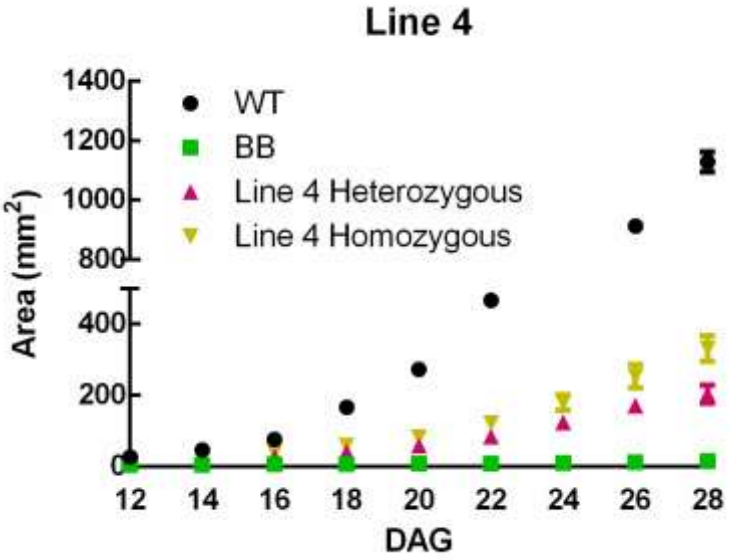
Line 4
1400
1200
1000
800
400
200
0
Area (mm2)
WT
BB
Line 4 Heterozygous
Line 4 Homozygous
12
14
16
18
20
22
24
26
28
DAG

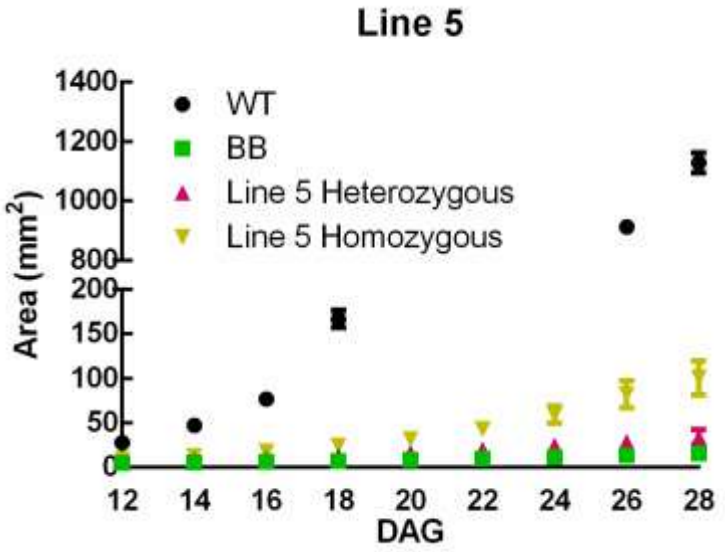
Line 5
WT
BB
Line 5 Heterozygous
Line 5 Homozygous
Area (mm2)
1400
1200
1000
800
200
150
100
50
0
12
14
16
18
20
22
24
26
28
DAG

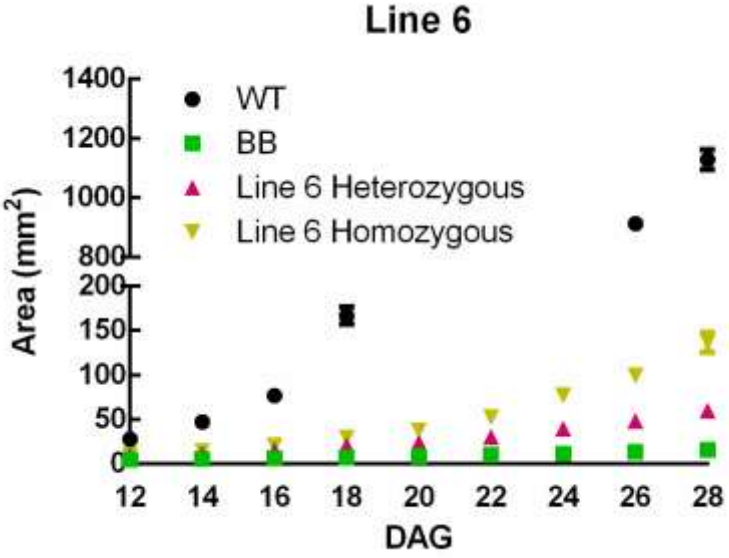
Line 6
WT
BB
Line 6 Heterozygous
Line 6 Homozygous
Area (mm2)
1400
1200
1000
800
200
150
100
50
0
12
14
16
18
20
22
24
26
28
DAG

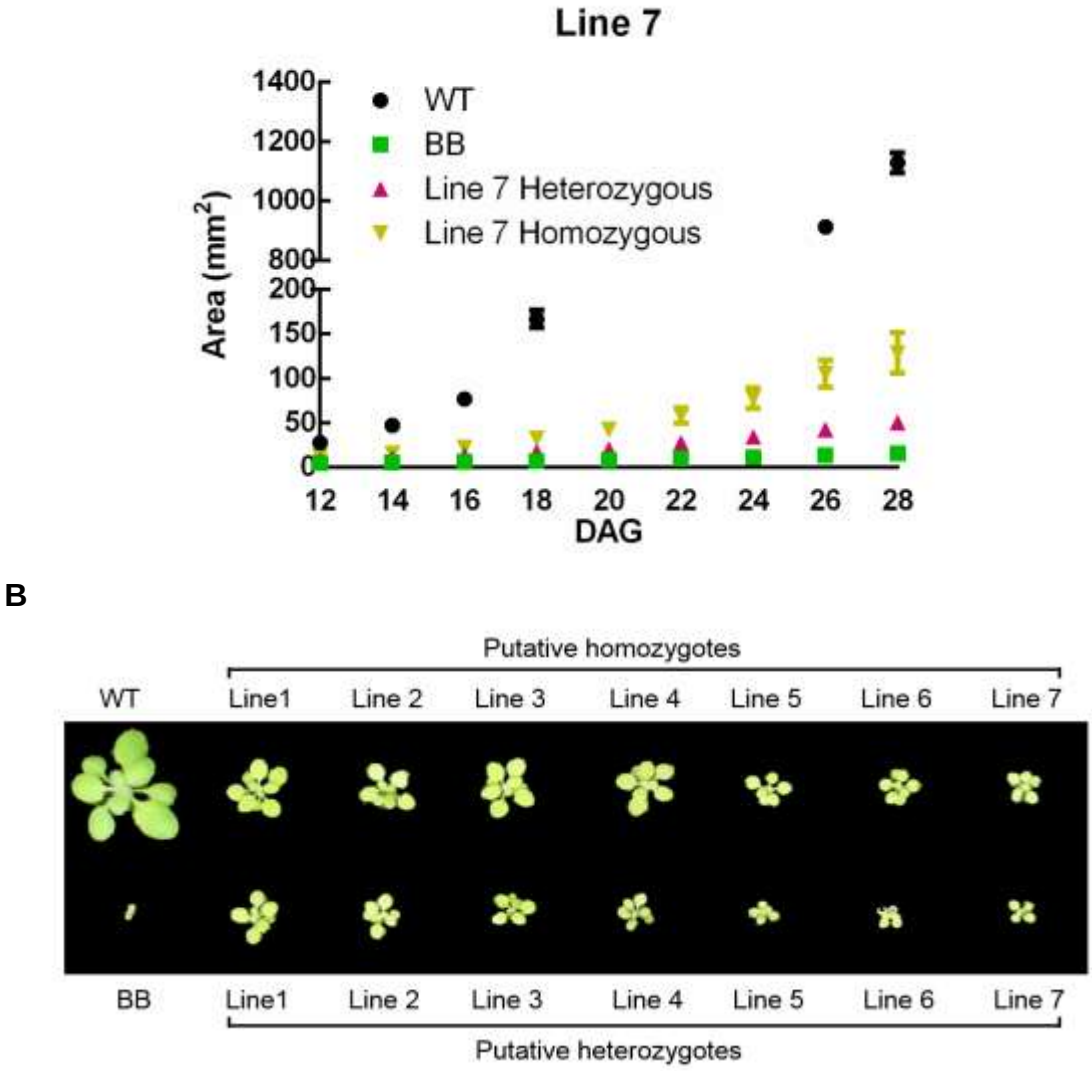

Figure 6.2. Growth of Chlamydomonas SSU complemented BigBoi lines. A) Rosette expansion of complemented lines in comparison to WT and BigBoi (BB) monitored from 12-28 days after germination (DAG). The values are means ± SE of measurements made on 6-8 individual rosettes. B) Representative images of 20-d-old rosettes of putative heterozygous and homozygous Chlamydomonas SSU complemented BigBoi lines**.**

A

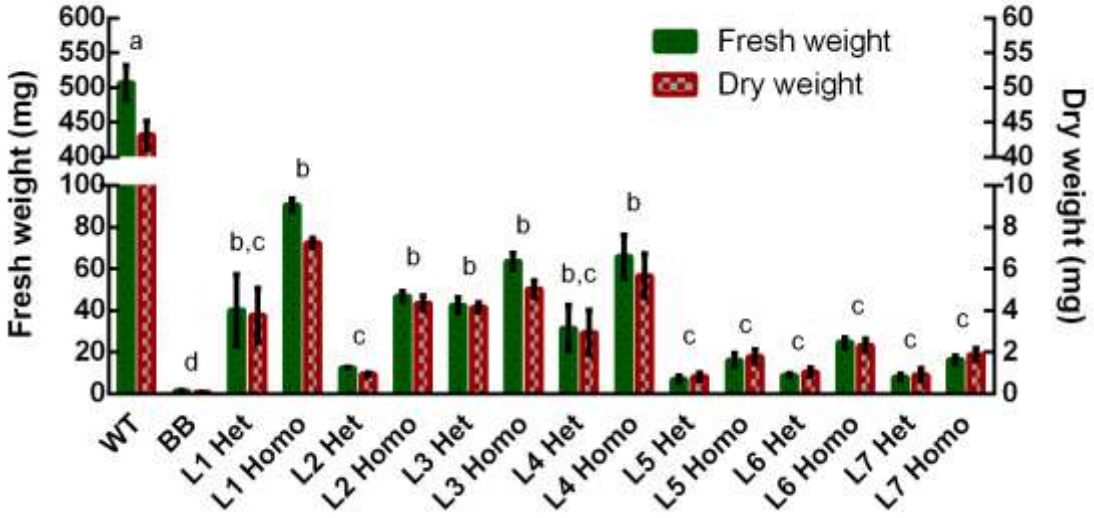
Fresh weight (mg)
Dry weight (mg)
Fresh weight
Dry weight
600
550
500
450
400
100
80
60
40
20
0
60
55
50
45
40
10
8
6
4
2
0
a
d
b,c
b
c
b
b
b
b,c
b
c
c
c
c
c
c
WT
BB
L1 Het
L1 Homo
L2 Het
L2 Homo
L3 Het
L3 Homo
L4 Het
L4 Homo
L5 Het
L5 Homo
L6 Het
L6 Homo
L7 Het
L7 Homo

B

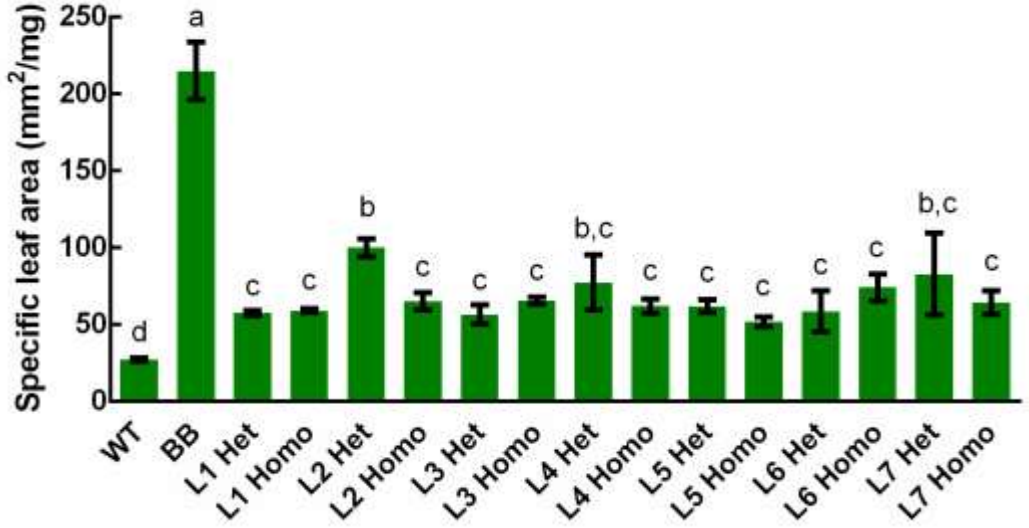
Specific leaf area (mm²/mg)
250
200
150
100
50
0
d
a
c
c
b
c
c
c
b,c
c
c
c
c
c
b,c
c
WT
BB
L1 Het
L1 Homo
L2 Het
L2 Homo
L3 Het
L3 Homo
L4 Het
L4 Homo
L5 Het
L5 Homo
L6 Het
L6 Homo
L7 Het
L7 Homo

C

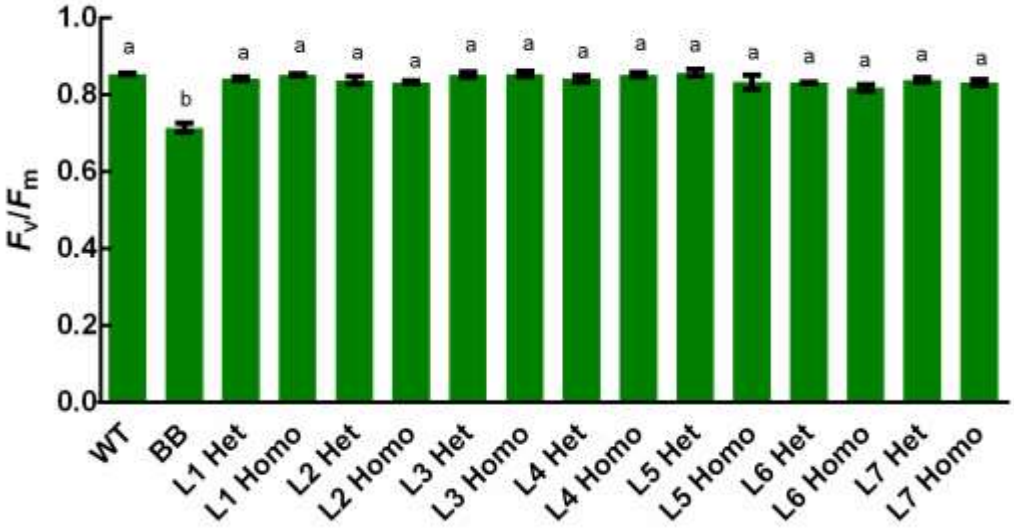
1.0
0.8
0.6
0.4
0.2
0.0
F_v/F_m
a
b
a
a
a
a
a
a
a
a
a
a
a
a
a
a
WT
BB
L1 Het
L1 Homo
L2 Het
L2 Homo
L3 Het
L3 Homo
L4 Het
L4 Homo
L5 Het
L5 Homo
L6 Het
L6 Homo
L7 Het
L7 Homo

D

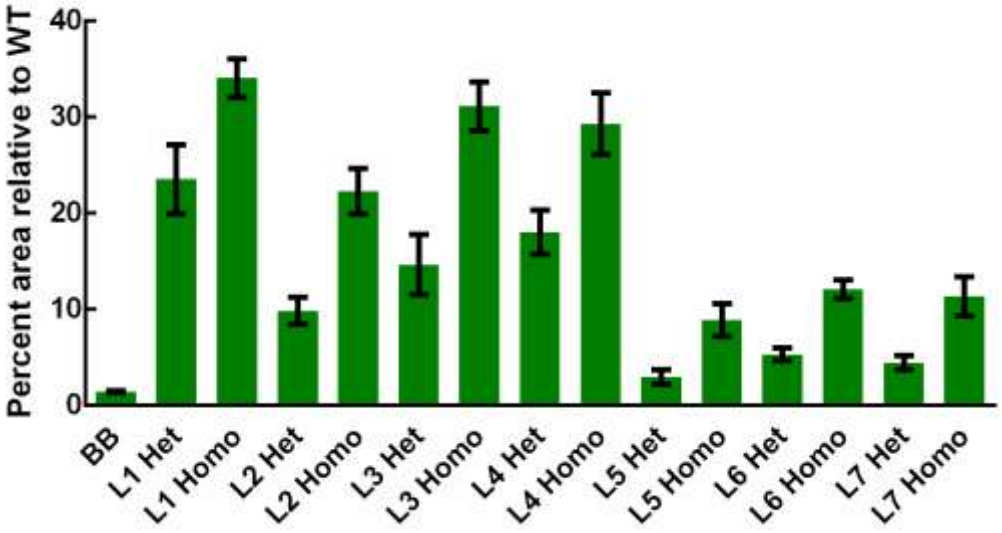
Percent area relative to WT
40
30
20
10
0
BB
L1 Het
L1 Homo
L2 Het
L2 Homo
L3 Het
L3 Homo
L4 Het
L4 Homo
L5 Het
L5 Homo
L6 Het
L6 Homo
L7 Het
L7 Homo

Figure 6.3. Growth analysis of BigBoi lines complemented with Chlamydomonas SSU in the T2 generation. A) Fresh and dry weight, B) specific leaf area, C) maximum potential quantum efficiency of PSII (F_v/F_m), D) Percent weight relative to WT. The values represent mean ± SEM of measurements made on 6-8 samples for fresh weight, dry weight and specific leaf area and four samples for F_v/F_m. Different letters above the bars indicate significant difference ($P < 0.05$) as determined by ANOVA followed by Tukey's HSD tests.

Discussion

In this chapter, preliminary data was presented to demonstrate that a Chlamydomonas SSU was successfully expressed in the triple KO mutant BigBoi and that a heterologous SSU was able to rescue the slow-growing phenotype. The transformation efficiency of BigBoi was comparable to that of WT (*ca.* 0.5%). However, more BigBoi plants were needed for floral-dipping to obtain an equal number of transformants because of lower flower and seed yields. The seven independent complemented lines displayed a range of growth rates, likely due differences in level of the heterologous SSU expression. These differences could arise from difference in location of chromosomal integration, spatial and temporal regulation of the transgene promoter activity relative to the chromosomal insert, (Hobbs *et al.,* 1990; Matzke and Matzke, 1998; Day *et al.,* 2000; Van Leeuwen *et al.,* 2001). Further characterisation of the insert should be performed on these lines to locate the insertion site (i.e. TAIL-PCR) and compare to the associated expression level.

BigBoi is a significant improvement over *1a3b* as a platform to test the effects of heterologous SSUs in Arabidopsis (Atkinson *et al.*, 2017). The only remaining native SSU isoform in BigBoi (1B) represents *ca.* 3% of the total SSU pool, which means that confounding factors attributed to native SSUs are more subdued. Moreover, 1B expression could be removed by CRISPR/Cas9 editing (as outlined in Chapter 4) following complementation with a heterologous SSU, which would result in a completely hybrid heterologous SSU: native LSU Rubisco. Future work should focus on removing 1B in homozygous T3 lines of the Chlamydomonas SSU complemented BigBoi lines, whereupon Rubisco content and Rubisco catalytic activities could be measured. The recently published protocols for chloroplast transformation in Arabidopsis (Yu *et al.*, 2017; Ruf *et al.*, 2019) add to the possibility of generating hybrid Rubisco where the native Arabidopsis LSU can also be modified, thus bolstering Arabidopsis as a powerful platform for the study of Rubisco catalysis *in planta*.

BigBoi may prove to have other useful applications and can be used as a model to answer questions about Rubisco. For example, it was previously hypothesised by Sawchuck *et al*. (2008) that 1B may modify Rubisco kinetics. BigBoi could be used to substantiate the hypothesis by measuring the Rubisco enzyme kinetics in comparison to that of WT and *1b* KO mutants generated in Chapter 4. In addition, as the contribution of the individual SSU to the Rubisco enzyme is still unclear, the triple mutant could be exploited as a model to knock in native SSUs tagged with different fluorescence probes (Ishida et al. 2010). This method would allow for the visualisation of composition of each SSU in the Rubisco enzyme.

Conclusive remarks

Rubisco has been a subject of scientific scrutiny for decades due to its central role in photosynthesis. Despite the importance, the enzyme is catalytically inefficient and modification through mutagenesis or re-engineering of subunits has observed marginal improvement on the catalytic activities. This difficulty not only highlights the complexity of Rubisco but also how much we can still learn about the functional roles of the subunits.

This thesis is a stepping stone to understanding the roles of Rubisco SSUs in Arabidopsis. To understand the functions of an enzyme, we first investigated the T-DNA insertion mutants in Arabidopsis. Due to the inherent limitations of T-DNA insertion mutants (outlined in Chapter 3), we improved on the system by using CRISPR/Cas9 editing to generate a suite of *rbcs* KO mutants, which includes novel mutants (*2b3b* and *1a2b3b*) that would not have been possible by T-DNA insertion method. These new KO knockout lines were characterised through molecular tools including RT-qPCR and Western blot to ensure gene and protein knockouts. In addition, we performed physiological characterisation of mutants and found that knocking out single SSU isoform did not affect growth of plants in standard conditions. The adverse effects to growth was observed in the *1a3b* mutant where Rubisco was *ca*. 45% of WT level. Growth was further stunted when Rubisco was decreased to *ca.* 15% in the triple mutant *1a2b3b* (BigBoi) as only the minor isoform 1B was the only remaining SSU responsible for photosynthetic growth.

Using CRISPR/Cas9 KO mutants as models, we explored the expression of the *RbcS* genes under different environmental conditions. We found that under high light

conditions, there was more demand for Rubisco and therefore knocking out major isoforms like 1A and 3B had negative effects on rosette area and/or weight (both fresh weight and dry weight). The expression of 2B and 3B varied more than that of 1A under changing temperatures as 2B and 3B were more highly expressed under high temperature and suppressed under low temperature. This evidence suggests the importance of 2B and 3B as temperature mediators of the *RbcS* gene family in Arabidopsis.

Lastly, we have established a platform for the study of SSU complementation using BigBoi as a model. BigBoi was complemented with SSU from Chlamydomonas and a rescue in growth of up to 40% of WT was observed. As there are structural differences between plant and algae SSUs, a WT-level of complementation was not expected. However, this platform could be used to further probe for regions of Rubisco that could be modified or test other heterologous SSUs to improve the catalytic properties.

BigBoi seeds and other KO mutants generated via CRISPR/Cas9 in this study will be available for the public through Nottingham Arabidopsis Seed Center (NASC) once the accompanying manuscript is published.

Supplemental information

Chapter 3

Supplemental table 3.1. Primers used PCR screening of T-DNA insertion mutants in chapter 3

Primer ID	Forward	Reverse	Amplicon (bp)
1A	CCATAAGGAAAGGGCCAAGT	CATTGTCCAGTACCGTCCATC	980
1B	ATAAAATTTTGTCTCGCGGTG	TACCGTCCATCGTAGTATCCG	1025
2B	TGGGTTCCTCTTGTTCATCAG	CACTTGTTGCGGAGAAGGTAG	1066
3B	TGCCTGAAAAATCTTAACAATTG	CACTTGTTGCGGAGAAGGTAG	1160
1A (*1a1b*)	GACCAAAGCACTAGACCAAACC	GATGGGGGATAAAGTTTTGAGG	879
1B (*1a1b*)	CAATCACTCATTTCCTCACAAA	TTGGGTTCCGGATAGTCAAC	1045
GABI T-DNA (left border)	ATATTGACCATCATACTCATTGC	-	-
SAIL T-DNA (left border)	GCCTTTTCAGAAATGGATAAATAGCCTTGCTTCC	-	-
SALK T-DNA (left border)	ATTTTGCCGATTTCGGAAC	-	-

Supplemental table 3.2. qPCR primers used for quantification of transcript abundance

Primer ID	Forward	Reverse	Amplicon (bp)
1A (Iz)	AATTTCCGGACTTAACGTTTGTTT	TCTATCGGATTCTCAACTGTCTGATG	69
1B (Iz)	GCCAAAGTGAAAAAACTGAAGGTT	TCTATTCATATCACTTCATTTCTGCTCTT	83
2B (Iz)	ACCCATTTCTATGTGGTCAATGC	GTTGAGGAACTATTGTTTGAAAGTGAA	80
3B (Iz)	CCTATTGTCTGTGTTCTTTTTCTCTTTATG	TGTAATTTATATATCCGTGCGTCTTGA	99
LSU (Iz)	GATGGGCTTACCAGCCTTGA	ACATCGAGCCCGTTCCAG	61
1A (Ca)	GGATCATCGGATTCGACAAC	TCCGGTTTGCGAGACATATT	217
1B (Ca)	GGATCATCGGATTCGACAAC	AGGTTTGTTTTTCTATCGTTTCCTC	205
2B (Ca)	GGATCATCGGATTCGACAAC	ATTGTGGCTCCTTTAAATTATCCTC	329
3B (Ca)	GGATCATCGGATTCGACAAC	TCGGATTGTCAAATGTCTGATTTA	196
LSU (Ca)	GTGTTGGGTTCAAAGCTGGT	GACAACTGTGTGGACCGATG	189

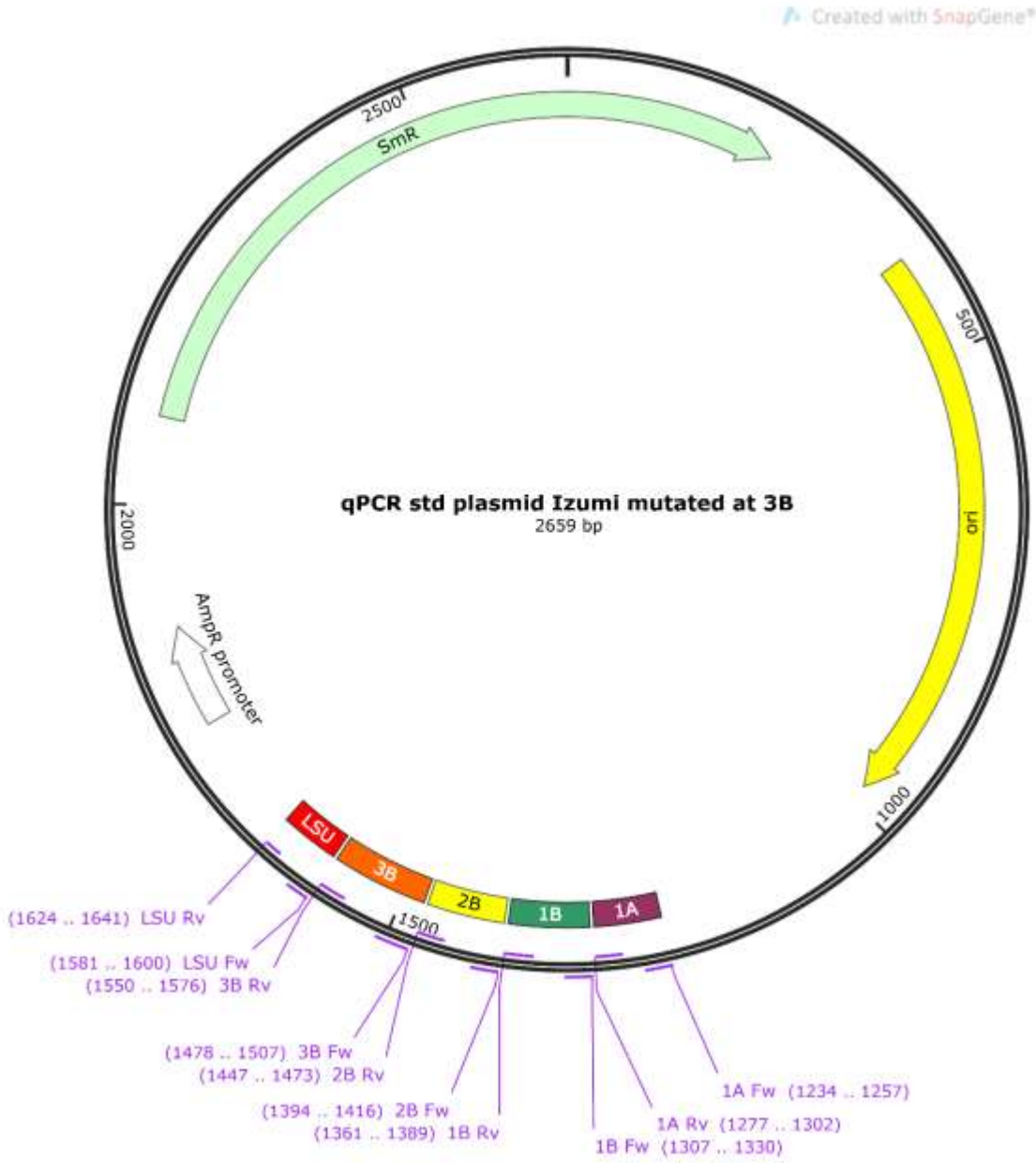

Supplemental figure 3.1. Standard plasmid used for RT-qPCR to construct the standard curve for *RbcS* and *RbcL* genes using specific primers. Regions in the 5'UTR for *RbcS* genes and a region spanning the exon-exon junction for the *RbcL* gene were synthesized and cloned into an L0 acceptor vector (pAGM9121) using Golden Gate assembly.

Chapter 4

Supplemental Table 4.1. gRNAs used in CRISPR/Cas9 editing

No.	Target	Name	Sequence	Location	Direction
1	1A	1AP11	TTGGAGTGATCGGAGGGTCT AGG	5'UTR	-
2	1A	1AP12	TATGCTCTCTTCCGCTACTA TGG	Exon 1	+
3	1A	1AP21	CGGAATCGGTAAGGTCAGGA AGG	Exon 2	-
4	1A	1AP22	ATATAAACTAGCTAGATCTT AGG	Intron 2	+
5	1B	1BP11	TATATAGTGAGAACCGTAAG AGG	5'UTR	-
6	1B	1BP12	GGAGGTAACCACAGCGGCAG AGG	Exon 1	-
7	1B	1BP21	TTACTTCCATCACAAGCAAT GGG	Exon 1	+
8	2B	2BP11	GGAATTCGAATTTATAGGTG TGG	Intron 1	+
9	2B	2BP12	TAAAGGATGCTTAGAGACAA AGG	Intron 2	-
10	2B	2BP21	TATATATCAATTGTATTGAA TGG	Intron 2	+
11	2B	2BP22	TGATCCTAATGAAGGCGCCA GGG	Exon 3	-
12	3B	3BP11	ATAAAGATGACAACACCAGT AGG	5'UTR	+
13	3B	3BP12	GGTCACCCGCAAGACCAACA AGG	Exon 1	+
14	3B	3BP21	TTAATTTGGAATTGGATTTG GGG	Intron 1	+
15	3B	3BP22	TTGTGTTGAATTCGAGTTAG AGG	Exon 2	+
16	1B, 3B	1B3B1	GGGAAGAGTTAGCTGCATGA AGG	Exon1	+
17	1B, 2B, 3B	1B3B2	GGAAGTTGAAGAATGCAAGA AGG	Exon 3	+

Supplemental Table 4.2. Primers used to amplify regions of *RbcS* genes for the screening of mutations

Primer ID	Forward	Reverse	Amplicon (bp)	Description
1A	TCCACACTCAAAATCCAACG	CCACATGTTACAAACCACTCAG	701	
1B	CAATCACTCATTTCCTCACAAA	TGGTGGCCACACCTATAATTC	469	
2B	GCTTCCTCTATGTTCTCCTCCA	TGCATTGACCACATAGAAATGG	834	
3B	AGTGGTGCGTACCGATAAGG	TCGGTTCTACAAAATCCGGTTA	696	
1A(1B3B)	GACCAAAGCACTAGACCAAACC	GATGGGGGATAAAGTTTTGAGG	879	Screening 1B3B lines
1B(1B3B)	CAATCACTCATTTCCTCACAAA	TTGGGTTCCGGATAGTCAAC	1045	Screening 1B3B lines
2B(1B3B)	GCTTCCTCTATGTTCTCCTCCA	TGGGTTCCAGAATAATCAACG	815	Screening 1B3B lines
3B(1B3B)	GCCTTTAGGGGGTTCTCATT	TCCTTTCAAGTGGACCATCC	1326	Screening 1B3B lines

Chapter 6

Supplemental table 6.1. Primer used to amplify the transgene in the Chlamydomonas SSU complemented BigBoi Lines

Primer ID	Forward	Reverse	Amplicon (bp)
CrSSU	GCCGAGAGCGATAAAGCCTA	CGGCCTCTGTACAAGGAACC	246

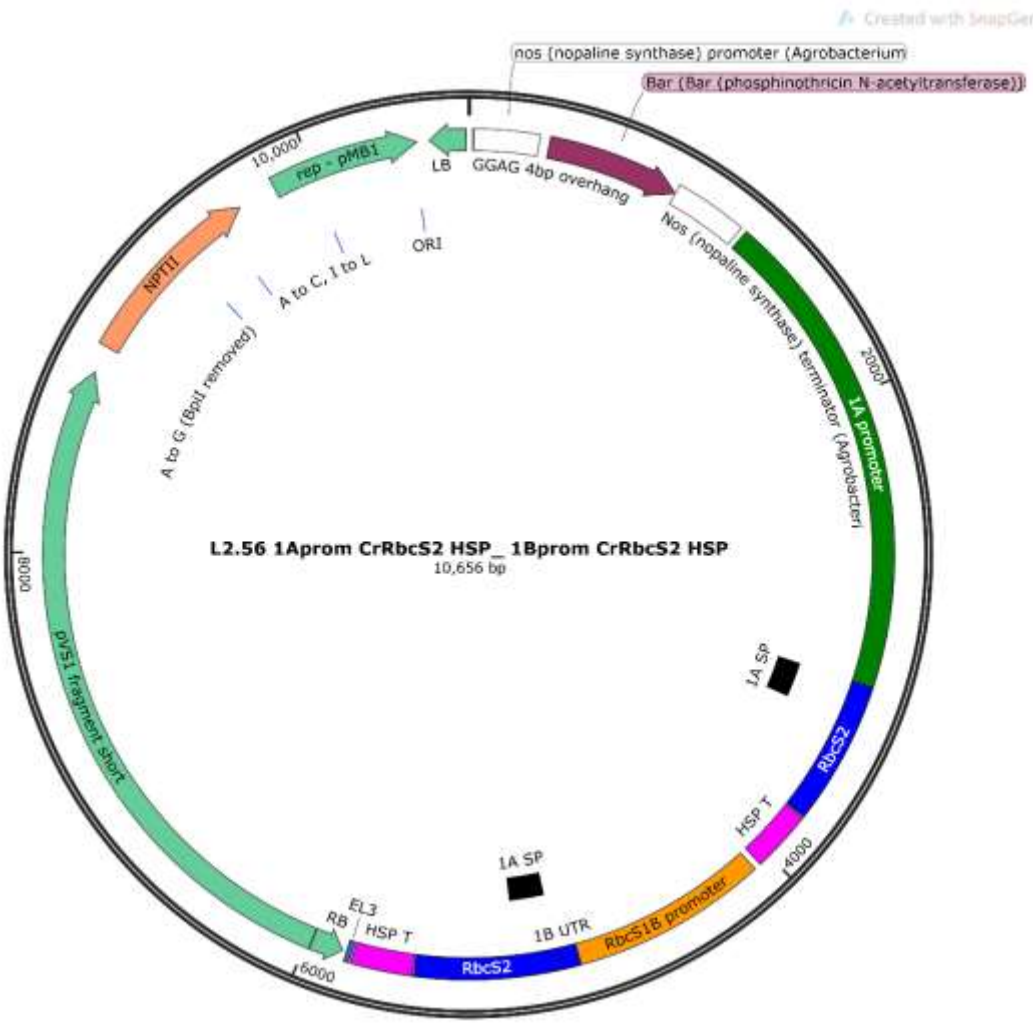

Supplemental Figure 6.2. Level 2 expression plasmid containing Chlamydomonas *RbcS2* driven by Arabidopsis 1A and 1B promoters and Arabidopsis heat shock protein (HSP) terminator. BASTA was used as a selection marker. SP is signal peptide.

References

Aigner H, Wilson RH, Bracher A, et al (2017) Plant RuBisCo assembly in E. coli with five chloroplast chaperones including BSD2. Science 358:1272–1278.

Alonso JM, Stepanova AN, Leisse TJ, et al (2003) Genome-wide insertional mutagenesis of Arabidopsis thaliana. Science 301:653–657.

Andersson I (1996) Large Structures at High Resolution: The 1.6 Å Crystal Structure of Spinach Ribulose-1,5- Bisphosphate Carboxylase/Oxygenase Complexed with 2-Carboxyarabinitol Bisphosphate. J Mol Biol 259:160–174.

Andersson I (2008) Catalysis and regulation in Rubisco. J Exp Bot 59:1555–1568.

Andersson I, Backlund A (2008) Structure and function of Rubisco. Plant Physiol Biochem 46:275–291.

Andersson I, Knight S, Schneider G, et al (1989) Crystal structure of the active site of ribulose-bisphosphate carboxylase. Nature 337:229–234.

Andersson I, Taylor TC (2003) Structural framework for catalysis and regulation in ribulose-1,5-bisphosphate carboxylase/oxygenase. Arch Biochem Biophys 414:130–140.

Andrews TJ (1996) The bait in the Rubisco mousetrap. Nat Struct Biol 3:3–7.

Andrews TJ, Lorimer GH (1985) Catalytic Properties of a Hybrid between Cyanobacterial Large Subunits and Higher-Plant Small Subunits of Ribulose Bisphosphate Carboxylase-Oxygenase. J Biol Chem 260:4632–4636

Atkinson N, Feike D, Mackinder LCM, et al (2016) Introducing an algal carbon-concentrating mechanism into higher plants: Location and incorporation of key components. Plant Biotechnol J 14:1302–1315.

Atkinson N, Leitão N, Orr DJ, et al (2017) Rubisco small subunits from the unicellular green alga Chlamydomonas complement Rubisco-deficient mutants of Arabidopsis. New Phytol 214:655–667.

Badger MR, Andrews TJ, Whitney SM, et al (1998) The diversity and coevolution of Rubisco, plastids, pyrenoids, and chloroplast-based CO2-concentrating mechanisms in algae. Can J Bot 76:1052–1071.

Barrangou R, Marraffini LA (2014) CRISPR-cas systems: Prokaryotes upgrade to adaptive immunity. Mol. Cell 54:234–244

Belhaj K, Chaparro-Garcia A, Kamoun S, et al (2015) Editing plant genomes with CRISPR/Cas9. Curr Opin Biotechnol 32:76–84.

Bock R (2015) Engineering Plastid Genomes: Methods, Tools, and Applications in Basic Research and Biotechnology. Annu Rev Plant Biol 66:211–241.

Bracher A, Whitney SM, Hartl FU, Hayer-Hartl M (2017) Biogenesis and Metabolic Maintenance of Rubisco. Annu Rev Plant Biol 68:29–60.

Bradford M (1976) A rapid and senstive method for the quantification of microgram quantities of protein utilizing the principle of protein-dye binding. Anal Biochem 72:248–254.

Castel B, Tomlinson L, Locci F, et al (2019) Optimization of T-DNA architecture for Cas9- mediated mutagenesis in Arabidopsis. PLoS One 10:1–20.

Cavanagh AP (2016) The role of the Rubisco small subunit in Arabidopsis thaliana. University of New Brunswick

Cen Y-P, Sage RF (2005) The Regulation of Rubisco Activity in Response to Variation in Temperature and Atmospheric CO 2 Partial Pressure in Sweet Potato . Plant Physiol 139:979–990.

Cermak T, Curtin SJ, Gil-Humanes J, et al (2017) A multi-purpose toolkit to enable advanced genome engineering in plants. Plant Cell 29:1196–1217.

Chang HHY, Pannunzio NR, Adachi N, Lieber MR (2017) Non-homologous DNA end joining and alternative pathways to double-strand break repair. Nat Rev Mol Cell Biol 18:495–506.

Chen Z, Chastain CJ, Chollet R, et al (1988) Reduced CO2/O2 specificity of ribulose-bisphosphate carboxylase/oxygenase in a temperature-sensitive chloroplast mutant of Chlamydomonas. Proc Natl Acad Sci U S A 85:4696–4699.

Cheng S-H, Moore B d., Seemann JR (1998) Effects of Short- and Long-Term Elevated CO 2 on the Expression of Ribulose-1,5-Bisphosphate Carboxylase/Oxygenase Genes and Carbohydrate Accumulation in Leaves of Arabidopsis thaliana (L.) Heynh. . Plant Physiol 116:715–723.

Clark K, Krysan P (2010) Chromosomal translocations are a common phenomenon in Arabidopsis thaliana T-DNA insertion lines. Plant J 64:990–1001.

Cong L, Ran F, Cox D, et al (2013) Multiplex genome engineering using CRISPR/Cas systems. Science 340:216–219.

Coruzzi G, Broglie R, Edwards C, Chua NH (1984) Tissue-specific and light-regulated expression of a pea nuclear gene encoding the small subunit of ribulose-1,5-bisphosphate carboxylase. EMBO J 3:1671–1679.

Crafts-Brandner SJ, Salvucci ME (2000) Rubisco activase constrains the photosynthetic potential of leaves at high temperature and CO2. Proc Natl Acad Sci 97:13430–13435.

Dalal J, Lopez H, Vasani NB, et al (2015) A photorespiratory bypass increases plant growth and seed yield in biofuel crop Camelina sativa. Biotechnol Biofuels 8:175.

Day CD, Lee E, Kobayashi J, et al (2000) Transgene integration into the same chromosome location can produce alleles that express at a predictable level, or alleles that are differentially silenced. Genes Dev 14:2869–2880.

Dean C, Pichersky E, Dunsmuir P (1989) Regulation of RbcS genes in higher plants. Annu Rev Plant Physiol Plant Mol Biol 40:1989.

Dean C, van den Elzen P, Tamaki S, et al (1987) Molecular characterization of the rbcS multi-gene family of Petunia. Mol Gen Genet 206:465–474.

Dedonder A, Rethy R, Fredericq H, et al (1993) Arabidopsis RbcS genes are differentially regulated by light. Plant Physiol 101:801–8.

Derocher EJ, Quigley F, Mache R, Bohnert HJ (1993) The six genes of the Rubisco small

subunit multigene family from Mesembryanthemum crystallinum, a facultative CAM plant. Mol Gen Genet 239:450–462.

Dodd AN, Borland AM, Haslam RP, et al (2002) Crassulacean acid metabolism: plastic, fantastic. J Exp Bot 53:569–580.

Du Y, Peddi SR, Spreitzer RJ (2003) Assessment of structural and functional divergence far from the large subunit active site of ribulose-1,5-bisphosphate carboxylase/oxygenase. J Biol Chem 278:49401–49405.

Duff AP, Andrews TJ, Curmi PMG (2000) The transition between the open and closed states of rubisco is triggered by the inter-phosphate distance of the bound bisphosphate. J Mol Biol 298:903–916.

Durr J, Papareddy R, Nakajima K, Gutierrez-Marcos J (2018) Highly efficient heritable targeted deletions of gene clusters and non-coding regulatory regions in Arabidopsis using CRISPR/Cas9. Sci Rep 8:1–11.

Eckardt NA, Snyder GW, Portis Jr AR, Ogren WL (1997) Growth and Photosynthesis under High and Low Irradiance of Arabidopsis thaliana Antisense Mutants with Reduced Ribulose-1,5-Bisphosphate Carboxylase/Oxygenase Activase Content. Plant Physiol 113:575–586.

Eid A, Ali Z, Mahfouz MM (2016) High efficiency of targeted mutagenesis in arabidopsis via meiotic promoter-driven expression of Cas9 endonuclease. Plant Cell Rep 35:1555–1558.

Emlyn-Jones D, Woodger FJ, Price GD, Whitney SM (2006) RbcX can function as a

Rubisco chaperonin, but is non-essential in Synechococcus PCC7942. Plant Cell Physiol 47:1630–1640.

Ernst D, Pfeiffer E, Schefbeck K, et al (1987) Phytochrome regulation of mRNA levels of ribulose-1,5-bisphosphate carboxylase in etiolated rye seedlings (Secale cereale). Plant Mol Biol 10:21–33.

Ethier GJ, Livingston NJ (2004) On the need to incorporate sensitivity to CO2 transfer conductance into the Farquhar-von Caemmerer-Berry leaf photosynthesis model. Plant, Cell Environ 27:137–153.

Ewing RM, Jenkins GI, Langdale JA (1998) Transcripts of maize RbcS genes accumulate differentially in C3 and C4 tissues. Plant Mol Biol 36:593–599.

Fauser F, Schiml S, Puchta H (2014) Both CRISPR/Cas-based nucleases and nickases can be used efficiently for genome engineering in Arabidopsis thaliana. Plant J 79:348–359.

Feng Z, Mao Y, Xu N, et al (2014) Multigeneration analysis reveals the inheritance, specificity, and patterns of CRISPR/Cas-induced gene modifications in Arabidopsis. Proc Natl Acad Sci U S A 111:4632–4637.

Feng Z, Zhang B, Ding W, et al (2013) Efficient genome editing in plants using a CRISPR/Cas system. Cell Res 23:1229–1232.

Fichtner K, Quick WP, Shulze E-D, et al (1993) Decreased ribulose-1, 5-bisphosphate carboxylase-oxygenase in transgenic tobacco transformed with “antisense” rbcS. Planta 190:1–9.

Flamholz AI, Prywes N, Moran U, et al (2019) Revisiting Trade-offs between Rubisco Kinetic Parameters. Biochemistry 58:3365–3376.

Fluhr R, Chua N-H (1986) Developmental regulation of two genes encoding ribulose-bisphosphate carboxylase small subunit in pea and transgenic petunia plants: Phytochrome response and blue-light induction. Proc Natl Acad Sci 83:2358–2362.

Fu Y, Foden JA, Khayter C, et al (2013) High-frequency off-target mutagenesis induced by CRISPR-Cas nucleases in human cells. Nat Biotechnol 31:822–826.

Fukayama H, Kobara T, Shiomi K, et al (2019) Rubisco small subunits of C 4 plants, Napier grass and guinea grass confer C 4 -like catalytic properties on Rubisco in rice. Plant Prod Sci 22:296–300.

Galili S, Galili G, Avivi Y, Feldman M (1992) Identification and chromosomal location of four subfamilies of the Rubisco small subunit genes in common wheat. Theor Appl Genet 83:385–391.

Genkov T, Meyer M, Griffiths H, Spreitzer RJ (2010) Functional hybrid rubisco enzymes with plant small subunits and algal large subunits: Engineered rbcS cDNA for expression in chlamydomonas. J Biol Chem 285:19833–19841.

Genkov T, Spreitzer RJ (2009) Highly conserved small subunit residues influence Rubisco large subunit catalysis. J Biol Chem 284:30105–30112.

Gesch RW, Boote KJ, Vu JCV, et al (1998) Changes in Growth CO 2 Result in Rapid Adjustments of Ribulose-1,5-Bisphosphate Carboxylase/Oxygenase Small Subunit Gene Expression in Expanding and Mature Leaves of Rice . Plant Physiol 118:521–

529.

Ghannoum O, Phillips NG, Conroy JP, et al (2010) Exposure to preindustrial, current and future atmospheric CO2 and temperature differentially affects growth and photosynthesis in Eucalyptus. Glob Chang Biol 16:303–319.

Goldschmidt-Clermont M, Rahire M (1986) Sequence, evolution and differential expression of the two genes encoding variant small subunits of ribulose bisphosphate carboxylase/oxygenase in Chlamydomonas reinhardtii. J Mol Biol 191:421–432.

Gray WM, Ostin A, Sandberg G, et al (1998) High temperature promotes auxin-mediated hypocotyl elongation in Arabidopsis. Proc Natl Acad Sci 95:7197–7202.

Gutteridge S, Rhoades DF, Herrmann C (1993) Site-specific mutations in a loop region of the C-terminal domain of the large subunit of ribulose bisphosphate carboxylase/oxygenase that influence substrate partitioning. J Biol Chem 268:7818–7824.

Hahn F, Mantegazza O, Greiner A, et al (2017) An Efficient Visual Screen for CRISPR/Cas9 Activity in Arabidopsis thaliana. Front Plant Sci 08:1–13.

Hahn F, Nekrasov V (2019) CRISPR/Cas precision: do we need to worry about off-targeting in plants? Plant Cell Rep 38:437–441.

Hobbs SLA, Kpodar P, DeLong CMO (1990) The effect of T-DNA copy number, position and methylation on reporter gene expression in tobacco transformants. Plant Mol Biol 15:851–864.

Howe CJ, Auffret AD, Doherty A, et al (1982) Location and nucleotide sequence of the gene for the proton-translocating subunit of wheat chloroplast ATP synthase. Proc Natl Acad Sci 79:6903–6907.

Hsu PD, Scott DA, Weinstein JA, et al (2013) DNA targeting specificity of RNA-guided Cas9 nucleases. Nat Biotechnol 31:827–32.

Hu X, Wang C, Liu Q, et al (2017) Targeted mutagenesis in rice using CRISPR-Cpf1 system. J Genet Genomics 44:71–73.

Hug N, Longman D, Cáceres JF (2015) Mechanism and regulation of the nonsense-mediated decay pathway. Nucleic Acids Res 44:1483–1495.

Hyun Y, Kim J, Cho SW, et al (2015) Site-directed mutagenesis in Arabidopsis thaliana using dividing tissue-targeted RGENof th e CRISPR/Cas system to generate heritable null alleles. Planta 241:271–284.

Ido A, Iwata S, Iwata Y, et al (2016) Arabidopsis Pol II-Dependent in Vitro Transcription System Reveals Role of Chromatin for Light-Inducible rbcS Gene Transcription. Plant Physiol 170:642–652.

Ingram JSI, Porter JR (2015) Plant science and the food security agenda. Nat Plants 1:15173.

Ishida T, Alexandrov M, Nishimura T, et al (2010) Selective detection of airborne asbestos fibers using protein-based fluorescent probes. Environ Sci Technol 44:755–759.

Ishikawa C, Hatanaka T, Misoo S, et al (2011) Functional incorporation of sorghum small

subunit increases the catalytic turnover rate of Rubisco in transgenic rice. Plant Physiol 156:1603–11.

Izumi M, Tsunoda H, Suzuki Y, et al (2012) RBCS1A and RBCS3B, two major members within the Arabidopsis RBCS multigene family, function to yield sufficient Rubisco content for leaf photosynthetic capacity. J Exp Bot 63:2159–2170.

Izumi M, Wada S, Makino A, Ishida H (2010) The Autophagic Degradation of Chloroplasts via Rubisco-Containing Bodies Is Specifically Linked to Leaf Carbon Status But Not Nitrogen Status in Arabidopsis. Plant Physiol 154:1196–1209.

Jiang F, Doudna JA (2017) CRISPR – Cas9 Structures and Mechanisms. AnnuRevBiophys 46:505–529.

Jiang W, Bikard D, Cox D, et al (2013a) CRISPR-assisted editing of bacterial genomes. Nat biotechnol 31:233–239.

Jiang W, Zhou H, Bi H, et al (2013b) Demonstration of CRISPR/Cas9/sgRNA-mediated targeted gene modification in Arabidopsis, tobacco, sorghum and rice. Nucleic Acids Res 41:1–12.

Kanevski I (1999) Plastome engineering of ribulose-1,5-bisphosphate carboxylase/oxygenase in tobacco to form a sunflower large subunit and tobacco small subunit hybrid. Plant Physiol 119:133–142.

Kaplan A, Reinhold L (1999) CO2 concentrating mechanisms in photosynthetic microorganisms. Annu Rev Plant Physiol Plant Mol Biol 50:539–570.

Karkehabadi S, Peddi SR, Anwaruzzaman M, et al (2005) Chimeric small subunits influence catalysis without causing global conformational changes in the crystal structure of ribulose-1,5-bisphosphate carboxylase/oxygenase. Biochemistry 44:9851–9861.

Karkehabadi S, Satagopan S, Taylor TC, et al (2007) Structural analysis of altered large-subunit loop-6/carboxy-terminus interactions that influence catalytic efficiency and CO2/O 2 specificity of ribulose-1,5-bisphosphate carboxylase/oxygenase. Biochemistry 46:11080–11089.

Kempton HR, Qi LS (2019) When genome editing goes off-target. Science 364:234–236.

Khrebtukova I, Spreitzer RJ (1996) Elimination of the Chlamydomonas gene family that encodes the small subunit of ribulose-1,5-bisphosphate carboxylase/oxygenase. Proc Natl Acad Sci U S A 93:13689–93.

Khumsupan P, Donovan S, McCormick AJ (2019) CRISPR/Cas in Arabidopsis: overcoming challenges to accelerate improvements in crop photosynthetic efficiencies. Physiol Plant 166:428–437.

Knight S, Andersson I, Branden CI (1990) Crystallographic analysis of ribulose 1,5-bisphosphate carboxylase from spinach at 2.4 A resolution: Subunit interactions and active site. J Mol Biol 215:113–160.

Knoll A, Fauser F, Puchta H (2014) DNA recombination in somatic plant cells: Mechanisms and evolutionary consequences. Chromosom Res 22:191–201.

Kostov R V., Small CL, McFadden BA (1997) Mutations in a sequence near the N-

terminus of the small subunit alter the CO2/O2 specificity factor for ribulose bisphosphate carboxylase/oxygenase. Photosynth Res 54:127–134.

Kozak J, West CE, White C, et al (2009) Rapid repair of DNA double strand breaks in Arabidopsis thaliana is dependent on proteins involved in chromosome structure maintenance. DNA Repair (Amst) 8:413–419.

Krapp A, Chaves MM, David MM, et al (1993) Decreased ribulose-1,5-bisphosphate carboxylase / oxygenase in transgenic tobacco transformed with 'antisensel rbcS . VIII. Impact on photosynthesis and growth in tobacco growing under extreme high irradiance and high temperature. Plant Cell Environ 17:945–953.

Krebbers E, Seurinck J, Herdies L, et al (1988) Four genes in two diverged subfamilies encode the ribulose-1,5-bisphosphate carboxylase small subunit polypeptides of Arabidopsis thaliana. Plant Mol Biol 11:745–759.

Krysan PJ, Young JC, Sussman MR (1999) T-DNA as an insertional mutagen in Arabidopsis. Plant Cell 11:2283–2290.

Laterre R, Pottier M, Remacle C, Boutry M (2017) Photosynthetic Trichomes Contain a Specific Rubisco with a Modified pH-Dependent Activity. Plant Physiol 173:2110–2120.

Lauerer M, Saftic D, Quick WP, et al (1993) Decreased ribulose-1,5-bisphosphate carboxylase-oxygenase in transgenic tobacco transformed with "antisense" rbcS - VI. Effect on photosynthesis in plants grown at different irradiance. Planta 190:332–345.

Lawrenson T, Shorinola O, Stacey N, et al (2015) Induction of targeted, heritable mutations in barley and Brassica oleracea using RNA-guided Cas9 nuclease. Genome Biol 16:258.

LeBlanc C, Zhang F, Mendez J, et al (2017) Increased efficiency of targeted mutagenesis by CRISPR/Cas9 in plants using heat stress. Plant J 9:377–386.

Li J, Aach J, Norville JE, et al (2013) Multiplex and homologous recombination-mediated plant genome editing via guide RNA/Cas9. Nat Biotechnol 31:688–691.

Li J, Chory J (1998) Preparation of DNA from Arabidopsis. Methods Mol Biol 82:55–60

Li J, Manghwar H, Sun L, et al (2019) Whole genome sequencing reveals rare off-target mutations and considerable inherent genetic or/and somaclonal variations in CRISPR/Cas9-edited cotton plants. Plant Biotechnol J 17:858–868.

Liang G, Zhang H, Lou D, Yu D (2016) Selection of highly efficient sgRNAs for CRISPR / Cas9-based plant genome editing. Sci Rep 19:1–8.

Lin MT, Stone WD, Chaudhari V, Hanson MR (2019) Enzyme kinetics of tobacco Rubisco expressed in Escherichia coli varies depending on the small subunit composition. bioRxiv 1–17.

Long SP, Marshall-Colon A, Zhu XG (2015) Meeting the global food demand of the future by engineering crop photosynthesis and yield potential. Cell 161:56–66.

Lorimer GH, Badger MR, Andrews TJ (1976) The activation of ribulose-1,5-bisphosphate carboxylase by carbon dioxide and magnesium ions. Equilibria, kinetics, a suggested

mechanism, and physiological implications. Biochemistry 15:529–536.

Mao Y, Zhang Z, Feng Z, et al (2016) Development of germ-line-specific CRISPR-Cas9 systems to improve the production of heritable gene modifications in Arabidopsis. Plant Biotechnol J 14:519–532.

Matzke AJM, Matzke MA (1998) Position effects and epigenetic silencing of plant transgenes. Curr Opin Plant Biol 1:142–148.

Meagher RB, Berry-Lowe S, Rice K (1989) Molecular evolution of the small subunit of ribulose bisphosphate carboxylase: Nucleotide substitution and gene conversion. Genetics 123:845–863.

Miki D, Zhang W, Zeng W, et al (2018) CRISPR/Cas9-mediated gene targeting in Arabidopsis using sequential transformation. Nat Commun 9:1–9.

Morell MK, Wilkin JM, Kane HJ, Andrews TJ (1997) Side reactions catalyzed by ribulose-bisphosphate carboxylase in the presence and absence of small subunits. J Biol Chem 272:5445–5451.

Morita K, Hatanaka T, Misoo S, Fukayama H (2014) Unusual small subunit that is not expressed in photosynthetic cells alters the catalytic properties of Rubisco in rice. Plant Physiol 164:69–79.

Nacry P, Camilleri C, Courtial B, et al (1998) Major chromosomal rearrangements induced by T-DNA transformation in Arabidopsis. Genetics 149:641–650

Nakamichi N, Kita M, Ito S, et al (2005) PSEUDO-RESPONSE REGULATORS, PRR9,

PRR7 and PRR5, Together play essential roles close to the circadian clock of Arabidopsis thaliana. Plant Cell Physiol 46:686–698.

Nekrasov V, Staskawicz B, Weigel D, et al (2013) Targeted mutagenesis in the model plant Nicotiana benthamiana using Cas9 RNA-guided endonuclease. Nat Biotechnol 31:691–693.

Nielsen TH, Krapp A, Röper-Schwarz U, Stitt M (1998) The sugar-mediated regulation of genes encoding the small subunit of Rubisco and the regulatory subunit of ADP glucose pyrophosphorylase is modified by phosphate and nitrogen. Plant, Cell Environ 21:443–454.

Nisbet EG, Grassineau N V., Howe CJ, et al (2007) The age of Rubisco: The evolution of oxygenic photosynthesis. Geobiology 5:311–335.

Onizuka T, Endo S, Akiyama H, et al (2004) The rbcX Gene Product Promotes the Production and Assembly of Ribulose-1,5-Bisphosphate Carboxylase/Oxygenase of Synechococcus sp. PCC7002 in Escherichia coli. Plant Cell Physiol 45:1390–1395.

Ordon J, Bressan M, Kretschmer C, et al (2019) Optimized Cas9 expression systems for highly efficient Arabidopsis genome editing facilitate isolation of complex alleles in a single generation Jana. Funct Integr Genomics 1:1–12.

Ordon J, Gantner J, Kemna J, et al (2017) Generation of chromosomal deletions in dicotyledonous plants employing a user-friendly genome editing toolkit. Plant J 89:155–168.

Ordon J, Gantner J, Kemna J, et al (2016) Generation of chromosomal deletions in

dicotyledonous plants employing a user-friendly genome editing toolkit. Plant J 89:155–168.

Osakabe Y, Watanabe T, Sugano SS, et al (2016) Optimization of CRISPR/Cas9 genome editing to modify abiotic stress responses in plants. Sci Rep 6:1–10.

Pannunzio N, Li S, Watanabe G, Leiber M (2014) NHEJ Often Uses Microhomology: Implications for Alternative End Joining. DNA Repair (Amst) 17:74–80.

Papikian A, Liu W, Gallego-bartolomé J, Jacobsen SE (2019) Site-specific manipulation of Arabidopsis loci using CRISPR-Cas9 SunTag systems Ashot. Nat Commun 10:1–11.

Paul K, Morell MK, Andrews TJ (1991) Mutations in the Small Subunit of Ribulosebisphosphate Carboxylase Affect Subunit Binding and Catalysis. Biochemistry 30:10019–10026.

Perchorowicz JT, Raynes DA, Jensen RG (1981) Light limitation of photosynthesis and activation of ribulose bisphosphate carboxylase in wheat seedlings. Proc Natl Acad Sci 78:2985–2989.

Petrillo E, Herz MAG, Barta A, et al (2014) Let there be light: Regulation of gene expression in plants. RNA Biol 11:1215–1220.

Pilgrim ML, McClung CR (1993) Differential Involvement of the Circadian Clock in the Expression of Genes Required for Ribulose-1,5-Bisphosphate Carboxylase/Oxygenase Synthesis, Assembly, and Activation in Arabidopsis thaliana. Plant Physiol 103:553–564.

Porra RJ, Thompson W a, Kriedemann PE (1989) Determination of Accurate Extinction Coefficients and Simultaneous-Equations for Assaying Chlorophyll-a and Chlorophyll-B Extracted with 4 Different Solvents - Verification of the Concentration of Chlorophyll Standards by Atomic-Absorption Spectroscopy. Biochim Biophys Acta 975:384–394.

Portis ARJ (1995) The regulation of Rubisco by Rubisco activase. J Exp Bot 46:1285–1291.

Pottier M, Gilis D, Boutry M (2018) The Hidden Face of Rubisco. Trends Plant Sci 23:382–392.

Price GD, Howitt SM, Harrison K, Badger MR (1993) Analysis of a genomic DNA region from the cyanobacterium Synechococcus sp. strain PCC7942 involved in carboxysome assembly and function. J Bacteriol 175:2871–2879.

Qi Y, Zhang Y, Zhang F, et al (2013) Increasing frequencies of site-specific mutagenesis and gene targeting in Arabidopsis by manipulating DNA repair pathways. Genome Res 23:547–554.

Qu L-J, Qin G (2014) Generation and Characterization of Arabidopsis T-DNA Insertion Mutants. In: Sanchez-Serrano J, Salinas J (eds) Arabidopsis Protocols. Methods in Molecular Biology (Methods and Protocols). Humana Press, Totowa, NJ, pp 241–258.

Quick WP, Schurr U, Scheibe R, et al (1991) Decreased ribulose-1,5-bisphosphate carboxylase-oxygenase in transgenic tobacco transformed with “antisense” rbcS - I.

Impact on photosynthesis in ambient growth conditions. Planta 183:542–554.

Raitskin O, Patron NJ (2016) Multi-gene engineering in plants with RNA-guided Cas9 nuclease. Curr Opin Biotechnol 37:69–75.

Ranty B, Lundqvist T, Schneider G, et al (1990) Truncation of ribulose-1,5-bisphosphate carboxylase/oxygenase (Rubisco) from Rhodospirillum rubrum affects the holoenzyme assembly and activity. EMBO J 9:1365–1373.

Read BA, Tabita FR (1992) A hybrid ribulosebisphosphate carboxylase/oxygenase enzyme exhibiting a substantial increase in substrate specificity factor. Biochemistry 31:5553–5560.

Robinson JJ, Cavanaugh CM, Robinson J, Cavanaugh M (2012) II Rubisco in chemoautotrophic I and form of form Expression for the interpretation , of symbioses : Implications stable carbon isotope values. Limnol Oceanogr 40:1496–1502.

Rodermel S, Haley J, Jiang CZ, et al (1996) A mechanism for intergenomic integration: abundance of ribulose bisphosphate carboxylase small-subunit protein influences the translation of the large-subunit mRNA. Proc Natl Acad Sci U S A 93:3881–5.

Salvucci ME, Crafts-Brandner SJ (2004) Relationship between the Heat Tolerance of Photosynthesis and the Thermal Stability of Rubisco Activase in Plants from Contrasting Thermal Environments. Plant Physiol 134:1460–1470.

Sasaki Y, Nakamura Y, Matsuno R (1987) Regulation of gene expression of ribulose bisphosphate carboxylase in greening pea leaves. Plant Mol Biol 8:375–382.

Satagopan S, Spreitzer RJ (2004) Substitutions at the Asp-473 Latch Residue of Chlamydomonas Ribulosebisphosphate Carboxylase/Oxygenase Cause Decreases in Carboxylation Efficiency and CO2/O2 Specificity. J Biol Chem 279:14240–14244.

Sawchuk MG, Donner TJ, Head P, Scarpella E (2008) Unique and overlapping expression patterns among members of photosynthesis-associated nuclear gene families in Arabidopsis. Plant Physiol 148:1908–1924.

Schneider G, Knight S, Andersson I, et al (1990) Comparison of the crystal structures of L2 and L8S8 Rubisco suggests a functional role for the small subunit. EMBO J 9:2045–2050.

Schwarte S, Tiedemann R (2011) A gene duplication/loss event in the ribulose-1,5-bisphosphate-carboxylase/oxygenase (rubisco) small subunit gene family among accessions of Arabidopsis thaliana. Mol Biol Evol 28:1861–1876.

Sharwood RE, Sonawane B V, Ghannoum O, Whitney SM (2016) Improved analysis of C4 and C3 photosynthesis via refined in vitro assays of their carbon fixation biochemistry. J Exp Bot 67:3137–3148.

Sharwood RE, Von Caemmerer S, Maliga P, Whitney SM (2008) The catalytic properties of hybrid rubisco comprising tobacco small and sunflower large subunits mirror the kinetically equivalent source rubiscos and can support tobacco growth. Plant Physiol 146:83–96.

Shih PM, Occhialini A, Cameron JC, et al (2015) Biochemical characterization of predicted Precambrian RuBisCO. Nat Commun 7:1–11.

Shimada TL, Shimada T, Hara-Nishimura I (2010) A rapid and non-destructive screenable marker, FAST, for identifying transformed seeds of Arabidopsis thaliana. Plant J 61:519–528.

Smith A, Coupland G, Dolan L, et al (2010) Plant Biology. Garland Sciences, London.

Song Y, Chen Q, Ci D, et al (2014) Effects of high temperature on photosynthesis and related gene expression in poplar. BMC Plant Biol 14:111–131.

South PF, Cavanagh AP, Liu HW, Ort DR (2019) Synthetic glycolate metabolism pathways stimulate crop growth and productivity in the field. Science 363:0–10.

Spreitzer RJ (2003) Role of the small subunit in ribulose-1,5-bisphosphate carboxylase/oxygenase. Arch Biochem Biophys 414:141–149.

Stec B (2012) Structural mechanism of RuBisCO activation by carbamylation of the active site lysine. Proc Natl Acad Sci U S A 109:18785–90.

Steinert J, Schiml S, Fauser F, Puchta H (2015) Highly efficient heritable plant genome engineering using Cas9 orthologues from Streptococcus thermophilus and Staphylococcus aureus. Plant J 84:1295–1305.

Suzuki Y, Makino A (2012) Availability of Rubisco Small Subunit Up-Regulates the Transcript Levels of Large Subunit for Stoichiometric Assembly of Its Holoenzyme in Rice. Plant Physiol 160:533–540.

Suzuki Y, Makino A (2013) Translational downregulation of RBCL is operative in the coordinated expression of Rubisco genes in senescent leaves in rice. J Exp Bot

64:1145–1152.

Tabita FR (1999) Microbial ribulose 1,5-bisphosphate carboxylase/oxygenase: A different perspective. Photosynth Res 60:1–28.

Tabita FR, Satagopan S, Hanson TE, et al (2008) Distinct form I, II, III, and IV Rubisco proteins from the three kingdoms of life provide clues about Rubisco evolution and structure/function relationships. J Exp Bot 59:1515–1524.

Tan J, Zhang F, Karcher D, Bock R for site-speci fi c single nucleotide replacement. Nat Commun.

Tang X, Lowder LG, Zhang T, et al (2017) A CRISPR-Cpf1 system for efficient genome editing and transcriptional repression in plants. Nat Plants 3:1–5.

Taylor TC, Andersson I (1996) Structural transitions during activation and ligand binding in hexadecameric Rubisco inferred from the crystal structure of the activated unliganded spinach enzyme. Nature 3:95–101.

Terashima I, Hanba YT, Tholen D, Niinemets Ü (2011) Leaf Functional Anatomy in Relation to Photosynthesis. Plant Physiol 155:108–116.

Tobin EM, Silverthorne J (1985) Light regulation of gene expression in higher plants. Annu Rev Plant Physiol Plant Mol Biol 36:569–593.

Ushio A, Mae T, Makino A (2008) Effects of temperature on photosynthesis and plant growth in the assimilation shoots of a rose. Soil Sci Plant Nutr 54:253–258.

Van Leeuwen W, Ruttink T, Borst-Vrenssen AWM, et al (2001) Characterization of

position-induced spatial and temporal regulation of transgene promoter activity in plants. J Exp Bot 52:949–959.

Von Caemmerer S, Furbank RT (2003) The C4 pathway: An efficient CO2 pump. Photosynth. Res. 77:191–207.

Wang M, Mao Y, Lu Y, et al (2017) Multiplex Gene Editing in Rice Using the CRISPR-Cpf1 System. Mol Plant 10:1011–1013.

Wang Z, Xing H, Dong L, et al (2015) Egg cell-specific promoter-controlled CRISPR / Cas9 efficiently generates homozygous mutants for multiple target genes in Arabidopsis in a single generation. Genome Biol 16:114–126.

Wanner LA, Gruissem W (1991) Expression dynamics of the tomato rbcS gene family during development. Plant Cell 3:1289–303.

Warner RM, Erwin JE (2005) Naturally occurring variation in high temperature induced floral bud abortion across Arabidopsis thaliana accessions. Plant Cell Environ 28:1255–1266.

Wasmann CC, Ramage RT, Bohnert HJ, Ostrem JA (1989) Identification of an assembly domain in the small subunit of ribulose-1,5-bisphosphate carboxylase. Proc Natl Acad Sci 86:1198–1202.

Whitney SM, Sharwood RE (2008) Construction of a tobacco master line to improve Rubisco engineering in chloroplasts. J Exp Bot 59:1909–1921.

Whitney SM, von Caemmerer S, Hudson GS, Andrews TJ (1999) Directed mutation of

the Rubisco large subunit of tobacco influences photorespiration and growth. Plant Physiol 121:579–88. oi: 10.1104/pp.121.2.579

Wilson RH, Hayer-Hartl M (2018) Complex Chaperone Dependence of Rubisco Biogenesis. Biochemistry 57:3210–3216.

Wolter F, Klemm J, Puchta H (2018) Efficient in planta gene targeting in Arabidopsis using egg cell-specific expression of the Cas9 nuclease of Staphylococcus aureus. Plant J 94:735–746.

Wolter F, Puchta H (2018) The CRISPR/Cas revolution reaches the RNA world: Cas13, a new Swiss Army knife for plant biologists. Plant J 94:767–775.

Wostrikoff K, Stern D (2007) Rubisco large-subunit translation is autoregulated in response to its assembly state in tobacco chloroplasts. Proc Natl Acad Sci 104:6466–6471.

Xie K, Minkenberg B, Yang Y (2015) Boosting CRISPR/Cas9 multiplex editing capability with the endogenous tRNA-processing system. Proc Natl Acad Sci 112:3570–3575.

Xie K, Yang Y (2013) RNA-Guided genome editing in plants using a CRISPR-Cas system. Mol Plant 6:1975–1983.

Xing H-L, Dong L, Wang Z-P, et al (2014) A CRISPR/Cas9 toolkit for multiplex genome editing in plants. BMC Plant Biol 14:327–337.

Yan L, Wei S, Wu Y, et al (2015) High-Efficiency Genome Editing in Arabidopsis Using

YAO Promoter-Driven CRISPR/Cas9 System. Mol Plant 8:1820–1823.

Yoon M, Putterill JJ, Ross GS, Laing W a (2001) Determination of the relative expression levels of rubisco small subunit genes in Arabidopsis by rapid amplification of cDNA ends. Anal Biochem 291:237–244.

Yoshida Y, Sarmiento-Mañús R, Yamori W, et al (2018) The Arabidopsis phyB-9 Mutant Has a Second-Site Mutation in the VENOSA4 Gene That Alters Chloroplast Size, Photosynthetic Traits, and Leaf Growth . Plant Physiol 178:3–6.

Young J, Zastrow-Hayes G, Deschamps S, et al (2019) CRISPR-Cas9 Editing in Maize: Systematic Evaluation of Off-target Activity and Its Relevance in Crop Improvement. Sci Rep 9:1–11.

Yu Q, Lutz KA, Maliga P (2017) Efficient Plastid Transformation in Arabidopsis. Plant Physiol 175:186–193.

Zhang XH, Webb J, Huang YH, et al (2011) Hybrid Rubisco of tomato large subunits and tobacco small subunits is functional in tobacco plants. Plant Sci 180:480–488.

Zsögön A, Čermák T, Naves ER, et al (2018) De novo domestication of wild tomato using genome editing. Nat Biotechnol EPub ahead of print.

Appendix

Published reviewed article “CRISPR/Cas in Arabidopsis: overcoming challenges to accelerate improvements in crop photosynthetic efficiencies” in Physiologia Plantarum 116: 428-437